UNIVERSITY OF SOUTHAMPTON

Faculty of Environmental and Life Sciences
School of Biological Sciences

Defining the Role of Epithelial LKB1 in Idiopathic Pulmonary Fibrosis

by

Zijian Xu

A thesis for the degree of
Doctor of Philosophy

March 17, 2024

University of Southampton

Abstract

Faculty of Environmental and Life Sciences
School of Biological Sciences

Doctor of Philosophy

Defining the Role of Epithelial LKB1 in Idiopathic Pulmonary Fibrosis

by Zijian Xu

Lung fibrosis, prevalent mainly among those over 50, is witnessing an increase in global cases, partly due to an ageing population and exacerbated by the COVID-19 pandemic's aftermath. Idiopathic pulmonary fibrosis (IPF), a form of this chronic disease, is characterized by a progressive buildup of extracellular matrix and lung parenchyma growth, with its root cause still unidentified. Despite its gradual onset, it eventually leads to symptoms like dry cough and breathing difficulties, thereby reducing survival rates. The ongoing challenge is to develop effective treatments, highlighting the need for innovative therapeutic strategies.

The mechanisms underlying fibrosis progression remain largely elusive. Previous studies have shown that inhibiting autophagy in alveolar epithelial cells can amplify myofibroblast differentiation in pulmonary fibrosis through paracrine signalling, thus fostering epithelial-mesenchymal transition (EMT). Autophagy, a cellular recycling process, is a potential treatment strategy in several medical fields. In the context of IPF, diminished autophagic activity, linked with ageing, accelerates bronchial epithelial cell ageing and promotes lung fibroblast differentiation, facilitating EMT. This reversible process, regulated by transcription factors like Snail and ZEB, has implications in various biological phenomena including cancer metastasis and organ fibrosis.

Our research reveals significant alterations in the global transcriptomics of ATII cells following LKB1 or *STK11* depletion, highlighting the activation of critical pathways like "TNFα signalling via NFκB" and "EMT". The data, confirmed through various analyses, underscore LKB1's pivotal role in initiating the EMT process in these cells. Further, we identified the primary pathway amplified by LKB1 depletion as "Hallmark_TNFα signalling via NFκB", confirmed by reporter assays. Our study further elucidated LKB1's influence on autophagy in ATII cells, indicating that its depletion disrupts autophagy, as revealed by western blot and immunofluorescence analyses. The study also explored the activation of the p62-NFκB pathway in ATII cells due to LKB1 depletion, indicating a potential regulatory mechanism involving

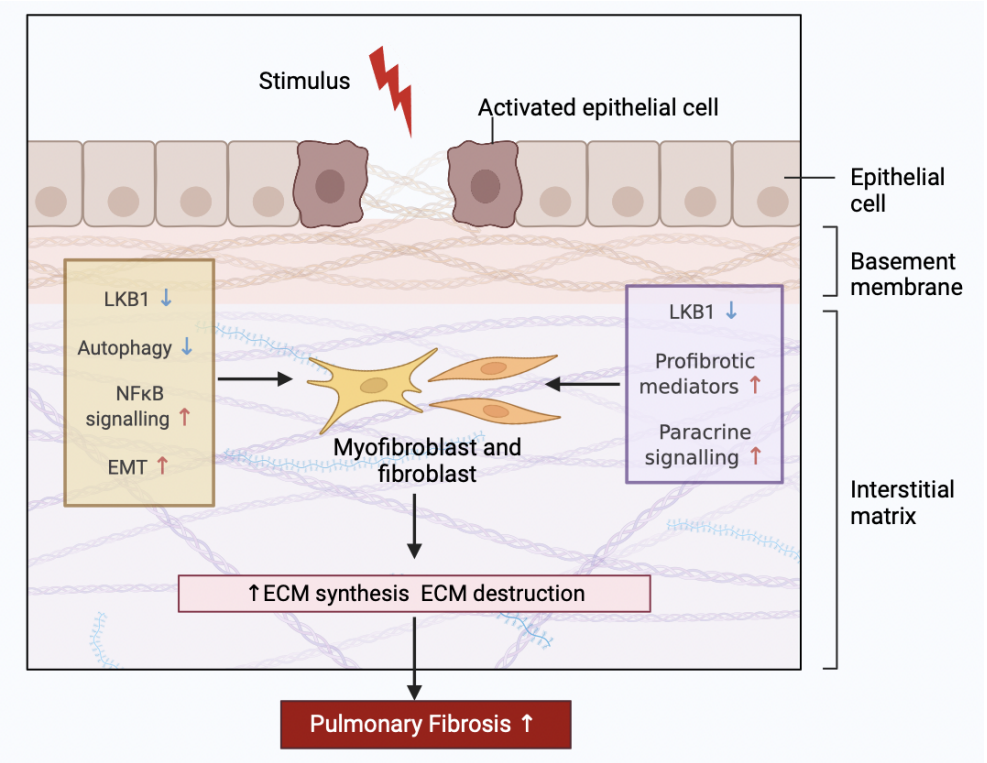

FIGURE 1: **The role of LKB1 of alveolar epithelial type II (ATII) cells in the development of pulmonary fibrosis**
Schematic representation showing depletion of LKB1 leads to altered global transcriptomics, emphasizing the activation of "TNFα signalling via NFκB" and "EMT". This inactivation disrupts autophagy and suggests a potential mechanism underlying direct initiation to epithelial-mesenchymal transition (EMT) (shown as yellow module) and indirect induction of epithelial-fibroblasts crosstalk via paracrine signalling (purple module). These molecular changes induced by LKB1 inhibition contribute to the progression of pulmonary fibrosis, highlighting the intricate interplay between ATII cells and fibroblasts.

p62 and p65 in controlling Snail2 expression. This suggests that LKB1 inactivation in ATII cells might foster EMT through the p62-NFκB pathway. In IPF-affected lungs, this is triggered by the downregulation of CAB39L, a vital component of the LKB1 complex. Our research, including 3D co-cultures and RNA-seq analyses, affirmed that the interaction between LKB1-depleted ATII cells and fibroblasts enhances myofibroblast differentiation. Preliminary studies in mice further corroborated the role of Lkb1 deletion in impairing lung functionality (Figure. 1).

In conclusion, our findings indicate that LKB1 inhibition-induced reduced autophagy can stimulate EMT in ATII cells, fostering fibrosis through abnormal epithelial-fibroblast interactions.

Contents

List of Figures

List of Tables

Declaration of Authorship

I declare that this thesis and the work presented in it is my own and has been generated by me as the result of my own original research.

I confirm that:

1. This work was done wholly or mainly while in candidature for a research degree at this University;
2. Where any part of this thesis has previously been submitted for a degree or any other qualification at this University or any other institution, this has been clearly stated;
3. Where I have consulted the published work of others, this is always clearly attributed;
4. Where I have quoted from the work of others, the source is always given. With the exception of such quotations, this thesis is entirely my own work;
5. I have acknowledged all main sources of help;
6. Where the thesis is based on work done by myself jointly with others, I have made clear exactly what was done by others and what I have contributed myself;
7. Parts of this work have been published as:

   Xu Z, Davies E R, Yao L, et al. LKB1 depletion-mediated epithelial–mesenchymal transition induces fibroblast activation in lung fibrosis[J]. Genes & Diseases, 2024, 11(3): 101065.

   Yao L, Xu Z, Davies D E, et al. Dysregulated bidirectional epithelial–mesenchymal crosstalk: A core determinant of lung fibrosis progression[J]. Chinese Medical Journal Pulmonary and Critical Care Medicine, 2024.

Signed:..... Date:.....

Acknowledgements

As I reach the conclusion of this significant chapter of my academic journey, I want to take a moment to acknowledge the support and encouragement I have received from many individuals and organizations.

Firstly, I would like to express my sincere gratitude to my supervisor, Dr Yihua Wang. Your guidance and support throughout this process have been invaluable. Your expertise and insights helped me navigate the complex landscape of my research field with confidence. Only when pursuing a Ph.D. do you realize that there's nothing more comforting in this world than hearing these words from your advisor: "It's okay, failure in experiments is normal. This result is very interesting. I think it's publishable. You can start writing your thesis now."

A special mention goes to all the colleagues in our lab. They always appear at the most appropriate moments, such as during the dull gaps in experiments, occupying the audience seats, cheering loudly during speeches, and being the heartiest laughers at tea breaks and dinner tables. Thanks to Liudi, who not only taught me all the experimental methods but also generously shared her personal precious experimental techniques, preventing me from taking detours in my research. And to Yilu, it was he who introduced me to bioinformatics and made me familiar with the field. And finally, to Siyuan and Ying, we might be different, but we share the same aspirations, enjoy the happiness we share, and give each other ample space to appreciate solitude.

I am thankful to my family for their constant support and encouragement. Your belief in me has been a pillar of strength, helping me persevere even during the most challenging times. My father is the most sensitive and generous person I have ever met. He is never hesitant to encourage, express love, and treat my mom and me like princesses.

I also want to thank all my friends. Qiang, who has stood by my side all the time, and Maggie, who offered moments of laughter and respite. To Qi, who is like a sibling to me, and my gym partners Xing and Yiyuan, thank you for reminding me to keep a balanced perspective on life.

I am grateful to the China Scholarship Council(CSC), the Medical Research Council (MR/S025480/1), the Academy of Medical Sciences /the Wellcome Trust Springboard Award (SBF0021038), and AAIR Charity for providing the necessary support to undertake this research. I would like to express my heartfelt gratitude to Elizabeth R. Davies, Julian Downward, Rob M. Ewing, Donna E. Davies and Mark G. Jones for their invaluable contributions, unwavering support, and collaborative spirit, which have significantly enriched this thesis. Your assistance has been instrumental in the realization of this project.

As I step forward, equipped with the knowledge and experiences gained during this period, I am reminded of the collective effort that has brought me to this point. Thank you for being a part of my journey.

To my parents, who have given me the greatest love and care.

Definitions and Abbreviations

CCL2	Monocyte chemoattractant protein-1 or MCP-1
LC3-II	Microtubule-associated protein 1A/1B-light chain 3 isoform II
α-SMA	α-smooth muscle actin
6MWT	six-minute walk test
ABCA3	ATP-Binding Cassette Subfamily A Member 3
ACTA2	Actin, Alpha 2, Smooth Muscle
ACTB	β-Actin
AE	Acute exacerbation
AECs	epithelial type 2 alveolar epithelial cells
AKT	Protein kinase B
AMPK	AMP-activated protein kinase
ATP11A	ATPase Phospholipid Transporting 11A
B-MSC	bone marrow
BH	Benjamini-Hochberg
BLM	bleomycin
BP	Biological process
CC	Cellular component
CCL17	Thymus and activation-regulated chemokine or TARC
CDH1	E-cadherin
CM	conditional media
COL1A1	Collagen Type I Alpha 1 Chain
COL3A1	Collagen Type III Alpha 1 Chain
CPFE	Combined pulmonary fibrosis and emphysema
Ct	cycle threshold
CXCL12	Stromal cell-derived factor 1 or SDF-1
DKC1	Dyskerin Pseudouridine Synthase 1
DLco	Diffusion of carbon monoxide
DM	Diabetes Mellitus
DPP9	Dipeptidyl Peptidase 9
DSP	Desmoplakin
EBV	Epstein-Barr virus
ECM	extracellular matrix

ECMO	extracorporeal membrane oxygenation
EDA–FN	extra domain A fibronectin
EGF	epidermal growth factor
EGFR	epidermal growth factor receptor
EMT	epithelial-mesenchymal transition
EMT-TFs	EMT transcription factors
ER	endoplasmic reticulum
FDR	false discovery rate
FFPE	Formalin-Fixed Paraffin-Embedded
FGF	Fibroblast growth factors
FGFR	fibroblast growth factor receptor
FiO2	fraction of inspired oxygen
FN	fibronectin
FN1	Fibronectin 1
FPKM	Fragments per Kilobase of exon per Million
GAP	Gender-Age-Physiology
GAPDH	Glyceraldehyde-3-Phosphate Dehydrogenase
GEO	Gene Expression Omnibus
GER	Gastroesophageal Reflux
GO	Gene ontology
GSEA	Gene set enrichment analysis
HA	hyaluronan
HFNC	high-flow nasal cannula
HHVs	human herpesviruses
HPC	High performance computing
HRCT	high resolution computed tomography
hTR	The human telomerase RNA
ICUs	intensive care units
IFN-γ	interferon-gamma
IGF-1	Insulin-like growth factor
IHC	Immunohistochemistry
IIPs	Idiopathic interstitial pneumonias
IL-13	interleukin-13
ISH	in situ hybridization
IT	Intratracheal Instillation
LAS	Lung Allocation Score
LC3	microtubule-associated protein light chain 3
LKB1(*STK11*)	Serine–threonine liver kinase B1
LMP1	latent membrane protein 1
MAPK	ERK-Mitogen-activated protein
MCID	minimal clinically important difference

MF	Molecular functions
MLE	maximum likelihood estimation
MMPs	matrix metalloproteinases
MO25	mouse protein 25
mtDNA	mitochondrial DNA
mTOR	mammalian target of rapamycin
MUC5B	mucin 5B
NAC	N-acetylcysteine
NAF1	Nuclear Assembly Factor 1
NES	Normalised enrichment score
NF-κB	nuclear factor kappa-light-chain-enhancer of activated B cells
NIV	Non-invasive ventilation
Nox4	NADPH oxidase-4
OBFC1	Oligonucleotide/Oligosaccharide-Binding Fold Containing 1
OSA	obstructive sleep apnea
p16	Cyclin-Dependent Kinase Inhibitor 2A (CDKN2A)
p21	Cyclin-Dependent Kinase Inhibitor 1A (CDKN1A)
Padj	adjusted P value
PARN	Poly(A)-Specific Ribonuclease
PCA	Principal component analysis
PCNA	proliferating cell nuclear antigen
PDE-5	phosphodiesterase 5
PDGFR	platelet-derived growth factor receptor
PE	pulmonary embolism
PE	phosphatidylethanolamine
PF	Pulmonary Fibrosis
PH	Pulmonary Hypertension
PPI networks	Protein-protein interaction (PPI) networks
PR	Pulmonary rehabilitation
PTEN	Phosphatase and tensin homolog
q-RT-PCR	Quantitative real-time PCR
RELA	nuclear factor NF-kappa-B p65 subunit
RIN	RNA integrity
RNAi	RNA interference
ROS	reactive oxygen species
RT	Room temperature
RTEL1	regulator of telomere elongation helicase 1
scRNA-seq	single-cell RNA sequencing
SFTPA1	Surfactant Protein A1
SFTPA2	Surfactant Protein A2
SFTPC	Surfactant Protein C

SGRQ	St. George's Respiratory Questionnaire
SHH	Sonic Hedgehog
SMAD	Mothers against decapentaplegic homolog (SMAD)
SNAI1	Snail Family Transcriptional Repressor 1
SNAI2	Snail Family Transcriptional Repressor 2
SNPs	single nucleotide polymorphisms
SP	surfactant protein
STK11	Serine/Threonine Kinase 11 (also known as Liver Kinase B1)
STRAD	STE20-related adaptor
TERT	Telomerase reverse transcriptase
TGF-beta	transforming growth factor beta
TINF2	TERF1 Interacting Nuclear Factor 2
TLC	Total lung capacity
TNF-α	tumour necrosis factor-alpha
TOLLIP	Toll Interacting Protein
tPA	Tissue-type plasminogen activator
TWIST1	Twist Family BHLH Transcription Factor 1
UIP	Usual interstitial pneumonia
VC	Vital capacity
VEGFR	vascular endothelial growth factor receptor
VIM	Vimentin
ZEB1	Zinc Finger E-box-Binding Homeobox 1
ZEB2	Zinc Finger E-box-Binding Homeobox 2

Chapter 1

Introduction

1.1 Overview

This chapter aims to provide a comprehensive background on the key areas that are covered in this thesis. The central focus of this chapter is on the lung disease known as IPF and its relevant mechanisms. To begin with, a brief introduction will be provided on the disease, followed by an exploration of its pathogenesis and risk factors. Additionally, the latest medical advances in IPF, including its diagnosis, treatments, and prognosis, will also be examined.

Throughout this thesis, The impact of the structure and function of epithelial and mesenchymal cells, which underlie cell-cell communication, will also be addressed concerning their contribution to IPF, and key signalling pathways that have also been scrutinized will be explicated. Notably, the contribution of liver kinase (LKB1) to IPF pathogenesis is substantial, including the LKB1-AMPK pathway. TGF-β1 pathway will also be discussed given its significance in the pathogenesis of IPF, as well as the utilization of TGF-β1 to elicit a myofibroblast phenotype.

Importantly, this chapter delves into the mechanisms of epithelial-mesenchymal transition (EMT) and the interplay between epithelial and fibroblasts, which are both relevant to IPF. Moreover, in terms of findings related to autophagy's crucial role in IPF within this project, the relationship between autophagy and LKB1 will also be highlighted in this chapter.

1.2 Idiopathic Pulmonary Fibrosis (IPF)

Lung fibrosis, also known as pulmonary fibrosis (PF) is a growing concern worldwide due to the ageing population, and its prevalence is on the rise (Strongman, Kausar,

and Toby M Maher 2018; Raghu, Weycker, et al. 2006). What was once considered a rare disease is now present in about 7% of the general population over the age of 50, resulting in increased mortality rates (hazard ratio 2.7). The recent COVID-19 pandemic has further exacerbated this problem, with reports of persistent interstitial changes following pneumonitis (T. Guo et al. 2021; X. Wu et al. 2021).

IPF is a specific type of chronic interstitial lung disease characterized by the deposition of extracellular matrix and the expansion of lung parenchyma (Raghu, Harold R Collard, et al. 2011a; Somogyi et al. 2019). Although the pathogenesis of IPF is not yet fully understood, disruptions in extracellular matrix homeostasis have been implicated in the development of the disease (Cook, Brass, and Schwartz 2002).

IPF is a progressive disorder that is often asymptomatic during the early stages. However, as scarring within the lungs progresses, patients may experience dry cough and dyspnea, resulting in poor survival rates (Raghu, Harold R Collard, et al. 2011a). The median survival is between two to five years (Strongman, Kausar, and Toby M Maher 2018; Bjoraker et al. 1998; KING JR et al. 2001; Ley, C. J. Ryerson, et al. 2012; Nathan et al. 2011). While some risk factors have been identified, effective treatment options remain elusive, highlighting an unmet need for therapies.

1.2.1 Epidemiology

Before the introduction of consistent histopathologic criteria, multiple terms were used to describe what would now be considered IPF, including different types of idiopathic interstitial pneumonias (IIPs) (Liebow 1969). In 1998, Katzenstein and Myers reorganised the previously distinct idiopathic pneumonias considering that there are several keys to reclassify as IPF, (Katzenstein and Myers 1998), which include extent of inflammation and honeycombing, fibroblastic foci, and present of heterogeneity of fibrosis or honeycombing. In 2000, the guidance published by the American Thoracic Society was termed IPF and was widely adopted (Society et al. 2000). In 2002, the American Thoracic Society and European Respiratory Society (ATS/ERS) published a consensus statement of classification of IIPs building upon Katzenstein and Myers's classification and extended more on clinical and radiographic diagnostic features (Travis et al. 2002). The most commonly encountered subgroup was termed "usual" interstitial pneumonia (UIP), which refers to the histopathological or radiological pattern of disease that, without any identifiable cause, is diagnostic of IPF. The histopathologic classification of UIP has remained unchanged since then.

IPF affects more than 3 million people worldwide (Martinez et al. 2017a; Luca Richeldi, Harold R Collard, and Mark G Jones 2017), with an estimated population of 300,000 in Europe and 130,000 in the US (Martinez et al. 2017a). The disease is more prevalent than previously recognized, with pulmonary interstitial

abnormality detected in 7% of the elderly population (age $>$ 50 years)(Putman et al. 2016; L. Yao, Yilu Zhou, et al. 2021). Incidence rates vary geographically, with North America and Europe reporting between 30 to 90 cases per million people per year, and Asia and South America reporting lower rates of between 5 to 42 cases per million people per year. (Strongman, Kausar, and Toby M Maher 2018; Raghu, Weycker, et al. 2006; Baddini-Martinez and Pereira 2015; H. Lee et al. 2016; Natsuizaka et al. 2014; Hutchinson et al. 2015; Gribbin et al. 2006; Navaratnam et al. 2011; Kornum et al. 2008; Raghu, S.-Y. Chen, et al. 2014; C.-C. Lai et al. 2012). Older males ($>$ 75 years old) are the most vulnerable population, with a five-fold higher incidence than others (Raghu, Weycker, et al. 2006). The disease is associated with poor prognosis, with a median survival following diagnosis between 2 to 5 years (Ley, C. J. Ryerson, et al. 2012; Nathan et al. 2011), and the estimated 3-year, 5-year, and 10-year survival rates for IPF patients being 50%, 34%, and 19%, respectively (Strongman, Kausar, and Toby M Maher 2018).

Moreover, IPF has a worse survival rate compared to many cancers (Martinez et al. 2017a; Vancheri et al. 2010). The progression period of IPF varies between individuals, with some patients only developing symptoms after many decades (Ley, Harold R Collard, and Talmadge E King Jr 2011a). Despite this, diagnosis typically takes 1-2 years on average following the onset of symptoms (ibid.). Prognosticating patient outcomes is challenging due to interpatient heterogeneity (Martinez et al. 2017a; Luca Richeldi, Harold R Collard, and Mark G Jones 2017), which makes developing effective treatments and improving prognostication an urgent and unmet need. Studies have shown that up to 20% of patients with IPF may die from other causes, such as cardiovascular disease or lung cancer, rather than directly from their pulmonary fibrosis (Ley, Harold R Collard, and Talmadge E King Jr 2011b; Michael Kreuter, Ehlers-Tenenbaum, et al. 2016). Because patients with significant comorbidities are often excluded from clinical trials, the short-term mortality rates reported in these studies may be lower than expected when compared to the general patient population (Ley, Bradford, et al. 2015).

1.2.2 Prognosis and monitoring of IPF

The prognosis of IPF has been validated by the guideline of Gender-Age-Physiology (GAP) model, including factors of age, gender and other clinical parameters such as total lung capacity (TLC), vital capacity (VC), the diffusion of carbon monoxide (DLco), or corrections by alveolar volume (KCO), six-minute walk test (6MWT), and greater extent of fibrosis on high resolution computed tomography (HRCT), among others (Ley, C. J. Ryerson, et al. 2012; Ley, Bradford, et al. 2015; Bois et al. 2011; A. U. Wells et al. 2003). Predicted factors at prognosis and monitoring stages have been suggested by (Fernández Fabrellas et al. 2018) in 2018 (Table. 1.1).

Apart from these, molecular biomarkers have attracted significant attention as potential tools to forecast the rate of IPF progression and to assist in identifying patients who would most likely benefit from IPF medications or require immediate assessment for lung transplantation (Table. 1.2) (Stankovic, Stjepanovic, and Asanin 2021; Drakopanagiotakis et al. 2018). This table illustrates the emerging spectrum of potential biomarkers in IPF diagnosis and prognosis. It showcases molecules implicated in alveolar epithelial cell injury, fibro-proliferation, matrix remodelling, and immune regulation, serving as prospective biomarkers. It highlights the association of genetic variants such as *TOLLIP* and *MUC5B* with differential responses to treatment and the potential influence on IPF development and prognosis. Additionally, it underscores the promising roles of bacterial signatures found in IPF lungs and mitochondrial DNA, as revealed through microbiome analyses, in serving as novel biomarkers. The figure also proposes the possibility of establishing comprehensive biomarker signatures through the combination of multiple biomarkers, a prospect that could potentially revolutionize current clinical and functional parameters employed in IPF management, albeit with further research and validation required to fully realize this potential. However, while several biomarkers can predict survival and disease progression, none has yet been validated to predict response to antifibrotic treatments, hence limiting their practical clinical usage. these specific genomic disorders(*MUC5B*, *SFTPC*, *SFTPA2*, *RTEL1*, *TERT*, and *hTR*) (Schwartz 2016), which will be discussed in more detail in the following subsection on risk factors, together with shorter telomere lengths in peripheral blood, seem to serve as molecular predictors of reduced survival time in patients diagnosed with idiopathic pulmonary fibrosis (Newton et al. 2019) (Table. 1.2). Despite the potential benefits, molecular biomarkers aren't widely accessible or routinely incorporated in the clinical management of IPF.

prognosis	**monitoring (6-12 months)**
Male gender; age $>$ 70 years	Grade of dyspnea increasing
Diagnosis delay	Exacerbation
Grade of dyspnea	Decline % FVC $>$ 10%
Cardiovascular comorbidities	Decline % DLco $>$ 15%
DLco $\leq$ 40%	Decline $>$ 50 m at 6 MWT
SpO2 $<$ 88% in 6 MWT	MCID variation in %FVC 2–6%
Distance 6 MWT $<$ 250 m	MCID variation in 6 MWT 24–45 m
Fibrosis extension in HRCT	Fibrosis extension increasing in HRCT
Pulmonary hypertension	Complications
Increase of fibroblastic foci in surgical lung biopsy	

TABLE 1.1: **Predicted factors for mortality of IPF**
DLco: diffusion of carbon monoxide; FVC: Forced Vital Capacity; SpO2: Oxygen saturation by pulse oximetry; 6 MWT: 6 min walking test; HRCT: High-resolution computed tomography; MCID: minimal clinically important difference. Information collected from (Fernández Fabrellas et al. 2018).

Biomarkers related to Idiopathic Pulmonary Fibrosis (IPF)		
immune dysfunction and inflammation:	fibrogenesis, fibroproliferation and extracellular matrix (ECM) remodeling:	alveolar epithelial cell damage and dysfunction
C-C chemokine ligand-18	MMPs and their inhibitors	Krebs von den Lungen
C-C chemokine 2	Osteopontin	Surfactant proteins
YKL-40	Periostin	
C-X-C motif chemokine 13	Insulin-like growth factors	The mucin MUC5B
S100A4,S100A8/9, S100A12	Fibulin-1	CA 15-3,CA 125,CA 19-9
Autoantibodies to heat shock protein 72	Heat shock protein 47	Defensins
Toll-like receptor 3	Circulating fibroblasts	Clara cell protein (CC16)
Soluble receptor for advanced glycosylated end products	Lysyl oxidase-like 2	
Endothelial damage markers: vascular endothelial growth factor, interleukin 8, endothelin 1	Extracellular matrix neoepitopes	Telomere shortening

TABLE 1.2: **Molecular biomarkers in IPF**
Data collected from (Stankovic, Stjepanovic, and Asanin 2021; Drakopanagiotakis et al. 2018).

Typically, at the initial stages of the IPF, patients are observed at regular intervals, ranging from three to six months, though the management and monitoring of patients with IPF lacks clear guidelines due to limited data and varying expert opinions (C. Ryerson and Ley 2020). Thus, monitoring strategies are tailored according to individual patient's needs. As the disease progresses, the monitoring approach adjusts, with a key focus on evaluating symptoms and assessing lung function throughout the IPF progression. In addition to regular monitoring, chest imaging and laboratory tests are also crucial for follow-up tracking and aiding in subsequent decision-making processes (Figure. 1.1). These comprehensive evaluations provide necessary insights for management more effectively. These aspects form the bedrock of IPF disease monitoring.

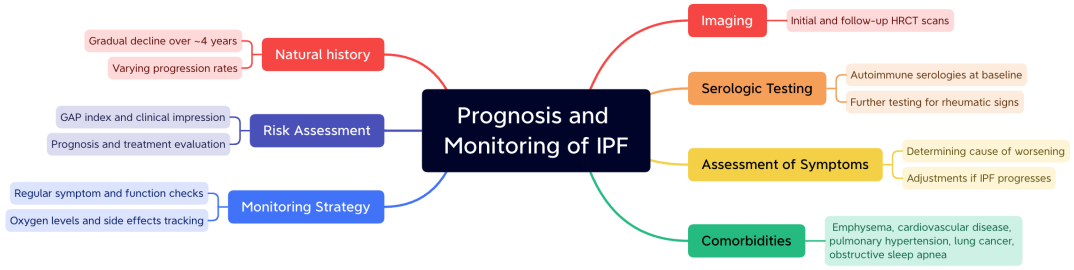

FIGURE 1.1: **Diagram of explanation for prognosis and monitoring of IPF**
This diagram emphasizes the classical prognostic factors influencing mortality, encompassing functional, clinical, and radiological parameters, while also highlighting recent advancements in understanding genetic factors and potential biomarkers that can aid in prognostic evaluations. Also the importance of continuous disease monitoring to enhance the prognosis of IPF patients, facilitating timely therapeutic interventions and potential early considerations for lung transplantation.

1.2.3 Risk factors

Although the underlying mechanisms that lead to the development of IPF are not yet fully comprehended, An increasing amount of evidence points towards both genetic and non-genetic factors playing a role in the onset of IPF. It is well-reported that genetic and non-genetic risk factors can impact the micro-injuries of the lung. Typically, a crucial factor in the development of IPF is the activation of immune cells. This activation is prompted by the discharge of pro-inflammatory cytokines, inducing increased production of interleukin and cytokines, notably transforming growth factor β1 (TGF- β) (Rockey, P. D. Bell, and J. A. Hill 2015). The ensuing chain of events encompasses the multiplication of fibroblasts, the enhancement of extracellular matrix formation, and the transformation of lung tissue from epithelial to mesenchymal (Thomas A Wynn and Ramalingam 2012). These pathological changes could potentially initiate fibrosis.

1.2.3.1 Genetic factors

Recent studies have reported multiple loci of interest through GWAS, identifying various single nucleotide polymorphisms (SNPs) that demonstrate significant association with IPF (Noth et al. 2013a; Fingerlin et al. 2013). However, despite these advancements, there remains a considerable gap in understanding the functional significance of most genetic associations. Importantly, discrete genetic variations have been linked to pathogenic mechanisms such as surfactant mutations, protein misfolding, endoplasmic reticulum stress, and telomere shortening associated with abnormalities in DNA repair(Table. 1.3).

Firstly, Evidence has delved into the role of telomeres and the genes that regulate the development of IPF. The genes *TERT* and *TERC*, which encode telomerase and its various components, are crucial for telomere synthesis. An issue arises when excessive shortening of telomeres occurs in mesenchymal cells and type 2 alveolocytes, leading to accelerated cell death and a higher risk of pulmonary fibrosis. Furthermore, mutations in genes that regulate telomerase function (*TERT*, *TERC*, *TINF2*, *DKC1*, *RTEL1*, *PARN*, *OBFC1*, and *NAF1*) (M. Y. Armanios et al. 2007; Kropski, Mitchell, et al. 2014; Stuart et al. 2015; Alder, Stanley, et al. 2015a; Noth et al. 2013b; Seibold et al. 2011), surfactant protein (SP) productions (*SFTPC*, *SFTPA2*,*ABCA3*,*SFTPA1*) (Campo et al. 2014; Takezaki et al. 2019; Yongyu Wang et al. 2009; A. Q. Thomas et al. 2002), host defences (*MUC5B*, *ATP11A*, *TOLLIP*, *TLR3*) (Seibold et al. 2011; O'Dwyer et al. 2013), and epithelial barriers (*DSP*, *DPP9*) (Table. 1.3) (El-Chemaly et al. 2010).

Next, we consider the effect of polymorphism in the *MUC5B* gene, which is responsible for mucociliary clearance (Seibold et al. 2011). This polymorphism increases the risk of developing sporadic and hereditary pulmonary fibrosis.

The role of wnt genes and the Sonic Hedgehog (*SHH*) gene family is also important. Wnt genes encode a family of 19 glycoproteins that interact with Frizzled receptors on cell membranes. This interaction triggers two signalling pathways: the β-catenin-mediated pathway leading to the upregulation of various genes and pathways, including those associated with pro-fibrotic activity and fibroblast proliferation, and a second pathway regulating cell differentiation and migration, key for tissue development and regeneration. *Wnt1*, *wnt7b*, *wnt10b*, and frizzled-2 and -3 receptors have all been associated with human IPF (B. T. MacDonald, Tamai, and X. He 2009; Chanda et al. 2019).

Lastly, the *SHH* gene family, which is pivotal for organ morphogenesis (including the lungs), is also a contributor to IPF. Increased signal transduction of *SHH* exacerbates pulmonary fibrosis by increasing fibroblast proliferation and resistance to cell death (Kugler et al. 2015).

Genetic variants of IPF pathogenesis		
Telomeres	*STN1*	Noth et al. (2013)
	PARN	Stuart et al. (2015)
	RTEL1	Cogan et al. (2015)
	DKC1	Kropski et al.(2014)
	TERC	Armanios et al. (2007)
	TERT	Armanios et al. (2007)
	OBFC1	Seibold et al. (2011)
	TINF2	Alder et al. (2015)
Mucin production	MUC5B	Seibold et al. (2011)
	MUC2	Fingerlin et al. (2013)
Surfactant	*ABCA3*	Campo et al. (2014)
	SFTPA1	Takezaki et al. (2019)
	SFTPA2	Wang et al. (2009)
	SFTPC	Thomas et al. (2002)
Cytokines and immune function	*FAM13A*	Seibold et al. (2011)
	HLA-DRB1	Xue et al. (2011)
	IL1RN	Korthagen et al. (2012)
	IL8	Ahn et al. (2011)
	IL4	Kishore et al. (2016)
	TGFB1	Xin et al. (2018)
Cell-cycle regulation	*CDKN1A*	Korthagen et al. (2012)
	KIF15	Allen et al. (2020)
	TP53	Korthagen et al. (2012a)
	MAD1L1	Allen et al. (2020)
Toll-like receptor signaling	*TLR3*	O'Dwyer et al. (2013)
	TOLLIP	Seibold et al. (2011)
	ATP11A	Seibold et al. (2011)
Cell adhesion and interaction	*DPP9*	Seibold et al. (2011)
	DSP	Seibold et al. (2011)
	MDGA2	Noth et al. (2013)
	MAPT	Seibold et al. (2011)
other Signalings	*DEPTOR*	Allen et al. (2020)
	AKAP13	Allen et al. (2017)
	SHH gene family	Kugler et al. (2015)
	Wnt gene family	Chanda et al. (2019)
	NOCH1, FBXO32	Wang et al. (2019) Yang et al. (2014)
DNA methylation	*H3K27*	Jiang et al. (2021)
	H3K9	Coward et al. (2018)
	MBD2	Wang et al. (2022)
	Thy-1 promoter region	Sanders et al. (2008)
	COX-2	Sun et al. (2021)
	14ARF	Cisneros et al. (2012)
	promoters of SFRP1 and SFRP4	Zhou et al. (2019)
	SMAD7, NOCH1, FBXO32	Yang et al. (2014)
DNA acetylation	*HDAC3*	Zheng et al. (2022)
	HDAC2, HDAC4	Li et al. (2017)
	HDAC8	Saito et al. (2019)
LncRNAs	*PFAR, MALAT1, H19, MEG3, TERRA*	Zhao et al. (2018) Yan et al. (2017) Zulkarneev et al. (2022)

TABLE 1.3: **Genetic variants of IPF pathogenesis**

1.2.3.2 Non-genetic factors

IPF is primarily influenced by non-genetic risk factors such as being older, male, a smoker, or living in unfavourable environments. The ageing process affects both type 1 alveolar cells and fibroblasts, potentially causing metabolic abnormalities in cellular proteins and damage to subcellular structures.

Ageing

The ageing process is complex and leads to a gradual decline in the body's ability to maintain homeostasis, increasing the susceptibility to diseases and mortality. IPF demonstrates a notable increase in incidence and prevalence with advancing age. While IPF is rare before the age of 50, its prevalence can reach as high as 300 cases per 100,000 individuals over the age of 60, highlighting a strong association between ageing and IPF. Many of the molecular and cellular hallmarks of ageing appear to be involved in the development and progression of IPF, including genomic instability, the erosion of telomeres, changes in epigenetic regulation, disruption of protein homeostasis, dysregulation of nutrient sensing, mitochondrial dysfunction, the accumulation of senescent cells, depletion of stem cells, and alterations in intercellular communication (Moisés Selman, Buendıa-Roldán, and Pardo 2016).

Normal ageing is associated with several changes in the respiratory system, including narrowing of intervertebral disk spaces and increased prevalence of hyperkyphosis (Lowery et al. 2013). Muscle function declines, leading to reduced strength in respiratory muscles. Ageing individuals may have difficulties meeting sudden increases in metabolic demand due to decreased mitochondrial ATP reserves, which can increase the risk of respiratory failure in acute lung diseases.

Lung elasticity decreases with age, particularly affecting small airways and alveolar septa. This can cause a premature collapse of peripheral airways during expiration, resulting in air-trapping (Fukuchi 2009). Alveolar ducts and alveoli may increase in size, but this is not emphysema as it lacks alveolar wall destruction. These changes contribute to an increase in residual volume over time. Studies have found pulmonary changes in older individuals without respiratory diseases, including fibrosis-like reticular opacities, airway dilation, bronchial thickening, and bronchiectasis. Mucociliary escalator dysfunction, reduced mucus clearance, and decreased cough strength are also observed in older individuals.

Physiologically, ageing is associated with a decline in forced expiratory volume in one second (FEV1) and forced vital capacity (FVC) by approximately 30 ml per year. The premature collapse of small airways and alterations in the pulmonary circulation leads to a heterogeneous distribution of ventilation/perfusion ratio. The diffusing lung capacity for carbon monoxide (DLCO) decreases, contributing to an age-related decline in arterial oxygen tension (PaO2). Approximately 20% of familial cases of IPF

can be attributed to mutations in telomerase components, which result in very short telomeres (Stanley and M. Armanios 2015). Additionally, a significant portion (20-30%) of sporadic IPF patients without telomerase mutations exhibit telomere lengths below the 10th percentile compared to control subjects (Cronkhite et al. 2008). It has been proposed that telomerase mutations in familial IPF or an exaggerated proliferative response in sporadic IPF lead to telomere shortening in alveolar epithelial type 2 (ATII), and this plays a critical role in the development of IPF. Recent studies using a mouse model lacking telomerase and exhibiting telomere dysfunction specifically in ATII cells have supported that the impairment of stem cell function in ATII cells due to telomere dysfunction resulted in senescence and limited alveolar repair. Furthermore, inducing telomere dysfunction in purified adult ATII cells led to cellular senescence, indicating the involvement of ATII cells-dependent telomere dysfunction and senescence in restricting alveolar repair and potentially contributing to mesenchymal abnormalities (Alder, Barkauskas, et al. 2015).

Cellular senescence

Cellular senescence, a state of permanent growth arrest accompanied by the release of inflammatory and tissue-remodelling factors, has been recognized as a critical event in biological ageing (Byun et al. 2015). In the lungs of IPF patients, alveolar epithelial cells (AECs) exhibit senescence characteristics, including increased staining of senescence markers such as β-galactosidase and p21/waf-1 (Minagawa et al. 2011). Telomere shortening is believed to contribute to the senescent phenotype observed in AECs. Fibroblasts within fibroblastic foci, another hallmark of IPF, also demonstrate features of senescence, with increased expression of p16, p21, and NADPH oxidase-4 (Nox4) (Hecker et al. 2014). The senescent fibroblasts in IPF display an accelerated entry to replicative senescence and exhibit myofibroblast-like properties characterized by high expression of alpha-smooth muscle actin (α-SMA) (Yanai et al. 2015).

In addition to cellular senescence, IPF patients may experience "systems senescence" involving immune senescence or endocrine senescence. Immune senescence is evident in IPF patients, as demonstrated by the downregulation of CD28 on circulating CD4 T-cells, a key co-stimulatory molecule responsible for optimal T-cell activation (Gilani et al. 2010). Endocrine system deterioration is also observed, with IPF patients showing disproportionate decreases in the circulating levels of dehydroepiandrosterone sulfate (DHEA-S), an adrenal steroid with potential antifibrotic effects on fibroblasts (Mendoza-Milla et al. 2013).

Mitochondrial dysfunction

Mitochondria play a vital role in cellular function and ageing. As individuals age, there is an expansion of dysfunctional mitochondria characterized by changes in dynamics and impaired quality control processes. This results in an imbalance between fission and fusion events and increased production of reactive oxygen species

(ROS) (López-Lluch et al. 2015). The accumulation of damaged mitochondrial DNA (mtDNA) and decreased mitophagy, the removal of dysfunctional mitochondria, contribute to cellular senescence and ageing (López-Otın et al. 2013). There is excessive ROS production and disruption of the oxidant/antioxidant balance in IPF (Lenz, Costabel, and Maier 1996). IPF patients exhibit elevated levels of oxidative stress markers and decreased levels of the antioxidant molecule glutathione (Psathakis et al. 2006). Studies have shown that ATII cells in IPF lungs have mitochondrial dysfunction, altered structure, and impaired mitophagy. The deficiency of the PINK1 enzyme is identified as a key factor in the accumulation of dysfunctional mitochondria in IPF. Animal models of ageing and *PINK1* deficiency mimic the mitochondrial abnormalities observed in IPF and demonstrate increased susceptibility to lung fibrosis (Bueno et al. 2015). Similar mitochondrial dysfunction and impaired mitophagy are also observed in other ageing-related diseases, suggesting a common phenomenon in age-associated conditions.

Loss of proteostasis

There is evidence of disrupted proteostasis in IPF. Autophagy, a complex process involving multiple proteins, has been studied about IPF (Avignat S Patel, Morse, and A. M. Choi 2013). Studies have shown that levels of LC3-II, a marker of autophagy, are lower in IPF lung tissue compared to control lungs (A. Patel et al. 2012). Inhibition of autophagy has been associated with fibroblast to myofibroblast differentiation and activation, as well as epithelial cell senescence and myofibroblast differentiation in lung fibroblasts. Abnormalities in the PTEN/Akt/mTOR axis have been found to suppress autophagic activity in IPF fibroblasts, resulting in a fibroblast phenotype resistant to apoptosis (Nho and Hergert 2014). Autophagy also plays a role in protecting epithelial cells against stress and apoptosis induced by bleomycin (Cabrera et al. 2015). Age-related decline in autophagy and selective targeting of mitochondria for autophagic degradation have been implicated in lung fibrosis. This reduction in autophagy may be exaggerated or accelerated in IPF (Sosulski et al. 2015). Oxidative stress, endoplasmic reticulum (ER) stress, and hypoxia, which are involved in the pathogenesis of IPF, can induce autophagy, but dysfunctional autophagy likely contributes to the disease. The ubiquitin-proteasome system, responsible for protein degradation, is relevant for preserving protein homeostasis in the lung. Inhibition of this system has shown antifibrotic effects in experimental models of lung damage (Balch et al. 2014). However, the regulation of proteasome function in IPF has not been extensively studied. Activation of the proteasome has been observed in TGF-β-induced myofibroblast differentiation, and elevated levels of ubiquitinated proteins have been found in IPF lungs, suggesting an involvement of the ubiquitin-proteasome system in fibrotic remodelling-specific to IPF (Mutlu et al. 2012; Semren et al. 2015).

Stem cell exhaustion

The balance between self-renewal and differentiation of stem cells is crucial for tissue homeostasis and the ability to repair and replace damaged tissues. The decreased function of adult stem cells has been implicated in the development of age-related diseases (Boyette and Tuan 2014). Although no studies have specifically focused on IPF, emerging evidence suggests that age-related changes in stem cell function could contribute to the disease. It is a study suggests that mesenchymal stem cells derived from the bone marrow (B-MSC) of old animals exhibited downregulation of chemokine receptors involved in migration, impairing their ability to migrate to sites of injury (Bustos et al. 2014). Furthermore, these aged stem cells produced insufficient amounts of anti-inflammatory agents compared to their younger counterparts. Similar differences were observed in mesenchymal stem cells obtained from young and aged human individuals, indicating a decline in activation and migration capabilities in aged cells. These findings highlight the importance of stem cell dysfunction in ageing and its potential relevance to age-related diseases. Further research is needed to elucidate the specific role of stem cells in the development and progression of IPF.

Deregulated nutrient-sensing

Insulin-like growth factor (IGF-1) and insulin signalling pathways regulate ageing and are involved in lung fibrosis. Studies show that abnormal activation of the mammalian target of rapamycin (mTOR) complexes, controlled by these pathways, contributes to lung fibrosis. Activation of mTOR in alveolar epithelial cells exacerbates fibrosis, while inhibition with rapamycin rescues lung injury. In IPF, overactivation of mTOR is observed in fibroblast foci and AECs. Targeting mTOR signalling could offer potential therapeutic strategies for managing fibrotic lung diseases (J. S. Park et al. 2014; W. Chang et al. 2014; Y.-S. Gui et al. 2015). However, current studies on this topic have been conducted with small cohorts and have produced diverse outcomes due to the limited genetic and epigenetic integrated data. The significance of ageing in the context of IPF will be detailed in the section related to autophagy.

Smoking

There is growing evidence suggesting various mechanisms that can partially explain the impact of smoking on the progression of IPF (Lederer and Martinez 2018). One theory involves the interaction between smoking and genetic risk factors related to telomerase activity. Telomerase RNA component (*TERC*) encodes important components of telomerase, such as human telomerase reverse transcriptase (*hTERT*) and human telomerase RNA (Rohde et al. 2000). It has been observed that the combination of genetic risk factors related to telomerase and smoking can lead to a shorter survival time in IPF patients. Nevertheless, Smoking is known to induce oxidative stress, which can accelerate the process of telomere shortening and contribute to cellular ageing (Białas et al. 2016). This, in turn, can lead to cell death and senescence of epithelial cells, thereby contributing to the progression of IPF

(M. S. Walters et al. 2014). Another explanation lies in the pulmonary epithelial barrier (Brune et al. 2015). Normally, the epithelium acts as a barrier, preventing growth factors or cytokines from interacting with their corresponding receptors. For instance, the epidermal growth factor receptor (EGFR) is located on the basolateral membrane of epithelial cells, while the epidermal growth factor (EGF) ligand is situated apically. This spatial arrangement prevents their interaction (Shaykhiev et al. 2013). However, smoking disrupts this homeostasis by increasing paracellular permeability, facilitating ligand-receptor interactions that can initiate disease progression.

Occupational exposures

Occupational exposures, such as those in farming, agriculture, construction, and industry, have been associated with pulmonary epithelial cell damage, particularly from particulate exposures like stone, silica, wood, and livestock (Hubbard 2001; Miyake et al. 2005). Of these, bird raising and exposure to vegetable/animal dust were most strongly associated with IPF, even after adjusting for age and smoking history (Baumgartner et al. 2000). Recent research from southern Italy highlighted a significant correlation between certain occupations and an elevated risk of developing Usual Interstitial Pneumonia (UIP). Specifically, farmers, veterinarians, gardeners, and workers in the metallurgical and steel industries exhibited higher odds of UIP, with the risk intensifying alongside longer exposure durations (Paolocci et al. 2018). Analysis of US mortality data, encompassing 84,010 IPF-related deaths, identified three occupational groups with increased IPF mortality risk, associated with exposure to wood and metal dusts: construction of wood buildings and mobile homes, metal mining, and production of fabricated structural metal products. Moreover, a national survey in Korea among 1,311 IPF patients revealed that those with occupational dust exposure had an earlier onset of IPF, longer symptom duration at diagnosis, and higher mortality compared to those without such exposure (S. H. Lee et al. 2015). This suggests a pathobiological link between occupational dust exposure and IPF and indicates a correlation with poorer clinical outcomes (Trethewey and G. I. Walters 2018).

Viral and bacterial infections

Viral infections, specifically human herpesviruses (HHVs), have also been linked to IPF. Patients with IPF have shown higher infection rates of Epstein-Barr virus (EBV), with the EBV marker latent membrane protein 1 (LMP1) highly expressed in their lung epithelium via the ERK-Mitogen-activated protein kinase (MAPK) (Jim J Egan et al. 1995). These viral infections may contribute to the endoplasmic reticulum (ER) stress and enhance epithelial-mesenchymal transition and cell migration through various pathways (Lasithiotaki et al. 2011).

Bacterial infections have also been associated with the worsening of IPF (Phillip L Molyneaux et al. 2014). IPF patients often exhibit high bacterial loads,

particularly from pathogenic types like Streptococcus spp (Knippenberg et al. 2015). and Staphylococcus spp. Some antimicrobial interventions have shown potential benefits in treating lung fibrosis, indicating a possible role for these microbes in the pathogenesis of IPF (E. C. Wilson et al. 2014). However, the exact causal mechanisms between these microbial infections and the development of IPF require further investigation. These factors contribute to pulmonary epithelial cell damage, EMT, and potential immune responses that play a role in the progression of the disease.

Immune cells

Consequently, the affected cells release signalling molecules that activate immune cells like polymorphic nuclear leukocytes, lymphocytes, monocytes, and macrophages. If we delve deeper into the Immune mechanisms of fibrosis development, we will see During inflammation, the release of interleukins, cytokines and other substances that activate both innate and acquired immunity occurs. The corresponding immune cells also synthesize interleukins and cytokines that stimulate the differentiation and proliferation of fibroblasts, ECM synthesis, and EMT of alveolocytes. An important role is played by classically or activated macrophages, since they can increase inflammation not only due to released cytokines, but also due to metalloproteinases, iNOS, ROS, and other enzymes that damage normal lung tissue (Hirahara et al. 2019; Henderson, Rieder, and Thomas A Wynn 2020). Other immune factors contribute to the development of IPF. Fibroblast growth factors (FGF-2, FGF-10, FGF-9, and FGF-18) have been implicated in IPF development (Hirahara et al. 2019). Eosinophils play a role in both allergy-related pulmonary fibrosis and IPF by synthesizing transforming growth factor beta 1 (TGF-β1) and interleukin-13 (IL-13). Lymphocytes, particularly a subpopulation of CD4+ Th17 cells, have a significant impact on fibrotic processes. Th17 cells secrete IL-17A, which promotes TGF-β synthesis and causes persistent neutrophilia. Th2 cells produce IL-13, which activates TGF-β synthesis and fibroblast proliferation. IL-4 and IL-5 also have profibrotic effects. Conversely, interferon-gamma (IFN-γ) produced by Th1 cells inhibits TGF-β and fibroblast proliferation.

TGF-β

TGF-β (transforming growth factor beta) is a polypeptide that is expressed in various organs and tissues during development. It plays a crucial role in regulating cell proliferation, differentiation, and apoptosis. The signalling of TGF-β involves the activation of SMAD 2/3 proteins, which transmit the signal to the nucleus. There are three isoforms of TGF-β, with TGF-β1 being the most active isoform in the pathogenesis of IPF (Chanda et al. 2019). In the context of IPF, the overexpression of TGF-β1 in type 2 alveolar cells leads to hyperplasia. In fibroblasts, TGF-β1 overexpression influences cell proliferation and increases the synthesis of the extracellular matrix, contributing to fibrotic processes. It is noteworthy that the levels of TGF-β1 sharply increase with age, suggesting its potential involvement in

age-related lung fibrosis. Furthermore, in vitro studies have demonstrated the induction of epithelial-mesenchymal transformation (EMT) in mouse type 1 alveolar cells when co-cultivated with M2 alveolar macrophages. This finding highlights the role of TGF-β1 in promoting EMT, a process implicated in the development and progression of IPF (Liangying Zhu et al. 2017). Further details regarding the process of EMT related to TGF-β in fibrosis will be described in the relevant chapter.

Epigenetic reprogramming in IPF

In the context of IPF, fibroblasts undergo significant epigenetic alterations that contribute to disease progression. One study focused on the transcriptomic and epigenetic profiling of fibroblasts from IPF patients, revealing that differential chromatin access might drive genetic differences in these fibroblasts compared to healthy ones. This research identified multiple motifs enriched in IPF fibroblasts, including those for *TWIST1* and *FOXA1*, and found 93 genes that could be annotated to differentially accessible regions (Hanmandlu et al. 2022). These findings suggest that modulation of chromatin access may be a crucial mechanism in the pathogenesis of lung fibrosis. Moreover, the significant role of DNA methylation changes in IPF. Researchers identified thousands of differentially methylated regions linked to gene expression in IPF, indicating a strong connection between DNA methylation and IPF pathology (I. V. Yang et al. 2014). This aberrant methylation correlates with altered gene expression profiles critical for fibroblast activation and collagen production. However, the complexity of cell-specific methylation patterns in lung tissue makes it challenging to pinpoint the exact cellular origins of these changes (Negreros et al. 2019). Furthermore, many studys reported significant histone modification changes in IPF fibroblasts, particularly in histone deacetylases (HDACs), impacting gene transcription associated with fibrotic process (Korfei, Mahavadi, and Guenther 2022).

1.2.4 Comorbidities and complications

The management of comorbidities in IPF is crucial due to their significant impact on life expectancy and quality of life. Here's a summary of the major comorbidities and complications associated with IPF:

1. Pulmonary Hypertension (PH): PH often complicates the clinical course of IPF and affects prognosis. It may be aggravated by other comorbidities, such as obstructive sleep apnea (OSA), pulmonary thromboembolic disease, emphysema, or cardiac abnormalities (Raghu, Amatto, et al. 2015).

2. Emphysema: Combined pulmonary fibrosis and emphysema (CPFE) are present in about 30% of IPF patients. This condition has distinct clinical, functional, radiological, and pathological characteristics and may be considered a phenotype of IPF (L. Zhang et al. 2016).

3. Obstructive Sleep Apnea (OSA): OSA is prevalent in IPF patients and can often go undiagnosed. It has been associated with more rapid clinical deterioration and worse prognosis (L. H. Lancaster et al. 2009).

4. Gastroesophageal Reflux (GER): GER and microaspiration have been proposed as risk factors for the development and progression of IPF. Both acid and non-acid reflux have been suggested as potential factors for worsening IPF progression (Raghu, Morrow, et al. 2016).

5. Cardiovascular comorbidities: Cardiovascular diseases in IPF patients are associated with shorter survival. Coronary artery disease has an estimated prevalence of 3–68% in IPF patients, sharing several risk factors such as male gender, increasing age, and smoking history (Kärkkäinen et al. 2018).

6. Lung Cancer: IPF is an independent risk factor for lung cancer in addition to smoking. Therapeutic interventions could provoke exacerbations of IPF (Sato et al. 2015).

7. Venous Thrombosis and Pulmonary Embolism: Reduced mobility with venous stasis and a probable involvement and activation of the coagulation cascade is involved in the pathogenesis of IPF, increasing the risk of venous thrombosis and, consequently, pulmonary embolism (PE) (Imokawa et al. 1997).

8. Diabetes Mellitus: Diabetes Mellitus (DM) could increase the risk for IPF, although no references regarding the impact on survival were made (Enomoto et al. 2003).

9. Hypothyroidism: A higher prevalence of hypothyroidism in patients with IPF has been reported. The link between hypothyroidism and IPF is not well established yet, but it is hypothesized that both may share a baseline autoimmune disorder (Oldham et al. 2015).

10.Anxiety and depression: Anxiety and depression are comorbidities commonly found in patients with interstitial lung diseases including IPF (I. N. Glaspole et al. 2017).

Acute exacerbation (AE) is a key complication of IPF that is associated with significant mortality risk (Harold R Collard, C. J. Ryerson, et al. 2016). AE-IPF typically presents as sudden and severe respiratory deterioration characterized by new bilateral ground-glass opacity and/or consolidation not attributed to heart failure or fluid overload. Risk factors include decreased forced vital capacity, rapid decline in FVC over six months, elevated alveolar-to-arterial oxygen pressure difference, pulmonary hypertension, gastroesophageal reflux, and exposure to air pollution (A. Suzuki and Kondoh 2017). Current treatment strategies for AE-IPF are mainly supportive, with corticosteroids often administered despite limited evidence for their efficacy. Some researchers advocate for a steroid avoidance strategy, while others propose the use of

azithromycin or procalcitonin-guided antibiotic therapy (Papiris et al. 2015). Lung transplantation is a potential option for suitable patients, and early referral to a transplantation centre is recommended (Kondoh, Cottin, and K. K. Brown 2017). Pharmacological treatments such as nintedanib and pirfenidone have shown promise in reducing AE-IPF risk and incidence, respectively (Harold R Collard, Luca Richeldi, et al. 2017). Another potential treatment under investigation is recombinant human soluble thrombomodulin, which possesses anti-inflammatory, anticoagulant, and antifibrinolytic properties (Matsumura et al. 2018). Other experimental therapies include hemoperfusion with polymyxin B-immobilized fibre column and autoantibody-targeting treatments (plasma exchange, rituximab, intravenous immunoglobulin). Some evidence suggests that statins and anti-acid treatments may help reduce AE-IPF incidence, but further research is needed to substantiate these claims (Michael Kreuter, Ulrich Costabel, et al. 2018).

1.2.5 Treatment

The treatment approach for idiopathic pulmonary fibrosis aims to slow down disease progression, relieve symptoms, and improve quality of life. Currently, there is no cure for IPF, but there are several treatment options available, including FDA-approved Antifibrotic Medications or some other non-pharmacotherputical treatments (M. E. Cho and Kopp 2010; Wollin et al. 2015). In severe cases, where lung function significantly deteriorates, lung transplantation may be considered as a treatment option. However, not all patients are suitable candidates for transplantation, and the availability of donor organs is limited. Managing symptoms and complications associated with IPF is essential, such as Oxygen Therapy, pulmonary Rehabilitation, medications to control cough and acid reflux, vaccinations to prevent respiratory infections, and supplemental nutrition support. It is also crucial for patients with IPF to work closely with a multidisciplinary healthcare team, including pulmonologists, respiratory therapists, and support groups, to develop an individualized treatment plan and receive ongoing monitoring and support (Thong, McElduff, and Henry 2023).

1.2.5.1 Pharmacotherapy

Over the past decade, the introduction of two anti-fibrotic drugs has marked a significant advancement in the treatment of IPF. Pirfenidone and nintedanib are approved medications used in multiple countries for managing IPF. Although these therapeutics provide substantial improvement in symptoms and survival rates for IPF patients, it's important to note that they can only slow down the progression of the disease and do not offer a cure (see table. 1.4).

Pharmacotherapy for IPF		
Anti-Fibrotic drugs	Pirfenidone	TGF-β inhibitor
	Nintedanib	Tyrosine Kinase Inhibitor
Novel Treatment	Pamrevlumab	Recombinant human antibody
	PRM 151	Recombinant human PTX2 protein
	GLPG 1690	autotaxin inhibitor
	BI 1015550	PDE type 4B compound
	PBI 4050	G-Protein Receptor analogue
	PLN 74809	Integrins αvβ6 and αvβ1 inhibitor
	BMS 986020	Lysophosphatidic acid receptor-1 inhibitor
	TD 139	Inhaled galectin 3 inhibitor
	TRK 250	siRNA-Based Oligonucleotide
	Dasatinib (D) + Quercetin (Q)	Tyrosine Kinase inhibitor/flavonoid
	PA 101	Inhaled Sodium Cromoglycate
Adjunctive Treatment	N-Acetylcysteine (NAC)	glutathione (GSH) enhancer
	Corticosteroids	steroid hormones
	Antacids	gastroesophageal reflux disease inhibitor
	Azithromycin	antibiotic with immunomodulatory effects
	Co-Trimoxazole	sulfonamide antibiotic for lung microbiome
	Phosphodiesterase 5 Inhibitor	treatment for arterial hypertension
	ganciclovir	Anti-Viral Therapy

TABLE 1.4: **Diagram of explanation for pharmaceutical treatment of Idiopathic Pulmonary Fibrosis**

Pirfenidone

Pirfenidone (known as Esbriet) with an anti-fibrotic effect is achieved by inhibiting the expression and activity of TGF-β (M. E. Cho and Kopp 2010), which reduces fibroblast differentiation, collagen synthesis, and extracellular matrix deposition (Iyer,

Gurujeyalakshmi, and Giri 1999; Ruwanpura, B. J. Thomas, and Bardin 2020). Pirfenidone also blocks the production of inflammatory cytokines and inhibits the formation of the NLRP3 inflammasome, resulting in an overall anti-inflammatory effect (Aimo et al. 2020; Yongliang Wang et al. 2013). When taken orally, pirfenidone is rapidly absorbed and primarily excreted through the kidneys (N.-Y. Huang et al. 2013). Dose adjustment is not required in mild renal or hepatic impairment but is contraindicated in severe impairment. Pirfenidone can cause photosensitivity due to its photoreactive properties, and precautions such as sunblock application and protective clothing are advised (Seto et al. 2013). Clinical trials have demonstrated the efficacy of pirfenidone in reducing disease progression in IPF. The CAPACITY and ASCEND trials showed significant improvements in forced vital capacity (FVC), 6-minute walk test, and progression-free survival in patients treated with pirfenidone compared to placebo. Common side effects include nausea and rash (P. W. Noble et al. 2011; Talmadge E King Jr, Bradford, et al. 2014).

Nintedanib

Nintedanib is a tyrosine kinase inhibitor used in the treatment of IPF. It works by deactivating tyrosine kinase receptors involved in fibroblast migration and proliferation, specifically platelet-derived growth factor receptor (PDGFR), fibroblast growth factor receptor (FGFR), and vascular endothelial growth factor receptor (VEGFR) (Wollin et al. 2015; Hostettler et al. 2014). When administered, nintedanib undergoes hydrolytic ester cleavage and is metabolized in the body. It is primarily excreted in the faeces. Nintedanib has a high plasma protein binding rate and achieves maximum plasma levels within 2 to 4 hours. It has a half-life of 10-15 hours. Drug interactions with cytochrome P450 enzymes are unlikely to affect its efficacy. Dose adjustment is recommended in mild hepatic impairment but not in moderate or severe impairment (Wind et al. 2019). The effectiveness of nintedanib has been demonstrated in large trials, such as INPULSIS 1 and 2. These trials compared the annual decline in forced vital capacity (FVC) between the nintedanib group and the placebo group over one year. The nintedanib group showed a significantly lower decline in FVC compared to the placebo group. The trials also evaluated secondary endpoints such as time to first exacerbation and reduction in St. George's Respiratory Questionnaire (SGRQ) score. Nintedanib demonstrated positive outcomes in these secondary endpoints as well (Luca Richeldi, Du Bois, et al. 2014). The most common side effects of nintedanib reported in the trials were diarrhoea and nausea.

Combination of pirfenidone and nintedanib

Combining pirfenidone and nintedanib, two approved therapies for IPF has shown potential synergistic effects by targeting different pathways involved in the development of the disease. Pirfenidone inhibits TGF-β, while nintedanib inhibits PDGF, FGF, and VEGF, leading to a reduction in fibroblast migration and

myofibroblast accumulation (W. A. Wuyts, Antoniou, et al. 2014). Studies on the safety and tolerability of combination therapy have been promising. The INJOURNEY trial, which compared combination therapy with monotherapy, showed that the combination was well-tolerated with a manageable safety profile. There was no increase in adverse events or plasma levels of nintedanib in the combination therapy group. Additionally, a 50% reduction in the rate of decline in lung function was observed with combination therapy compared to nintedanib alone (Carlo Vancheri et al. 2018). However, it is important to note that the INJOURNEY trial was only 12 weeks in duration, limiting the ability to conclude long-term efficacy. Further trials with longer follow-up periods are needed to assess the effectiveness of combination therapy over an extended duration.

Novel treatment

Although pirfenidone and nintedanib effectively slow down disease progression in IPF, several compounds are currently being studied in clinical trials as potential alternatives, replacements, or combination therapies that could potentially halt or reverse fibrosis progression in IPF. These ongoing trials aim to explore new treatment options for this challenging disease (see table. 1.4). Numerous novel treatments are being investigated for IPF, aiming to overcome the limitations of current therapies. Compounds such as pamrevlumab (Sgalla et al. 2020), PRM-151 (N. Cox, Pilling, and Gomer 2014), GLPG 1690 (Toby M Maher, Aar, et al. 2018), BI 1015550 (S. Huang et al. 2007), PBI 4050 (L. Gagnon et al. 2018), PLN 74809 (Decaris et al. 2021), BMS 986020 (Palmer et al. 2018), TD 139 (Hirani et al. 2021), inhaled sodium cromoglycate (Birring et al. 2017), TRK 250 (ibid.), and the combination of dasatinib and quercetin (Justice et al. 2019) show promise in halting or potentially reversing fibrosis progression. These treatments target various mechanisms involved in fibrosis, such as connective tissue growth factor inhibition, pentraxin-2 modulation, autotaxin inhibition, phosphodiesterase type 4B inhibition, galectin-3 inhibition, integrin inhibition, lysophosphatidic acid receptor-1 modulation, and senescent cell targeting. Ongoing clinical trials are evaluating their efficacy and safety to provide new therapeutic options for IPF patients (Table. 1.5).

Supportive treatment

Several older drugs have been investigated for the treatment of IPF before the emergence of anti-fibrotic therapies. N-acetylcysteine (NAC) (Demedts et al. 2005), corticosteroids (Turner-Warwick, Burrows, and A. Johnson 1980), antacids (Khor et al. 2022), azithromycin (Berkhof et al. 2013), co-trimoxazole (Shulgina et al. 2013), anti-viral therapy (Blackwell et al. 2021), phosphodiesterase 5 inhibitors (PDE-5 inhibitors) (Galiè et al. 2005), and inhaled sodium cromoglycate are among the drugs studied. However, the results have been largely disappointing, with limited or no significant benefits observed in preserving lung function or improving clinical

Drug Name	Target	Mechanism of Action
Pamrevlumab	CTGF	Inhibits CTGF to prevent pro-fibrotic signalling
PRM 151	Pentraxin-2 (PTX2)	Modulates wound healing and fibrotic remodeling
GLPG 1690	Autotaxin	Inhibits autotaxin to reduce fibroblast accumulation
BI 1015550	Phosphodiesterase type 4B	Enhances cAMP levels to inhibit fibroblast functions
PBI 4050	GPR40 and GPR84	Regulates fibrosis via modulating macrophages and fibroblasts
PLN 74809	Integrins $\alpha v\beta 6$ and $\alpha v\beta 1$	Inhibits integrins to suppress TGF-β
BMS 986020	LPA1 receptor	Antagonizes LPA1 to regulate fibroblast recruitment
TD 139	Galectin-3	Inhibits Gal-3 to regulate fibrotic processes
Inhaled Sodium Cromoglycate	Mast cells	Stabilizes mast cells to reduce inflammation
TRK 250	TGF-β1 mRNA	Produces siRNA to inhibit TGF-β1 transcription
Dasatinib + Quercetin	Senescent cells	Induces apoptosis in senescent cells

TABLE 1.5: Summary of novel treatments for IPF, their targets, and mechanisms of action.

outcomes. These drugs have shown mixed efficacy, and their use in IPF treatment is not recommended or is mainly reserved for specific situations such as acute exacerbations or symptom management. Despite their potential as more accessible and economical options, further research is needed to determine their role in combination with anti-fibrotic therapies and their long-term effectiveness in IPF patients.

1.2.5.2 Non-Pharmacotherapies

In addition to pharmacological treatments, nonpharmacological interventions play a crucial role in the management of IPF to enhance patients' quality of life. These interventions focus on various aspects of care and support. Some key

nonpharmacological strategies include general measures, pulmonary rehabilitation, oxygen therapy, ventilation, or lung transplant (Table. 1.6).

Category	Description
General Measures	Nutritional counselling, Smoking cessation, Vaccination (annual influenza and anti-pneumococcal)
Oxygen Therapy	Exertional hypoxemia treatment, Ambulatory oxygen for final stage patients, Oxygen therapy for comorbidities (e.g., pulmonary hypertension, right heart failure)
Support Therapies	in Acute Life-Threatening Hospitalizations and high-concentration oxygen therapy, ICU admission for severe cases, High-flow nasal cannula (HFNC) oxygen therapy, Non-invasive ventilatory support (NIV), Invasive ventilatory support (restricted use), Extracorporeal membrane oxygenation (ECMO)
Lung Transplantation	Consideration at time of diagnosis, Evaluation for transplantation based on set criteria, Use of Lung Allocation Score (LAS)
Pulmonary Rehabilitation	Exercise training, Education, Behavior change
Palliative Care and Psychological Support	Symptom management, Emotional and psychological support, End-of-life decision planning, Patient support groups

TABLE 1.6: **Summary of non-pharmacological treatments for IPF**

Patients diagnosed with IPF often experience heightened breathlessness and an increased metabolic state, resulting in elevated resting oxygen consumption. This can lead to weight loss, decreased muscle mass, and reduced functional capacity. Nutritional guidance is imperative in effectively managing IPF patients, especially those being considered for lung transplantation. Stopping smoking is of utmost importance as it raises the risk of severe comorbidities, including lung cancer and emphysema. Quitting smoking is a fundamental aspect of IPF management. While specific studies on vaccination in IPF patients are limited, similar to other respiratory conditions, they are more vulnerable to respiratory infections. Therefore, annual flu and pneumococcal vaccinations are recommended for all individuals diagnosed with IPF (Millan-Billi et al. 2018).

Oxygen therapy

Exertional hypoxemia is commonly observed in IPF, and oxygen therapy may be prescribed to alleviate breathlessness, improve gas exchange, and potentially benefit comorbidities such as pulmonary hypertension and right heart failure. However, the existing evidence on the efficacy of oxygen therapy in interstitial lung disease, including IPF, is scarce and lacks clinical randomized trials. Retrospective studies have yielded contradictory results regarding the survival benefit of oxygen therapy in IPF (ibid.). Some studies have shown no improvement in survival rates among patients receiving oxygen therapy, while others consider it a critical component of IPF management (Douglas, Ryu, and D. R. Schroeder 2000). The confusion in the results

may be attributed to the fact that patients with more severe and progressive diseases are more likely to receive oxygen therapy. Ongoing studies aim to evaluate the effects of ambulatory oxygen during daily life on health status and breathlessness in fibrotic lung disease, which may provide more evidence on the use of oxygen in IPF patients (J. Egan 2011). Exertional dyspnea significantly impacts the quality of life in IPF, and hypoxia during the 6-minute walk test (6-MWT) has been identified as an independent prognostic factor for mortality and disease progression (Hallstrand et al. 2005). Studies have shown that appropriate titration of oxygen flow during the 6-MWT can improve exercise capacity in IPF patients (Lettieri et al. 2006; Hook et al. 2012). Furthermore, the use of long-term oxygen therapy in chronic obstructive pulmonary disease (COPD) patients has demonstrated improved health outcomes, although this evidence is not directly applicable to IPF (Hardinge et al. 2015). While the survival benefit of ambulatory oxygen in IPF remains uncertain, guidelines recommend considering oxygen therapy in patients with resting or nocturnal hypoxemia (SpO2 ¡ 88%) (Raghu, Harold R Collard, et al. 2011b). Additionally, performing a 6-MWT and titrating the oxygen flow rate based on exertional hypoxemia is recommended (GROUP* 1980). The indications and use of oxygen therapy in IPF are largely extrapolated from the experience in COPD, where long-term oxygen therapy has shown established benefits.

Support therapies in acute life-threatening hospitalizations

In cases of acute life-threatening hypoxemia during the process of IPF, various ventilatory support options may be considered. Oxygen therapy, including high-flow nasal cannula (HFNC) oxygen, is commonly used in IPF hospitalizations, especially during acute exacerbations, to address significant hypoxia resulting from ventilation/perfusion (V/Q) mismatch and severe diffusion impairment. HFNC oxygen therapy provides high flows and a high fraction of inspired oxygen (FiO2) delivery, reducing the rate and work of breathing, improving oxygenation, and enhancing secretion clearance. It is a promising treatment option that can be applied outside of intensive care units (ICUs) and may be used to avoid more invasive procedures in exacerbations while specific aetiology treatment is adjusted or while waiting for a lung transplant (Faverio et al. 2018). However, the specific role of HFNC in ILD is not well-defined, and more studies are needed to evaluate its benefits and guide appropriate indications. Invasive mechanical ventilation in IPF patients with acute respiratory failure admitted to the ICU has been associated with a very poor prognosis and high mortality rates. As a result, the general recommendation is to avoid invasive ventilator treatment except in certain circumstances, such as while waiting for lung transplantation. Non-invasive ventilation (NIV) has shown promise in improving dyspnea and may be an appropriate option in these cases (Vianello 2014). Studies have demonstrated improved survival rates in IPF patients treated with NIV compared to invasive ventilation. However, NIV responsiveness does not appear

to impact the overall prognosis of the disease. It is important to note that compliance with NIV can be challenging due to poor patient-ventilator adaptation caused by intense breathlessness and a high respiratory rate. In cases of acute worsening in IPF patients awaiting lung transplantation, extracorporeal membrane oxygenation (ECMO) or veno-venous ECMO may be considered (Rozencwajg and Schmidt 2016). ECMO has been used as a bridge to transplant in ILD patients (Trudzinski et al. 2016), including those with IPF, who experience severe respiratory failure. Awake-ECMO, which involves ECMO without intubation, has also been explored as a strategy to reduce ventilator-associated complications, allow early rehabilitation, and potentially prevent ventilator-induced lung injury. Studies have shown promising outcomes, with high survival rates in awake-ECMO patients who undergo lung transplantation.

Lung transplantation

While pharmacological treatments have shown promise in slowing disease progression, lung transplantation remains an important option for enhancing survival. The timing of referral and listing for transplant can be challenging, but guidelines have been developed to assist physicians in this decision-making process. The International Society for Heart and Lung Transplantation (ISHLT) released guidelines in 2015 that define the timing of referral for lung transplant candidates (Weill et al. 2015). This includes various criteria such as histopathologic or radiographic evidence of interstitial pneumonitis, abnormal lung function, dyspnea or functional limitation, oxygen requirement, and lack of improvement with medical therapy in inflammatory ILD. The guidelines also outline situations for listing patients for transplant, such as a significant decline in lung function, desaturation or decline in exercise capacity, presence of pulmonary hypertension, and hospitalization due to respiratory decline or acute exacerbation. Adequate nutritional status and social support are also important considerations. The Lung Allocation Score (LAS) is another initiative that helps improve the selection of candidates for lung transplant (Kistler et al. 2014). It calculates a score based on various measures of a patient's health and estimates their survival probability with or without transplantation. The LAS has increased the number of IPF patients receiving lung transplants and has made interstitial lung disease, particularly IPF, the second most common indication for lung transplant (D. C. Chambers et al. 2017). Regarding the type of procedure, both single and bilateral lung transplantations are performed in IPF patients, and there is ongoing debate about the optimal method (Force et al. 2011). While randomized trials comparing the two procedures are lacking, some retrospective studies suggest that survival may be improved with bilateral lung transplantation (Gulack et al. 2015). Lung transplantation has been shown to significantly reduce the risk of death for IPF patients compared to those remaining on the waiting list. However, waiting list mortality is higher for IPF patients compared to those with cystic fibrosis and emphysema. The overall median survival for adult lung recipients is 6 years, with IPF

transplanted patients having a median survival of 4.5 years. Post-transplant mortality at 3 months is higher for IPF patients compared to those with COPD, likely due to age and comorbidities (Adamali et al. 2012). Based on international guidelines and the evidence available, early referral for evaluation and consideration of lung transplant is recommended for IPF patients at the time of diagnosis. This allows for timely assessment and potential inclusion on the transplant list.

Pulmonary rehabilitation

Pulmonary rehabilitation (PR) is a comprehensive intervention aimed at improving the physical and psychological condition of individuals with chronic respiratory diseases. In IPF, exercise intolerance and reduced physical activity are common, by improving exercise tolerance and quality of life (Rochester et al. 2015). While the duration and components of PR programs for ILD and IPF patients vary, they typically involve muscle training and respiratory reeducation techniques. However, the exact duration and program details are not well-established due to limited research in this population. Emerging evidence suggests short-term benefits of PR in ILD patients, including IPF, with improvements in functional exercise tolerance, dyspnea, and quality of life. However, the magnitude of these benefits may be smaller compared to chronic obstructive pulmonary disease (COPD) (Dowman, CJ Hill, and A. Holland 2014). The efficacy of maintenance exercise programs following structured PR training in IPF is still unclear (Huppmann et al. 2013). Current international guidelines weakly recommend PR for IPF patients, as the long-term benefits are uncertain. Further large randomized controlled trials are needed to establish IPF-specific PR protocols, determine optimal duration and aftercare strategies, and assess long-term outcomes (Jackson et al. 2014).

Palliative care and physicological support

The management of IPF focuses not only on the control of physical symptoms but also on psychological care. As IPF significantly impacts patients' quality of life, this approach is also extended to their families and caregivers. Palliative care plays an essential role in this process. As defined by the World Health Organization, palliative care is an approach that improves the quality of life of patients and their families facing life-threatening diseases. It involves the prevention and alleviation of suffering through early identification, impeccable evaluation, and treatment of pain and other physical, psychological, and spiritual problems. This is particularly relevant to many IPF patients, given the progressive nature of the disease. To implement comprehensive and integrated care, a multidimensional assessment of needs, including symptoms, functional status, nutritional status, cognition, emotions, and social aspects, is performed (Gómez-Batiste et al. 2010). This assessment takes into account the prognosis of the disease and any comorbidities and is used to adapt treatment, identify patient preferences, and plan advance decisions. However, a

significant challenge is identifying which patients need palliative intervention and the timing for initiating such an intervention (Michael Kreuter, Bendstrup, et al. 2017). Psychological assessments, particularly for depression and anxiety linked to diagnosis and prognosis, are recommended as they are prevalent in IPF patients and have a significant impact on their quality of life. Though few studies have evaluated the role of palliative care in IPF, they have revealed gaps in symptom control, psychological care, and end-of-life planning. These studies also suggest the need for strategies for evaluating, treating, and monitoring the palliative needs of patients, aiming to improve quality of life and symptom control (M. Kalluri et al. 2018).

1.2.6 Mechanism of IPF: a continuous positive loop

IPF is indeed characterized by abnormal wound-healing responses in the lungs. The primary process is thought to be initiated by an injury to the alveolar epithelial cells, which comprise the lining of the lung alveoli. This injury can be triggered by a variety of factors including environmental exposures (e.g., cigarette smoke, dust), genetic predisposition, ageing, and potentially viral infections. Upon injury, AECs release a variety of pro-fibrotic mediators that contribute to the recruitment, proliferation, and activation of fibroblasts, which are cells responsible for wound healing and the production of the extracellular matrix (ECM) (A. Santos and Lagares 2018). These fibroblasts can transform into a more active form, known as myofibroblasts, under the influence of certain mediators such as Transforming Growth Factor-beta (TGF-β). Myofibroblasts play a crucial role in the progression of IPF (K. K. Kim, Sheppard, and H. A. Chapman 2018). They can evade apoptosis (programmed cell death), and they produce excess amounts of ECM proteins, including collagen, which leads to the thickening and stiffening of the lung tissue - a hallmark of fibrosis. This disrupts the normal architecture of the lung and impairs its function, leading to the clinical manifestations of the disease. Moreover, the ECM itself is a complex network of proteins and polysaccharides that not only provides structural support to tissues but also plays an active role in cell signalling. In IPF, the ECM is significantly altered and becomes a bioactive reservoir for a range of secreted mediators, exerting a pivotal role in various physiological activities such as apoptosis, proliferation, migration, invasion, and differentiation. Furthermore, it's suggested that there are self-sustaining positive feedback loops between the altered ECM and activated myofibroblasts in IPF (Parker et al. 2014). This means that ECM stiffening contributes to and is a result of fibrogenesis. In return, ECM stiffness enhances myofibroblast activation and collagen synthesis while inhibiting several anti-fibrotic molecules. Therefore, understanding the distinct roles and interactions of the epithelial cells and ECM during the progression of fibrosis is crucial for developing effective therapeutic interventions for this progressive and often fatal disease and signallings involved crosstalk between epithelial cells and mesenchymal is also important (Figure. 1.2).

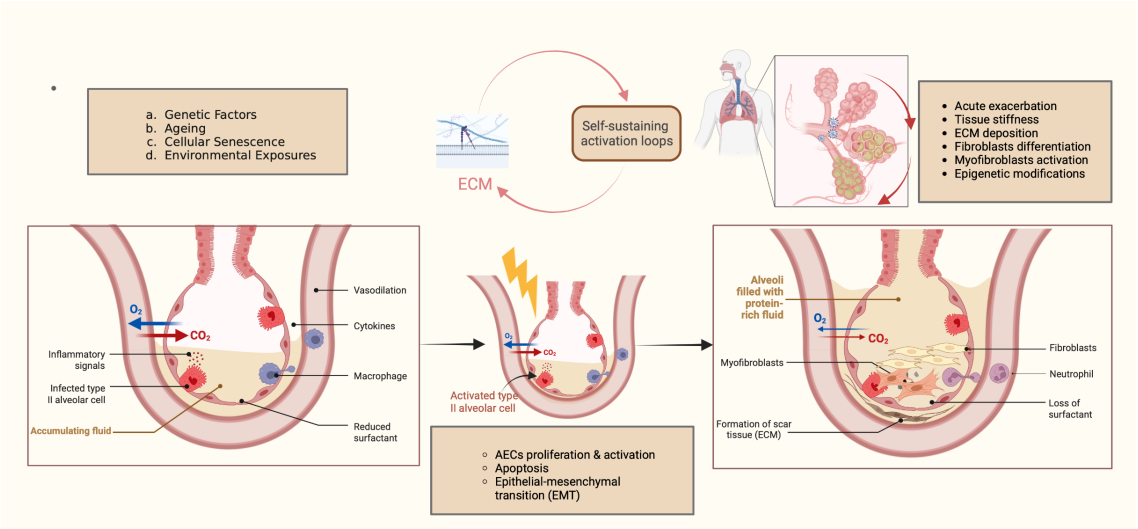

FIGURE 1.2: **Diagram summarising the mechanisms of lung fibrosis**
The injury of the alveolar epithelium is initiated by a range of risk factors, such as ageing, environmental exposures, genetic susceptibility, and epigenetic reprogramming. This leads to Epithelial-Mesenchymal Transition, apoptosis, proliferation, and activation of Alveolar Epithelial Cells. These aberrant AECs become the primary source of pro-fibrotic mediators, playing a critical role in the recruitment, proliferation, and differentiation of fibroblasts. The activation of myofibroblasts allows them to evade apoptosis and induce the deposition of Extracellular Matrix (ECM). The ECM acts as a bioactive reservoir for a variety of secreted mediators, playing a crucial role in physiological activities such as apoptosis, proliferation, migration, invasion, and differentiation. The self-sustained positive feedback loops between the altered ECM and activated myofibroblasts in IPF suggest that ECM stiffening is both a pathological cause and a consequence of fibrogenesis. This ECM stiffness, in turn, enhances myofibroblast activation and collagen synthesis, while inhibiting several anti-fibrotic molecules. Diagram adapted from (W. A. Wuyts, Agostini, et al. 2013).

1.2.6.1 Epithelial cells in IPF

The lung alveoli, which are the primary sites for gas exchange in the respiratory system, are indeed made up of a variety of different cell types and structures. They are lined by two types of epithelial cells known as type I and type II alveolar epithelial cells (ATI cells and ATII cells, also referred to as pneumocytes type I and II). Type I alveolar epithelial cells, or ATI cells, are thin, flat cells that cover the majority of the alveolar surface (about 90-95%) (Féréol et al. 2008). Due to their thinness and extensive surface area, they are ideally suited for the exchange of gases between the air in the alveoli and the blood in the surrounding capillaries. Oxygen from the inhaled air diffuses across the ATI cells and the adjacent capillary endothelium to enter the bloodstream, while carbon dioxide diffuses in the opposite direction to be exhaled. Type II alveolar epithelial cells, or ATII cells, are more cuboidal and cover a smaller portion of the alveolar surface (about 7%). Despite their smaller coverage, they play several crucial roles in lung function. ATII cells are responsible for the production

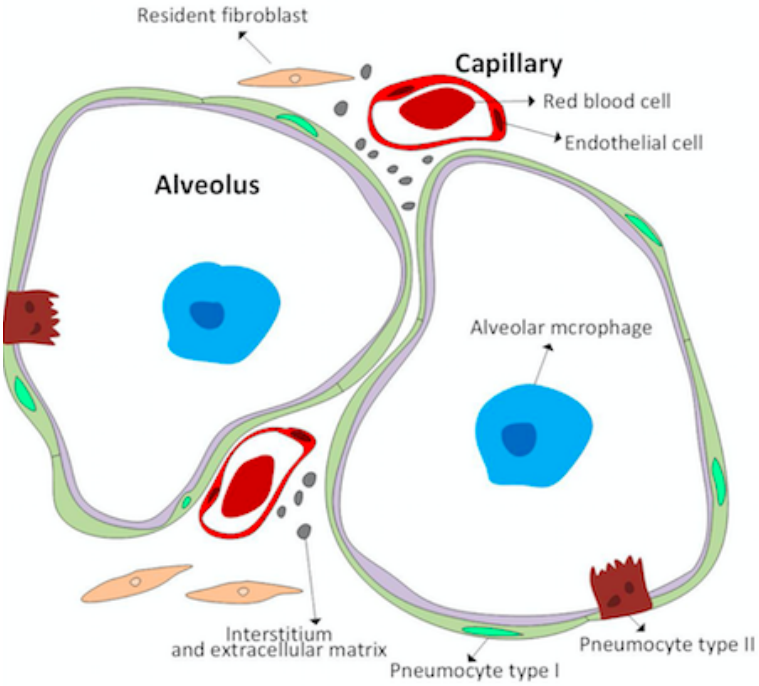

FIGURE 1.3: **Structural scheme of an alveolus structure in the lung**
Diagrams illustrate a lung alveoli unit, composed of an epithelial layer and an extracellular matrix, encapsulated by capillaries. Both type I (Pneumocyte) and type II alveolar cells are situated on the alveolar wall along with macrophages. The type I cells constitute the region for gas exchange, while the interstitium of the alveoli is enveloped by the resident fibroblast and the extracellular matrix.

and secretion of surfactant, a substance that reduces the surface tension within the alveoli and prevents them from collapsing during exhalation. They also serve as progenitor cells for the type I cells, meaning they can proliferate and differentiate into type I cells to repair the alveolar epithelium following injury. In addition to these epithelial cells, the alveoli also contain alveolar macrophages (Féréol et al. 2008). These immune cells are responsible for removing inhaled particles, pathogens, and cellular debris from the alveoli to keep them clean and functioning properly. Surrounding these cells is the extracellular matrix (ECM), which provides structural support and also plays an active role in cell signalling. The ECM in the alveoli is produced by resident fibroblasts. Finally, the alveolar-capillary barrier is formed by the ATI cells and the endothelial cells of the capillaries, with the basement membrane in between. This barrier is where the exchange of gases takes place, allowing oxygen to enter the bloodstream and carbon dioxide to be removed (Figure. 1.3).

The role of alveolar epithelium damage and malfunction in the onset of IPF is significantly recognized (Thomas A Wynn 2011a), yet the factors that dictate the transition from normal wound healing to detrimental extracellular matrix (ECM) remodelling remain unclear. In IPF, changes in alveolar epithelial cells have been documented (Pardo and Moisés Selman 2002; Plataki et al. 2005). For instance, both in

IPF patients and in bleomycin-induced fibrotic mouse models, the presence of apoptotic AECs has been significantly reported (C. G. Lee et al. 2004; Kuwano et al. 2001). Moreover, there is evidence that apoptosis in epithelial cells alone is sufficient to induce fibrosis (T. E. King, Pardo, and Moisés Selman 2011). The severity of fibrosis appears to be proportionate to the levels of apoptosis and can be reversed by using a caspase inhibitor. Interestingly, apoptotic AECs and α-SMA positive myofibroblasts are often found together near fibroblast foci, suggesting that aberrant AECs play a crucial role in lung fibrogenesis (Liang et al. 2016). In healthy lungs, Type II alveolar epithelial (ATII) cells serve as stem cells with the ability to renew Type I cells (T. J. Desai, Brownfield, and Krasnow 2014). However, in fibrotic mice, ATII cells show a diminished renewal ability, which could be partially linked to the toll-like receptor 4 (TLR4) or the Wnt/ β-catenin pathway (Königshoff, Kramer, et al. 2009; Qunn et al. 2002).

Alongside apoptosis, hyperplastic alveolar epithelial cells found near the honeycombing regions in IPF lungs also exhibit an increased capacity for proliferation, as indicated by proliferating cell nuclear antigen (PCNA) markers (J. Yang et al. 2013). These accumulating AECs actively produce almost all mediators involved in subsequent extracellular matrix (ECM) remodelling and disease progression (Zissel et al. 2000). Altered phenotypes in alveolar epithelial cells in IPF have been characterised (Pardo and Moisés Selman 2002; Moisés Selman and Pardo 2014). A significant finding of a single-cell RNA sequencing study published recently is the identification of a significant shift in epithelial cell phenotypes in the peripheral lung in PF, including several previously unrecognized epithelial cell phenotypes. Notably, they found a pathologic epithelial cell population (KRT5-/KRT17+) that produces an extracellular matrix (ECM) and is highly enriched in PF lungs. Trajectory analysis suggested that this phenotype evolved from a transitional stage of AT2 cells, and these transitional cells could originate from either the original form of AT2 cells or SCGB3A2+ basal cells (Arun C Habermann et al. 2020). There have also been reports suggesting that a small fraction of AECs may undergo a Transforming Growth Factor Beta (TGFβ)-mediated process of Epithelial-Mesenchymal Transition, characterized by the expression of various mesenchymal-associated genes and enhanced collagen synthesis. However, lineage-tracing studies using transgenic mice have produced inconclusive results, indicating that the proportion of these fibroblast-like Type II alveolar cells (ATII) is almost negligible (Humphreys et al. 2010; LeBleu et al. 2013).

Numerous risk factors such as infection, environmental and occupational exposures, smoking, and genetic mutations can cause micro-injuries to alveolar epithelial cells, leading to the start of fibrogenesis (section 1.2.3). However, recent evidence has called this theory into question. While it's widely accepted that abnormal regeneration in IPF lungs commences with continuous exogenous micro-injuries to the alveolar epithelial cells, some researchers propose that changes in the integrity of these cells, even in the

absence of injuries, might offer an alternative initiation point for IPF (Naikawadi et al. 2016) (Kropski, Pritchett, et al. 2015). It's been suggested that telomere shortening in type II alveolar cells (ATII) triggers fibrogenesis. For instance, in a mouse model, the absence of telomere repeat binding factor 1 (TRF1) in ATII cells spontaneously started age-associated remodelling and fibrotic responses. As a type of shelterin, TRF1 allows damaged telomeres to be recognized (Alder, Stanley, et al. 2015b). It's hypothesized that abnormalities in telomerase may lead to impaired stem cell function in ATII cells, thus inducing fibrosis. Consistently, the persistent accumulation of premature senescence in ATII cells has been implicated in IPF lungs (Moisés Selman, López-Otın, and Pardo 2016; Minagawa et al. 2011). Interestingly, senescence detected in myofibroblasts has been shown to inhibit fibrogenesis in many organs such as the liver, heart, and kidney (Muñoz-Espın and Serrano 2014). In pulmonary fibrosis, senescence mainly occurs in the alveolar epithelial cells and is reported to be harmful. However, there is contradicting evidence suggesting that failure of alveolar renewal associated with reduced telomerase integrity only predisposes patients to pulmonary fibrosis following endogenous injuries (Martinez et al. 2017b). This suggests that the loss of telomere integrity is a risk factor, rather than a direct cause, for IPF.

When injuries occur, alveolar epithelial cells that have been abnormally activated produce several pro-fibrotic regulators, leading to the formation of highly contractile myofibroblasts. As a result, these abnormal alveolar epithelial cells contribute to the deposition of the extracellular matrix (ECM) and the progression of the disease. These pro-fibrotic mediators primarily include growth factors, matrix metalloproteinases (MMPs), chemokines, coagulation factors, and developmental pathways (Moisés Selman and Pardo 2014; Moisés Selman and Pardo 2020)(Table. 1.7, 1.8, 1.9, Information collected from (Moisés Selman and Pardo 2014; Moisés Selman and Pardo 2020)). Among these, growth factors, such as TGFβ, TNF-α, osteopontin, angiotensinogen, PDGF, CTGF, endothelin-1, and IGF-1, are the most commonly secreted by the alveolar epithelial cells (Nasreen Khalil et al. 1996; HN Antoniades et al. 1990; PF Piguet et al. 1993; S.-T. Uh et al. 1998; Dina Saleh et al. 1997). Studies have indicated that these mediators play a crucial role in the pathogenesis of IPF by inducing epithelial to mesenchymal transition (EMT), controlling fibroblast migration and proliferation, promoting myofibroblast differentiation, and increasing ECM production. MMP family members, on the other hand, exert their pro-fibrotic effects mainly on the alveolar epithelial cells, encouraging migration and proliferation (Herrera et al. 2013; Fukuda et al. 1998). Additionally, during the progression of the disease, alveolar epithelial cells may release several chemokines, including CCL2, CCL17, and CXCL12 (Scotton et al. 2009; Yogo et al. 2009; Andersson-Sjöland et al. 2008). Also, some of the released regulators are related to coagulation, such as the TF/FVIIa/FX complex, protease-activated receptors 1 and 2, and PAI-1 (Kotani et al. 1995; Wygrecka et al. 2011). It's also worth noting that the activation of certain developmental pathways (e.g., Wnt and Sonic Hedgehog) can regulate fibrogenesis in

an alternative manner, primarily through their interaction with TGFβ (Alfredo Lozano Bolaños et al. 2012).

Mediator	**Biopathological effect**
Growth factors	
Transforming growth factor-beta (TGF-β)	The strongest profibrotic factor. Induces fibroblast to myofibroblast differentiation, epithelial to mesenchymal transition, and extracellular matrix production.
Platelet-derived growth factor (PDGF)	Through the activation of PDGFR exerts mitogenic, motogenic, and chemoattractant effects, on fibroblasts.
Connective-tissue growth factor (CTGF)	CTGF/CCN2 a members of the CCN family of matricellular proteins. It may promote the progression of fibrosis directly or function as a downstream factor of transforming growth factor β.
Tumor necrosis factor-alpha (TNF-α)	Induces loss of fibroblast Thy-1 surface expression which is associated with myofibroblast differentiation.
Osteopontin	Induces migration and proliferation of fibroblasts and epithelial cells. It shows a bidirectional profibrotic relationship with MMP-7.
Insulin-like growth factor-I (IGF-I)	IGF-1 stimulate the proliferation and differentiation of lung fibroblasts into myofibroblasts, increase collagen synthesis, and protect myofibroblasts from apoptosis.
Insulin-Like Growth Factor Binding Proteins 3 and 5	Induce migration of lung fibroblasts and extracellular matrix production.
Angiotensinogen	Enhances fibroblast migration and proliferation, and ECM synthesis. It induces epithelial cell apoptosis.
	to be continued

TABLE 1.7: **Pro-fibrotic mediators in epithelial cells of IPF (1)**

Mediator	Biopathological effect
Matrix metalloproteinases (MMP)	
MMP-1	Induces alveolar epithelial cell migration and proliferation protects from apoptosis and represses mitochondrial oxygen consumption. Induces fibroblast migration.
MMP-7	Cleaves E-cadherin and may induce epithelial cell migration. Cleaves osteopontin, potentiating its effect.
MMP-2	Basement membrane degradation.
Chemokines	
CCL17/Thymus and activation-regulated chemokine (TARC)	Associated with a Th2 (profibrotic) profile.
CCL2/monocyte chemotactic protein-1	Involved in the profibrotic effects of thrombin. It stimulates collagen synthesis and up-regulation of TGFβ.
CXCL12	Acts as a potent chemotactic factor for fibrocytes through the CXCL12/CXCR4 axis
Coagulation factors	
TF/FVIIa/FX ternary complex	FXa is a potent inducer of the myofibroblast differentiation.
Plasminogen activator inhibitor-1	Promotes the proliferation and activation of lung fibroblasts. Inhibits fibroblast apoptosis.
Protease-activated receptor-1 and -2	Activation of PAR1 may lead to increased local CCL2 release. The PAR-2/TF/FVIIa axis may contribute to the coagulation cascade. PAR-1 mediates thrombin's effects on fibroblast function.
to be continued	

TABLE 1.8: **Pro-fibrotic mediators in epithelial cells of IPF (2)**

Mediator	**Biopathological effect**
Developmental pathways	
Wnt-pathway components	It induce epithelial cell proliferation and differentiation, epithelial-to-mesenchymal transition, fibroblast migration, and myofibroblast differentiation.
Sonic Hedgehog	It increases proliferation, migration, extracellular matrix production, and survival of fibroblasts. Smoothened, the obligatory signal transducer of the pathway is required for TGF-β1-induced fibroblast to myofibroblast differentiation.
Others mediators	
Pigment epithelium-derived factor	It has angiostatic and neurotrophic activities. Colocalizes with TGF-β1, prominently within the epithelium overlying the fibroblastic focus.
Autotaxin	A secreted phosphodiesterase that produces lysophosphatidic acid which promotes fibroblast migration and resistance to apoptosis.
Sphingosine-1-phosphate	A pleiotropic bioactive lipid mediator. Stimulates extracellular matrix synthesis and increases the expression of profibrotic mediators such as CTGF.
Neuregulin NRG1α	Regulates mucus cell differentiation and has a paracrine effect influencing bronchiolization and *MUC5B* expression.
Growth and differentiation factor 15 (GDF15)	Epithelial stress signal, senescence.
Transmembrane protease serine 4 (TMPRSS4)	Promote migration and facilitate epithelial to mesenchymal transition.

TABLE 1.9: **Pro-fibrotic mediators in epithelial cells of IPF (3)**

To summarise, the initiation and progression of IPF is largely attributed to epithelial cells, which when affected, result in severe scarring and organ dysfunction, leading to premature death. The factors influencing lung epithelium are multifactorial and not yet completely understood. However, it is generally agreed that three factors are critical:

1. Genetic predisposition that impacts the integrity and regenerative capacity of epithelial cells.

2. Accelerated lung ageing in adulthood, characterized by abnormal shortening of telomeres, mitochondrial dysfunction, and other age-related cellular and molecular alterations.

3. Epigenetic reprogramming, likely stochastic, closely related to ageing and certain environmental exposures like smoking.

A wide variety of mediators derived from the epithelium work in both synergy and opposition, enhancing the recruitment and activation of fibroblasts, leading to abnormal ECM deposition and ultimately, respiratory failure. The convergence of these factors can result in abnormal activation of alveolar and airway epithelial cells and disrupted communication between these cells and their surrounding environment. It is noted that IPF lungs exhibit a variety of abnormal epithelial cells with a significant reduction in normal alveolar epithelial cells. These atypical cells produce factors that trigger fibroblast activation and transdifferentiation into myofibroblasts, leading to excessive extracellular matrix secretion. This results in progressive disorganization and stiffness, destroying the lung architecture.

1.2.6.2 Extracellular Matrix (ECM) of IPF

Composition of extracellular matrix

The extracellular matrix (ECM) of the lungs, including the epithelial and endothelial cell basement membranes and the interstitial matrix of tissue stroma, is crucial for the architecture, stability, and function of the lungs (Burgstaller et al. 2017). It comprises a variety of molecules, with collagens, elastin, glycoproteins, and proteoglycans as the main components (Schiller et al. 2015). Maintaining the balance between matrix synthesis and degradation is crucial for normal lung development, homeostasis, and physiological repair. However, disruptions in this balance can lead to tissue destruction or fibrosis. Changes in the ECM components of IPF are observed. There is an increase in fibrillar collagens, proteoglycans like versican and decorin, and glycoproteins, particularly fibronectin (T. Kulkarni et al. 2016). The increased synthesis of neoepitopes for collagen types III and VI distinguish individuals with

progressive disease, suggesting an imbalance of synthesis and degradation of different collagens may play a role in IPF progression (Organ et al. 2019).

Several ECM components such as elastin, fibronectin, and periostin play critical roles in fibrogenesis. Elastin, highly expressed in fibrotic lung areas, may influence myofibroblast differentiation (Rozin et al. 2005). Fibronectin is essential for fibrogenesis, with mice lacking extradomain A (EDA) of fibronectin showing less lung fibrosis post-bleomycin treatment (Muro et al. 2008). Periostin promotes ECM deposition, mesenchymal cell proliferation, and wound closure, contributing to lung fibrosis, and is essential for the proliferation of IPF fibroblasts (Naik et al. 2012). Deficiency in periostin protects mice from bleomycin-induced lung fibrosis (M. Uchida et al. 2012; Ashley et al. 2017).

Other matrisome components like fibulin 1 (G. Liu et al. 2019), osteopontin (Pardo, K. Gibson, et al. 2005), and tenascin-C are increased in IPF lung and can induce cellular activation and fibrosis (Estany et al. 2014; Booth et al. 2012). The composition of the basement membrane also changes during pathological lung remodelling. In IPF, alveolar basement membrane components like laminins, agrin, and collagen IV are lost. The loss of basement membrane integrity is a critical factor in determining the progression of pathological lung remodelling and fibrosis (Strieter 2008). Restoration of the basement membrane, as seen with increased amounts of laminin $\alpha 3$, laminin $\beta 2$, and laminin $\gamma 2$ during the resolution phase in the bleomycin model, is key to the resolution of fibrosis (Schiller et al. 2015).

Extracellular matrix on lung environment

The extracellular matrix (ECM) of the lung, an array of collagens, elastin, glycoproteins, and proteoglycans, provides essential biochemical and biomechanical cues for cell differentiation, tissue remodelling, and homeostasis (Frantz, Stewart, and Weaver 2010). Pathological alterations in the lung ECM, such as stiffening, induce differentiation of lung fibroblasts into a highly synthetic and contractile phenotype, and drive fibrotic ECM deposition, thereby forming a profibrotic positive feedback loop in fibrotic ECM during IPF progression (Xiangwei Huang et al. 2012; Marinković et al. 2012; Yong Zhou et al. 2013; F. Liu et al. 2010; Booth et al. 2012).

Beyond fibroblasts, the ECM also affects alveolar epithelial cells, with increased matrix stiffness inducing epithelial mesenchymal transition (EMT), a process that has been proposed to contribute to fibrosis through the generation of myofibroblasts (Dunsmore and Rannels 1996; R. Kalluri, Weinberg, et al. 2009; Calle et al. 2015; K. K. Kim, Kugler, et al. 2006). Furthermore, other cells such as pericytes and pulmonary mesothelial cells are suggested to undergo a phenotypic transition into myofibroblasts when exposed to a fibrotic ECM (Hung et al. 2013; Rock et al. 2011; Sava et al. 2017; Habiel and Hogaboam 2017).

The force-induced activation of transforming growth factor-beta (TGF-β), a mediator of fibrogenic responses, is one potential mechanism through which increased matrix stiffness affects cell phenotype. TGF-β can be activated through integrin binding and mechanical stretch in fibrotic lung tissue, and stiff matrices can promote fibroblasts to liberate active TGF-β from the matrix (Giacomini et al. 2012; Froese et al. 2016; Mih et al. 2012). These findings highlight the significant role of ECM in lung fibrosis and the complex interplay between cells and their microenvironment in disease progression.

1.2.6.3 Myofibroblasts in IPF

In 1971, myofibroblasts were first identified by Gabbiani et al. as large, fibroblast-like cells present in granulation tissue. These cells were notable for having filamentous fibres composed of actin, myosin, and α-smooth muscle actin (α-SMA) spanning their cytoplasm. This distinct structure imbued myofibroblasts with the ability to exert contractile force, which is roughly twice that of fibroblasts when cultured on substrates with high elastomer stiffness (GRGB Gabbiani, Ryan, and Majno 1971; Majno et al. 1971; Omar Skalli et al. 1986; Darby, Skalli, and Gabbiani 1990; Wrobel et al. 2002; Hinz, Celetta, et al. 2001). Morphologically, myofibroblasts are larger and irregularly shaped compared to fibroblasts, and they have strong cell–matrix interactions and intracellular gap junctions (Pakshir and Hinz 2018).

Myofibroblasts are also known for their increased production of extracellular matrix (ECM) components such as type I and type III fibrillar collagens, hyaluronan (HA), fibronectin (FN), and extra domain A fibronectin (EDA–FN) (Klingberg, Hinz, and E. S. White 2013). They are key drivers of progressive organ fibrosis and have been implicated in tumour development and metastasis (Gabbiani 1981; Lieubeau et al. 1994; De Wever et al. 2008). Furthermore, recent studies suggest that myofibroblasts have additional roles beyond wound contraction and scar formation, including macrophage-like phagocytosis, immunomodulation, and autophagy (M. Nakaya et al. 2017; Gargus et al. 2015; M. Bernard et al. 2014).

Myofibroblasts can originate from various cell types depending on the tissue type, including resident fibroblasts, pericytes, circulating bone-marrow-derived fibrocytes, tissue-derived mesenchymal stem cells, local epithelial and endothelial cells, de-differentiated smooth muscle cells, other hepatic stellate cells, mesangial cells, Schwann cells, and even monocytes and macrophages (Vierhout et al. 2021; Schuster et al. 2021; Pakshir, Noskovicova, et al. 2020; Hinz, Phan, et al. 2007). The process of myofibroblast development from resident fibroblasts is the most well-documented. Resting fibroblasts, present within most organs and connective tissues, produce ECM and matrix proteases needed for homeostatic turnover. Upon activation, fibroblasts become highly migratory, and proliferative, and increase the production of ECM,

enzymes, and cytokines, leading to a state known as the proto-myofibroblast (G. Laurent et al. 2007; T. J. Shaw and Rognoni 2020; T. J. Shaw and P. Martin 2016). These proto-myofibroblasts exhibit a rearrangement of the actin cytoskeleton from largely membrane-associated monomeric G-actin to polymerized cytoplasmic F-actin stress filaments (Hinz, Celetta, et al. 2001; Tomasek et al. 2002). The absence of α-SMA within these stress fibers distinguishes proto-myofibroblasts from myofibroblasts (Tomasek et al. 2002). As proto-myofibroblasts mature into myofibroblasts, α-SMA-positive stress fibers appear (Hinz 2006) (Figure. 1.4).

In a healthy lung, after epithelial dysfunction, a series of vital processes occur, including recruitment, migration, and proliferation of fibroblasts (Kuhn and McDonald 1991). This culminates in the activation of specific contractile cells, namely myofibroblasts, which are typically characterized by increased expression of α-smooth muscle actin (α-SMA). This leads to wound resolution. However, in the case of IPF, repeated stimuli lead to damages in the lung epithelium, causing malfunctions in tissue repair (Kendall and Feghali-Bostwick 2014). An essential characteristic of the myofibroblasts in this context is their anti-apoptotic properties. These activated myofibroblasts play a critical role as they continuously produce substantial amounts of extracellular matrix (ECM) components in regions known as fibroblast foci. This results in the thickening of interstitial tissues and eventually leads to permanent scarring (ibid.).

The origins of these myofibroblasts remain a topic of discussion and controversy. Recent evidence has pointed to three primary sources, although it is difficult to estimate the extent to which each contributes to the development of IPF. In mouse models, nearly 30% of myofibroblasts are thought to originate from the bone marrow, while epithelial-mesenchymal transition accounts for approximately 20% (Tanjore, X. C. Xu, et al. 2009). However, the contribution of EMT may be overestimated, as lineage tracing results from transgenic mice have indicated that fibroblast-like ATII cells contribute very little (Humphreys et al. 2010; Grande et al. 2015). Nonetheless, these mouse models suggest that over 50% of activated myofibroblasts originate from resident local fibroblasts.

1.3 Signallings in IPF

Shared fibrotic signalling responses, including Transforming Growth Factor-beta (TGF-β), Platelet-Derived Growth Factor (PDGF), WNT, and Hedgehog signalling, are key drivers of disease progression in the later stages of fibrotic diseases (Distler et al. 2019).

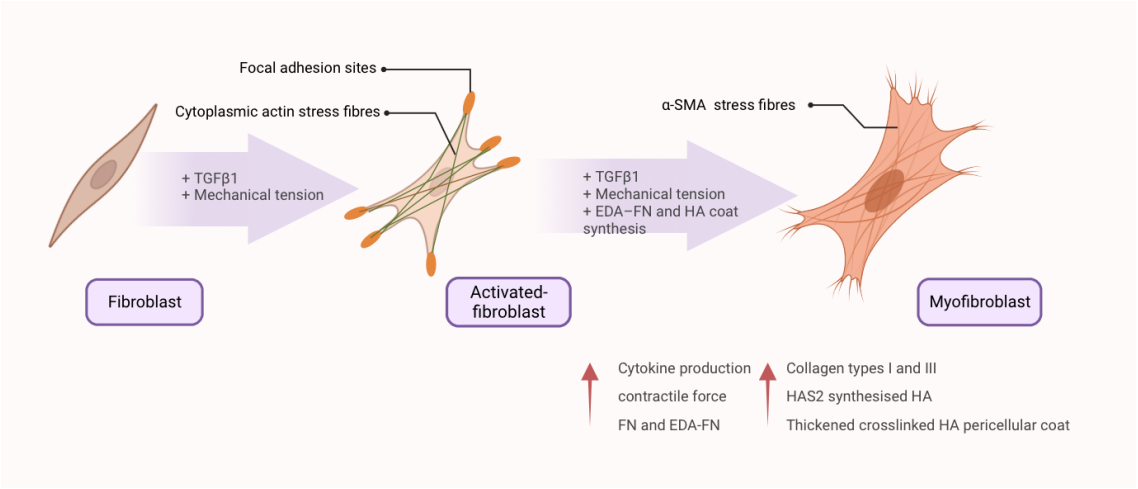

FIGURE 1.4: **Myofibroblasts activation**
The transformation from fibroblast to myofibroblast involves a few crucial steps: (1) initiation of the TGF-β1/Smad signalling pathway; (2) signal transmission from cell to ECM due to mechanical forces; and (3) production of modulators, like EDA–FN and HAS2-produced HA, that encourage and sustain the myofibroblast characteristics. The stage that lies in-between, known as the proto-myofibroblast, is characterized by an increase in cell proliferation and migration, as well as a shift from cortical, membrane-associated actin to cytoplasmic filamentous actin stress fibres that create focal adhesion points at the interface between the membrane and the ECM. The fully developed myofibroblast displays thick and crosslinked HA pericellular coats, and is filled with α-SMA+ cytoplasmic actin stress fibres, which establish mature focal adhesion plaques at membrane–ECM junctions, providing enhanced contractile strength. (TGFβ1: Transforming Growth Factor Beta 1; αSMA: α-smooth muscle actin; FN: fibronectin; EDA-FN: extra domain A fibronectin; HA: hyaluronan.) Information integrated from (Tai et al. 2021).

1.3.1 TGF-β signalling in IPF

Transforming Growth Factor-Beta (TGF-β) is a multi-functional cytokine with diverse physiological roles (Moustakas and Heldin 2009). It is part of a larger superfamily of proteins, which also includes bone morphogenic proteins, activins, and inhibins. There are three isoforms of TGF-β in mammals: TGF-β1, TGF-β2, and TGF-β3. Despite sharing the same high-affinity cell surface receptors (TGF-β type I and type II receptors), each isoform performs different biological functions (Annes, Munger, and Rifkin 2003). For instance, TGF-β1 null mice experience severe inflammation and die within a few weeks of birth (Shull et al. 1992; A. B. Kulkarni et al. 1993). In contrast, TGF-β2 null mice die perinatally due to cyanotic heart disease and pulmonary insufficiency (Sanford et al. 1997)]. TGF-β3 null mice, on the other hand, exhibit craniofacial defects, most notably cleft palate (Proetzel et al. 1995). These phenotypes suggest that TGF-β signalling is crucial for tissue growth and morphogenesis during embryonic development and for maintaining tissue homeostasis after birth.

In the context of pulmonary fibrosis, TGF-β has a pro-fibrotic role, regulating several key processes including the recruitment, proliferation, and differentiation of fibroblasts into myofibroblasts, and stimulating the production of extracellular matrix (Sheppard 2006a). This is evidenced by experiments where the administration of TGF-β to the lungs of rodents induced pulmonary myofibroblast accumulation and fibrosis (Kenyon et al. 2003; Sime et al. 1997). Conversely, inhibiting TGF-β with neutralizing antibodies or a type I receptor inhibitor suppressed experimental pulmonary fibrosis (Kenyon et al. 2003; Bonniaud et al. 2005).

The activation of TGF-β is a critical step in its biological function. All three TGF-β isoforms are present in tissues as inactive latent precursors, known as small latent complexes (SLCs), which often associate with latent TGF-β binding proteins (LTBPs) to form large latent complexes (LLCs). These complexes are stored in the extracellular matrix through the covalent binding of LTBPs to extracellular matrix proteins like fibrillin and fibronectin (Vallance et al. 2005; Kenyon et al. 2003). For TGF-β to exert its effects, it must be activated from these latent complexes. This can occur through either non-proteolytic or proteolytic mechanisms that induce conformational changes or cleave the latency-associated peptide (LAP), respectively (Annes, Munger, and Rifkin 2003; Stephen L Nishimura 2009; Hayashi and T. Sakai 2012).

Epithelial cells can induce these activating conformational changes in latent TGF-β complexes through their integrins. Integrins are cell adhesion molecules and transmembrane receptors that connect the cytoskeleton to the extracellular matrix. They are composed of α and β subunits that heterodimerize to form various $\alpha\beta$ combinations (Coward, Saini, and Jenkins 2010). Eight of these, including all five αv-containing integrins ($\alpha v\beta 1$, $\alpha v\beta 3$, $\alpha v\beta 5$, $\alpha v\beta 6$, and $\alpha v\beta 8$), can bind ligands with an arginine-glycine-aspartate (RGD) motif. The latency-associated peptides (LAPs) of TGF-$\beta 1$ and TGF-$\beta 3$ have RGD sequences, and these two TGF-β isoforms can be activated in vitro by at least four of the αv-containing integrins ($\alpha v\beta 3$, $\alpha v\beta 5$, $\alpha v\beta 6$, $\alpha v\beta 8$) (ibid.).

A critical integrin for the activation of latent TGF-β is $\alpha v\beta 6$. Genetic deletion or antibody blockade of $\alpha v\beta 6$ suppresses TGF-β signalling in the lung after injury and protects mice from the development of pulmonary fibrosis induced by bleomycin or radiation (Munger et al. 1999; Horan et al. 2008). The expression of $\alpha v\beta 6$ is increased in the lungs of mice after bleomycin challenge and in human lungs with usual interstitial pneumonia (UIP) pattern pulmonary fibrosis (Horan et al. 2008; Aluwihare and Munger 2008). This increase may itself be driven by active TGF-β, suggesting a feed-forward loop of increased TGF-β activation and $\alpha v\beta 6$ expression (A. Wang et al. 1996; Bates et al. 2005; Jun Araya, Cambier, et al. 2007).

Upon activation, TGF-β interacts with its receptors on fibroblasts, leading to a range of pro-fibrotic behaviours. This interaction involves both canonical and non-canonical

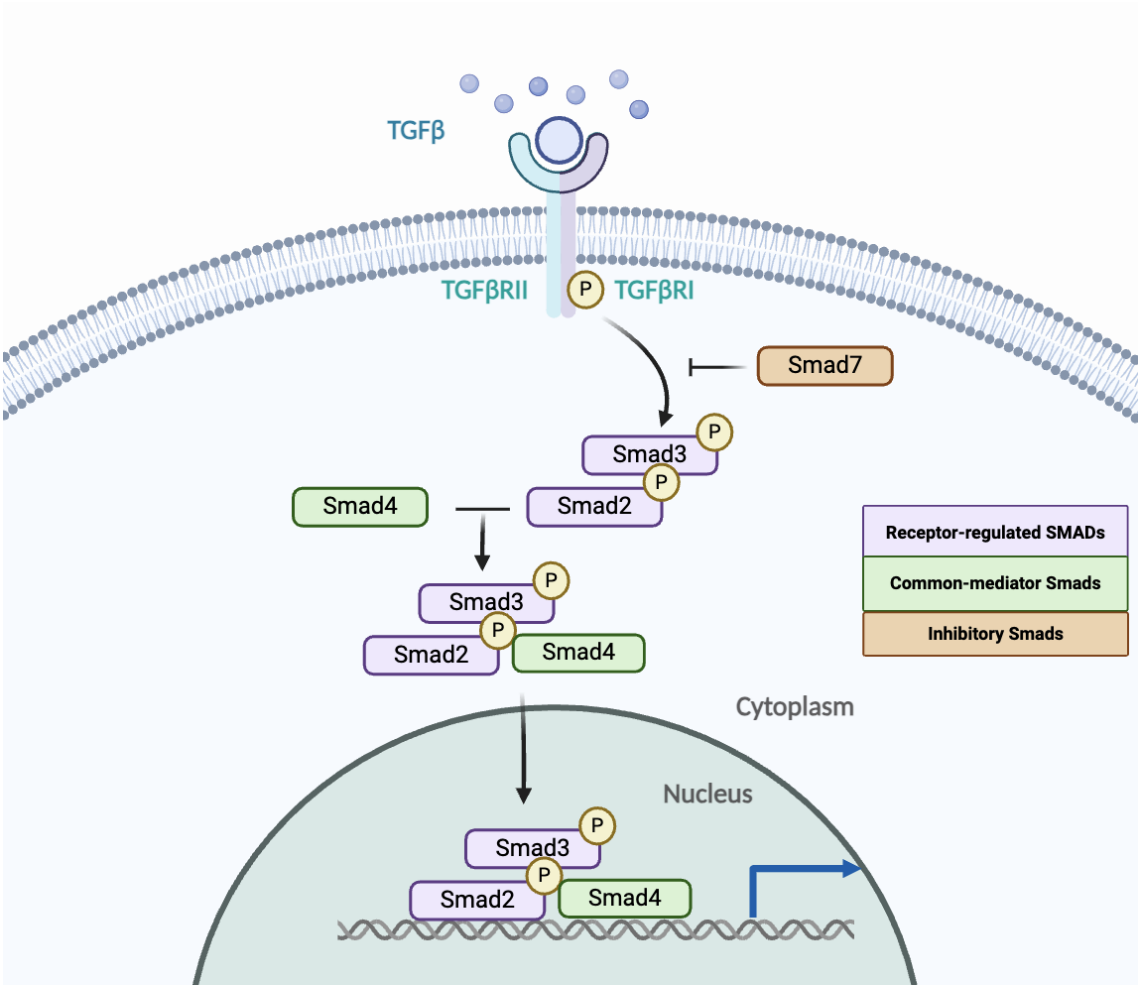

FIGURE 1.5: **TGF-β signalling pathway.**
The TGF-β signalling pathway initiates when TGF-β binds to its receptors (TGF-β Receptors I and II) on the cell surface, leading to receptor activation and autophosphorylation. This activation triggers the phosphorylation of Smad2 and Smad3 proteins in the cytoplasm. These phosphorylated proteins then associate with Smad4 to form a complex that translocates to the nucleus. Within the nucleus, this Smad complex collaborates with other transcription factors to regulate the expression of genes involved in cell proliferation, differentiation, and extracellular matrix production. Additionally, the pathway includes inhibitory mechanisms via Smad proteins such as Smad6 and Smad7, which modulate the intensity and duration of TGF-β signalling to prevent over-activation.

signalling pathways. In the canonical pathway, activated TGF-β receptor type I (TBRI) phosphorylates effector Smad proteins (Smad2 and Smad3), which heterodimerize with Smad4 to form Smad2/4 or Smad3/4 complexes (Figure. 1.5). These complexes translocate to the nucleus, where they bind to Smad response elements in the promoter regions of pro-fibrotic genes, such as type I collagen, fibronectin, and αSMA (Castelino and Varga 2010). This canonical signalling is integral to fibrosis, in Smad3-deficient mice.

1.4 Epithelial-mesenchymal transition (EMT)

Alveolar epithelial cells in IPF show a high degree of plasticity, transforming into various mesenchymal cells, such as fibroblasts and smooth muscle cells, in response to certain signals or injuries. This transformation process, known as epithelial-to-mesenchymal transition (EMT), results in the loss of typical epithelial characteristics like cell polarity and cell-cell adhesion, and the acquisition of mesenchymal traits like increased motility and invasiveness (Charlotte Hill and Yihua Wang 2020; Yihua Wang, Bu, et al. 2014; Yihua Wang, Hua Xiong, et al. 2019)

EMT can be triggered by multiple factors, including infections, endoplasmic reticulum (ER) stress, and the signalling molecule TGFβ (Pozharskaya et al. 2009; Tanjore, D.-S. Cheng, et al. 2011). Particularly, TGFβ is a potent driver of EMT, with SNAI1 being a key mediator (Goldmann et al. 2018; Kasai et al. 2005; K.-J. Chen et al. 2016; T. Wang et al. 2017; Willis and Borok 2007). Overexpression of SNAI has been identified in AECs from lungs of patients with IPF, and blocking SNAI expression can counteract TGFβ-induced EMT (Jayachandran et al. 2009).

Several studies have proposed that myofibroblasts in IPF lungs could originate from epithelial cells undergoing EMT. Supporting this, AECs from IPF patients have been found to express several mesenchymal markers, such as α-SMA and N-cadherin (K. K. Kim, Kugler, et al. 2006; Willis, Liebler, et al. 2005). Concurrently, epithelial-specific proteins like keratin 18 have been found in IPF myofibroblasts (Larsson et al. 2008). Moreover, colocalization of epithelial and mesenchymal markers has been observed in IPF lungs (Willis, Liebler, et al. 2005; J. S. Park et al. 2014; Lomas et al. 2012; Harada et al. 2010).

However, the exact contribution of EMT to the population of myofibroblasts in IPF is still debated. Some studies strongly support the theory that EMT-originated cells contribute significantly to the myofibroblast population (Tanjore, X. C. Xu, et al. 2009; K. K. Kim, Kugler, et al. 2006; Degryse et al. 2011), while others argue that this contribution may be negligible (Rock et al. 2011; Humphreys et al. 2010; LeBleu et al. 2013; Grande et al. 2015). It is suggested that rather than directly forming the myofibroblast population, EMT may mainly affect the microenvironment,

contributing to fibrosis in this indirect manner (Charlotte Hill, Mark G Jones, et al. 2019). Understanding the mechanisms of EMT in lung fibrosis could therefore be instrumental in the development of novel IPF interventions.

1.5 Epithelial-mesenchymal crosstalk

IPF progression is considered a complex process involving the deterioration of the lung, characterized by aberrant communication between epithelial cells and myofibroblasts, leading to the formation of fibrotic tissue. While the pathogenesis of IPF is known to require abnormal crosstalk between these cell types, the precise mechanisms and evidence supporting these interactions remain largely elusive and require further elucidation. Moreover, the factors underlying why scarring prevails over regular tissue repair in IPF progression remain undefined.

Once myofibroblast foci are established, the interplay between epithelial and mesenchymal cells is thought to exacerbate the progression of IPF through the modulation of the microenvironment. This intercellular dialogue creates a self-perpetuating vicious cycle, wherein damaged alveolar epithelial cells enhance the proliferation, recruitment, and activation of fibroblasts, resulting in abnormal deposition of extracellular matrix (ECM). In response, these myofibroblasts induce epithelial injury and promote apoptosis, further contributing to disease progression. Similar epithelial-mesenchymal interactions have been observed in the development of fibrosis in various organs, where the co-localization of fibroblasts and epithelial cells is a common feature (N. Sakai and Tager 2013).

In kidney fibrosis, for instance, epithelial micro-injuries can create a pro-fibrotic microenvironment by releasing mediators such as transforming growth factor-beta (TGFβ) or connective tissue growth factor (CTGF) (L. Yao, Yilu Zhou, et al. 2021; N. Sakai and Tager 2013; Prunotto and al. 2012; Madhusudhanan Bhaskaran and al. 2003; Jungwook Kim et al. 2009; Brezniceanu and al. 2010), thus enhancing myofibroblast accumulation. Conversely, these resultant myofibroblasts induce apoptosis of epithelial cells through molecules like angiotensin II (ANG II) or reactive oxygen species (ROS), establishing a self-sustaining feedback loop (L. Yao, Yilu Zhou, et al. 2021; N. Sakai and Tager 2013).

Similar crosstalk has been observed in the context of pulmonary fibrosis, where a range of pro-fibrotic mediators acting on fibroblasts derived from AECs have been strongly implicated in IPF (N. Khalil et al. 1996; H. Antoniades and al. 1990; L. Pan and al. 2001; Pierre Piguet et al. 1993; Pardo and al. 2005; Xiaoming Li and al. 2006; Daniel Saleh and al. 1997; Moisés Selman and al. 2004). These mediators include various growth factors (e.g. TGFβ, PDGF, CTGF, TNF-α, osteopontin, angiotensinogen, and endothelin-1) as well as developmental pathways (e.g.

Wnt/β-catenin and Sonic hedgehog) (Königshoff and al. 2009; Ana L. Bolaños and al. 2012; Cigna and al. 2012). In response to injury, AECs secrete mediators that enhance the pathogenic functions of fibroblasts, thereby contributing to ECM deposition. For instance, injured AECs stimulate the secretion of TGFβ, which, in turn, increases fibroblast proliferation, recruitment, and activation (Sheppard 2006b; Yoh Morishima and al. 2001). Additionally, secreted TGFβ1 and endothelin-1 are crucial for preventing fibroblast apoptosis by regulating the protein kinase B (Akt) pathway (Talmadge E King Jr, Pardo, and Moisés Selman 2011; Prabha Kulasekaran and al. 2009). Conversely, under the same microenvironment, AECs from IPF patients become more susceptible to apoptosis, partly due to decreased expression of prostaglandin E2 (Talmadge E King Jr, Pardo, and Moisés Selman 2011; Toby M. Maher and al. 2010; Victor J. Thannickal and Jeffrey C. Horowitz 2006).

In addition, research has shown that RAS-activated ATII cells can provide paracrine signals that augment fibroblast activation (L. Yao, Franco Conforti, et al. 2019). Moreover, zinc finger E-box binding homeobox factor 1 (ZEB1) has been identified as a key transcription factor secreted during EMT and has been associated with increased mesenchymal gene expressions (Yujing Liu et al. 2008). The matrix-derived protein SPARC secreted by IPF fibroblasts could also disrupt the integrity of alveolar epithelium by interfering with junctional contacts (F. Conforti and al. 2020). Additionally, Thy-1 deficiency in IPF fibroblasts has been linked to increased synthesis of metalloproteinase-9 (MMP-9), which can disrupt the alveolar basement membrane by inhibiting collagen IV production (Ramírez and al. 2011; Pardo and Moisés Selman 2006)[. Conditioned media (CM) from IPF fibroblasts have been shown to promote apoptosis of AECs when compared to media conditioned by healthy fibroblasts (N. Sakai and Tager 2013; Bruce D. Uhal and al. 1995). Several mediators have been identified in this regulatory effect, including Angiotensin II (ANG II) and hydrogen peroxide (H_2O_2). ANG II, a key mediator found in conditioned media harvested from IPF fibroblasts (Rui Wang and al. 1999), can be produced under low oxygen tension (Abdul-Hafez, Shu, and B. D. Uhal 2003). Studies in WT mice have demonstrated that both epithelial apoptosis and bleomycin-induced fibrosis can be attenuated by treating with ANG II type 1 receptor (AT1R) antagonist or antisense oligonucleotides (Koslowski et al. 2003; Xiangde Li and al. 2007). Similarly, mice with AT1R-deficiency were protected from pulmonary fibrosis (Koslowski et al. 2003). Hydrogen peroxide (H_2O_2), another fibroblast-derived mediator, is responsible for alveolar apoptosis (Waghray and al. 2005), and increased secretion of H_2O_2 has been correlated with IPF severity (K. Psathakis and al. 2006). Exogenous H_2O_2 has been shown to inhibit migration and induce apoptosis of primary AECs (Geiser et al. 2004; Victor J. Thannickal and Fanburg 2000).

It is worth noting that several mediators have bidirectional effects and can be synthesized by both fibroblast and epithelial cell populations. ANG II and TGFβ are

particularly crucial in mediating this bidirectional epithelial-mesenchymal crosstalk, impacting the microenvironment and exacerbating pulmonary fibrosis. For example, fibroblast-derived ANG II has been shown to induce apoptosis in AECs through paracrine signalling (Rui Wang and al. 1999; Koslowski et al. 2003; Xiangde Li and al. 2007), while AECs can also synthesize ANG II (Xiaoming Li and al. 2006; Xiangde Li and al. 2003). Similarly, TGFβ, a potent cytokine secreted by AECs, regulates various pro-fibrotic functions in fibroblasts (Grahovac and A. Wells 2014; Sheppard 2006b; Yoh Morishima and al. 2001). Recent studies suggest that latent TGFβ may be produced by activated myofibroblasts in an integrin αvβ5-dependent manner, leading to the induction of epithelial apoptosis (Yang Zhou et al. 2010; Hagimoto and al. 2002; Solovyan and Keski-Oja 2006; M. Li and al. 2011).

1.6 Dysregulated epithelial-mesenchymal crosstalk in IPF

Dysregulated epithelial-mesenchymal crosstalk plays a pivotal role in the pathogenesis of fibrosis, particularly in interstitial lung fibrosis, mirroring mechanisms observed in kidney fibrosis. (Prunotto and al. 2012). This crosstalk is characterized by a bi-directional profibrogenic feedback loop between activated epithelial cells and fibroblasts, perpetuating a chronic wound environment conducive to fibrosis progression rather than healing. Central to this process is the ZEB1-tPA axis, which orchestrates paracrine signalling between RAS-activated alveolar type II (ATII) cells and fibroblasts (L. Yao, Franco Conforti, et al. 2019). In our studies, This signalling enhances fibroblast migration and augments TGFβ-induced fibroblast activation, while TGFβ-activated fibroblasts, in turn, induce RAS activation in ATII cells, partially via the secreted protein SPARC (Figure. 1.6).

The interplay of risk factors in interstitial lung fibrosis leads to micro-injuries of alveolar epithelial cells, triggering epithelial-mesenchymal transition (EMT) and loss of apical-basal polarity, which further affects fibroblast function and fosters a migratory mesenchymal phenotype capable of signalling to surround fibroblasts (Talmadge E King Jr, Pardo, and Moisés Selman 2011; Moisés Selman, Pardo, and Kaminski 2008). Our findings reveal that ATII cells undergoing EMT not only enhance TGFβ-induced profibrogenic responses in lung fibroblasts through ZEB1-mediated paracrine signalling but also exhibit increased expression of profibrotic genes upon exposure to conditioned media from RAS-induced EMT, explaining the enhanced effects of exogenous TGFβ (L. Yao, Franco Conforti, et al. 2019). Further investigations revealed that this epithelial-mesenchymal crosstalk affects the sensitivity of fibroblast activation induced by TGFβ through tissue plasminogen activator (tPA) (Hebert et al. 2016). In a mouse model of kidney fibrosis, tPA binding to the low-density lipoprotein receptor-related protein 1 (LRP1) enhances integrin-linked kinase (ILK) dependent formation of the β1-integrin/LRP1 complex,

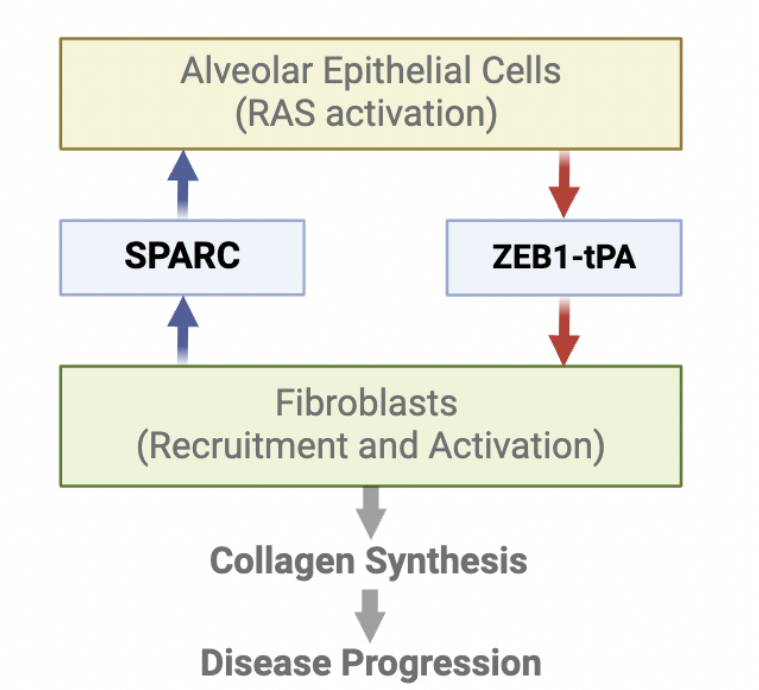

FIGURE 1.6: **Aberrant epithelial-mesenchymal crosstalk provides self-sustainable activation signals driving disease progression.**
Dysregulated epithelial-mesenchymal crosstalk in fibrotic progression: RAS-activated ATII cells and fibroblasts interact through ZEB1-tPA and SPARC-mediated paracrine signalling, enhancing fibroblast recruitment and TGFβ activation. This interaction promotes collagen secretion by myofibroblasts, driving IPF advancement.

contributing to fibroblast surveillance and fibrogenesis (Hu et al. 2007). In our studies, we found that fibroblasts from pulmonary fibrosis exhibit altered pathogenic properties, including enhanced migration compared to fibroblasts from control lungs (Ramos and al. 2001; Pierce and al. 2007; Suganuma and al. 1995).

Moreover, the origin of TGFβ, a critical mediator in fibrogenesis, has been linked to the inflammatory response following lung injury, where epithelial cells release mediators that trigger a coagulation cascade, leading to platelet activation and leukocyte recruitment (Kolb and al. 2001), which further secretes pro-fibrotic cytokines, including TGFβ (Thomas A. Wynn 2011b; Kolb and al. 2001). This study also highlights the role of SPARC in dysregulating alveolar barrier integrity and enhancing alveolar cell migration, suggesting a complex network of signalling pathways that contribute to the fibrotic process. These insights into the dysregulated epithelial-mesenchymal crosstalk in fibrosis underscore the complexity of fibrotic diseases and identify potential therapeutic targets aimed at modulating these intricate cellular interactions. we also found that alveolar epithelial cells from IPF lung tissue express high levels of TGFβ2 and Snai2. Damaged bronchial epithelial cells have been shown to promote autocrine activation of EGFR while increasing production of TGFβ2 independent of EGFR activation (Puddicombe and al. 2000). Therefore, we observed

enhanced expression of TGFβ2 in scraped ATII cells in proportion to the injury severity. The increased expression of TGFβ2 indicates the potential of RAS-ZEB1 and Snail2-TGFβ that synergistically activate the underlying fibroblasts by paracrine signalling. We propose that two parallel pathways are operating within these damaged and repairing epithelial cells. Some pathways control the production of profibrogenic growth factors such as TGFβ independently of EGFR, while others promote epithelial-mesenchymal crosstalk to augment the profibrogenic microenvironment, dependent on RAS signalling.

1.7 Autophagy

Impaired proteostasis, which involves the stabilization and degradation of proteins, is associated with ageing and age-related diseases. Ageing is characterized by disturbed proteostasis, leading to an accumulation of intracellular damage and contributing to age-related disorders. Autophagy, a process involved in protein quality control, and the ubiquitin-proteasome system are two principal proteolytic systems implicated in proteostasis (Moisés Selman, Buendıa-Roldán, and Pardo 2016).

Autophagy is a process where cells degrade and remove various cellular waste products, such as damaged organelles and misfolded proteins, to maintain homeostasis (Yorimitsu and Klionsky 2005). This process is crucial for cell survival and is generally preserved across different species and cell types, including tumour cells (Komatsu, Waguri, et al. 2007). Autophagy can break down these waste products into useful components such as amino acids and fatty acids, which can then be recycled by the cell for energy and protein synthesis (Z. Yang and Klionsky 2010). While the precise mechanisms by which autophagy collaborates with apoptosis to regulate cell survival and death are not yet fully understood, it is clear that maintaining a basic and low level of autophagy activity is necessary for cellular stability (Rabinowitz and E. White 2010).

As a cellular degradation process, Autophagy is categorized into three types based on the generation process: macroautophagy, microautophagy, and chaperone-mediated autophagy (CMA) (Mizushima and Komatsu 2011). Macroautophagy, the most researched type, is characterized by the formation of a double-layered, cup-shaped phagophore (H. Wu et al. 2015). Microautophagy involves the direct engulfment of cytoplasmic components by lysosomes (Kunz, H. Schwarz, and Mayer 2004). CMA requires molecular chaperones such as Hsp70, which facilitate the translocation of unfolded proteins into the lysosomal membrane (Kunz, H. Schwarz, and Mayer 2004; Chiang et al. 1989).

Under normal cellular conditions, autophagy maintains a low level but is activated by various intracellular and extracellular stimuli. Intracellular stimuli include metabolic

stress, misfolded or aggregated proteins, and damaged organelles, while extracellular stimuli encompass nutrient deficiency, oxygen shortage, and growth factor withdrawal (Martinet et al. 2006). Upon receiving these signals, cells synthesize autophagy-related proteins and form a phagophore, which expands to sequester cytoplasmic components. The phagophore then closes, creating an autophagosome, which subsequently fuses with a lysosome to form an autolysosome where degradation occurs. The breakdown products are recycled, while residues are expelled or remain in the cytoplasm (Mizushima 2007). The highlighted role of P62 has been pointed out by (Y. Chen et al. 2020). When cells perceive signals from within or outside their boundaries, the enlargement of phagophores commences, encapsulating elements of the cytoplasm. The UBA domain of p62 acts as a magnet for misfolded protein clumps. Subsequently, the phagophores close off, morphing into fully enclosed autophagosomes with a spherical structure. The synergy between p62 bodies and LC3 plays a pivotal role in the genesis of autophagosomes. As the final step, autophagosomes unite with lysosomes, giving rise to autolysosomes that facilitate the breakdown of protein aggregates (Figure. 1.7). Lamark et al. found that during the selective autophagy process, p62 serves as a "cargo" receptor for the degradation of ubiquitinated target substrates (Ichimura and Komatsu 2018). Intracellular protein aggregates marked for degradation are labelled by ubiquitination and accompanied by the presence of p62. For instance, p62 has been identified in ubiquitinated protein inclusions such as Alzheimer's disease-related neurofibrillary tangles (NFTs) and nonalcoholic steatohepatitis (NASH) Mallory bodies (MBs) (Strnad et al. 2008). By interacting with ubiquitinated substrates and LC3 through its UBA and LIR domains, respectively, p62 can facilitate the selective autophagy process.

P62 levels can indicate autophagy levels, as p62 can be degraded via binding to LC3 through its LIR domain as an autophagic substrate. When detecting autophagy flux using p62, it is important to take into account lysosomal activity and gene expression (Rusten and Stenmark 2010). Autophagy flux is capable of reflecting p62 expression, and autophagy serves as a key factor in regulating p62 levels. Conversely, Autophagy reduction or suppression usually results in p62 accumulation.

As selective autophagy has a critical function in both physiological and pathological processes, evaluating its levels is necessary to avoid functional imbalances. LC3, a well-established autophagy marker, is involved in this process. LC3-I (a cytoplasmic form of LC3) is enzymatically cleaved, losing a small peptide and transforming into LC3-II (an autophagosome membrane form) during autophagy (Aparicio et al. 2016). Therefore, determining the LC3-II/LC3-I ratio under conditions involving autophagy inhibitors or activators is a practical approach for assessing autophagy levels, often termed autophagy flux (Larsen et al. 2010).

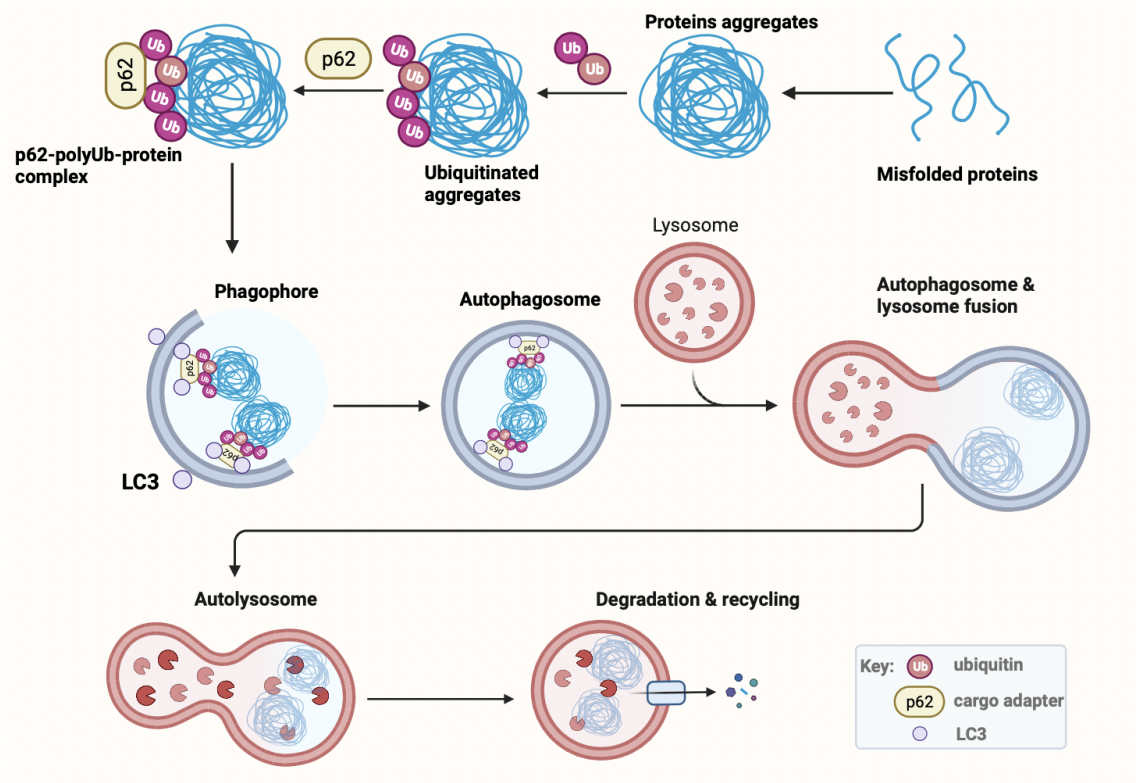

FIGURE 1.7: **Illustration depicting the stages of p62-mediated selective autophagy** The process commences with the recruitment of misfolded protein aggregates to the p62's UBA domain, triggered by intra or extracellular signals. This initiates the phagophore expansion encapsulating cytoplasmic components, eventually sealing to form autophagosomes. These structures, facilitated by p62-LC3 interactions, later merge with lysosomes to create autolysosomes, where the aggregated proteins are ultimately degraded. Information collected from (Y. Chen et al. 2020).

1.8 LKB1 complex

LKB1 is a serine/threonine protein kinase that plays an important role in regulating various cellular processes, including cell polarity, proliferation, and metabolism. It was first identified as a causal mutation in patients with Peutz-Jeghers syndrome (PJS), a rare genetic disorder characterized by the development of benign tumours in the gastrointestinal tract and other organs (Hemminki et al. 1998a). Since its discovery, LKB1 has been extensively studied as a tumour suppressor, and it has been shown to regulate many important cellular processes involved in tumour development and progression.

LKB1 plays a critical role in cell cycle regulation by phosphorylating and activating AMP-activated protein kinase (AMPK) and other downstream targets (Tiainen, Ylikorkala, and Mäkelä 1999). Through this pathway, LKB1 regulates the progression of cells through the cell cycle, preventing uncontrolled proliferation that can lead to tumour formation. LKB1 also has been shown to regulate apoptosis, or programmed

cell death, mediated by the tumour suppressor protein p53 (Ossipova et al. 2003). Specifically, LKB1 phosphorylates and activates the protein kinase NUAK1, which promotes p53-dependent apoptosis in response to cellular stress (Jose M Lizcano et al. 2004a). In addition to this, LKB1 regulates the Wnt signalling pathway, which is involved in cell proliferation and differentiation (Ossipova et al. 2003). LKB1 phosphorylates and activates the protein kinase MARK4, which in turn regulates the activity of the Wnt signalling pathway (Jose M Lizcano et al. 2004a).

LKB1 has been shown to regulate the transforming growth factor beta (TGFβ) signalling pathway, which is involved in cell proliferation, differentiation, and apoptosis. Distinctly, LKB1 phosphorylates and activates the protein kinase STRAD, which in turn regulates the activity of the TGFβ signalling pathway (N.-S. Li et al. 2016). Relatively, LKB1 has been shown to play a role in regulating cell transformation induced by the RAS oncogene in terms of that LKB1 can regulate the activity of the protein kinase MST2, which is involved in RAS-induced cell transformation (Khan et al. 2019). LKB1 regulates these processes through its ability to phosphorylate and activate various downstream targets, including AMP-activated protein kinase (AMPK), which is a key regulator of cellular energy metabolism. LKB1 also plays a role in regulating the activity of the mTOR pathway, which is involved in protein synthesis and cell growth (D. Han et al. 2013).

LKB1 activation occurs via allosteric binding of LKB1 to STE20-related adaptor (*STRAD*) and mouse protein 25 (MO25, encoded by *CAB39* and *CAB39L*) (Figure. 1.8) (Momcilovic and D. Shackelford 2015b), and its best-known function is the activation of AMPK, a fundamental regulator of cell growth and metabolism. AMPK is activated by ATP depletion and acts as a bioenergetics sensor, coordinating growth and metabolism (Figure. 1.8). The AMPK plays a role in coordinating growth and metabolism as a bioenergetics sensor. The activation of AMPK not only can be led by the nucleotide-binding (Oakhill et al. 2011) (Maria M Mihaylova and Reuben J Shaw 2011b). While LKB1 has other substrates besides AMPK, only AMPK is activated under low-energy conditions. There is mounting evidence linking the function of LKB1 to the AMPK signalling pathway in various microenvironments, with AMPK activation reversing established lung fibrosis and impairments in AMPK activity implicated in the development of IPF (Sunad Rangarajan et al. 2018; L. Li et al. 2015). Kidney-specific deletion of LKB1 induces severe renal fibrosis (Seung Hyeok Han et al. 2016), and thymoquinone has been shown to alleviate hepatic fibrosis by activating the LKB1-AMPK signalling pathway in mice (Ting Bai et al. 2014). In summary, LKB1 plays a crucial role in regulating cell metabolism and growth through its activation of AMPK and represents an important therapeutic target for the treatment of fibrotic diseases.

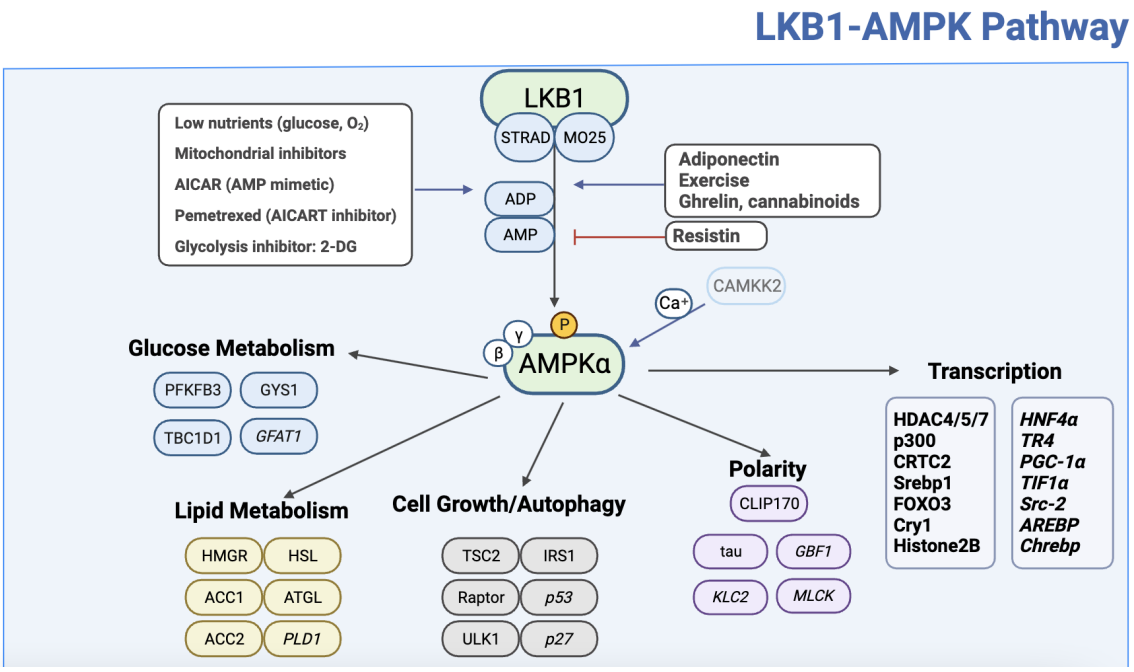

FIGURE 1.8: **LKB1-AMPK signalling pathway**
Diagram showing activation of AMPK occurs on AMP and ADP levels elevated by physiological stresses or even exercise. LKB1 as the upstream kinase activates AMPK in response to AMP. AMPK is activated by phosphorylating plenty of substrates to impact cell growth and metabolism and mediate long-term metabolic reprogramming. Shown are all the best-established substrates to date needing further in vivo examination. Question marks denote candidate substrates whose identified phosphorylation sites diverge from the established optimal substrate motif. Information collected from (Maria M Mihaylova and Reuben J Shaw 2011a).

1.8.1 LKB1 as a tumor suppressor

LKB1, also known as STK11, is commonly recognized as a tumour suppressor gene. Its hereditary mutation is responsible for cancer syndrome, while somatic inactivation of LKB1 is found in non-small cell lung cancer (NSCLC), melanoma, and cervical cancers. Unlike other tumour suppressors that typically suppress cell proliferation or promote cell death, one of the unique functions of LKB1-regulated AMPK signalling is to suppress cell proliferation and promote cell survival under conditions of energetic stress.

On the one hand, LKB1 is known to selectively inhibit the growth of cancer cells, particularly under conditions of metabolic stress and hypoxia (low oxygen levels). When cancer cells face energy deprivation, the LKB1-AMPK signalling pathway is activated, leading to the inhibition of anabolism and the induction of cell cycle arrest, ultimately suppressing cancer cell growth (Hardie and Alessi 2013). The inhibition of anabolism in cancer cells is achieved through AMPK activation by LKB1, resulting in the suppression of key enzymes involved in fatty acid, sterol, and protein synthesis (ibid.). Moreover, LKB1 induces cell cycle arrest in cancer cells through AMPK

signalling. AMPK activators, like metformin, can effectively inhibit cancer cell growth by promoting cell cycle arrest through AMPK activation. This effect is associated with the inhibition of mTOR, a key regulator of cell growth, through the phosphorylation of tuberous sclerosis 2 (TSC2) (Xiang et al. 2004; Hardie 2005; Zakikhani et al. 2006). Additionally, AMPK can induce cell cycle arrest through persistent activation of p53, leading to cellular senescence (R. G. Jones et al. 2005). Furthermore, LKB1 may inhibit cancer cell growth through AMPK-mediated regulation of cyclooxygenase-2 (COX-2) signalling, a key player in cell cycle control (Hwang et al. 2006; Wagner, Mullally, and Fitzpatrick 2006). LKB1's role in cell cycle arrest is also dependent on p21 and p53. LKB1 can upregulate the expression of the CDK inhibitor p21WAF1/CIP1, leading to G1 cell cycle arrest. This effect is not influenced by the presence of certain G1 cyclins, making it p53-independent. However, LKB1 also physically interacts with p53 in the nucleus, stabilizing p53 and directly or indirectly phosphorylating specific sites necessary for LKB1-dependent G1 cell cycle arrest (Tiainen, Vaahtomeri, et al. 2002; P.-Y. Zeng and Berger 2006). In addition to these mechanisms, LKB1 may also inhibit cancer cell growth by regulating hypoxia-inducible factor 1 (HIF-1) under hypoxic conditions. HIF-1 is a transcription factor that enables cancer cells to survive and grow in a hypoxic tumour environment. LKB1-AMPK signalling negatively regulates mTORC1, which has been reported to upregulate HIF-1. In LKB1-deficient tumours, both mTORC1 and HIF-1 levels are significantly increased, suggesting that LKB1-AMPK-mTORC1 signalling may suppress HIF-1 expression and its target genes responsible for cell survival. (W. R. Wilson and M. P. Hay 2011; Powis and Kirkpatrick 2004; Reuben J Shaw, Bardeesy, et al. 2004; G. V. Thomas et al. 2006).Furthermore, LKB1 exerts its tumour suppressor effect through interactions with STRAD and BRG1. The depletion of endogenous STRAD disrupts G1 cell cycle arrest, emphasizing the crucial role of STRAD in LKB1's tumour suppressor function. Additionally, LKB1 can interact with and activate BRG1, which leads to cell growth arrest (A. Baas et al. 2003; Marignani, Kanai, and Carpenter 2001).

On the other hand, regarding cancer cell death, LKB1 mediates both p53-dependent and p73-dependent cell death pathways (Karuman et al. 2001). In certain cancer cell lines, LKB1-induced apoptosis is p53-independent but occurs through the activation of p73 (JH Lee et al. 2006). Moreover, LKB1 can induce cell apoptosis through activation of the JNK pathway. In osteosarcoma cells, LKB1 is essential for TRAIL and DAP3-induced apoptosis, and a kinase-dead mutant of LKB1 inhibits this apoptotic process (Takeda et al. 2007). Interestingly, LKB1 can also induce autophagy, a cellular process with dual effects on cancer cell fate. Autophagy can sustain the survival of cancer cells with apoptosis defects, but it can also induce cell death under certain conditions. LKB1-AMPK signalling, when activated by metabolic stress like hypoxia and energy deprivation, phosphorylates and activates TSC2, leading to mTOR and mTORC1 inhibition and the subsequent activation of autophagy. The role of LKB1-regulated autophagy in cancer cell survival or death remains context-dependent

and may vary based on tumour micro-environmental conditions (Reuben J Shaw 2009). Also, studies have demonstrated that LKB1 plays a crucial role in suppressing cancer cell invasion and metastasis. For instance, in breast cancer cells lacking LKB1 expression, the introduction of wild-type LKB1 leads to a significant inhibition of cancer cell invasion and metastasis both in laboratory settings and in animal models. This inhibition is accompanied by the downregulation of matrix metalloproteinase 2 and 9 (MMP-2 and MMP-9), as well as vascular endothelial growth factor (VEGF) (Zhuang et al. 2006). Furthermore, LKB1 is essential for the inhibitory effects of adiponectin on the migration and invasion of breast cancer cells. This effect is dependent on the activation of AMPK and the inhibition of p70S6 kinase (Taliaferro-Smith et al. 2009). As a cancer promoter, LKB1-deficient cells experience increased cell death under energy deprivation (Reuben J Shaw, Kosmatka, et al. 2004). Introducing LKB1 in lung adenocarcinoma cells inhibits glucose starvation-induced cancer cell death through AMPK-mediated fatty acid synthesis inhibition (Jeon, Chandel, and N. Hay 2012). Knockdown of LKB1 downstream molecules AMPK and NUAK1 induces cell apoptosis in osteosarcoma cells with c-Myc overexpression (L. Liu et al. 2012). Phenformin, an AMPK activator, shows enhanced efficacy in treating non-small cell lung cancer when tumours lack a functional LKB1-AMPK pathway. Caution is needed when targeting the LKB1 pathway for cancer treatment due to its dual role in promoting and inhibiting cancer growth (David B Shackelford, Abt, et al. 2013).

1.8.2 LKB1-STRAD-MO25 COMPLEX

LKB1 functions as a master kinase that regulates various cellular processes by forming a heterotrimeric complex with STRAD and MO25 (CAB39). The most studied isoform of this complex is LKB1-STRADα-MO25α, but other combinations like LKB1-STRADα-MO25β and LKB1-STRADβ-MO25α have also been reported with lower activity (S. Hawley et al. 2003). This complex activates downstream kinases, and suppressed LKB1 expression or activity is linked to cancer development, particularly in Peutz-Jeghers syndrome, where inactivating mutations are common (David B Shackelford and Reuben J Shaw 2009; A. Baas et al. 2003). LKB1 has been identified as a tumour suppressor in lung, breast, thyroid, and liver cancers (Kou et al. 2022; C. T. King et al. 2022). While not statistically significant, higher LKB1 expression levels show a trend towards improved outcomes in hepatocellular carcinoma.

STRADα/β are pseudokinases that interact with LKB1 to activate it (A. Baas et al. 2003). The primary variant, STRADα (Veleva-Rotse et al. 2014), is the main focus in LKB1 complex research, although studies have suggested its role in regulating cellular polarity and invasion through PAK1 signalling in LKB1-null cells (Eggers et al. 2012). Higher STRADα and STRADβ expression levels in hepatocellular carcinoma show a

trend towards improved outcomes and a statistically significant survival benefit, respectively.

CAB39, also known as MO25, is a scaffolding protein that enhances LKB1 signalling by stimulating STRAD's activation of LKB1 and facilitating cytoplasmic translocation (Jérôme Boudeau, Annette F Baas, et al. 2003a). Briefly, LKB1 functions both in the nucleus and cytoplasm, being inactive in the nucleus but activated when it migrates to the cytoplasm. The adaptor protein STRAD plays a crucial role in this process by facilitating LKB1's export to the cytoplasm and enhancing its catalytic activity, while MO25 stabilizes the activated LKB1 complex (Zeqiraj et al. 2009). The level of LKB1 in the cell is regulated by the ubiquitin-proteasome system, with poly-ubiquitination leading to its degradation. CAB39 has been associated with tumour suppression in the brain, pancreas, lung, colon, and liver (H.-M. Wang et al. 2020; Kai Li et al. 2020). Interestingly, for the CAB39L variant, there was a statistically significant survival benefit for patients with higher levels of CAB39L mRNA expression. This suggests that CAB39L may play a more significant role in tumour suppression and could be a potential target for therapeutic interventions in hepatocellular carcinoma.

The LKB1-STRAD-MO25 complex can be isolated from mammalian cell expression systems, and the three components are present in a similar stoichiometry, indicating a high affinity among the individual subunits (Annette F. Baas et al. 2003; Jérôme Boudeau, Annette F. Baas, et al. 2003b). Notably, LKB1 is mainly localized in the nucleus when overexpressed alone, but a small fraction is found in the cytoplasm (Sapkota et al. 2002). The N-terminal noncatalytic region of LKB1 contains a nuclear localization signal, and mutations in this motif result in cytoplasmic localization of LKB1 (Hemminki et al. 1998b). Notably, the overexpression of MO25α enhances the amount of STRADα associated with LKB1, and siRNA-mediated knockdown of MO25α reduces the amount of endogenous STRADα bound to LKB1 (Sanchez-Cespedes 2007; Jérôme Boudeau, Annette F. Baas, et al. 2003b). The pseudokinase domain of STRAD isoforms directly binds to the kinase domain of LKB1, and there are likely to be multiple interaction sites between them. In addition to interacting with STRAD and MO25 isoforms, a pool of cellular LKB1 is associated with a chaperone complex consisting of heat shock protein 90 (Hsp90) and Cdc37 kinase-specific targeting subunit for Hsp90. Hsp90 stabilizes and prevents degradation of LKB1, indicating a potential role in facilitating LKB1 assembly into the complex with STRAD and MO25 (Nony et al. 2003; Jérôme Boudeau, Maria Deak, et al. 2003).

1.8.3 LKB1-dependent signallings

LKB1, as a master upstream kinase, regulates various biological processes by activating AMPK and 12 AMPK-related kinases (Jose M Lizcano et al. 2004b). AMPK

is a major target of LKB1, and its activation under metabolic stress enhances ATP production through improved mitochondrial function, glycolysis, and fatty acid oxidation, while also limiting energy consumption by blocking synthetic pathways and inducing mild autophagy. These effects help cells adapt to energy deficiency and ischemia and also restrict cell growth (Woods et al. 2003; Altarejos et al. 2005; K. Sakamoto et al. 2006; Suter et al. 2006). Additionally, LKB1 targets other kinases such as MARK, BRSK, NUAK1, and SIK1, which play roles in controlling cellular polarity, adhesion, detachment, and invasion (Alvarado-Kristensson et al. 2009; H. Cheng et al. 2009; Zagórska et al. 2010).

The role of LKB1 in regulating lung cancer invasion and metastasis is an emerging area of research. Studies in Drosophila suggested that LKB1 is involved in regulating cell polarity, which may be related to epithelial-to-mesenchymal transition (EMT). In a mutant Kras mouse model, the loss of Lkb1 was found to accelerate tumour progression and promote metastasis, providing in vivo evidence of LKB1's involvement in cancer metastasis. Further analysis indicated that LKb1-deficient tumours exhibited activation of SRC and FAK, and LKB1 was found to suppress FAK activity in human cancer cell lines. These findings suggest that LKB1-deficient cancer cells may have hyper-activated SRC/FAK function, making them susceptible to inhibition of these kinases using drugs like dasatinib (Src inhibitor) and defactinib (FAK inhibitor). Clinical trials are ongoing to investigate whether these inhibitors can prevent metastasis in LKB1-mutant tumours.

1.9 Summary and aims of thesis

To summarise, a few relevant findings have been confirmed:

1. LKB1-AMPK pathway activation reverses established lung fibrosis in a bleomycin model.

Numerous studies have explored the role of LKB1-AMPK in the progression of lung fibrosis. However, the existing literature may provide limited details specifically concerning LKB1 in the context of lung fibrosis. LKB1 is widely recognized as a tumour suppressor gene, and its hereditary mutation is associated with cancer syndrome. Somatic inactivation of LKB1 has also been observed in various cancers, such as non-small cell lung cancer, melanoma, and cervical cancers. Unlike typical tumour suppressors that mainly regulate cell proliferation or cell death, LKB1, when regulated by AMPK, plays a unique role in suppressing cell proliferation to promote cell survival during energetic stress conditions. Recent evidence suggests that LKB1-AMPK also inhibits tumour invasion and migration by downregulating downstream factors of TGF-β signalling, such as MMPs and Snail. AMPK has been reported to impede TGF-β-induced EMT. Moreover, in a bleomycin-induced mouse model of lung fibrosis, therapeutic administration of metformin accelerates the resolution of well-established fibrosis in an AMPK-dependent manner. Given these intriguing findings, it becomes crucial to investigate the function of LKB1 in epithelial cells, particularly its role in driving AMPK activation in the context of lung fibrosis. Additionally, researchers should evaluate whether and how epithelial LKB1 impacts the microenvironment of epithelial-fibroblast interactions. Understanding these aspects can provide valuable insights into the mechanisms underlying lung fibrosis and potentially uncover new therapeutic targets for this condition.

2. Autophagy promotes p65/RELA mediated transactivation of an EMT transcription factor in lung fibrosis.

Previous studies have provided evidence that the loss of essential autophagy genes leads to endothelial-to-mesenchymal transition (EndMT) and induces myofibroblast differentiation and cellular senescence in bronchial epithelial cells. Additionally, inhibition of autophagy promotes EMT in alveolar epithelial cells. EMT is a reversible process where epithelial cells acquire migratory and invasive properties by losing cell polarity and cadherin-mediated cell-cell adhesion. This process is implicated in various biological events, including embryonic development, wound healing, cancer metastasis, and organ fibrosis. Specific transcription factors known as EMT transcription factors (EMT-TFs), including Snail, ZEB, and TWIST, play a role in promoting the repression of epithelial features and induction of mesenchymal features.

In our research group, it has been demonstrated that autophagy inhibition in alveolar epithelial cells promotes EMT, partly through increased expression of sequestosome 1 (p62/SQSTM1). This leads to p65/RELA mediated-transactivation of Snail2 (SNAI2), which not only controls EMT but also regulates the production of locally acting profibrogenic mediators. This suggests that autophagy inhibition-induced EMT of alveolar epithelial cells contributes to fibrosis, not only by affecting the epithelial phenotype but also through aberrant epithelial-fibroblast crosstalk.

However, the specific factors that inhibit autophagy in epithelial cells to promote the expression of Snail2 and further induce EMT have not been fully elucidated. This critical aspect forms a central aim for my thesis, as identifying the key upstream regulator that inhibits autophagy and triggers Snail2 expression can provide valuable insights into the mechanisms driving fibrosis and may uncover potential therapeutic targets for this condition.

3. Aberrant epithelial-mesenchymal crosstalk maintains a wound-healing phenotype and provides self-sustaining pro-fibrotic signals.

The origin of myofibroblasts in the context of lung fibrosis has been a subject of debate, with epithelial-to-mesenchymal transition (EMT) being proposed as a potential source for the transformation of epithelial cells into myofibroblasts that produce extracellular matrix (ECM). However, lineage tracing studies in transgenic mice have indicated that the contribution of EMT to the population of myofibroblasts is negligible.

In a previous study, we uncovered a novel regulatory axis involved in lung fibrosis, where EMT plays a role in the fibrotic process through paracrine activation of fibroblasts. Our research team demonstrated that the epidermal growth factor receptor (EGFR)-RAS-extracellular signal-regulated kinase (ERK) signalling pathway induces the transcription factor ZEB1. This transcription factor not only controls EMT but also regulates the production of locally-acting mediators. Specifically, we identified tissue plasminogen activator (tPA) as a downstream effector of ZEB1 transcriptional activity, enhancing TGFβ-induced profibrogenic responses in fibroblasts through paracrine signalling. Immunostaining showed increased ZEB1 nuclear expression in alveolar epithelium adjacent to sites of ECM deposition in IPF lung tissue. Consequently, our findings suggest that ZEB1-dependent EMT of alveolar type II (ATII) cells contribute to fibrosis via epithelial-fibroblast crosstalk. This suggests that the activation of ZEB1 and its role in paracrine signalling at sites of local ECM deposition in IPF lung tissue contributes to the development of a profibrogenic microenvironment, ultimately leading to interstitial lung fibrosis.

1.9.1 Hypothesis

It is crucial to further investigate the dynamics of epithelial-fibroblast crosstalk in the microenvironment during lung fibrosis. Additionally, it becomes imperative to elucidate whether and how the function of LKB1 in epithelial cells influences fibroblast behaviour in the context of lung fibrosis. Understanding these intricate interactions between epithelial and fibroblast cells can provide valuable insights into the mechanisms driving lung fibrosis and may lead to potential therapeutic interventions targeting this complex disease. Based on these, we hypothesise that:

1. LKB1 plays a significant role in epithelial cells, promoting the process of EMT through the induction of signalling pathways by various mediators.
2. The depletion of LKB1 in epithelial cells is proposed as a crucial factor that could mediate autophagy inhibition, subsequently leading to the upregulation of Snail2 expression.
3. LKB1 functions both as a crucial upstream regulator of autophagy, facilitating the epithelial-mesenchymal transition (EMT) during lung fibrosis progression, and as a mediator altering the epithelial-mesenchymal microenvironment. This dual role is proposed to occur through the specific depletion of LKB1 in alveolar type II (ATII) epithelial cells.

1.9.2 Objectives

The main aim of this thesis is therefore to characterise the mechanisms of epithelial LKB1 underlying EMT in the pathogenesis of IPF. Determining whether ECM-producing fibroblasts are derived from epithelial targets is critical in understanding the pathogenesis of IPF. LKB1-regulated AMPK signalling pathway has been proposed as a changer of established lung fibrosis. Elucidating the molecular mechanisms of epithelial LKB1-induced EMT, in fibrogenesis, will provide insight into disease pathogenesis. The specific objectives of my Thesis are:

1. **To assess the influence of LKB1 status on epithelial type II cells:** We plan to meticulously analyze the RNA-Seq raw data derived from both LKB1-depleted epithelial cells and controls utilizing advanced bioinformatics approaches. The objective is to delineate the biological behaviours that are altered following the inactivation of LKB1. We aim to corroborate these findings at both the protein and mRNA levels, thereby establishing a comprehensive view of the repercussions of LKB1 depletion in epithelial cells.

2. **To explore the role of LKB1 in mediating epithelial-fibroblast crosstalk in lung fibrosis and IPF Development:** This segment of the study is designed to probe the mechanisms through which LKB1 in ATII cells orchestrates the interaction between epithelial cells and fibroblasts during lung fibrosis establishment or IPF progression. Employing RNA-Seq and protein/mRNA analyses within a 2D/3D co-culturing model, we aim to accurately replicate the epithelial-fibroblast microenvironment. This initiative will involve the transfection of ATII cells with LKB1 siRNA or control vectors, followed by co-cultivation with fibroblasts, to elucidate the underlying pathways and interactions.

3. **To verify the inhibition of the LKB1 regulated pathway in IPF and mouse models:** The third objective is centred on substantiating the hypothesis that the LKB1 regulated pathway is suppressed in IPF and analogous mouse models. Utilizing RNA-scope strategies, we intend to pinpoint the presence of LKB1 components within the pathological sections of IPF patient samples, contrasting these findings with data from healthy individuals. This analysis will be informed by existing patient databases and histological sections. Furthermore, we propose to explore the interstitial modifications induced by LKB1 deletion using mouse lung tissues isolated from inducible Cre recombinase Lkb1 $^{-/-}$ mice, thereby offering a multifaceted perspective on the role of LKB1 in IPF progression.

Chapter 2

Materials and Methods

2.1 Global transcriptomic processing

This study utilized two bulk RNA sequencing datasets. The first dataset involved the examination of transcriptomic changes in ATII cells upon LKB1 depletion. The second dataset was obtained using a novel 3D bio-printing assay, where ATII cells were co-cultured with fibroblasts to simulate the alveolar interstitial tissue and study the cellular cross-talk between epithelial cells and fibroblasts. The RNA-seq data from both datasets have been deposited in the Gene Expression Omnibus (GEO) database under the accession code GSE205970. A secure token (ifstmcyadrqvler) has been created to allow review of this record while it remains in private status. Briefly, ATII cells were transfected with either control siRNA or LKB1 siRNA for 3 days. Total RNA was isolated by RNeasy mini kit (Qiagen) according to the manufacturer's instructions and quantified using a Nanodrop Spectrophotometer 2000c (Thermo Fisher Scientific). A total amount of 3 μg RNA per sample was used as input material for library construction. Sequencing libraries were generated using NEBNext® Ultra^{T}M RNA Library Prep Kit for Illumina® (NEB, Ipswich, Massachusetts, USA) following the manufacturer's instructions. Libraries were pooled in equimolar and sequenced using the paired-end strategy (2 $\times$ 150) on the Illumina NovaSeq 6000 platform following the standard protocols (Novogene, UK). 20516 genes have an expression in this total 6 samples assayed by the company of Novogene, Cambridge.

2.1.1 Raw counts preparation

For each sample, 3 μg of total RNA was used for library construction. The NEBNext UltraTM RNA Library Prep Kit was employed, following the manufacturer's protocols. The resulting libraries were pooled and sequenced using the paired-end strategy (2x150) on the Illumina NovaSeq 6000 platform by Novogene. The raw

RNA-seq data was subjected to quality control using FastQC(http://www.bioinformatics.babraham.ac.uk/projects/fastqc), and Trim Galore(https://github.com/FelixKrueger/TrimGalore) was used to trim adapters and filter out reads with low quality (phred score $<$ 30) and short length ($<$ 50 bp). The filtered data was then mapped to the Human genome Ensembl GRCh38 using Hisat2. Sam files were converted to bam files using samtools, and featureCounts was used to summarize the read counts for each specific gene. All these data processing steps were conducted using Conda installed on Iridis5 of HPC Soton with a Linux system. After mapping, the read counts were analyzed in RStudio using the DESeq2 R package (version 1.26.0).

2.1.2 Differentially expressed genes(DEGs) analysis

The raw read counts were analyzed in Rstudio software for gene expression analysis. The data were normalized using the variance stabilization normalization (Vsn) method to minimize sample differences. The Vsn package in R was used to implement the Vsn method with the just-vsn function. The normalized data were then transformed into log2 format. Differentially expressed genes (DEGs) were identified using the DESeq2 package (version 1.26.0) in R, with a significance threshold of < 0.05 and Log[Fold change]> 1. Transcripts with low abundance (below 10 counts across all samples) were removed from the analysis.

For gene ontology (GO) enrichment analysis and Hallmark pathway enrichment analysis, ToppGene website (https://toppgene.cchmc.org/) or GSEA software was utilized. The parameters were set with a false discovery rate (FDR) < 0.05. Hallmark pathway enrichment analysis was conducted using Metascape. Data processing and visualization were performed using the R programming language. The ggplot2 package was used to generate principal component analysis (PCA) plots and heatmaps. For gene ontology treemaps, R code was generated using GOrilla, and modifications were made to improve the quality of the plots.

2.1.3 Gene set enrichment analysis

Gene set enrichment analysis (GSEA) was performed using the Broad Institute's dedicated GSEA software or package in R. (downloadable at http://www.gsea-msigdb.org/gsea/index.jsp) (Subramanian et al. 2005). Gene set enrichment analysis (GSEA) is a method that uses software or R to rank two classes of genes based on their correlation with class definition. The software then performs a gene set enrichment analysis on this ranked list to determine which pre-defined gene sets are enriched at the top and bottom. To determine the significance of these gene sets, the class labels are rearranged and a null distribution for the gene set is

calculated. The ranked gene list and the enrichment scores are recalculated for this null distribution, and significance is determined by comparing the original ES distribution with the null ES distribution. This helps identify which gene sets are significantly enriched or depleted in the ranked list of genes.

The results of the gene set enrichment analysis are adjusted for multiple hypothesis testing, and a false discovery rate is calculated based on the normalized enrichment scores. Gene sets from different databases, such as gene ontologies, KEGG pathways, and hallmark gene sets, are used for the analysis. Gene ontologies contain genes associated with molecular functions, cellular components, and biological processes, while KEGG pathways specifically refer to gene sets involved in the same molecular pathway. Hallmark gene sets are highly curated and represent gene co-expression networks associated with specific biological states or processes. These gene sets are refined from multiple other gene sets to reduce redundancy and variation, and are taken from the molecular signatures database(MsigDB), which was originally developed for use with GSEA (ibid.).

2.2 Single cell RNAseq data analysis

Single-cell RNAseq counts data, associated metadata and cell-type definition, was downloaded from the Gene Expression Omnibus (GEO) database (GSE135893) (Arun C Habermann et al. 2020). Counts data was processed using the Seurat R package(172). Routine data processing was done in R 3.6 running on Mac. massive dataset was running via high-performance computing (HPC) provided by the Iridis 5 service of the University of Southampton.

2.3 Cell component analysis by CibersortX

CibersortX is a deconvolution method that utilizes v-Support Vector Regression (SVR), a machine learning technique, to estimate the proportions of different cell types in a sample. The input to CibersortX is a mixture of data and a signature matrix, and it outputs a model coefficient representing the estimated fractions of each cell type in the sample. The optimization procedure in CibersortX involves minimizing a specific objective function to allow for a margin of error and reduce data point errors outside this margin. CibersortX is the ability to handle expression matrices generated from different platforms or methods. This is important because technical differences between these platforms can be as significant as the biological differences between cell types. CibersortX addresses this by assuming that a mixture sample expression profile can be modelled as a linear combination of a signature matrix comprised of cell-type

reference profiles. Batch correction can be directly applied to the mixture sample and the signature matrix to ensure comparability between batches, avoiding estimation artefacts and the need for paired samples profiled on both platforms. CibersortX offers two reliable normalization strategies: B-mode and S-mode. B-mode batch correction removes technical differences between a signature matrix derived from bulk-sorted reference profiles (e.g., bulk RNA-seq or microarrays) and an input set of mixture samples. However, in cases with excessive technical variation, B-mode may not be effective. In such instances, S-mode is recommended as it adjusts the signature matrix instead of the bulk sample matrix. Significant improvement has been observed when the signature matrix is generated from droplet single-cell techniques.

2.4 Quantitative real-time PCR (q-RT-PCR)

2.4.1 RNA quantification and extraction

To quantify mRNA expressions, RNA was extracted using RNeasy mini kits (Qiagen, Germany) as per the manufacturer's instructions. Briefly, in a 6-well plate, cells were lysed using 350 μl buffer RLT, and mixed with an equal volume of 70% ethanol (Sigma Aldrich, UK) before being transferred to a Qiagen RNeasy column. Cells were washed by 700 μl of Buffer RW1 once and 500 μl of Buffer RPE twice sequentially with centrifugation (13,000g, 2 min) after each wash. Finally, each column was transferred into a new Eppendorf, and 40 μl of RNase-free water (Qiagen, Germany) was used to elute the RNA by centrifuging at 13,000g for 1 min. RNA concentration was quantified on a Nanodrop Spectrophotometer 2000c (ThermoFisher Scientific) and stored in a -80$^{\circ}C$ freezer until further qPCR analysis. Diluted RNA samples with a final concentration of 20ng/μl in RNase-free water (Qiagen, Germany) were used.

2.4.2 Quantitative real-time PCR (qRT-PCR)

Real-time PCR was performed using a QuantiNova SYBR Green RT-PCR kit (Qiagen, Germany) according to the manufacturer's instructions. The reaction set-up, the QuantiTect gene-specific primers (Qiagen, Germany), and the thermocycling conditions were as follows: (details are provided in table. 2.1, table. 2.2, table. 2.3, respectively). Triplicates were performed for each sample in a 96-well plate on a StepOnePlus^{TM} Real-Time PCR System (Thermo Fisher Scientific, UK).

During the amplification, the fluorescent dye was released, and the point when intensity exceeded the threshold was recorded, determining the Ct value. A higher Ct value indicated that the intensity exceeded the threshold later, corresponding to lower expression of the specific gene. Gene expression of each sample was estimated by the

ΔΔCt (delta-delta Ct) value utilizing *ACTB* (β-Actin) as a control (details in section 736), and the results were summarized using GraphPad Prism (version 9.4.1) (GraphPad Software Inc, CA, USA). In terms of ΔΔCt, briefly, an amplification plot was produced to determine the cycle threshold (Ct) value in the quantitative real-time PCR (qRT-PCR) analysis, which represents the point at which the reaction curve intersects with the threshold line. The Ct value indicates the number of PCR cycles required for the fluorescent signal to intercept with the threshold, marking the point of exponential amplification in the PCR reaction.

To calculate the relative gene expression levels, the $2^{-\Delta\Delta Ct}$ method is used. First, the average Ct value for all replicates of each sample is determined. The change in Ct (ΔCt) is then calculated by subtracting the average Ct of the target gene of interest from the average Ct of the housekeeping gene (reference gene). Next, the ΔΔCt is calculated by subtracting the average ΔCt of the control sample (e.g., baseline or untreated sample) from the ΔCt of the treatment conditions (e.g., experimental samples). The $2^{-\Delta\Delta Ct}$ is then computed, which represents the fold change in gene expression between the treatment conditions and the control.

2.4.3 Data analysis

The data obtained from qRT-PCR analysis is presented as the mean and standard deviation unless otherwise specified. Statistical analysis is performed using a two-tailed unpaired Student's t-test to compare two groups with independent samples. A significance level of $P < 0.05$ is considered statistically significant.

To quantify the mRNA expression level of specific genes (Chapter. 4), total RNA was extracted using RNeasy mini kit (Qiagen) following the manufacturer's instructions. RNA concentration was quantified on a Nanodrop Spectrophotometer 2000c (ThermoFisher Scientific, UK), with detailed methods described above. Diluted RNA samples with a concentration of 100 ng/ml were used. Real-time PCR was carried out using gene-specific primers (Table. 2.3), QuantiNova SYBR Green RT-PCR kits (Qiagen) and QuantiTect Primer Assays(Qiagen) according to manufacturer's instruction. The set-up conditions are listed in table. 2.1. The PCR running condition for each cycle was listed in table. 2.2. Triplicates were performed for each sample in a 96-well plate on an ABI PRISM 7000 Sequence Detection Systems (ThermoFisher Scientific, UK). The RNA level for Glyceraldehyde 3-phosphate dehydrogenase (*GAPDH*) or β-actin was used as a control for normalisation of the transcript level using GraphPad Prism. Method of statistical analysis see subsection 2.15.

Condition	Temperature	Time	Cycles
Initial	95°C	15min	1
Denaturation	94°C	15s	35
Annealing	55°C	15s	35
Extension	72°C	30s	35

TABLE 2.1: **Settings for PCR machine (StepOnePlus, ThermoFisher)**

Name of component	Volume (μl)
RNA (100mg/μl)	1
Gene specific primer	1
2x Rotor-Gene SYBR Green PCR Master Mix	10
10x QuantiTect Primer Assay	2
RNase free H_2O	Add to 20 μl

TABLE 2.2: **PCR reaction set up and reaction Conditions**

Gene Name	Reference Code
SNAI1	QT00010010
SNAI2	QT00044128
ZEB1	QT00008555
ZEB2	QT00008554
TWIST1	QT00011956
STK11	QT01008980
GAPDH	QT01192646
ACTA2	QT00088102
COL1A1	QT00037793
COL3A1	QT00058233
FN1	QT00038024
ACTB	QT01680476

TABLE 2.3: **List of qPCR QuantiTect primers (Qiagen, Germany)**

2.5 Western blotting

2.5.1 Protein extraction

Cells were washed with PBS before the addition certain volume(100-200 μl) of 8M urea lysis buffer (Appendix. A.2) and scraped for 1 min. lysed cells were incubated on ice for 30 minutes. The lysate was centrifuged (13,000 g, 10 min, 4°C) each time before quantification.

2.5.2 Protein quantification

Protein lysate was quantified and the concentration was determined using the Bio-Rad Protein Assay Dye Reagent Concentrate (Bio-Rad). Bovine serum albumin (BSA) dilutions (0, 0.5, 1, 2, 4 μl) in 200 μl reagent dye were used to produce a protein concentration standard curve. 1 μl of sample lysate was added to 200μl of diluted reagent dye (1:5) into each well in a Falcon 96 well plate. Triplets were performed for each sample to minimize the random error. Samples were mixed on the plate reader for 1 min before measuring. Protein concentrations were measured via absorbance using a FLUOstar Optima microplate reader (BMG Labtech, UK) and the absorbance was normalized by linear regression using the Optima software.

2.5.3 SDS-PAGE Gel running and nitrocellulose membrane transferring

7 μl of 4 $\times$ NuPAGE LDS sample buffer (Thermo Fisher Scientific) (with 5 % β-mercapoetahnol) was added to 10-30 μg of protein and boiled at 100 $^{\circ}C$ for 5 min before separating on a 10% SDS-PAGE using a Mini Protean tetra cell (Bio-Rad, USA). 1-2 μl of hyperspace pre-stained protein marker (Bioline) was used to separate the proteins according to different sizes. Gels were run at 80 V in SDS for 60 mins and then 150 V for about another 60 min. Gel and running buffer preparation has been attached to Appendix. A.3 and A.4.

After SDS-PAGE separation, proteins were transferred onto a nitrocellulose membrane (GE Healthcare Life Science, UK) at 80 V, 350 amps for 3 hours in a cooled TE 22 mini tank transfer unit (GE Healthcare Life Science) filled with transfer buffer (Appendix. A.5).

2.5.4 Membrance blocking and antibody Incubation

After the transfer process, the nitrocellulose membrane was washed twice with dH_2O and then briefly stained with Ponceau S stain (Sigma Aldrich, UK) for 1 minute. Following three quick rinses with dH_2O, the visualized bands were used to check the transfer's quality and confirm equal loading of each sample. Subsequently, the membrane was blocked in 5% milk TBST for 1 hour on an RT shaker. Primary antibodies (details in Table. 2.4), diluted in blocking buffer, were incubated with the membranes at 4 $^{\circ}$C for 16 hours. After incubation, the membranes were washed for 5 minutes in TBST (see Appendix. A.6) on an RT shaker for three cycles. The secondary antibody (680LT anti-mouse and 800CW anti-rabbit) from LI-COR bioscience, USA, was diluted 1:5000 in 5% fat-free milk.

Antibody	Supplier	Cat-No
β-actin	Santa Cruz	sc-47778
Snail2	Santa Cruz	sc-10436
β-tubulin	Abcam	ab6046
α-SMA	Cell Signalling Technology	14968
LKB1/*STK11*	Cell Signaling Technology	D60C5F10
Snail2	Cell Signalling Technology	9585
β-tubulin	Cell Signalling Technology	86298
LC3	Cell Signalling Technology	2775
p62/*SQSTM1*	Cell Signalling Technology	5114
p65/*RELA*	Cell Signalling Technology	8242
Phospho-Smad2	Cell Signalling Technology	3104
E-Cadherin	BD Transduction Laboratories	610405

TABLE 2.4: **List of Primary Antibodies with Supplier and Cat-No Information**

2.5.5 Blots imaging

Protein bands were visualized using two different infrared channels (680nm/800nm) on the Odyssey imaging systems (LI-COR Bioscience) based on the species of secondary antibodies used. Western blot quantification was carried out using the ImageJ software (National Institutes of Health, USA). The background of the protein bands was first subtracted to minimize noise and improve accuracy. Each band of interest was outlined with a rectangle, ensuring that the size of the rectangle was consistent across all samples for comparability. The integrated density for each band was measured, which represents the sum of the values of the pixels within the selected area. To account for variations in loading and transfer efficiency, the intensity of the target protein bands was normalized against a housekeeping protein, typically β-actin or GAPDH, which was detected on the same membrane. The relative expression levels of the proteins of interest were then calculated based on these normalized values. This method allows for the quantitative comparison of protein levels across different samples under various experimental conditions.

2.6 Cell culture

2.6.1 Cell lines and trypsinisation of cells

All cell lines were maintained in Corning tissue culture (TC) treated flasks or culture dishes incubated at $37°C$ with 5% CO_2 in a humidified incubator, and The capacity of flasks and dishes was chosen based on the number of cells required for the experiments. The complete media for cell culture were obtained from Life Technologies (Paisley, UK) unless specified otherwise. To ensure their viability and

proper growth, regular cell passage was performed with varying frequencies: ATII cells were passaged three times a week, and MRC5 fibroblasts every 4-5 days. To provide essential nutrients for cell growth, complete media were refreshed regularly, typically every other day. Confluency of cells was monitored using a microscope, and when it reached over 90% but not 100%, the adherent cell monolayer was passaged for experiments or routine maintenance. Passage involved the use of 1x phosphate-buffered saline to remove traces of FBS that could interfere with trypsin activity. After trypsinization, cells were centrifuged and re-suspended in fresh complete media for further cultivation. These meticulous procedures ensured the cell lines' proper health and behaviour, preventing complications from over-confluency and maintaining their suitability for experimental purposes. The details of the cell lines and maintenance procedures can be found in table. 2.5.

Cell Line	Originated from	media composition
MRC5	Lung fibroblasts isolated from a male fetus	DMEM with 10% heat-inactivated FBS, 50U/ml Penicillin, 50µg/ml Streptomycin,2mM L-glutamine, 1mM sodium pyruvate, and 1mM non-essential amino acids)
ATII	Type II pneumocytes	DCCM-1 (Biological Industries Ltd, Beit HaEmek, Israel) with 10% heat-inactivated Foetal Bovine Serum (FBS), 1% penicillin, 1% streptomycin and 1% L-glutamine

TABLE 2.5: **Preparation of cell culture media**

2.6.2 Cell thawing and viable cell count

Cells were thawed from either liquid nitrogen or an -80°C freezer and immediately defrosted in a $37°C$ water bath for approximately 1 minute. Once thawed, the cells were transferred to a tissue culture hood, mixed by flicking the tubes, and then added to a new falcon tube. Fresh complete media was added to achieve a final DMSO concentration below 1%, and the cell suspension was mixed by pipetting up and down. After a short centrifugation (300g, 5 minutes), the cells' pellet was resuspended in 10ml of complete media in a T75 TC treated flask and incubated at $37°C$ with 5% CO_2.

After 24-hour cultivation, the cells were refreshed with new complete media to remove any traces of DMSO. For cryopreservation, the cells were trypsinized following the previously mentioned procedures and counted as described. The cell pellet was then re-suspended in freezing media containing 90% FBS (Life Technologies, UK) and 10% DMSO (Sigma-Aldrich, UK). The final cell suspension concentration was adjusted to 1x10 ^{6} cells/ml, and 1ml of this suspension was transferred into each cryogenic vial (STARLAB Ltd, Blakelands, UK). The vials were placed into a Mr. Frosty freezing container (Sigma-Aldrich, UK) overnight at an -80 $^{\circ}C$ freezer before being transferred into liquid nitrogen for long-term storage.

2.7 siRNA reverse transfection

siRNA oligos again LKB1 was purchased from Dharmacon (USA) (Table. 2.6). DharmaFECT 2 (Dharmacon) was used to knock down target genes according to the manufacturer's instructions. ATII cells were seeded in 21cm^2 dishes at 40% confluency the day before transfection. Cells transfected with the indicated siRNA oligos at a final concentration of 35 nM using DharmaFECT 2 reagent (Dharmacon) and Hank's buffered salt solution (HBSS). siGENOME RISC-Free siRNA (Dharmacon) was used as a negative control. After 3 days post-transfection (cells at 37$^{\circ}C$ with 10% CO_2). The fully transfected reaction in ATII cells is ready for Protein or RNA extraction, in the meantime, the conditional medium of absence of LKB1 collected from the Plates is stored in -80$^{\circ}C$ or used for the CM experiment directly.

siRNA	Catalog Number	Company
STK11(LKB1)	MU-005035-02-0010	Dharmacon
SQSTM1(p62)	MU-010230-00-0002	Dharmacon
RELA(p65)	MU-003533-02-0002	Dharmacon

TABLE 2.6: **List of Short Interfering RNA (siRNA) with Catalog Number Information**

2.8 Conditional medium assay

Conditioned media, also known as the cell secretome, consists of proteins processed through the classical secretion pathway with a signal peptide. It also includes proteins shed from the cell surface and intracellular proteins released through non-classical pathways or exosomes. These secreted proteins, such as enzymes, growth factors, cytokines, and hormones, play crucial roles in cell growth, differentiation, invasion, and angiogenesis by regulating cell-to-cell and cell-to-extracellular matrix interactions.

To further investigate the role of LKB1-depleted alveolar epithelial cells in affecting epithelial-fibroblasts microenvironment, conditional media (CM) from ATII cells siRNA transfection with knockdown of LKB1 was seeded at 60% according to the above protocol. MRC5 cells were in the absence or presence of 5 ng/ml TGF- β 1(PeproTech, UK). Similarly, CM from ATII cells treated normal and LKB1(*STK11*) depleted ATII cells were also collected and dosed the MRC5 cells in the absence or presence of 5 ng/ml TGF- β1 (PeproTech, UK). Both the control ATII cells and ATII cells with indicated treatment/CM were incubated for 48 hours ($37^{\circ}C$, 10% CO_2). To eliminate the effect of TGF-β on the conditional media. Fibroblasts were treated with TGF-β1 (PeproTech, UK) at 1:2000 for 2 days prior to a day withdrawal. At the same time, the ATII cell was seeded at 60% confluency the day before dossing the CM. Conditional media were collected from both the control fibroblasts and the TGF-β activated fibroblasts and dosed on ATII cells transfected *STK11* siRNA or control siRNA for 48 hours before further analysis.

2.9 Luciferase reporter assay

Cells were transfected using Lipofectamine 3000 (Life Technologies) in a 96-well plate with 100 ng of Renilla along with 100 ng of NFκB reporter per well. Cells were washed with 1 $\times$ PBS and lysed by trypsin (0.05% trypsin, Gibco), then centrifuged at 500 g for 5 minutes. The cell pellet was then re-suspended in a certain amount of complete media before plating on a 96-well plate (usually 100 μl of medium for each well) at 70-80% confluency. For each well to be transfected, 0.1 μl of Lipofectamine 3000 reagent (Life Technologies) was diluted in 5 μl of Opti-MEM medium. The mixed reagent was made and short-vortexed. Diluted plasmids and Lipofectamine 3000 were mixed by pipetting up and down, and the lipid-DNA mixture was incubated at room temperature for 15 minutes. Cells were transfected at $37^{\circ}C$ for 48 hours before analysis. The transcriptional assay was carried out using the Dual-Luciferase reporter assay system (Promega, UK) following the manufacturer's protocol. Cells were washed with 1 $\times$ PBS prior to lysis in a 96-well plate. Cells were lysed in 100 μl of passive lysis buffer and put on a room temperature shaker for 15 minutes. Freezing lysates at -20 facilitated the lysis. Five μl of lysate was analyzed for each well in a 96-well white plate. Triplets were used for each transfection, and 25 μl LAR II was first added and mixed by pipetting to measure the firefly luciferase activity. Another 25 μl of Stop & Go reagent was then added to help identify the Renilla activity. The final Dual-Luciferase Reporter activity was normalized based on both measurements.

2.10 Generation of Lkb1 KO mice

All animal studies and breeding were carried out under a UK Home Office project license (Julian Downward's lab, project licence PPL No. 70/8095). Mouse lung tissue isolated from inducible Lkb1 $^{-/-}$ mice where deletion of Lkb1 is initiated by the introduction of adenovirus expresses Cre recombinase and the viral delivery method when initiating an experiment. delivered Cre to the lungs of anaesthetized mice using intratracheal instillation (IT) (Figure. 2.1) to infect the whole pulmonary alveoli. Briefly, Cre recombinase is an enzyme derived from the bacteriophage P1. It is widely used in genetic engineering and molecular biology to facilitate site-specific recombination between DNA sequences. Cre recombinase recognizes specific DNA sequences called loxP sites and catalyzes the excision or inversion of DNA segments flanked by these loxP sites. This system is commonly used to create conditional knockout mice, where a gene of interest can be selectively deleted in specific tissues or at specific developmental stages by crossing with mice containing tissue-specific promoters driving Cre expression. Intra-tracheal instillation is a technique used to deliver substances, such as viral vectors or drugs, directly to the lungs. It involves introducing the substance into the trachea (windpipe) of an anaesthetized mouse. The substance is then distributed throughout the entire pulmonary alveoli, which are small air sacs in the lungs responsible for gas exchange. Intra-tracheal instillation is a common method for viral delivery to the lungs in mouse models, as it allows for efficient and targeted transduction of lung cells. It is particularly useful for investigating the effects of gene manipulation or delivering therapeutic agents to study lung-related diseases and conditions. In this study, Cre recombinase was used to induce the deletion of the Lkb1 gene in inducible Lkb1 $^{-/-}$ mice. The intra-tracheal instillation technique was employed to deliver adenovirus expressing Cre recombinase directly to the lungs of the mice, leading to the specific and efficient deletion of Lkb1 in the pulmonary alveoli.

2.11 Harvesting of murine Lungs

During the process of harvesting lung tissue for analysis, several meticulous steps were undertaken to ensure successful extraction and subsequent preservation. Initially, the liver was gently pulled down to reveal the diaphragm, and a small incision was made to collapse the lungs. Careful cutting along the midline of the rib cage followed, with utmost caution taken to avoid damaging the lungs. As many ribs as possible were removed to facilitate access. Delicate forceps were then used to expose the trachea in the neck area, and the thin lining around it was gently torn. Two pieces of 2" suture material were threaded under the trachea and loosely tied. With precision, a small incision was made in the trachea, and a cannula was inserted into

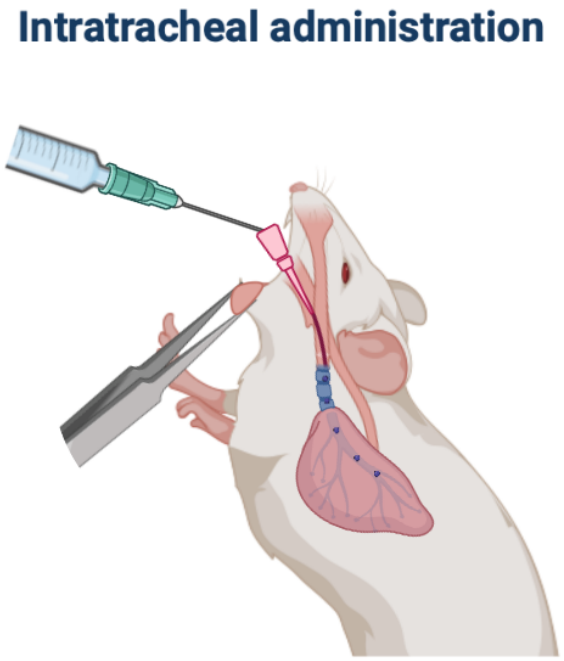

FIGURE 2.1: **Technique of intra-tracheal infection**
The imaging shows the anaesthetized mice placed on the platform and chest hanging vertically. The catheter is inserted into the trachea where the virus can be injected. The mouse illustrations were generated using BioRender.

the thoracic cavity, securely held in place by the tied suture. For lung perfusion, needles were inserted into the right ventricle and left atrium to remove blood. Further access to all lung lobes was gained by severing connections in the abdominal cavity. A 3" suture material was inserted under the right bifurcation of the lung, and the lobes were carefully pulled through and tightly knotted. Subsequently, the lobes on the lung side of the suture were removed, with the inferior lobe preserved in RNA later and the remaining three snap-frozen for protein analysis. The left lobe was inflated with 4% PFA at a stable pressure for a brief period. Afterwards, the lower suture of the trachea was tied off, closing off the PFA, and the cannula was removed. The trachea was fully cut above the ties, and the rib cage on each side was carefully cut to free the lungs, ensuring no damage to the lung tissue. Finally, the lungs were placed in a 30ml tube containing 10ml of 4% PFA for further processing.

2.12 3D spheroid building and co-culture assay

Aggregation of 3D co-cultures was achieved using Nanoshuttle-PL (Greiner Bio-One). Briefly, MRC5 fibroblasts at 80% confluence were treated with Nanoshuttle-PL for 24 h, before trypsinisation as normal. Cells were then pipetted onto cell-repellant 96-well plates sat on a magnetic drive and left to incubate at 37 $^{\circ}C$ and 5% CO2 for a minimum of 3 h on the magnetic drive to enable the spheroid to form. The process

was then repeated for control or LKB1-depleted ATII cells so they could then grow around the existing fibroblast spheroid. LKB1-depleted ATII cells were generated by transfection with LKB1 (STK11) siRNA oligos at a final concentration of 35 nM using DharmaFECT2 reagent (Dharmacon). Details see in Chapter 5.

2.13 Histology

2.13.1 Immunohistochemistry staining (IHC)

Samples were de-paraffinized and rehydrated. Antigen retrieval was done using 0.01 M sodium-citrate buffer (pH 6.0) in a microwave oven. To block endogenous peroxidase activity, the sections were treated with 0.5% hydrogen peroxide in methanol for 10 minutes. After 1 h pre-incubation in 10% normal goat serum to prevent nonspecific staining, the samples were incubated with anti-LKB1 (1:100. Cell Signalling Technology, 13031T), at 4 $^{\circ}C$ overnight. The sections were then incubated with a biotinylated secondary antibody (Vector Laboratories, PK-6101, 1:200) and then incubated with avidin-biotin peroxidase complex solution (1:100) for 30 min at room temperature. Colour was developed with the DAB solution. Counterstaining was carried out using Mayer's haematoxylin. Dehydrate through graded alcohols and tissue clear solution before mounting.

2.13.2 Haematoxylin and eosin staining (H&E)

Dewax embedded sections through Tissue Clear twice and graded IMS, leaving slides in the dH2O for 5 mins. Stain in Mayer's haematoxylin for 5 mins and rinse them in the running tap water for a while before transferring to eosin. After another 5 mins staining, dehydrate through 100% IMS and Tissue Clear before mounting. The Nuclei should be shown as colour Blue, Muscle fibres should be deep pinky red, and the cytoplasm should be varying shades of pink.

2.13.3 RNAscope ISH Assay

The ISH assay is an advanced technique by utilises a unique probe design strategy coupled with an amplification system, it offers high sensitivity and specificity, enabling the observation of target gene expression even at the single-molecule level. One of the standout features of RNAscope is its versatility, as it can be applied to a range of sample types, notably formalin-fixed, paraffin-embedded (FFPE) tissues commonly used in clinical research. Additionally, the assay's multiplexing capability allows for the simultaneous detection of multiple targets within a single tissue,

shedding light on gene co-expression patterns. Importantly, since RNAscope operates within the tissue's cellular architecture, it offers invaluable spatial and morphological context to RNA expression, enhancing our understanding of cellular behaviours and interactions. This method is not only pivotal for basic research but also finds applications in translational and clinical research, including disease diagnosis and biomarker validation. In this chapter, it was designed to detect and visualize RNA molecules within individual cells in tissue samples. The procedure consists of the following steps outlined below. tissue sections were baked for 1 h at 60 $^{\circ}C$, deparaffinized, and treated with pre-treat 1 for 10 min at room temperature (RT). Target retrieval was performed for 15 min at 100 $^{\circ}C$, followed by protease treatment for 15 min at 40 $^{\circ}C$. Probes were then hybridized for 2 h at 40 $^{\circ}C$ followed by RNAscope amplification followed by DAB chromogenic detection.

2.13.4 Immunofluorescence microscopy

Cells were fixed in 4% PBS-paraformaldehyde for 15 min, incubated in 0.1% Triton X-100 for 5 min on ice, then in 0.2% fish skin gelatin in PBS for 1 h and stained for 1 h with an anti-P62 antibody). Protein expression was detected using Alexa Fluor (1:400, Molecular Probes) for 20 min. DAPI (Invitrogen) was used to stain nuclei (1:1000). Samples were observed using a confocal microscope system (Leica SP8). Acquired images were analysed using Photoshop (Adobe Systems) according to the guidelines of the journal.

2.14 Clinical IPF samples and donors transcriptomic profiling database

All human lung tissue samples for primary cell culture were approved by the Southampton and South West Hampshire and the Mid and South Buckinghamshire Local Research Ethics Committees, and all subjects gave written informed consent. Clinically indicated IPF lung biopsy tissue samples and non-fibrotic control tissue samples (macroscopically normal lung sampled remote from a cancer site) were assessed as surplus to clinical diagnostic requirements. All IPF samples were from patients subsequently receiving a multidisciplinary diagnosis of IPF according to international consensus guidelines laser capture microdissection was performed upon Formalin-Fixed Paraffin-Embedded (FFPE) control non-fibrotic lung tissue (alveolar septae, (n=10)) and usual interstitial pneumonia/idiopathic pulmonary fibrosis FFPE lung tissue (fibroblast foci, (n=10) and adjacent non-affected alveolar septae, (n=10)). Total RNA was isolated, and cDNA libraries were prepared using the Ion Ampli-Seq-transcriptome human gene expression kit (Life Technologies, Paisley, UK)

and sequenced using the Ion Torrent Proton Sequencer. A two-stage mapping strategy was used to map the reads to the UCSC hg19 human genome. Cufflinks were used to calculate Fragments per Kilobase of exon per Million (FPKM) values.

2.15 Statistical analysis

Statistical analyses were performed in GraphPad Prism v9.4.1 (GraphPad Software Inc, San Diego, CA) unless otherwise indicated. No data were excluded from the studies, and for all experiments, all attempts at replication were successful. For each experiment, the sample size reflects the number of independent biological replicates and is provided in the figure legend. The normality of distribution was assessed using the D'Agostino-Pearson normality test. Statistical analyses of single comparisons of two groups utilized Student's *t*-test or Mann-Whitney *U*-test for parametric and non-parametric data, respectively. Where appropriate, individual *t*-test results were corrected for multiple comparisons using the Holm-Sidak method. For multiple comparisons, one-way or two-way analysis of variance (ANOVA) with Dunnett's multiple comparison test or Kruskal-Wallis analysis with Dunn's multiple comparison test were used for parametric and non-parametric data, respectively. Results were considered significant if $P < 0.05$, where $* \; P < 0.05$, $** \; P < 0.01$, $*** \; P < 0.001$, $**** \; P < 0.0001$.

Chapter 3

Global transcriptomic changes in LKB1-depleted alveolar type II (ATII) cells

Results shown throughout this chapter are part of the following publication: [1]

3.1 Abstract

It was reported previously that activation of LKB1's downstream effector, AMP-activated protein kinase (AMPK), in myofibroblasts from IPF lungs displays a lower fibrotic activity (Sunad Rangarajan et al. 2018). To determine if, and how, ATII cells responded to the alteration of LKB1 activity, we characterized the global transcriptomic changes in ATII cells upon RNA interference (RNAi)-mediated LKB1 depletion by performing RNA-seq.

Differentially expressed genes (DEGs) were defined by a false discovery rate (FDR)-adjusted P value (Padj) less than 0.05 and $||\text{Log}_2\text{FoldChange}||$ above 1. In total, 763 up-regulated and 664 down-regulated DEGs were identified. Gene Ontology (GO) enrichment analysis was performed and grouped into molecular function, biological process and cellular component. Interestingly, several EMT-related terms were identified, including cell junction, chemotaxis and regulation of cell migration. To provide further mechanistic insights, Gene Set Enrichment Analysis (GSEA) 17 was performed and several Hallmark pathways were identified, including "TNFα signalling pathway via NFκB" and "EMT" as top up-regulated pathways in LKB1-depleted ATII cells, showing as normalized enrichment score(NES) of TNFα

[1] ***Xu Z***, *Davies E R, Yao L, et al. LKB1 depletion-mediated epithelial–mesenchymal transition induces fibroblast activation in lung fibrosis. Genes & Diseases, 2023, ISSN 2352-3042, https://doi.org/10.1016/j.gendis.2023.06.034.*

signalling pathway via NFκB signallings was 2.45 and EMT was 2.03, both FDR of hallmark pathways was significantly less than 0.001.

3.2 Introduction and rationale

IPF is a chronic, progressive, fibrotic lung disease of unknown aetiology (Velagacherla et al. 2022). In IPF the current paradigm of disease pathogenesis proposes that the delicate alveolar architecture of the lung is disrupted by extracellular matrix (ECM) deposition as a consequence of repetitive micro-injuries to the alveolar epithelium, resulting in tissue scarring, increased stiffness and impaired gas exchange.

Gas exchange in the lungs occurs in the alveolar sacs, which are lined with two types of epithelial cells - squamous alveolar type I (ATI) and surfactant-secreting alveolar type II (ATII). While ATI cells are responsible for gas exchange, ATII cells produce surfactant that helps to reduce the surface tension within the alveoli and prevent their collapse.

LKB1 as one of the epithelial targets, is an evolutionarily conserved serine/threonine protein kinase, which acts as an important regulator of cell polarity, proliferation, and cell metabolism in epithelial cells (Lars Kullmann and Michael P Krahn 2018). on the other hand, Many of the best-known functions of LKB1 are attributable to its ability to activate AMPK, which is an important conserved regulator of cell growth and metabolism (Maria M Mihaylova and Reuben J Shaw 2011c). It was reported recently that activation of AMPK in myofibroblasts from IPF lungs displays lower fibrotic activity. In a bleomycin mouse model of lung fibrosis, metformin accelerates the resolution of well-established fibrosis in an AMPK-dependent manner (Sunad Rangarajan et al. 2018).

3.3 Aims and objectives

- To identify the Key signalling pathways and processes that will be altered in LKB1-depleted ATII cells by global transcriptomics analysis. Defined differentially expressed genes(DEGs) can enrich up or downregulated signalling.
- To confirm the role of LKB1 in epithelial cells and downstream biological behaviours' activity via further bioinformatic strategies.

3.4 Methodology

The ATII cells were treated and transfected with siRNA against indicated siRNAs for 48h. The cell culture processes and siRNA reverse transfection methods used in this study are outlined in Chapter 2, Sections 2.6 and 2.7, respectively. Total RNA was isolated using RNeasy mini kit (Qiagen) according to the manufacturer's instructions and quantified using a Nanodrop Spectrophotometer 2000c (Thermo Fisher Scientific). For information on processing the global transcriptomics dataset utilized in this study, please refer to Section 2.1 in Chapter 2. Briefly, a total amount of 3 μg RNA per sample was used as input material for library construction. Sequencing libraries were generated using NEBNext ® UltraTM RNA Library Prep Kit for Illumina ® (NEB, Ipswich, Massachusetts, USA) following manufacturer's instruction. Libraries were pooled in equimolar and sequenced using the paired-end strategy (2×150) on the Illumina NovaSeq 6000 platform following the standard protocols (Novogene, UK). Raw read counts were imported into RStudio (version 4.2.0) and analyzed by using DESeq2 (Love, Huber, and Anders 2014a) (version 1.26.0). Transcripts with low abundance (under 10 counts across all samples) were removed. The R codes were provided in the Supplementary Materials. Genes with a false discovery rate (FDR) adjusted P value using the Benjamini-Hochberg (BH) method less than 0.05 and $\|\text{Log}_2\text{FoldChange}\|$ above 1 were considered as differentially expressed genes (DEGs). DEGs in LKB1-depleted ATII cells are provided in the Supplementary tables.

The collection of Hallmark gene sets generated from the gene set enrichment analysis (GSEA) software (version 4.1.0) (with registration) (Subramanian et al. 2005). Gene Ontology (GO) terms and Hallmark enrichment analysis of DEGs were generated through DAVID website tools (https://david.ncifcrf.gov) with default parameters. FDR-adjusted P values by the Benjamini-Hochberg (BH) method were used to estimate the statistical significance. Details for GO enrichment analysis and Gene Set Enrichment Analysis (GSEA) are provided in Supplementary information and section 2.1.3.

3.5 Results

3.5.1 Identification of Differentially Expressed Genes (DEGs) using integrated bioinformatics.

We first conducted a comprehensive analysis of the transcriptomic changes in alveolar epithelial type II cells that were transfected with either siRNAs against LKB1 (siLKB1) or control siRNA (Control). After ensuring the quality of the RNA samples, we outsourced the RNA-sequence assay to Novogene. Subsequently, the raw data was

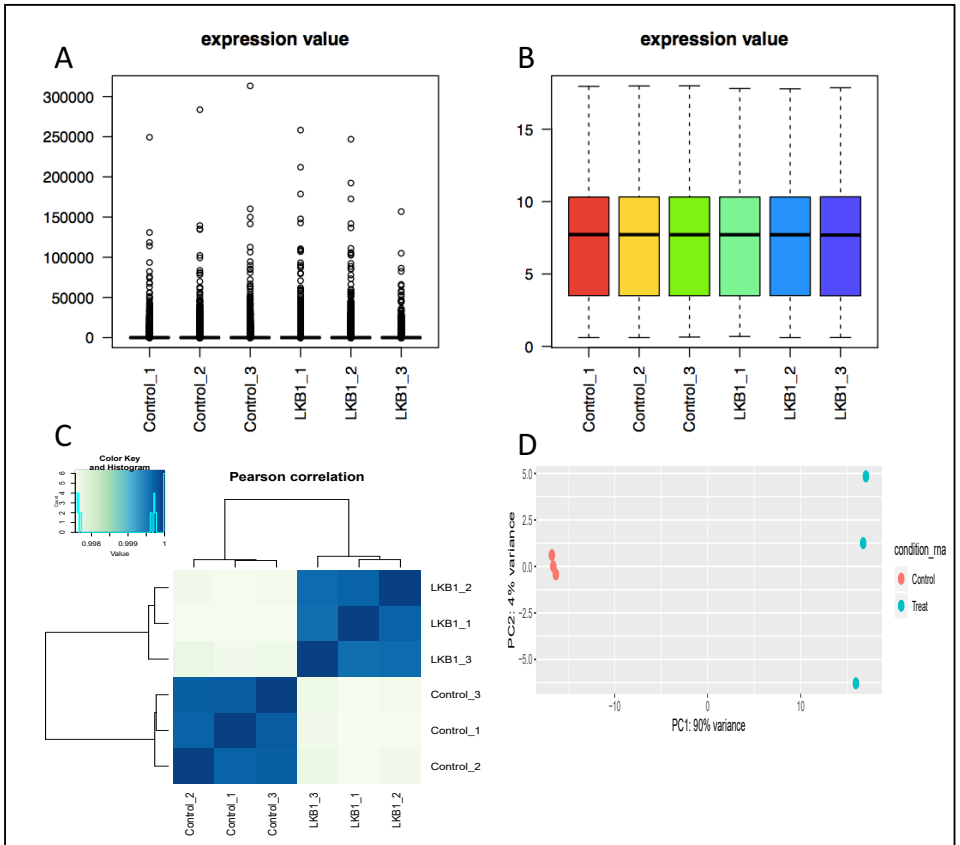

Figure 1. The normalized distribution in the RNA-seq dataset by knockdown of LKB1 in ATII cells.

FIGURE 3.1: **Qualified distribution of LKB1 depletion in ATII cell VS Control** ATII cells were transfected with LKB1 siRNA or control siRNA for 3 days, followed by RNA-Seq analysis. and Covariance of all samples and built a matrix that represents the overall feature of the data shown by scatter plot (A), box plot (B), correlation heatmap (C), and principal component analysis (PCA) (D). indicated samples by control siRNA (Control, in red) or siRNA against LKB1 (LKB1, in blue). Each point represents an RNA-Seq sample. Samples that have similar gene expression patterns are clustered together. LKB1 depletion and control expression data, 3 replicates each.

normalized and analyzed for differential gene expression enrichment. To be included in the analysis, a gene needed to have at least two valid quantification values from the three replicates, and a false discovery rate (FDR) adjusted P value less than 0.05 was used to identify differentially expressed genes (DEGs). Following normalization and imputation of the raw data, a total of 20,516 qualified expressed genes were identified under standard conditions. To better visualize and compare the relationship between the treatment groups and replicates, we presented all data using a heatmap of Pearson correlation and principal components analysis (PCA) (Figure. 3.1). The results indicated that the group of replicates was primarily distinguished by the different treatments administered.

The present study conducted a differential expression analysis on a given dataset. In the absence of foldchange consideration, a total of 4,581 up-regulated and 4,478 down-regulated differentially expressed genes (DEGs), with a significant differential expression ($Pvalue < 0.05$), were observed between LKB1 siRNA transfected ATII

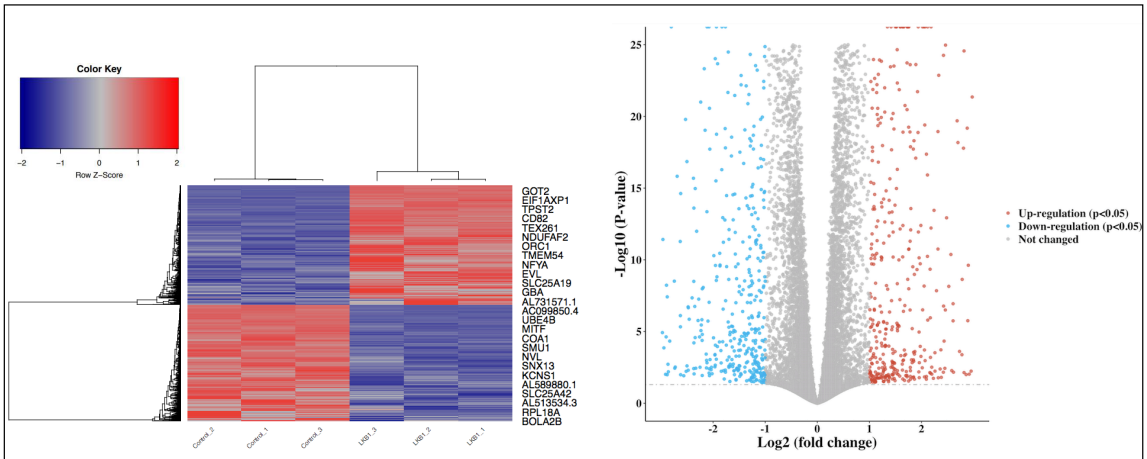

Figure 2. Heatmap and Volcano plot of DEGs in siLKB1 RNA-seq dataset. P-value<0.05; log(FDR)>1; red indicates up-Regulation and blue down regulation.

FIGURE 3.2: **Distribution of up and down-regulated DEGs in ATII cells transfected with siRNA against LKB1 vs control siRNA**

(A) Heatmap showing the top 15 DEGs in RNA-Seq dataset from siLKB1 VS control in ATII cells. $P - value < 0.05$. The colours red and blue indicate up-regulation and down-regulation, separately. (B)Volcano plot showing the distribution of DEGs. Grey dotted lines indicate the threshold for P-value =0.05. Blue and red points represent down-regulated and up-regulated differentially expressed genes respectively.

cells and control group. DEGs with a P value < 0.05 and Log[Foldchange] > 1 were considered significant. The top 15 DEGs for the entire dataset were visualized using a heatmap, and all DEGs were highlighted in a Volcano plot (Figure. 3.2).

3.5.2 Gene Ontology (GO) functional and Hallmark pathway enrichments analysis

We conducted gene ontology (GO) enrichment analysis of differentially expressed genes (DEGs) using the PANTHER tool, categorizing the results into molecular functions (MF), cellular component (CC), and biological process (BP) groups. Our focus was on the cohort of up-regulated DEGs, as previous evidence has suggested that LKB1 loss plays a crucial role in exacerbating metabolism. Additionally, up-regulated genes and proteins are known to be associated with cell-cell communication and several EMT-related terms were identified in the GO analysis, including cell junction, chemotaxis and regulation of cell migration (Figure. 3.3). Our findings showed that knocking down LKB1 in ATII cells led to an ATP level imbalance due to the energy sensor feature, and GO analysis revealed the identification of several disease-related pathological terms, including ribonucleoprotein complex biogenesis, regulation of cellular stress response, and cell death (Figure. 3.4).

Limma is a widely used package in R for analyzing differential gene expression from RNA sequencing data. It allows for robust comparison of normalized gene expression values between different sample sets. Limma uses a linear model to estimate the fold changes and p-values for each gene between the two sample sets, and it corrects for

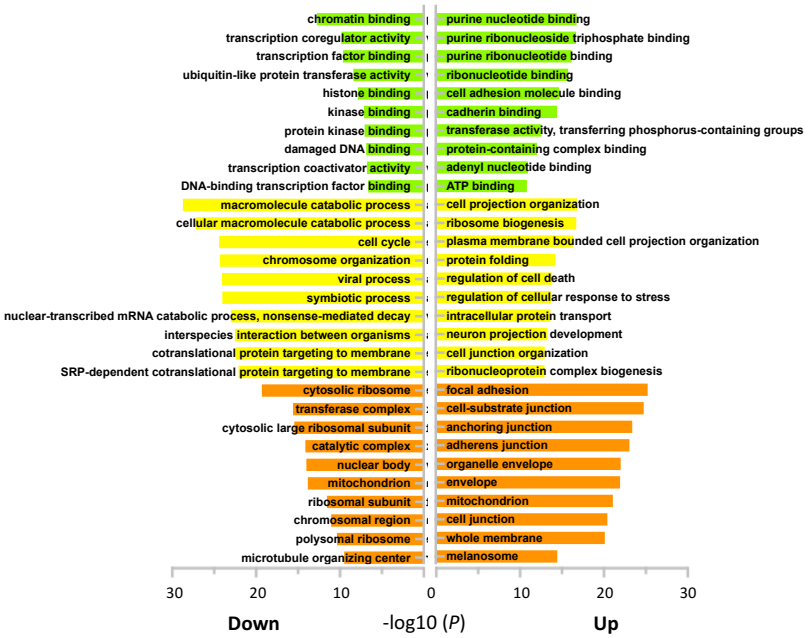

FIGURE 3.3: **Bar plot of Gene Ontology (GO) enrichment of upregulated and down-regulated differentially expressed genes (DEGs) in 3 groups**
Cellular component (orange), biological processes (yellow), and molecular functions (green) exhibits, Respectively. The top 10 enriched GO terms are arranged in -Log10(P-value).

multiple testing using methods such as the Benjamini-Hochberg procedure, and ANOVA test. However, differential expression analysis alone may not provide a complete picture of the biological processes and pathways involved in the phenotype differences between the two sample sets. GSEA is a complementary analysis that allows for the identification of enriched molecular phenotypes, by taking into account the entire set of genes associated with a particular process or pathway, rather than just those that are significantly differentially expressed.

To perform GSEA, a pre-defined list of genes associated with a particular process, such as a gene ontology or Hallmark dataset, is used. The Limma output is then ranked based on differential expression between the two sample sets, and GSEA is used to determine whether the pre-defined gene set is enriched at the top or bottom of the ranked list. GSEA provides a more holistic and quantitative way of identifying enriched phenotypes than classical differential expression analysis, as it considers all genes associated with a particular phenotype.

As demonstrated above, We utilized Gene Set Enrichment Analysis (GSEA) to perform enrichment analysis of differentially expressed genes (DEGs) in our dataset, and the most significantly enriched pathways were analyzed using Hallmark genes hit analysis. Among the up-regulated genes, the top three enriched pathways were TNF α signalling via nuclear factor- κB (NF κB), epithelial-mesenchymal transition (EMT), and KRAS signalling Up, as revealed by gene set enrichment of Hallmark

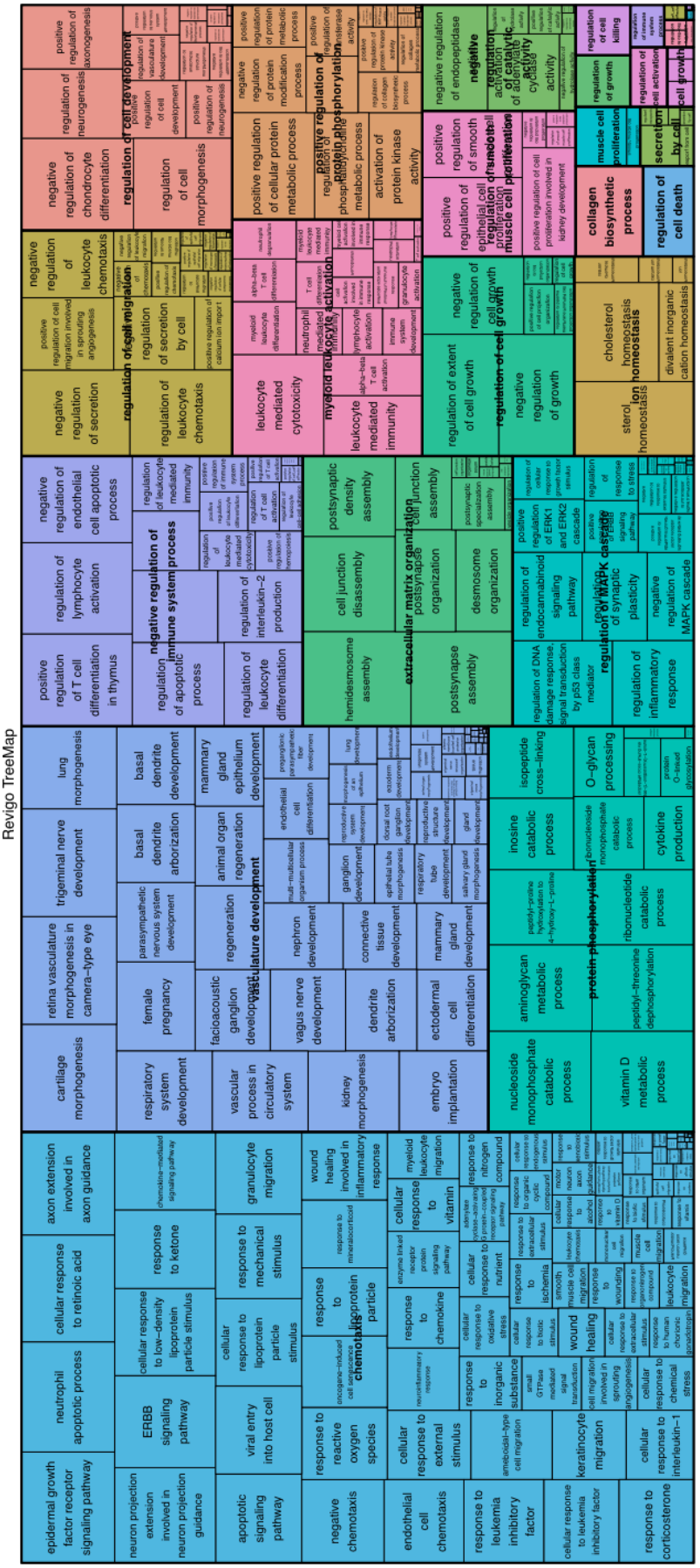

FIGURE 3.4: **REVIGO TreeMap of Biological Process of Gene Ontology (GO) analysis for upregulated differentially expressed genes (DEGs) in LKB1-depleted ATII cells**

Common colours represent groupings based on parent GO terms, and each rectangle is a percentage of the relative enrichment of the Biological processes compared with the whole genome. Genes with a false discovery rate (FDR) less than 0.05 and —Log2FoldChange— above 1 were considered DEGs.

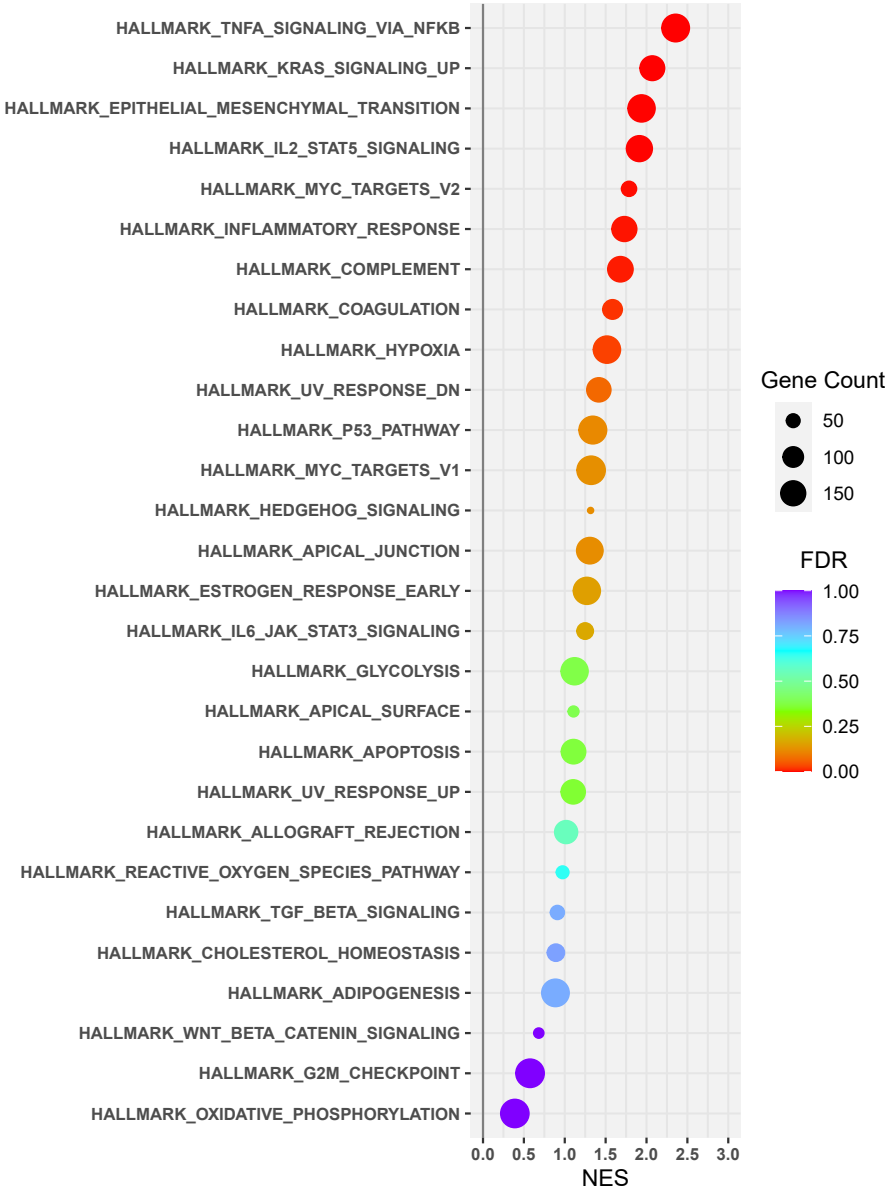

FIGURE 3.5: **Scatter plot showing Gene Set Enrichment Analysis (GSEA)** Results are ranked by the normalised enrichment score (NES). The colour and size of the dots represent the false discovery rate (FDR) and gene counts, respectively.

pathways analysis (Figure. 3.5, B.1). In addition, the knockdown of LKB1 resulted in the inflammatory response, and several common situations in patients with IPF, such as hypoxia and apoptosis, were also enriched in the down-regulated gene list (Figure B.2).

3.6 Discussion

Our investigation focused on elucidating the response of alveolar type II (ATII) cells to alterations in LKB1 activity. By employing RNA interference (RNAi) to deplete LKB1, we characterized the global transcriptomic changes in ATII cells using RNA-seq. Our analysis identified 763 up-regulated and 664 down-regulated differentially expressed genes (DEGs), with several enriched terms related to epithelial-to-mesenchymal transition (EMT), such as cell junction, chemotaxis, and regulation of cell migration. Moreover, Gene Set Enrichment Analysis (GSEA) revealed significant up-regulation of hallmark pathways, notably including the "TNF α signalling pathway via NF κB" and "EMT". These findings shed light on the molecular mechanisms underlying LKB1-mediated regulation of ATII cells and provide potential therapeutic targets for conditions such as idiopathic pulmonary fibrosis (IPF) associated with LKB1 dysregulation.

Regarding the analytical approach, employing siRNA for gene knockdown in signalling pathway studies offers specificity, temporal control, reversibility, and cost-effectiveness. This method allows precise manipulation of target genes, and observation at various stages, facilitates recovery studies, and is suitable for pathway analysis. Analyzing global transcriptomic changes following LKB1 knockdown in epithelial cells provides comprehensive insights into the downstream effects, cellular responses, signalling pathways, and potential therapeutic implications associated with LKB1 dysfunction. In gene function research, the focus is often on analyzing upregulated genes and pathways post-gene knockout, as they directly unveil the gene's functions and biological impacts. These upregulated elements commonly signify compensatory responses or pathological changes resulting from gene knockout, and they may present potential therapeutic targets. Neglecting downregulated genes and pathways risks overlooking critical biological information and disease mechanisms. A comprehensive analysis that encompasses both upregulated and downregulated genes provides a more thorough understanding of the effects of gene knockout.

Research into the role of LKB1 in lung cancer invasion and metastasis is gaining momentum. On the one hand, Studies in Drosophila indicate its involvement in regulating cell polarity, potentially linked to epithelial-to-mesenchymal transition (EMT) (Thiery et al. 2009). In LKB1-knockdown cells exhibiting a mesenchymal phenotype, the expression of Yes-associated protein (YAP) positively correlates with that of ZEB1. This suggests a direct regulatory relationship between the Hippo pathway effector YAP and ZEB1. In the context of LKB1 dysfunction affecting EMT in epithelial cells, it remains uncertain whether ZEB1 or other transcription factors mediate this process. Our transcriptomic analysis in this chapter does not provide

conclusive evidence to definitively attribute the regulation of EMT solely to ZEB1 or any specific transcription factor.

It is not unexpected to find the involvement of the TNF α signalling via nuclear factor- κB in this context. NF-κB is a dimeric transcription factor that plays a crucial role in responding to cellular stress by modulating the expression of target genes (Mulero et al. 2019). This protein complex is found in the cytoplasm of all cells and, upon activation, translocates to the nucleus. Activation of NF-κB can be triggered by free radicals and toxins. Once activated, NF-κB regulates the expression of various inflammatory agents, including enzymes like COX-2 and iNOS, as well as mediators such as IL-1β, IL-6, TNF-α, and TGF-β. These mediators are closely associated with the development of pulmonary fibrosis, particularly TGF-β (Serasanambati and Chilakapati 2016; Tilborghs et al. 2017; Qin et al. 2018).

NF-κB impacts various cellular processes by controlling the expression of numerous genes, particularly those related to immune and inflammatory responses. As a result, it has a crucial role in governing inflammation, cell growth, and programmed cell death (Serasanambati and Chilakapati 2016; Jin'en Wu et al. 2018). Moreover, NF-κB significantly influences multiple cellular functions, including the proliferation of cells such as fibroblasts, inflammation management, and cell differentiation (Alvira 2014; Hou et al. 2018).

Researchers have highlighted the crucial role of inflammatory mediators, such as transforming growth factor beta (TGF-β) and tumour necrosis factor-alpha (TNF-α), in promoting the proliferation and thickening of the smooth muscle layer (J. Liu et al. 2016). Similarly, evidence emphasized that bleomycin (BLM) triggers oxidative stress, leading to increased production of reactive oxygen and nitrogen species (Zaafan et al. 2016). These reactive species, in turn, activate numerous genes involved in cell growth and cell death processes. This can be attributed to the fact that numerous inflammatory cells are attracted to and proliferate in damaged areas, leading to the production of various cytokines that cause further recruitment of cells and remodelling of the matrix, ultimately resulting in an excessive production of collagen and other matrix components (Fanny et al. 2018). Additionally, several inflammatory cytokines, particularly TGF-β, are generated from the damaged lung tissue, primarily through the activation of the NF-κB pathway, which in turn stimulates the production of fibroblasts (L. Zhao et al. 2019). TGF-β can be secreted in the lung via macrophages, alveolar epithelial cells, endothelial cells, and fibroblasts including myofibroblasts (Frangogiannis 2020; Border and N. A. Noble 1994). Moreover, activation of TGF-β will stimulate the recruitment and proliferation of macrophages and fibroblasts (Comeglio et al. 2019; Shamskhou et al. 2019), which subsequently results in increased collagen deposition (A. Okamoto et al. 2017). Similarly, in a study, four weeks of BLM administration led to an overexpression of NF-κB in the lung tissue, observing a significant increase in the percentage area of positive immune reaction in the lungs of

the BLM-treated group compared to the control groups (El-Bassouny et al. 2021). Much evidence showed that the NF-κB signalling pathway can be activated by BLM and plays an important role in controlling inflammation (S.-L. Tian et al. 2018; H. Tang et al. 2016). As well as it has an important role in BLM-induced pulmonary fibrosis (Alvira 2014; Hou et al. 2018). In addition, the Activation of Toll-like receptor 4 (TLR-4) signalling in fibroblasts, which is a regulator of NF-κB, leads to increased collagen deposition and elevated expression of various genes involved in tissue repair and extracellular matrix (ECM) regulation (Sabry 2020).

In the next chapter, further investigation is needed to understand how the loss of LKB1 in epithelial cells promotes the occurrence of EMT through the mediation of the NF-κB pathway, and what factors are responsible for activating the NF-κB pathway due to the loss of LKB1. Is the loss of LKB1 in epithelial cells, potentially due to the activation of the aforementioned pathways, a critical factor in the development of pulmonary fibrosis?

Chapter 4

LKB1 depletion leads to autophagy inhibition-mediated EMT via the p62-NFκB-Snail2 pathway in ATII cells.

Results shown throughout this chapter are part of the following publication: [1]

4.1 Abstract

As stated previously in the chapter, GSEA identified "Hallmark_EMT" positively enriched upon LKB1 (*STK11*) depletion in ATII cells. In the RNA-seq analysis, knockdown of LKB1 (siRNA *STK11*) in ATII cells led to significant increases in the expressions of *VIM* (Vimentin, a mesenchymal marker) and several EMT-transcriptional factors, in particular *SNAI2* (Snail2), and a reduction in *CDH1* (E-cadherin, an epithelial marker). The changes in their mRNA levels were verified with real-time qPCR. In addition, the increased protein level of Snail2 and decreased E-cadherin were observed upon LKB1 depletion in ATII cells as shown by western blot. Together, these results demonstrate that LKB1 inactivation can activate the EMT programme in ATII cells. The top enriched pathway upon LKB1 depletion in ATII cells was the "Hallmark_TNFα signalling pathway via NFκB". To verify this, we assessed NFκB activity using a reporter assay under different conditions. LKB1 depletion in ATII cells increased NFκB activity above 2-fold.

[1] ***Xu Z***, *Davies E R, Yao L, et al. LKB1 depletion-mediated epithelial–mesenchymal transition induces fibroblast activation in lung fibrosis. Genes & Diseases, 2023, ISSN 2352-3042, https://doi.org/10.1016/j.gendis.2023.06.034.*

We have previously demonstrated that autophagy inhibition-induced accumulation of p62/SQSMT1 can activate the NFκB pathway (Charlotte Hill, Juanjuan Li, et al. 2019; Yihua Wang, Hua Xiong, et al. 2019). The impact of LKB1 on autophagy activity in ATII cells was explored. LKB1 depletion in ATII cells led to autophagy inhibition, as demonstrated by a decreased level of LC3-II and increased p62 by western blot analysis as well as p62 puncta staining by immunofluorescence. We then checked if LKB1 depletion induces EMT via the p62-NFκB-Snail2 pathway in ATII cells. Depletion of p62 abolished the increase in NFκB activity induced by LKB1 knockdown, suggesting that LKB1 depletion in ATII cells triggers the NFκB pathway via p62. Functionally, p65 or p62 knockdown abolished the increase in the Snail2 expression induced by LKB1 depletion in ATII cells. Taken together, these results demonstrate that LKB1 inactivation in ATII cells triggers autophagy inhibition and promotes EMT via a p62-NFκB pathway.

4.2 Introduction and Rationale

Autophagy is a meticulously regulated biological process conserved through evolution, responsible for the degradation of long-lived proteins and damaged organelles. Currently, manipulating autophagy is being explored as a therapeutic strategy in several fields, including neurodegenerative diseases and cancer. However, diminished autophagic activity has been observed in a variety of human diseases, including Idiopathic Pulmonary Fibrosis. In the context of IPF, ageing stands as a primary risk factor, contributing to its development, with cases being rare in individuals below 50 years of age. Ageing has been associated with reduced autophagy in several contexts, including IPF. This study substantiates these findings, illustrating prominent p62/SQSTM1 immunostaining in IPF epithelial cells within thickened alveolar septae, a contrast to the weak signals found in control lungs. Furthermore, a significant decrease in SQSTM1 (p62) mRNA levels was noted in IPF epithelial cells compared to controls, suggesting an increase in p62/SQSTM1 protein levels due to reduced autophagic activity. Together with previous data, these results suggest a down-regulation of autophagic activity in IPF epithelial cells.

The concept of Epithelial-Mesenchymal Transition (EMT) is well established in embryonic development and also plays critical roles in wound healing, cancer metastasis, and fibrosis. The orchestration of EMT involves complex signalling pathways, including TGF-β, fibroblast growth factor, Wnt/β-catenin, and epidermal growth factor (*EGF*), among others. A pivotal event in EMT is the loss of E-cadherin, which is suppressed by potent repressors such as Snail1/2, ZEB1/2, and other basic helix-loop-helix factors. While EMT's role in cancer is detrimental, it can facilitate beneficial responses to injury through wound healing; however, an exaggerated wound-healing process can lead to fibrosis. Recent research illustrates the interaction

between autophagy and EMT in several disease contexts, with one study demonstrating that autophagy inhibition induces EMT via the p62/SQSMT1-NFκB/RELA pathway in RAS-mutated cancer cells, predominantly through ZEB1 upregulation. In contrast, in lung alveolar epithelial cells, autophagy inhibition induces EMT sans RAS activation, exclusively via Snail2 upregulation, highlighting the cellular context dependency of this effect. The significance of Snail2 in IPF is further underscored, with elevated levels noted in IPF lung epithelial cells compared to controls, potentially contributing to the fibroblast pool through Snail2-mediated EMT, fostering fibroblast activation via Snail2-regulated paracrine signalling.

4.3 Aims and Objectives

The objectives of Chapter 3 were to identify the signalling activated by LKB1 underlying epithelial-mesenchymal transition (EMT) in ATII cells.

Thus, in this chapter, we aimed to:

- confirms the role of LKB1 depletion associated with EMT in alveolar epithelial type II cells via confirming the A group of transcription factors (EMT-TFs).
- investigate whether LKB1 can induce EMT and can cause autophagy inhibition and NFκB signalling pathway activation by immunofluorescence staining or DNA reporters.
- verify whether the aforementioned signalling pathways or biological behaviours are interrelated with each other Utilizing double STK11 siRNA and p62 (autophagy cargo) siRNA or p65 (subunit of the NFκB complex) siRNA knockdown at a cellular level to verify their correlations. For instance, whether the EMT induced by LKB1 depletion is due to the suppression of autophagic activity initiating the NFκB pathway.

4.4 Methodology

4.4.1 Cell biology

Cell Lines of ATII cells used in this stage were listed in table. 2.4 and the details of cell processing referring to 2.6. Briefly, Cells were thawed from liquid nitrogen and diluted in corresponding media (Life technology) and the media was changed after a 48-hour cultivation at $37°C$. Cells were incubated at $37\ °C$ supplied with 10% CO_2.

Adherent cells were passaged 2-3 times per week. 2 ml of PBS was added to wash the cells before 0.05% trypsin (Life technology) was added and incubated. The detached cells were observed using an EVOS XL Core microscope (Life technology). The mixture was then centrifuged at 400 g for 5 mins and the cells were re-suspended in fresh pre-warmed medium for further use, normally diluting 1:2-1:5 for further plating. For cell counting, A sample of cells was diluted using an equal volume of trypan blue (Sigma Aldrich). The number of cells was determined by a light EVOS XL Core microscope (Life technology) and the average number of unstained cells in 8 Neubauer counting chambers $\times$ 104 indicated the total number of living cells in a plate. The number of cells in a 6-well plate before transfection was 4 $\times$ 104 cells with 2 ml of medium while the number for a 10 cm dish was 2 $\times$ 105 cells with 10 ml of media.

The further molecular analysis and validations, such as Western Blots, immunofluorescence staining, reporter assays, and qRT-PCR For detailed descriptions of the methodologies employed, please refer to section 2.5, 2.13.4, 2.9, and 2.4.2 in the respective sections of chapter 2. These are conducted based on insights obtained from global transcriptomic studies, particularly those identified through Gene Set Enrichment Analysis (GSEA) (Details are in section 2.1.3).

4.5 Results

4.5.1 LKB1 depletion in ATII cells induces EMT.

Our recent global transcriptomic analysis aligns well with our previous findings, indicating significant changes in the behaviour of epithelial cells. We observed an increase in the expression levels of *Vimentin*, *Snail2*, and *ZEB1/2*, and a decrease in *CDH1*(E-cadherin) expression. This suggests that the epithelial cells are losing their polarity, promoting the activation of fibroblasts.

Given our findings, we sought to evaluate the potential role of EMT in the pathogenesis of IPF, by utilising the hallmark EMT gene set (M5930, https://www.gsea-msigdb.org/). Raw counts in the RNA-seq dataset were matched to those in the hallmark EMT gene set to determine expression. The global transcriptomics changes in LKB1-depleted ATII cells indicated that the EMT is activated in ATII cells upon LKB1 depletion (Figure. 4.1). Besides the global transcriptomic results, To confirm this finding and investigate whether the EMTIFs altered by LKB1 were abolished in epithelial cells, we conducted qRT-PCR analysis on ATII cells transfected with LKB1 siRNA (cells incubated for 2 days and processed protein assay). it suggested that significant up-regulation of *CDH1*, *Vimentin*, *SNAI2*, *ZEB1* and *ZEB2*, consistent with our RNA-Seq results (Figure. 4.2). We also observed

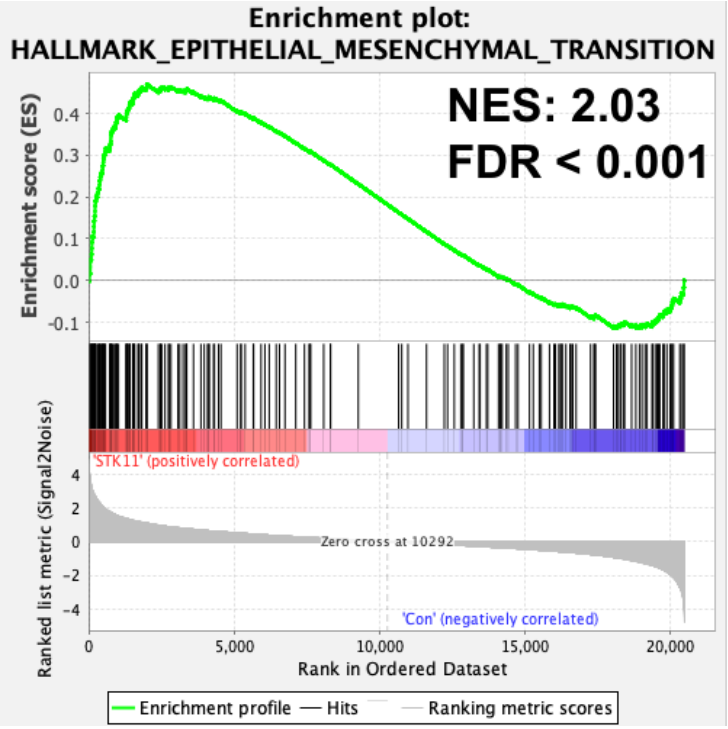

FIGURE 4.1: **Gene Set Enrichment Analysis (GSEA) plot showing the enrichment of Hallmark_Epithelial-Mesenchymal Transition in LKB1-depleted ATII cells**
Normalised enrichment score (NES) and false discovery rate (FDR) are indicated.

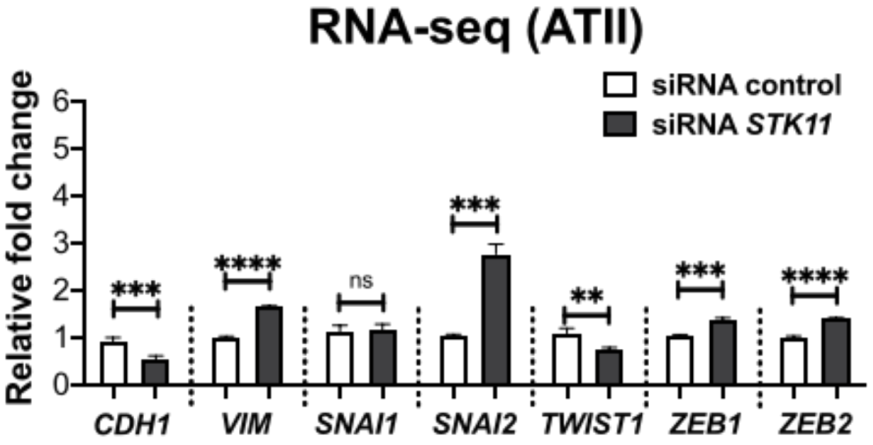

FIGURE 4.2: **RNA-seq data showing relative expressions of *CDH1*, *Vimentin*, *SNAI2*, *ZEB1* and *ZEB2* in LKB1-depleted ATII cells vs. control**
$*$ $P < 0.05$, $**$ $P < 0.01$, $***$ $P < 0.001$, $****$ $P < 0.0001$ ns: not significant.

a significant down-regulation of E-cadherin protein expression in ATII cells transfected with LKB1 siRNA (Figure.4.3). Together, these results demonstrate that LKB1 inactivation can activate the EMT programme in ATII cells.

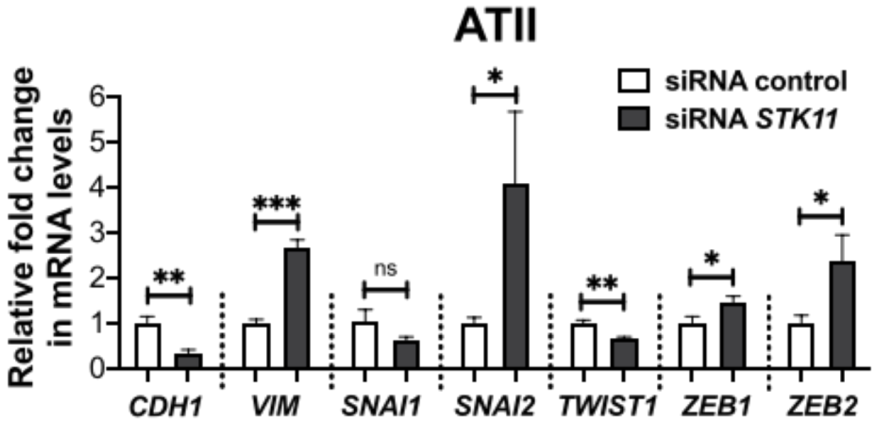

FIGURE 4.3: **Relative fold changes in mRNA levels of *CDH1* (E-cadherin), *VIM* (Vimentin), *SNAI1* (Snail1), *SNAI2* (Snail2), TWIST1, ZEB1 and ZEB2 in LKB1-depleted ATII cells vs. control**
β-actin normalised mRNA levels in ATII cells were used to set the baseline value at unity. Data are mean $\pm$ s.d; $n = 3$ samples in each group. $* P < 0.05$, $** P < 0.01$, $*** P < 0.001$, $**** P < 0.0001$ ns: not significant.

4.5.2 LKB1 depletion leads to autophagy inhibition-mediated EMT via the p62-NFκB-Snail2 pathway in ATII cells.

Initially, when we started exploring LKB1 in our group, we suspected that its role in ATII cells was closely linked with ZEB1, primarily due to the KRAS upregulation induced by ZEB1, as referenced in figure. 4.4, 4.5), performed by Dr. Yihua Wang. However, as we progressed, it became clear that ZEB1's role as a mediator between LKB1 and EMT is minor compared to the substantial effect observed when Snail2 is up-regulated by suppressing LKB1 in ATII cells. This observation is further emphasized in our Protein-Protein Interaction (PPI) network, which highlights the significant role of Snail2 when LKB1 is silenced in ATII cells, as shown in figure. 4.6.

To understand better the function of LKB1 in facilitating communication between epithelial cells with others, we utilized a combination of bioinformatics tools and PPI analysis. This approach helped us identify a group of up-regulated genes (DEGs) that respond to LKB1 depletion in ATII cells. We then integrated the predicted secreted proteins with RNA-seq data, contrasting LKB1 depletion with control scenarios. Using the STRING database and Cytoscape software (Doncheva et al. 2018), we constructed a PPI network of these up-regulated and secreted genes, refining it by removing isolated and partially connected nodes. The finalized network points to MMP9 and SNAI2 as central figures in the protein network following LKB1 depletion in ATII cells, as depicted in figure 4.6. This data indicates that MMP9 and SNAI2 might be critical in guiding the interaction between epithelial cells and fibroblasts, especially in the context of LKB1 depletion.

Notably, *SNAI2* showed the highest up-regulation, with a fourfold increase (Figure. 4.7). Our previous research has demonstrated that *SNAI2* is not only an EMT transcription factor but also regulated by autophagy inhibition mediated by p62

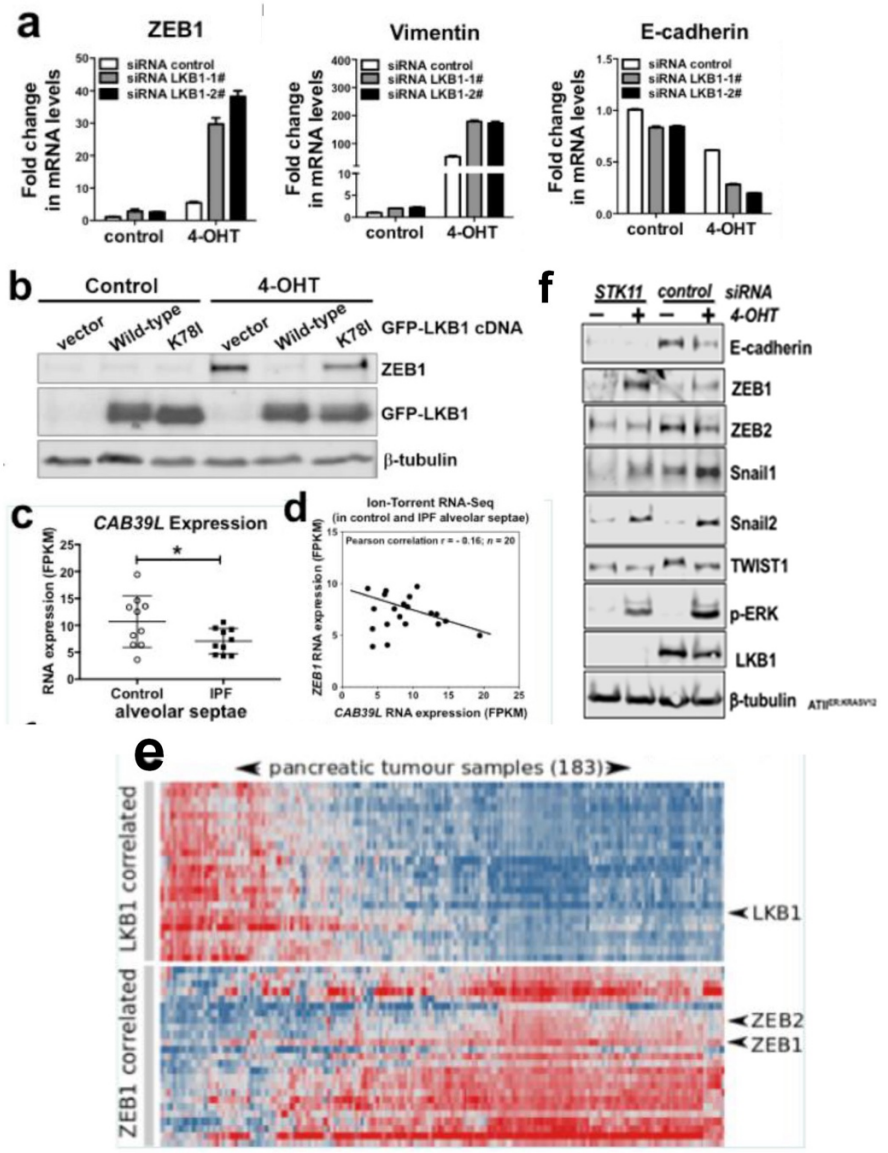

FIGURE 4.4: **Evidence for LKB1 related to ZEB1 expression induced by RAS**
(A) mRNA expression of ZEB1, Vimentin, and E-cadherin in RAS-inducible cells with indicated treatments. mRNA levels normalised by β-actin in control siRNA transfected cells were used to set the baseline value at unity. (B) Cells were transfected with wild-type or the kinase-dead K78I mutant GFP-LKB1. Expression of ZEB1 was analysed by western blotting. (C) CAB39L expression is decreased in IPF alveolar septae. (D) Expression of CAB39L and ZEB1 is anti-correlated in alveolar septae. (E) Top-25 most correlated expression profiles for LKB1 (upper panel) and ZEB1 (lower panel) across a big dataset. Heatmap: Red=maximum, blue=minimum. (F) A representative image is shown in Western blots analysis. LKB1 depletion in ATII cells combined with Ras activated by 4-OHT increased the expression of Snail2, and ZEB1 and decreased the E-cadherin.

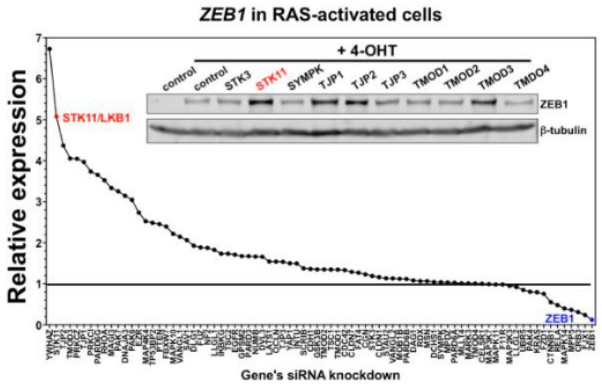

FIGURE 4.5: **Knocking down *STK11* as top hit promotes ZEB1 expression**
Protein levels of ZEB1 in RAS-activated cells with the indicated siRNA transfection. Cells transfected with control siRNA or siRNA against individual genes for 3 days were treated with 4-OHT for another day. Protein levels normalised by β-tubulin in control siRNA transfected 4-OHT-treated cells were used to set the baseline value at unity. Data are average from 2 independent experiments. Inserts are western blots of ZEB1 with the indicated siRNA transfection.

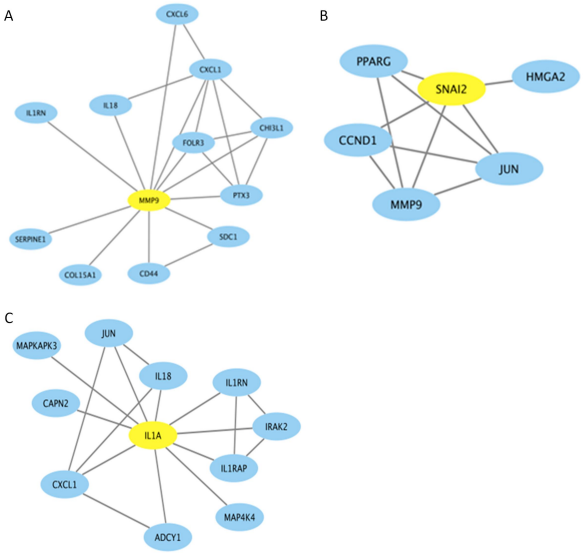

FIGURE 4.6: **PPI network analysis of up-regulated proteins/genes correlation in siLKB1 RNA-seq dataset generated in String.db (v. 11) and visualized in Cytoscape (v. 3.7.1)**
(A)(B) Representative local association graphs in PPI networks. (C) Representative secreted proteins graphs in PPI networks. Nodes indicate proteins/genes and lines indicate protein-protein interaction.

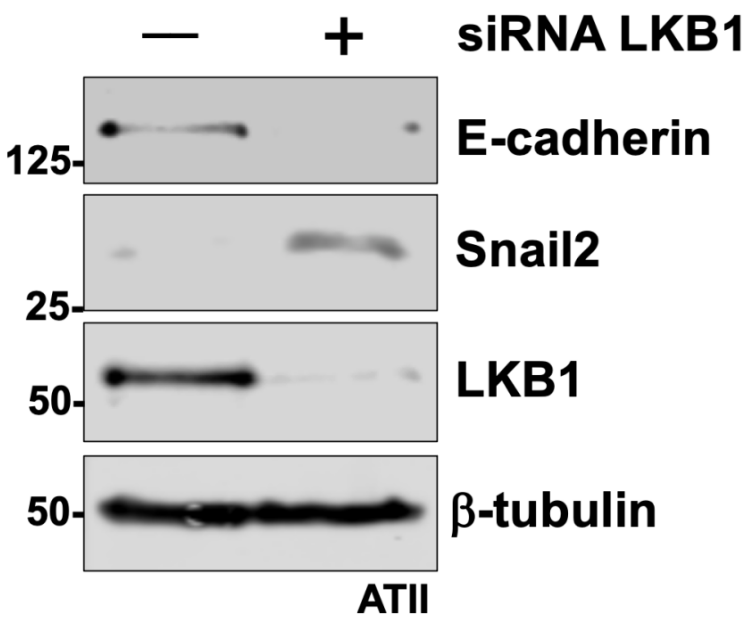

FIGURE 4.7: **Protein expressions of E-cadherin, Snail2, and LKB1 in ATII cells transfected with the indicated siRNA**
β-tubulin was used as a loading control.

deposition (Charlotte Hill, Juanjuan Li, et al. 2019). Therefore, the involvement of autophagy in pulmonary fibrosis, EMT and NF κB signalling pathways in the context of LKB1 depletion is not surprising. The lungs are constantly exposed to various cellular stressors, making gas exchange epithelial cells organ-specific in their roles. Growing evidence highlights the significance of autophagy in the pathogenesis of pulmonary fibrosis and cancer. Our previous findings have suggested that autophagy inhibition promotes EMT, which is induced by NF κB signalling in cancer (Yihua Wang, Hua Xiong, et al. 2019). Consistently, the involvement of NF κB signalling has been shown by GSEA results, as the top enriched pathway upon LKB1 depletion in ATII cells was "Hallmark_TNF α signalling pathway via NF κB" (Figure. 4.8 a; normalized enrichment score, $NES = 2.45$; FDR <0.001). To verify this, we assessed NF κB activity using a reporter assay under different conditions. Briefly, ATII cells were transfected with the LKB1 siRNAs for 48 h in 24-well plates, followed by 24-h transfection with 250 ng of NFKB reporter and 10 ng of phRL-CMV (Promega, E2261), the transcription assay was carried out using the Dual-luciferase® reporter assay system (Promega, E1960) following the manufacturer's protocol. LKB1 depletion in ATII cells increased NF κB activity above 2-fold (Figure. 4.8 b; $P < 0.01$), suggests that LKB1 depletion in ATII cells leads to activation of NF κB signalling and increased Snail2 expression, thereby promoting EMT.

We have previously demonstrated that autophagy inhibition-induced accumulation of p62/SQSTM1 can activate the NFκB pathway(Charlotte Hill, Juanjuan Li, et al. 2019), and triggering of the NFκB pathway by P62/SQSTM1 is involved in the EMT induced

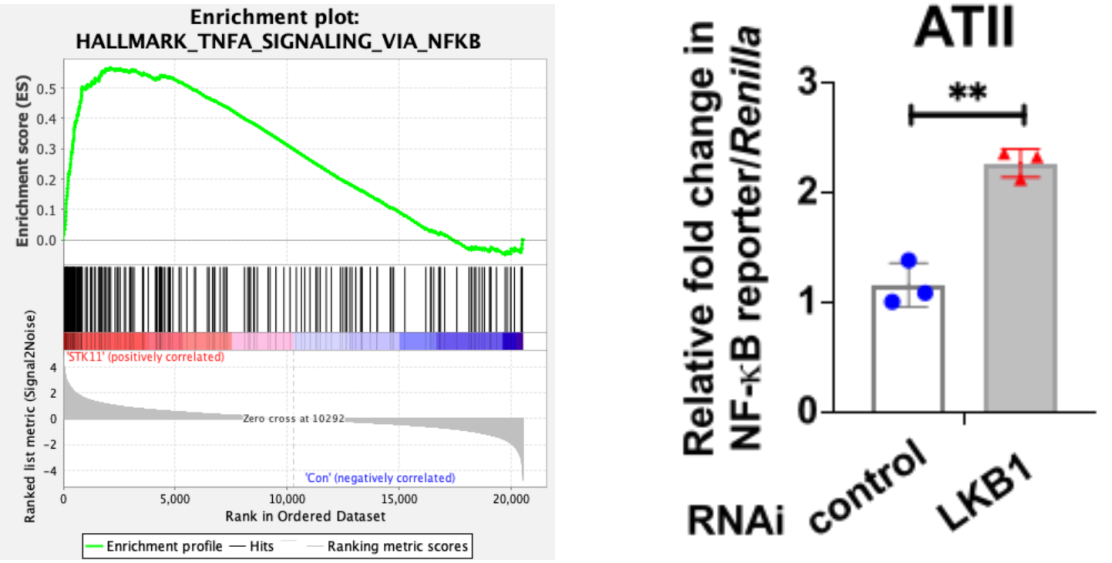

(A) (B)

FIGURE 4.8: **LKB1 depletion leads to NF κB pathway in ATII cells.**
(A) Gene set enrichment analysis (GSEA) plot showing enrichment of Hallmark TNFα Signaling Via NFκB in LKB1 depleted ATII cells. Normalised enrichment score (NES) and false discovery rate (FDR) are indicated. (B) NF κB reporter assays in ATII cells transfected with the indicated siRNA. Values represent the relative fold of firefly luciferase about Renilla luciferase, normalised against control (1.0). Data are mean$\pm$s.d.; $n = 3$ samples in each group. **p-value < 0.01.

by autophagy inhibition in RAS-mutated cells (Yihua Wang, Hua Xiong, et al. 2019). Theoretically, inhibition of autophagy in the presence of a strong RAS signal causes an accumulation of P62/SQSTM1, resulting in super-activation of the NFκB pathway, which leads to EMT Taking the evidence of involvement of NFκB signallings in LKB1 induced EMT. Unfortunately, Although we have discovered that autophagy is involved in the NFκB activation-mediated EMT pathway, the upstream factors responsible for autophagy suppression remain unknown.

Autophagy is a tightly regulated and evolutionarily conserved mechanism that has a convoluted connection with EMT in malignancy. Many studies have found that ageing as a risk factor for IPF causes defective autophagy response in IPF lungs (Charlotte Hill and Yihua Wang 2022). LC3-II and p62 are commonly used as a marker for autophagy activity, as LC3-II's levels increase during autophagy induction and decrease when autophagy is inhibited (Kimura, Fujita, et al. 2009), and p62 is selectively degraded by autophagy (Bjørkøy et al. 2005; Komatsu and Ichimura 2010). Briefly, LC3-II is a form of the microtubule- associated protein light chain 3 (LC3) that is involved in the process of autophagy, which is the cellular process by which cytoplasmic components and organelles are delivered to lysosomes for degradation (Tanida, Ueno, and Kominami 2008). LC3-II is generated from LC3-I through proteolytic cleavage and lipidation, which results in the formation of a

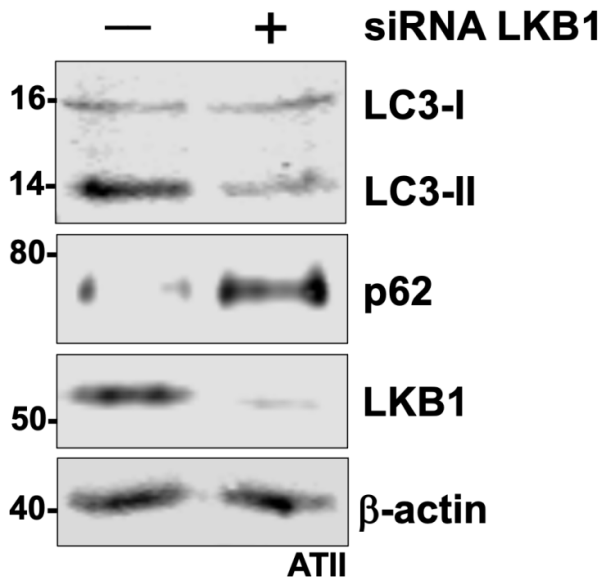

FIGURE 4.9: **Protein expressions of LC3-I, LC3-II, p62 and LKB1 in ATII cells transfected with the indicated siRNA**
β-actin was used as a loading control.

phosphatidylethanolamine (PE) conjugate that is associated with autophagosomal membranes (P. Jiang and Mizushima 2015). As for p62, it binds to ubiquitinated protein aggregates and damaged organelles and targets them for degradation by autophagy (Moscat and Diaz-Meco 2012). During autophagy, p62 is incorporated into autophagosomes and degraded along with its cargo (Johansen and Lamark 2011). Therefore, the levels of p62 are often used as an indicator of autophagy activity. If autophagy is impaired, p62 accumulates because it is not efficiently degraded. Additionally, the number and size of p62 puncta observed by fluorescence microscopy can also be used as a measure of autophagy activity (Kimura, Noda, and Yoshimori 2007). we therefore investigated autophagy activity by Inspecting those markers' protein expression. A decreased level of LC3-II and increased p62 by western blot analysis (Figure. 4.9) indicated the autophagy has been inhibited by LKB1 transfected into ATII cells compared to control, as well as p62 puncta staining by immunofluorescence (Figure. 4.10).

Previously evidence showing the P62-NFκB-EMT axis involved in pulmonary fibrosis by augmenting myofibroblast differentiation gives us reason to believe that LKB1 inhibition may potentially play a role on this signalling pathway as the important upstream effector. We then checked if LKB1 depletion induces EMT via the p62-NF κB-Snail2 pathway in ATII cells by performing a "double knocking-down" system. Briefly, In the context of knocking down LKB1 by transecting siRNA in ATII cells, we also abolish either p62 or p65 under the same culturing conditions in the same batch of cells to test whether there are potential interactions between two of these factors. The results as expected that Depletion of p62 abolished the increase in

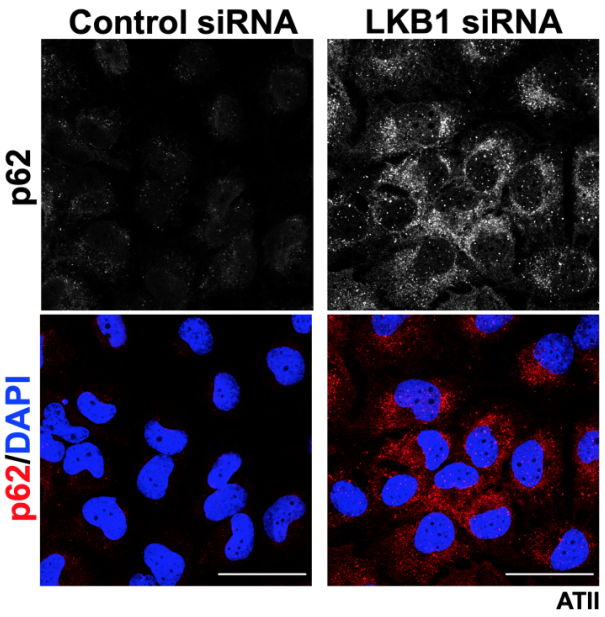

FIGURE 4.10: **Immunofluorescence staining of p62 (red) in ATII cells transfected with the indicated siRNA**
DAPI (blue) was used to stain nuclei. Scale bar: 40 μm.

NF κB activity induced by LKB1 knockdown (Figure. 4.11), suggesting that LKB1 depletion in ATII cells triggers the NF κB pathway via p62. Compared to no snail2 significant changes in double knocking-down LKB1 and p65/p62, LKB1 knocking-down in ATII cells leads to a significant up-regulation of snail2 has to be processed in the absence of knockdown of either p65 (Figure. 4.12 a or p62(Figure. 4.12 b), suggesting p65 or p62 knockdown abolished the increase in the Snail2 expression induced by LKB1 depletion in ATII cells.

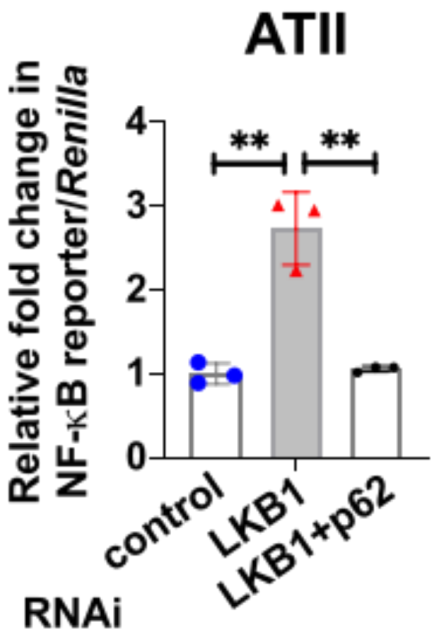

FIGURE 4.11: **NFκB reporter assays in ATII cells with the indicated treatment**
Values represent the relative fold of Renillaluciferase, normalised against control (1.0). Data are mean ± s.d.$n = 3$ samples per group. $** P < 0.01$

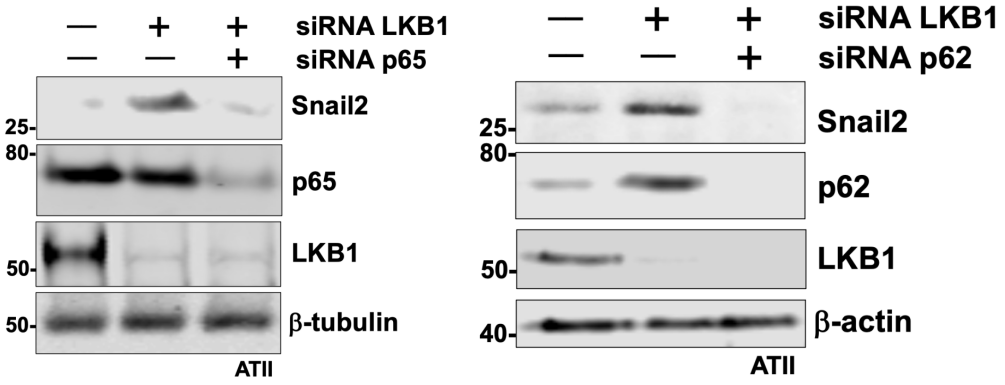

(A) (B)

FIGURE 4.12: **Protein expression of Snail2, (A) p65 (B) p62 and LKB1 in ATII cells with the indicated treatment**
β-tubulin was used as a loading control.

4.6 Discussion

A summary of the evidence we have gathered so far in this section, there are several cellular behaviours have been verified associated with ATII cells transfected with LKB1 siRNA, which points to deposited p62 inhibiting autophagy, NFκB signallings activation and snail2 induced EMT. Previous studies have posited that inhibited autophagy can activate the NFκB pathway, thereby inducing the epithelial-mesenchymal transition (EMT) process (Charlotte Hill, Juanjuan Li, et al. 2019). However, at that time, our colleagues were uncertain about the specific factors that inhibit autophagy in epithelial cells, and which subsequently trigger the NFκB-Snail2-EMT axis. Intriguingly, when examining the global transcriptomic alterations resulting from LKB1 depletion in ATII cells, we observed that the up-regulated differentially expressed genes (DEGs) were strongly associated with both EMT and NFκB pathway activation. This hinted at a possible link between LKB1 and autophagy inhibition. Furthermore, the pronounced upregulation of Snail2 expression due to LKB1 depletion provided compelling evidence for this connection. In this chapter, we not only confirm that LKB1 depletion in ATII cells can induce EMT, but we also delve into whether and how LKB1 inhibition can upregulate NFκB and EMT. More importantly, we explore whether these signalling pathways are hierarchically linked at the cellular intercommunication level and whether autophagy inhibition plays a role within these pathways.

There is a strong correlation between autophagy and NF-κB signalling both in the context of tumorigenesis and lung fibrosis. The NF-κB pathway is a crucial regulator of inflammation and immune response, which plays a significant role in cellular survival (Sundaram et al. 2011). Activation of this pathway has been linked to various mechanisms, including the promotion of ROS production, facilitating tumour cell proliferation and differentiation, and stimulating the expression of genes responsible for neoangiogenesis and cancer cell invasion (Y. Chen et al. 2020).

Autophagy, on the other hand, is a cellular process that degrades and recycles damaged or unnecessary cellular components. It plays a crucial role in maintaining cellular homeostasis and responding to stress (Carroll et al. 2018). Dysregulation of autophagy has been implicated in the development of several diseases, including cancer. Based on the above descriptions, p62 is suggested to be a potential target profiting from its close interaction with selective autophagy and Nrf2 regulation (Inami et al. 2011). This adaptor protein is distributed in organs and tissues throughout the whole body. In other words, p62 is a universal regulatory protein in vivo. When autophagy is inhibited or cells undergo oxidative stress, the expression level of p62 is detected to be abnormal in various disease processes as mentioned before (D. D. Zhang and Hannink 2003). Since its aberrant expression in illnesses, p62 can be considered a clinical diagnostic marker for several disorders. The quantitative

analysis technique of p62 should be put forward because p62 can serve as a pathological indicator. It has been expected to be a good prognostic marker for human hepatocellular carcinoma (HCC) and ovarian cancer (Umemura et al. 2016). p62 accumulation is frequently combined with autophagy deficiency, leading to misfolded protein aggregation, which is a significant factor in disease occurrence and development. The level of autophagy flux can be evaluated by detecting the p62 expression, and the p62 level inversely correlates with the activity of autophagy. In that case, p62 accumulation is the reflection of autophagy dysfunction for that p62 is an autophagy substrate and can be selectively degraded. It is beneficial for symptomatic improvement by reducing the accumulation of p62 and recovering the regular degradation function of autophagy.

In the context of tumorigenesis, p62, an adaptor protein involved in selective autophagy, has been shown to play a central role in the activation of the NF-κB pathway. This activation occurs through the interaction of p62 with TRAF6 (Wooten et al. 2005), ultimately leading to the induction of pro-inflammatory cytokines such as IL-1, TNF, and NGF receptors (Anagnostopoulou et al. 2013). The involvement of p62 in NFκB activation has been demonstrated in various types of cancer, including lung cancer and PDAC. Moreover, a feed-forward loop between p62, NF-κB, and Ras has been identified, which promotes tumour cell survival during pancreatic ductal adenocarcinoma (PDAC) development. Ras, an oncogenic protein, is essential for cancer initiation and progression. When elements of this loop are disrupted, it leads to increased cell death and decreased tumorigenicity. Furthermore, Ras-dependent carcinogenesis development is positively associated with autophagy expression. LKB1-AMPK axis is related to autophagy in IPF has also been discussed, in terms of the fact that ROS-associated autophagy induction is associated with liver kinase B1/AMP-activated protein kinase (LKB1/AMPK1) metabolic pathway and AMPKs function as 'energy-sensing' are activated upon metabolic stress or ATP consumption, this promotes catabolic processes globally and subsequently, AMPK (SFN1, the yeast ortholog) was implicated in autophagy (Alexander et al. 2010; Z. Wang et al. 2001; Meley et al. 2006), it is also expected that p-AMPK was shown to be increased in IPF by immunoblot (Avignat S Patel, Ling Lin, et al. 2012). Based on the last section demonstrating that LKB1 deletion in ATII cells can activate the NF κB pathway, we further explored the impact of LKB1 on autophagy activity in ATII cells.

The interference between inhibited autophagy and EMT-related paracrine signals in IPF is intricate and appears to be context- and tissue-dependent. The suppression of autophagy alone is capable of accelerating both bronchial epithelial cell senescence and the differentiation of lung fibroblasts into myofibroblasts (Jun Araya, Kojima, et al. 2013). Janus Kinase 2 (*JAK2*) and signal transducer and activator of transcription 3 (STAT3) have been identified as autophagy-driven EMT pathways in IPF (Milara et al. 2018). Cheng et al. also proposed that protein phosphatase 1 regulatory subunit

13B (*PPP1R13B*) controls circ-012091 via ER stress and autophagy to increase fibroblast migration and proliferation (Y. Cheng et al. 2019). In addition, inhibition of autophagy via the PI3K/Akt/mTOR pathway can augment signals in TGF β1-induced EMT (X. Gui et al. 2018). IL17A is increased in IPF, and it has been shown to induce EMT and is responsible for the secretion of synthesis and secretion collagen in a TGF β1-dependent manner (Mi et al. 2011; Hong Liu et al. 2013).

In this chapter, these results demonstrate that LKB1 inactivation in ATII cells triggers autophagy inhibition and promotes EMT via a p62-NF κB pathway. After determining the role of LKB1 in epithelial cells, we will further investigate whether the epithelial LKB1 will impact the fibroblasts' behaviours via epithelial-mesenchymal crosstalk.

Chapter 5

A role of paracrine signalling in augmenting myofibroblast differentiation

Results shown throughout this chapter are part of the following publication: [1]

5.1 Abstracts

Our previous report suggests that reduced autophagy activity contributes to fibrosis via aberrant epithelial-fibroblast crosstalk (Charlotte Hill, Juanjuan Li, et al. 2019). To determine if it is also the case for LKB1 depletion in ATII cells, 3D co-cultures of ATII cells and lung fibroblast MRC5 coupled with RNA-seq were performed. To analyse the influence of LKB1 depletion in ATII cells on fibroblasts, we utilised a machine learning method called CIBERSORTx (Newman et al. 2019). Cell deconvolution based on an epithelial or a mesenchymal cell signature matrix derived from the single-cell RNA-seq (GSE135893) (A. Habermann et al. 2020) showed a decrease in the epithelial population and an increase in the mesenchymal population. Further characterisation based on a fibroblast subtype signature matrix (GSE135893) suggested an eminent increase in the myofibroblast population, suggesting that myofibroblast differentiation is induced upon LKB1 depletion in ATII cells.

A comparison of collagen genes in control vs. LKB1-depleted ATII cells demonstrated that ATII cells upon LKB1 inactivation-induced EMT did not express significantly more collagen genes. By contrast, data from 3D co-cultures of ATII cells and MRC5 showed a strong upregulation in a majority of collagen genes upon LKB1 depletion in

[1] ***Xu Z***, *Davies E R, Yao L, et al. LKB1 depletion-mediated epithelial–mesenchymal transition induces fibroblast activation in lung fibrosis. Genes & Diseases, 2023, ISSN 2352-3042, https://doi.org/10.1016/j.gendis.2023.06.034.*

ATII cells. We then quantified the changes in collagen gene expression using Gene Set Variation Analysis (GSVA) (Hänzelmann, Castelo, and Guinney 2013), showing a significant increase in 3D co-cultures of ATII cells and MRC5, but not in 2D-cultured ATII cells.

These findings in 3D co-cultures were supported by checking the expressions of *ACTA2* (encoding α-smooth muscle actin, α-SMA, a myofibroblast marker) and other ECM genes, including *COL1A1*, *COL3A1* and *FN1* in the RNA-seq analysis, showing an increase in the majority upon LKB1-depletion in ATII cells. The changes in their mRNA levels were further confirmed with real-time qPCR. Together with our earlier reports (Charlotte Hill, Juanjuan Li, et al. 2019; L. Yao, Franco Conforti, et al. 2019), this suggested collagen production in IPF lungs was unlikely due directly to EMT but rather epithelial cells exhibiting an indirect effect on myofibroblast differentiation via paracrine signalling.

5.2 Introduction and rationale

When AECs are damaged, they release these signalling molecules, which promote fibroblast proliferation, recruitment, and activation, leading to abnormal ECM deposition. In turn, the resulting myofibroblasts cause further damage to the epithelial cells and induce apoptosis, exacerbating the cycle of epithelial-mesenchymal crosstalk and myofibroblast accumulation.

Epithelial-mesenchymal crosstalk in IPF is mediated by paracrine signalling molecules that are released by the damaged alveolar epithelial cells (AECs) and act on fibroblasts in the surrounding microenvironment. These signaling molecules include growth factors such as TGFβ (Moises Selman et al. 2004; Nasreen Khalil et al. 1996), PDGF (HN Antoniades et al. 1990), CTGF (LH Pan et al. 2001), TNF- α (PF Piguet et al. 1993), osteopontin (Pardo, K. Gibson, et al. 2005), angiotensinogen (Xiaopeng Li et al. 2006), and endothelin-1 (Dina Saleh et al. 1997), as well as pro-fibrotic mediators and developmental pathways like AMPK (Maria M Mihaylova and Reuben J Shaw 2011c), Wnt/-catenin (Königshoff, Kramer, et al. 2009), and Sonic hedgehog (Alfredo Lozano Bolaños et al. 2012).

In kidney fibrosis, epithelial micro-injuries also promote pro-fibrotic circumstances by secreting TGF β and connective tissue growth factor (CTGF) to enhance myofibroblast formation. Similarly, myofibroblasts trigger apoptosis in epithelial cells via angiotensin II (ANG II) or reactive oxygen species (ROS) in a self-sustaining vicious circle to enhance myofibroblast accumulation. These paracrine signalling interactions between epithelial cells and fibroblasts are thought to contribute to the onset of multiple organ fibrosis, where both cell types co-localize (Prunotto, Budd, et al. 2012; Madhu Bhaskaran et al. 2003).

Investigations have shown that activated AECs in IPF release a set of mediators that promote pathogenic fibroblast growth, suggesting that they may contribute to ECM deposition. For instance, injured AECs stimulate TGF β secretion, increasing fibroblast proliferation, recruitment, and activation (Sheppard 2006a; Yuko Morishima et al. 2001). Meanwhile, secreted TGF β1 and endothelin-1 are required to prevent fibroblast apoptosis by regulating the protein kinase B (Akt) pathway (Priya Kulasekaran et al. 2009). However, AECs from IPF patients become more vulnerable to apoptosis in the same milieu, owing to reduced expression of prostaglandin E2 (Toby M Maher, I. C. Evans, et al. 2010).

Our lab has investigated the response of fibroblasts and their subtypes to AECs via disordered epithelial-mesenchymal communication in human 2D and 3D in vitro studies for several years. The previous evidence showed that RAS-activated alveolar epithelial type II (ATII) cells provide paracrine signals to augment fibroblast activation (L. Yao, Franco Conforti, et al. 2019). While zinc finger E-box binding homeobox factor 1 (ZEB1) knock-out mice presented with less mesenchymal gene expressions (Yongqing Liu et al. 2008). In summary, human fibroblasts treated with conditional media (CM) derived from RAS-activated ATII cells with or without ZEB1 RNAi demonstrated that ZEB1 is a major regulator of paracrine signalling between ATII cells and fibroblasts. In line with the previously published dataset (Y. Xu et al. 2016), our colleagues also have performed a quantitative proteomic analysis of the CM from control or 4-OHT-treated AECs and presented PLAT (tPA) as a transcriptional target of ZEB1 in response to RAS activation in ATII cells and mediates epithelial-mesenchymal crosstalk by upregulating TGF β expression (L. Yao, Franco Conforti, et al. 2019) (Figure. 5.1). As a sustaining-negative loop, we also reported that signalling occurs between fibroblasts and ATII cells leading to RAS activation and induction of ZEB1 and that this effect is augmented by CM from fibroblasts that have been differentiated into myofibroblasts by TGF β or by CM from IPFFs independently of exogenous (L. Yao, Yilu Zhou, et al. 2021). These findings point to a two-directional process in which epithelial-mesenchymal interaction causes a negative feedback loop in the fibrotic microenvironment.

Given the aforementioned significance of EMT and epithelial-mesenchymal communication in the study of lung fibrosis, coupled with our lab's exploration of key regulators triggering myofibroblast differentiation, my research now turns to investigate the role of LKB1 depletion in ATII cells contributes to fibroblasts' behaviour. We aim to decipher whether the LKB1-depletion-induced EMT can influence paracrine signalling mechanisms, thereby potentially enhancing myofibroblast differentiation—a pivotal process in lung fibrosis progression. These investigations are directly informed by our previous findings that LKB1 inactivation in ATII cells inhibits autophagy and promotes EMT via a p62-NF κB pathway.

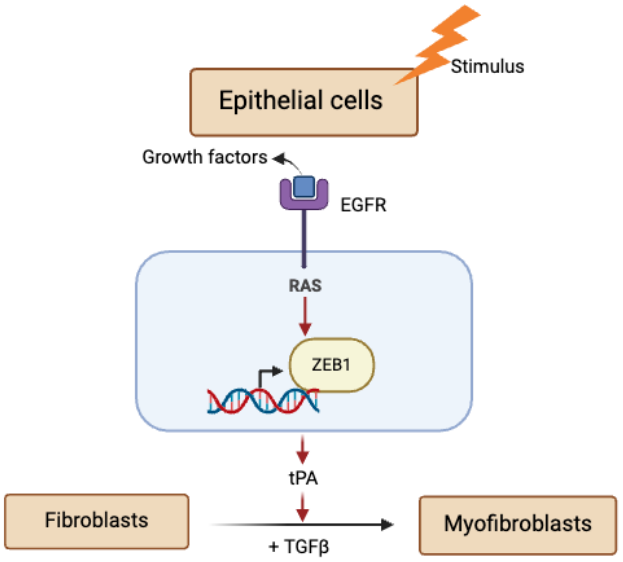

FIGURE 5.1: **Illustration of the ZEB1-tPA Axis in Epithelial-Mesenchymal Crosstalk and Its Role in Idiopathic Pulmonary Fibrosis (IPF) Development.**
This diagram highlights how the ZEB1 and tPA axis facilitate paracrine activation of human lung fibroblasts, contributing to the progression of IPF. The figure also demonstrates the interaction with TGFβ, underscoring its significance in fibroblast activation and fibrosis formation. Note: ZEB1 and tPA are key mediators in the epithelial-mesenchymal communication critical to IPF pathology. The diagram is adapted from (L. Yao, Franco Conforti, et al. 2019).

5.3 Objectives

In this chapter, we aim to:

- Identify whether depletion of LKB1 in ATII cells can induce global transcriptomic changes in the epithelial-mesenchymal environment by performing RNA sequencing analysis using 2D and 3D co-culturing models.
- Determine if depleting LKB1 in ATII cells can influence fibroblast behaviours and myofibroblast differentiation, initiating epithelial-mesenchymal crosstalk, by utilizing CibersortX to deconvolute the different types of fibroblasts present.

5.4 Methodology

5.4.1 Three-dimensional (3D) co-cultures

Three-dimensional (3D) cell cultures were carried out using the Bio-AssemblerTM kit designed for 96 well plates (n3D-Biosciences Inc, Houston, TX, USA). In short, NanoShuttles^{TM} (Badr-Eldin et al. 2022) were added in a T-25 flask with a ratio of 1 μL of NanoShuttles ^{TM} per 5,000 MRC5 cells and incubated at 37 $^{\circ}C$ and 5% CO_2 overnight. Then, the MRC5 cells were detached by treating them with 5 mL of trypsin for 5 min and washed by centrifugation (600 g/5 min) with a balanced salt solution (PBS, Nutricell). Cell viability was determined by trypan blue (1% w/v in PBS) exclusion method MRC5 cells conjugated with NanoShuttles ^{TM} was seeded in the 96-well ultralow-attachment plate (ULA, Cellstar® Greiner Bio-one, Kremsmünster, Austria) at final volume of 200 μL/well. The 3D culture was achieved by incubating (37 $^{\circ}C$ and 5% CO_2) the plates under a magnetic field, first using a bioprint drive for 20 minutes, which was followed by a levitation drive for all culture periods. This procedure promotes MRC5 cells to grow as aggregates. The 3D culture plate was replenished with fresh medium every 2 days until the moment of cell aggregate use. The co-culture would be processed after 24h. Pre-treated ATII cells with nanoshuttles as above procedure overnight were driven by a magnetic field to surround the established MRC5 spheroids (Figure. 5.2).

5.4.2 Conditioned media

The conditioned media derived from cultured cells is abundant in proteins, offering a fertile ground for biomarker identification (H. Xue, Bingjian Lu, and M. Lai 2008). Notably, some of these cell-secreted proteins transition into the bloodstream, potentially serving as indicators for disease presence or gauging treatment efficacy.

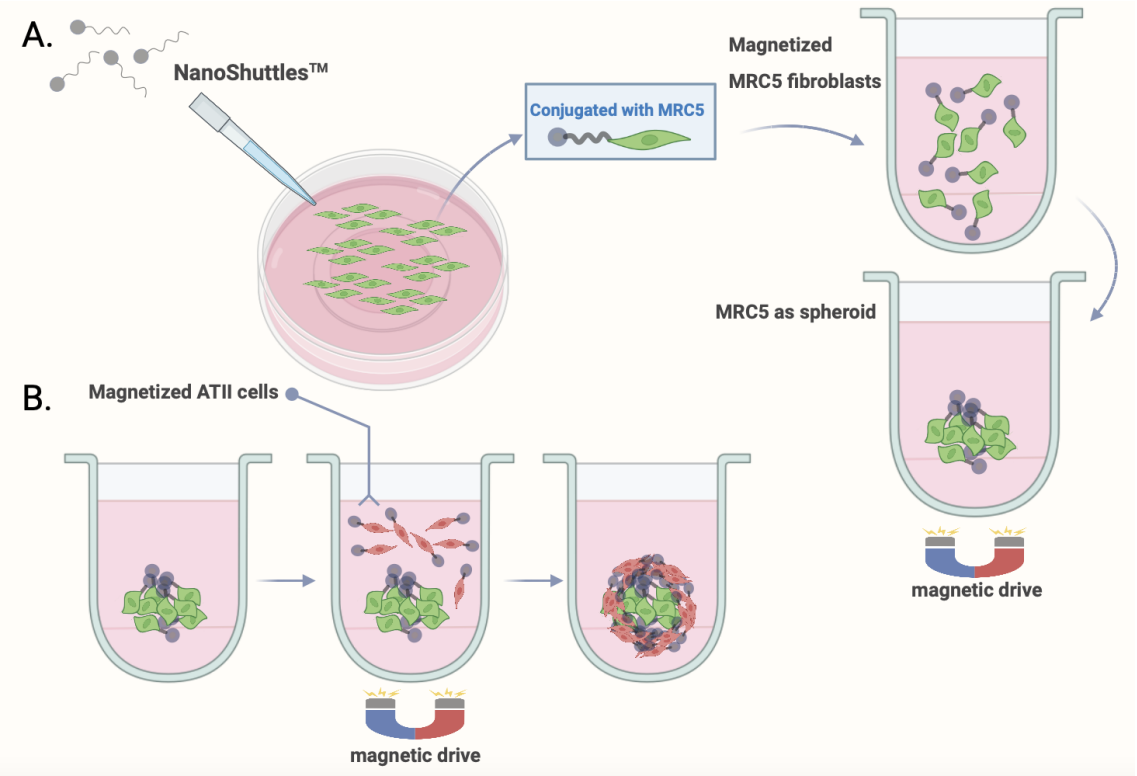

FIGURE 5.2: **MRC5-ATII Three-dimensional (3D) co-culturing model by bioprinting magnetic drive**
The Schematic diagram of A represents the process of MRC5 cells conjugated with NanoShuttles driven as 3D spheroids. Figure B shows that pre-treated ATII cells with nanoshuttles as above procedure were driven by a magnetic field to surround the established MRC5 spheroids.

This strategy is a more straightforward and less invasive alternative to directly analyzing clinical samples and holds promise for unearthing novel biomarkers. Through meticulous research on cell populations, a rich array of secreted proteins has surfaced as promising biomarker candidates. Preliminary tests on clinical samples have shown that many of these proteins offer reliable diagnostic accuracy (L. Zhong et al. 2008; Volmer et al. 2005). This chapter continued with an investigation of global transcriptomic changes in epithelial-mesenchymal microenvironments, A conditioned medium was utilised to evaluate the biomarkers of fibroblasts and myofibroblasts. Briefly, type II epithelial cells were transfected with *STK11* siRNA to knock down LKB1 expression or transfected with control siRNA to be a control. After 48h, the indicated conditioned culturing medium was transferred to growing fibroblasts treated or not treated with TGFβ (see figure. 5.3). The percentage of conditional media has been optimized. I used 30%, 50%, 70%, and 100% media collected from the growing environment of ATII cells to treat MRC5 fibroblasts for 24, 48, and 72 hours. This was done to elucidate the effects of metabolic inhibition caused by LKB1 depletion and to determine the optimal timing of TGFβ action. Ultimately, collecting 100% conditional media from ATII cells after 48 hours and applying it to MRC5 cells,

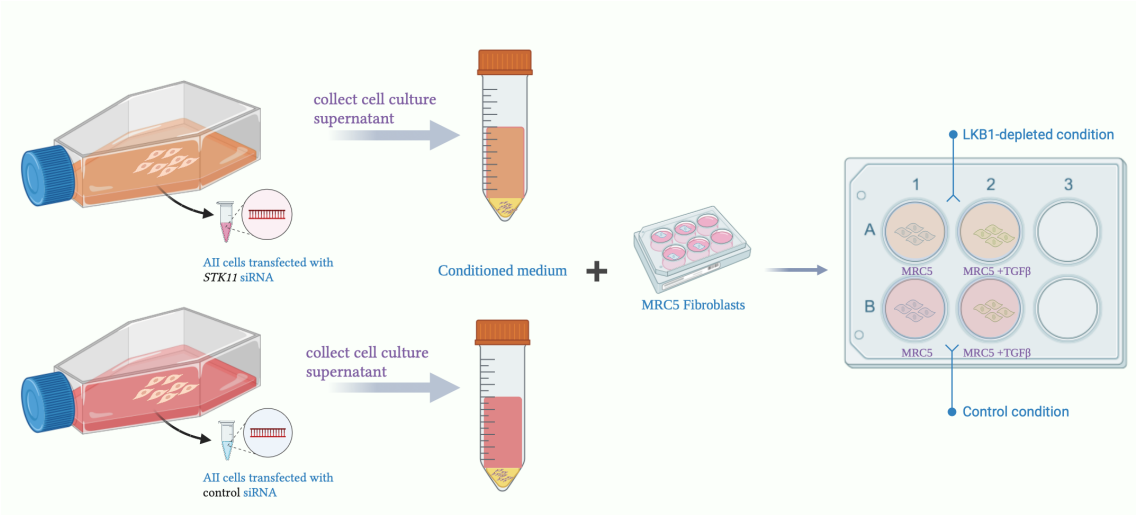

FIGURE 5.3: **Flowchart of 2D co-culturing model by collecting conditioned medium and treat MRC5 lung fibroblasts**
The diagram represents the process of harvesting conditioned medium from a specific cell culture and subsequently using it to treat or influence MRC5 lung fibroblasts. This method is commonly employed to study the impacted fibroblasts and myofibroblasts by LKB1 in epithelial type II cells.

both with and without TGFβ induction, could mimic the microenvironment of MRC5 affected by LKB1 depletion.

5.5 Results

5.5.1 Gobal transcriptomic changes identify several potential key paracrine factors mediating epithelial-mesenchymal crosstalk.

As demonstrated above, due to factors involved in paracrine signallings related to Epithelial-fibroblasts crosstalk reduced autophagy activity contributes to fibrosis via aberrant epithelial-fibroblast crosstalk (Charlotte Hill, Juanjuan Li, et al. 2019). To determine the role of LKB1 in the epithelial-fibroblast microenvironment, we used a novel 3D bio-printing assay by co-culturing the ATII cells with fibroblasts, to mimic the alveolar interstitial tissue and the cellular cross-talk between epithelial cells and fibroblasts. The cells were fluorescently labelled green (fibroblasts) or red (ATII) to visualise the proximity of the cells (Figure. 5.4). In brief, fibroblast aggregations were formed on an ultra-low attachment plate on a magnetic drive (the first image in Figure. 5.4), before ATII cells underwent the same process (the middle image in Figure. 5.4)to form an outer layer on the existing spheroid (column 3 in Figure. 5.4). Once this was established, this method was used to compare LKB1-depleted ATII cell cross-talk with fibroblasts. The 3D bio-printing assay and cell tracker staining were conducted by Elizabeth R. Davies.

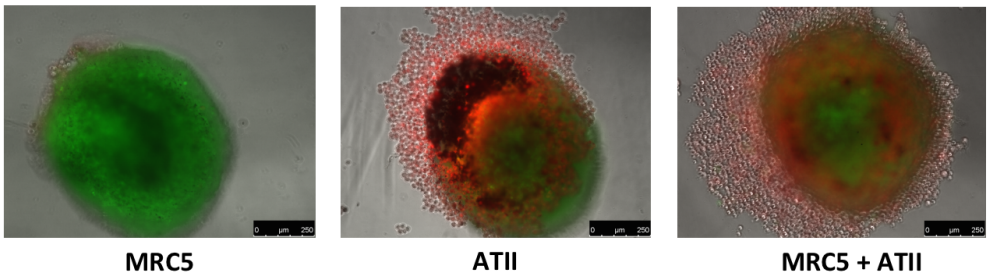

FIGURE 5.4: **Bioprinting 3D co-culturing spheroids**
Representative images showing 3D co-culture spheroid of MRC5 lung fibroblasts (green) and ATII cells (red). The co-culture formation process has been shown from left to right. MRC5 fibroblasts form initial spheroids, followed by ATII cells encasing the spheroids, resulting in a layered structure. Scale bar: 250 μm.

we then performed the RNA sequencing by purifying RNA in the ATII-MRC5 co-culturing model to compare the LKB1 depletion-initiated epithelial changes and whether would impact the fibroblast's activity. Samples (6 in total) were prepared either by transfecting LKB1 siRNA into ATII cells co-culturing with human fibroblasts MRC5 or control siRNA into ATII cells co-culturing with MRC5, 3 samples in each group. For each sample, 3 μg of total RNA was utilised as the input for library construction. we first checked the distribution of all samples to confirm the 6 samples can be clustered as 2 groups by raw counts conducted by Novogene. In this part, we utilized hierarchical clustering (hclust) and PCA analysis to identify patterns and relationships between data points.

Hclust is a method of cluster analysis that seeks to build a hierarchy of clusters. It is a popular unsupervised machine learning technique used in data science and statistical analysis. In hierarchical clustering(Figure. 5.6), the data is recursively partitioned into smaller and smaller clusters until the desired number of clusters is reached. Dendrogram shows the relationship between control ATII + MRC5 and LKB1 depleted ATII + MRC5 as clearly different clusters, as the horizontal axis displays the samples sorted by the treatment group, with control samples (control siRNA transfected into ATII co-culturing with MRC5) on the top and treated samples (siLKB1 transfected into ATII co-culturing with MRC5) on the below (Figure. 5.5).

The workflow for the differential gene expression analysis with DESeq2. The steps in the analysis are Estimate size factors, estimate gene-wise dispersion, fit curve to gene-wise dispersion estimates, shrink gene-wise dispersion estimates, and GLM fit for each gene. This is particularly important to reduce false positives in the differential expression analysis. After shrinking the gene-wise dispersion estimates toward the expected dispersion values to reduce false positives, dispersion plots as expected show the 3D RNAseq data to generally scatter around the curve, with the dispersion decreasing with increasing mean expression levels. This curve is displayed as a red line in the figure, which plots the estimate for the expected dispersion value for genes

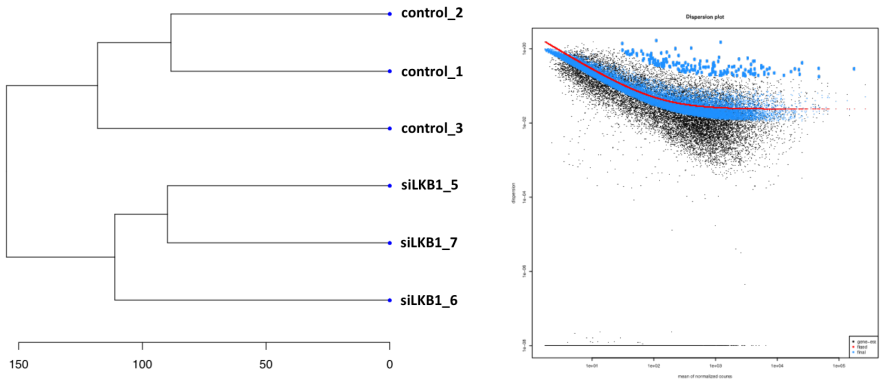

(A) A (B) B

FIGURE 5.5: **Distribution of RNAseq dataset for LKB1 depleted ATII co-culturing with MRC5**
(A) The dendrogram represents the hierarchical clustering of gene expression data based on Euclidean distance and Ward's linkage method. The vertical axis represents the distance between samples, with shorter distances indicating greater similarity. (B) the shrinkage estimation of within-group variation using DESeq2 for a set of genes with varying mean expression levels. The blue line represents the shrinkage estimate of dispersion, which combines the individual gene-wise estimates with the curve-fit estimate. Shrinkage estimation provides more accurate estimates of within-group variation for each gene, allowing for more reliable differential expression analysis between groups.

of a given expression strength. Each black dot is a gene with an associated mean expression level and maximum likelihood estimation (MLE) of the dispersion (Love, Huber, and Anders 2014b).

Furthermore, the DEGs analysis was explored. I demonstrated the distribution of differentially expressed genes (DEGs) in ATII cells co-cultured with MRC5 cells and transfected with siRNA against LKB1 compared to those transfected with control siRNA (Figure. 5.6). The DEGs were defined by a p-value of less than 0.05 and a log-fold change greater than 1. The REVIGO TreeMap (Figure. 5.7) provides a visual representation of the enriched Gene Ontology items (Molecular Function, Biological Process, and Cellular Component) in DEGs from co-cultures of LKB1-depleted ATII cells and MRC5. The upregulation of "extracellular matrix organization" and "extracellular matrix constituent" suggests a potential role for ECM remodelling in the fibroblast's response to LKB1 depletion in ATII cells, highlighting a promising avenue for our perspective.

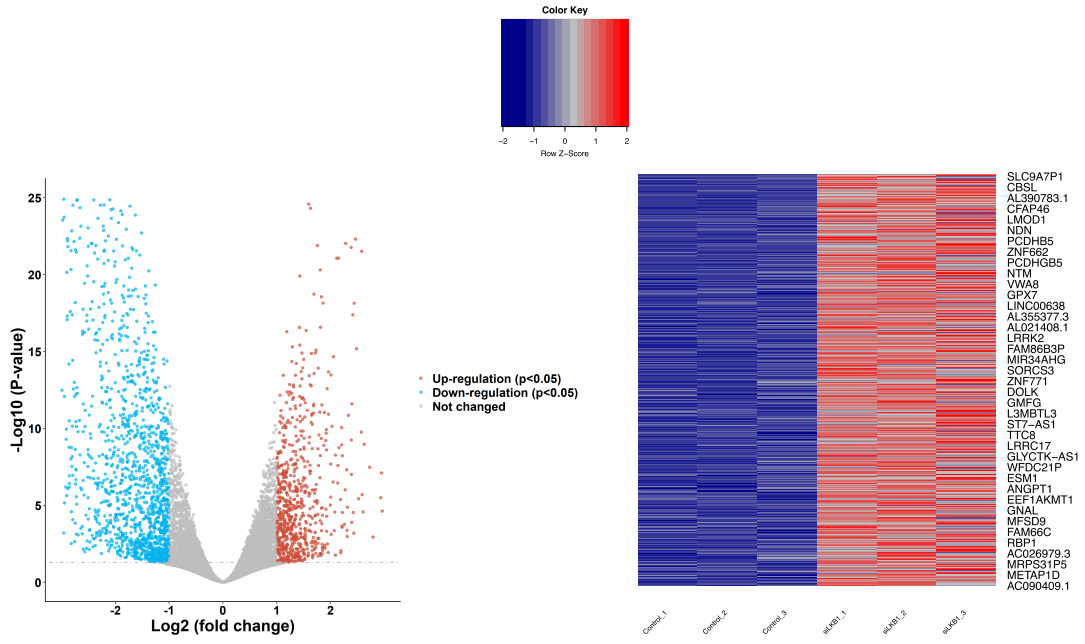

FIGURE 5.6: **Distribution of up and down-regulated DEGs in MRC5 co-culturing ATII cells transfected with siRNA against LKB1 vs control siRNA**
(A)Volcano plot showing the distribution of DEGs. Grey dotted lines indicate the threshold for P-value = 0.05. Blue and red points represent down-regulated and up-regulated differentially expressed genes respectively. (B) Heatmap showing the top 15 DEGs in RNA-Seq dataset from siLKB1 VS control in ATII cells. DEGs were defined by P-value$<$ 0.05 and Log[Foldchange] $>$ 1. Colours of red and blue indicate upregulation and downregulation, separately.

5.5.2 LKB1 depletion induces fibroblast changes via epithelial-mesenchymal crosstalk.

To discern the broader implications of LKB1 depletion in ATII cells, particularly its role in epithelial-to-mesenchymal transition (EMT) and its influence on epithelial-fibroblast crosstalk, we undertook a comprehensive analysis integrating two RNAseq datasets in both 2D and 3D culturing model. Our primary objective was to delineate the exclusive effects of LKB1 depletion on fibroblasts within this microenvironment while controlling for direct impacts on epithelial cells. Briefly, We commenced by identifying differentially expressed genes (DEGs) meeting specific criteria: those not significantly up-regulated in the 2D model (comparing LKB1 siRNA transfected ATII cells against controls) yet were notably up-regulated in the 3D co-culturing model (comparing LKB1-depleted ATII cells co-cultured with MRC5 fibroblasts against control ATII cells in similar co-culture). By intersecting these two gene sets, we aimed to uncover the signalling pathways and molecular mechanisms

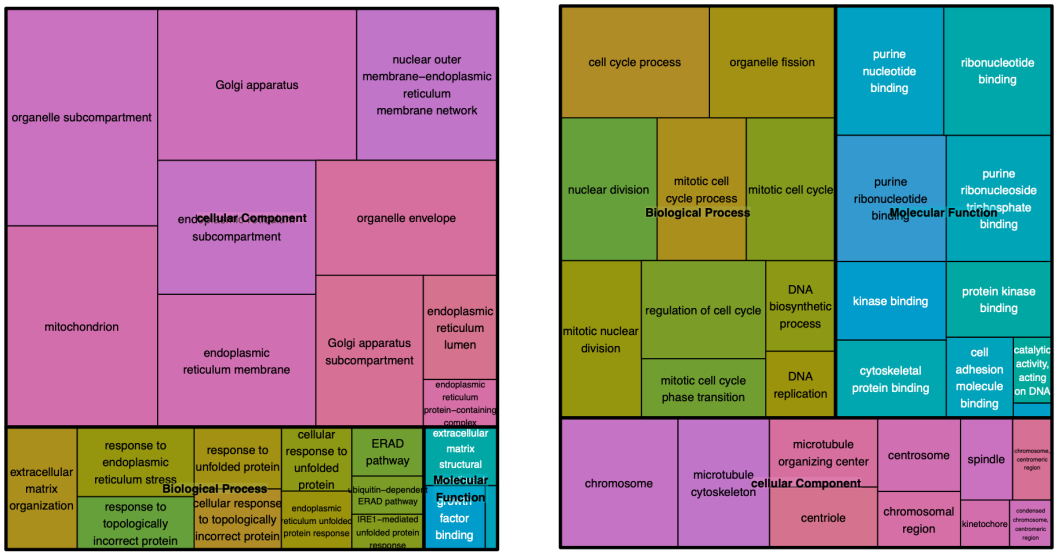

(A) Top 10 upregulation

(B) Top 10 downregulation

FIGURE 5.7: **LKB1 depletion induces global changes via epithelial-mesenchymal crosstalk**
REVIGO TreeMap showing top 10 Gene Ontology (GO) items enriched by up-regulated or down-regulated differentially expressed genes (DEGs) in 3D models of LKB1-depleted ATII cells co-culturing with MRC5.Common colours represent groupings based on parent GO terms, and each rectangle is a percentage of the relative enrichment of the GO term compared with the whole genome. Genes with a false discovery rate (FDR) less than 0.05 and Log[Foldchange] > 1 were considered as DEGs.

predominantly elevated, offering insights into the genuine effects of LKB1 depletion in epithelial cells on fibroblast behaviour (Figure. 5.8).

A total of 749 DEGs are related to the interaction between ATII and MRC5, which is evaluated by overlapping up-regulated DEGs in a 3D group with not up-regulated DEGs in the 2D group. furthermore, The online analysis tool of Metascape (Yingyao Zhou et al. 2019) was utilised to explore the relatively enriched disease, KEGG pathways and Gene Ontology to explore whether there are some fibroblasts changes influenced by epithelial-mesenchymal interaction. By delving into the details of treemap (Figure. 5.9), liver fibrosis, Idiopathic pulmonary fibrosis, and Pulmonary fibrosis have been shown in the chunk of Disease related to the interacted DEGs, suggest that the impacted fibroblasts by LKB1 depleted ATII cells Displayed characteristics of the relevant diseases. Moreover, pathways associated with extracellular remodelling including Extracellular matrix organization, Collagen formation, Genes encoding collagen proteins, etc. categories of Gene Ontology especially biological processes also suggest a significant extracellular structure reorganization and fibroblasts relative to other biological processes have been changed (Figure. 5.9).

To delve deeper into this area of study, I constructed a tree diagram focusing exclusively on relevant biological processes (BP) in Gene Ontology (GO) items. Within this diagram (Figure. 5.10), it becomes evident that several items, which positively influence fibroblast growth and migration, are notably up-regulated. These include ”regulation of growth”, ”regulation of mesenchymal cell proliferation”, ”positive regulation of fibroblast proliferation”, and ”fibroblast proliferation”, among others. These observations emphasize that by specifically studying the interacted DEGs and excluding the direct effects caused by LKB1 depletion in epithelial cells, we can discern that LKB1 depletion indirectly influences fibroblast behaviour through epithelial-mesenchymal crosstalk. Furthermore, this behaviour is likely mediated predominantly through mechanisms impacting cell growth.

5.5.3 A paracrine signalling between LKB1-depleted ATII cells and fibroblasts via inducing ECM remodelling.

Concerning the observation of extracellular matrix (ECM) remodelling and reorganization in overlapping differentially expressed genes (DEGs) within RNA-sequencing datasets, we have employed several approaches to explore the impact of LKB1 deficiency in epithelial tissue on ECM organization. Concerning Type I Collagen Alpha 1 Chain (COL1A1) and Collagen Type III Alpha 1 Chain (COL3A1) as the main components of collagen, and Fibronectin 1 (FN1) as an essential glycoprotein present in the extracellular matrix (ECM), we evaluated their expression levels in both 2D and 3D RNA-sequencing data (Figure. 5.11). Furthermore, Dr. Elizabeth R. Davies confirmed the mRNA levels in 3D co-cultured spheroids. Compared to the down-regulated expression of ECM markers in 2D LKB1-depleted ATII cells, the ECM markers demonstrate up-regulation in the co-culture RNA-sequencing dataset. The qRT-PCR results provide strong evidence that the expression of COL1A1, COL3A1 and FN1 on mRNA level is significantly up-regulated in LKB1-depleted ATII cells co-cultured with MRC5, as compared to the control group (Figure. 5.14a).

Additionally, when control or LKB1-depleted ATII cells were co-cultured with MRC5 fibroblasts, there was a marked upregulation of a large number of collagen genes upon LKB1-depletion in ATII cells (control ATII + MRC5 vs. LKB1-depleted ATII + MRC5; Figure. 5.12), showing in the heatmap. Quantification of the changes in collagen gene expression using Gene Set Variation Analysis (GSVA) (Hänzelmann, Castelo, and Guinney 2013) Briefly, Gene Set Variation Analysis (GSVA) is a non-parametric, unsupervised method used for gene set enrichment analysis, providing a way to determine the relative enrichment of free-defined gene sets across samples in a dataset. The algorithm transforms a gene-by-sample expression matrix into a gene-set-by-sample enrichment score matrix. It does this by ranking genes for

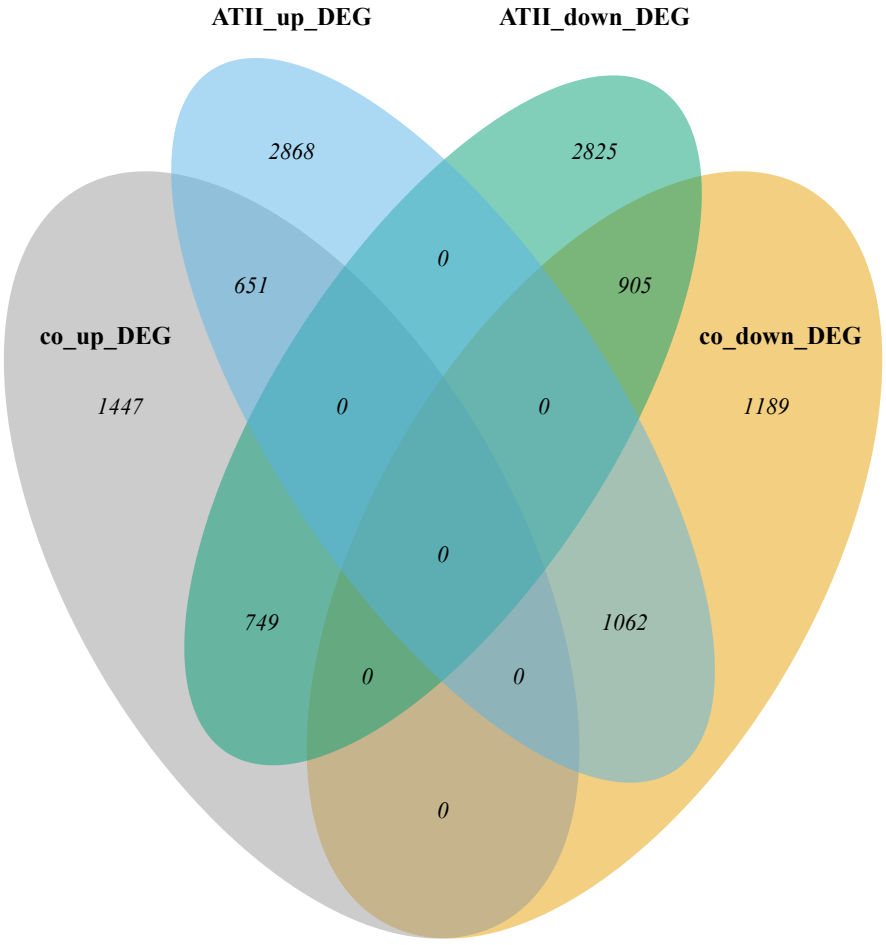

FIGURE 5.8: **Comparative Analysis of DEGs Between 2D and 3D Models Following LKB1 Depletion in ATII Cells**
Venn diagram showing the interactions among differentially expressed genes (DEGs) in two distinct experimental setups: the 2D model and the 3D co-culturing model. In the 2D model, DEGs were identified by comparing LKB1 siRNA transfected ATII cells to their respective controls. Meanwhile, in the 3D co-culturing model, DEGs were distinguished by contrasting LKB1-depleted ATII cells co-cultured with MRC5 fibroblasts against control ATII cells co-cultured similarly. Numbers within each segment of the Venn diagram indicate the count of DEGs specific to that category.

FIGURE 5.9: **REVIGO TreeMap showing top 10 up-regulated items in Molecular Function, Biological Process, and Cellular Component in GO items and pathways and disease enriched by interacted DEGs**
Common colours represent groupings based on parent terms, and each rectangle is a percentage of the relative enrichment of the GO term compared with the whole genome. Genes with a false discovery rate (FDR) less than 0.05 and Log[Foldchange]> 1, Random sampling size was set as 5000 and Min. feature count was 2.

each sample and calculating an enrichment score, much like how the GSEA method works, but at the sample level. One of its key strengths is the flexibility in defining gene sets. Unlike other methods that rely on predefined gene sets, GSVA allows users to customize and define their own gene sets based on specific biological interests or hypotheses. In my context, I have employed GSVA to quantify changes in the expression of those respective collagen genes to quantify the changes by enrichment score. The result identified a significant effect of LKB1 depletion in 3D co-cultures of ATII cells and MRC5 (Figure. 5.13; $P < 0.01$), but not in 2D-cultured ATII cells ($P > 0.05$).

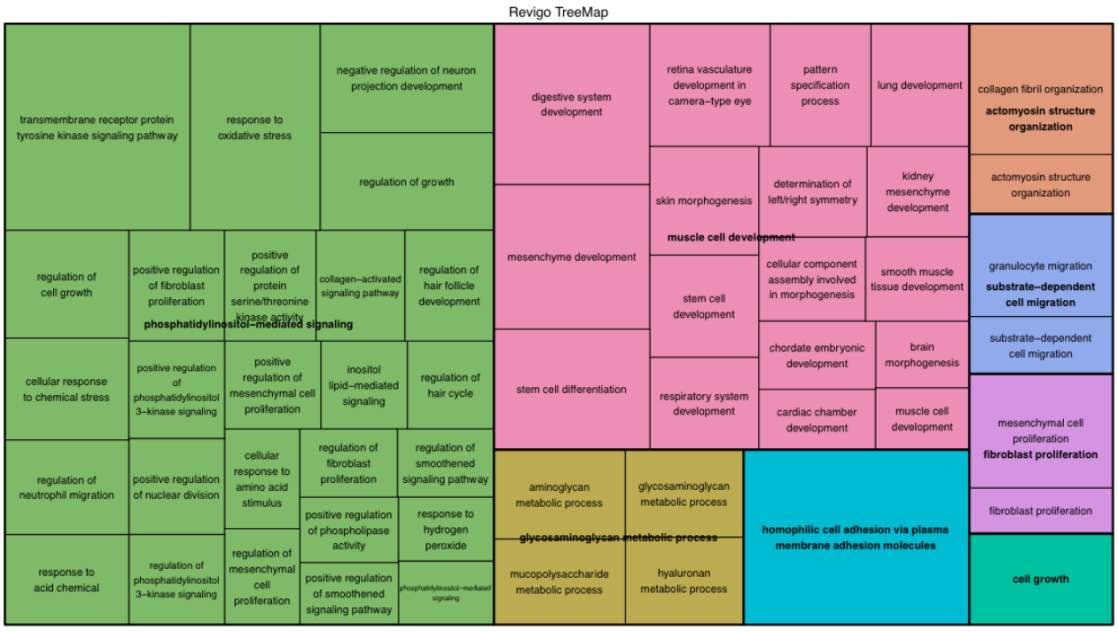

FIGURE 5.10: **REVIGO TreeMap showing Biological Process changes in Gene Ontology (GO) analysis of interacted DEGs**
Common colours represent groups based on parent GO terms, and each rectangle is the percentage of the relative enrichment of the GO term compared with the whole genome.

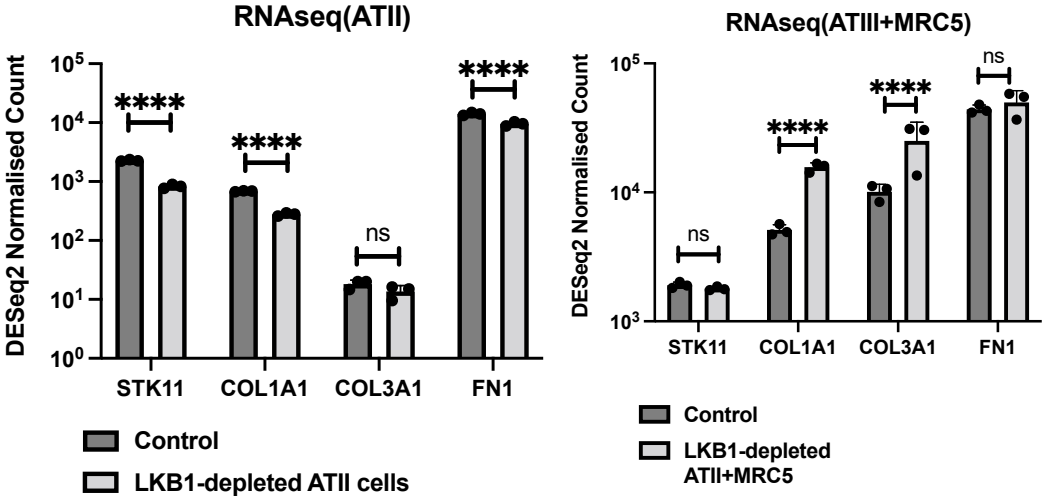

(A) 2D RNA-seq dataset

(B) 3D RNA-seq dataset

FIGURE 5.11: **DEGSeq2 was used to determine the relative normalized counts of *STK11*, *COL1A1*, *COL3A1*, and *FN1* in LKB1-depleted ATII cells compared to control in a 2D (A) or 3D(B) RNA-seq dataset**
β-actin normalised mRNA levels in ATII cells were used to set the baseline value at unity. Data are mean ± s.d; n = 3 samples in each group. *P <0.05; **P <0.01; ***P <0.001 and ns: not significant.

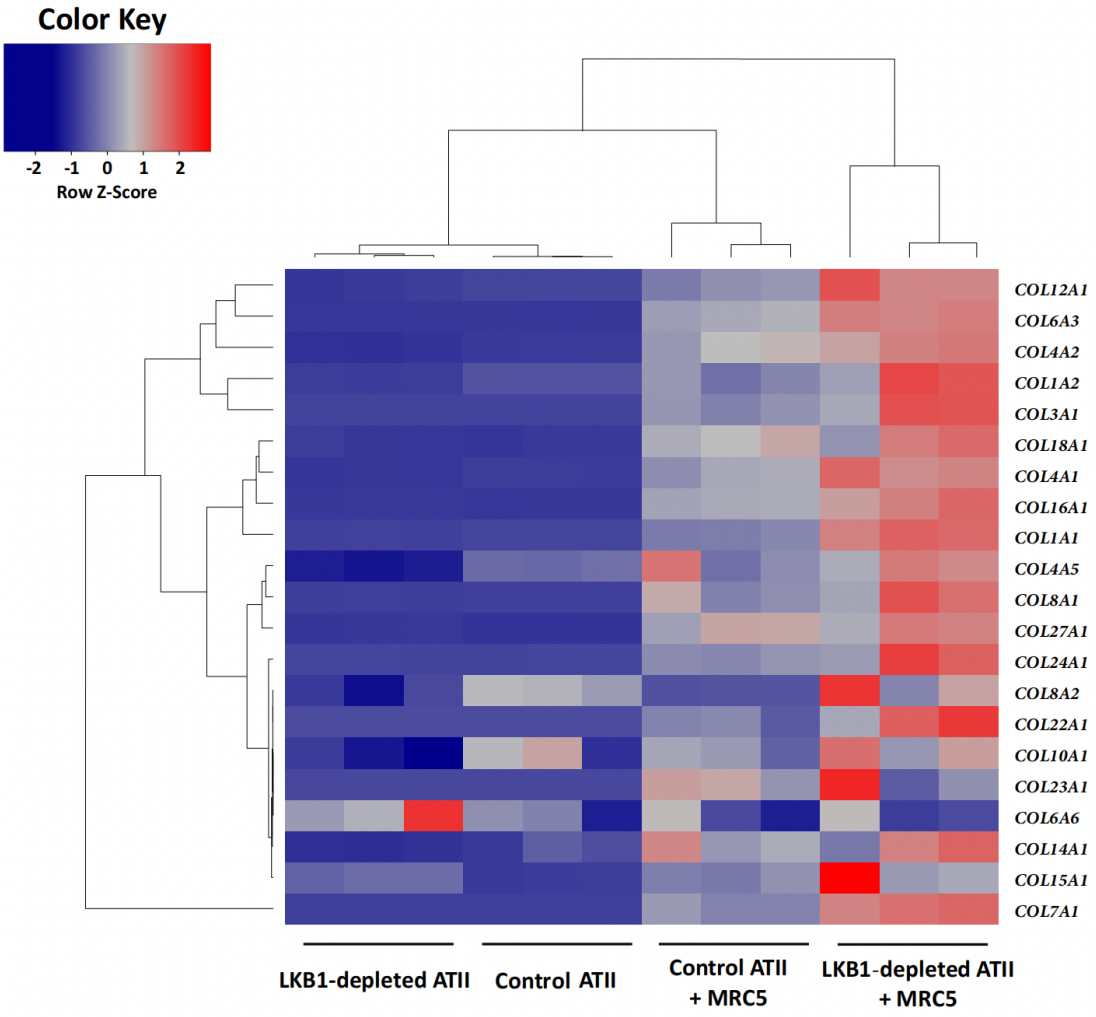

FIGURE 5.12: **Heatmap and hierarchical cluster analysis of multiple collagen genes in 2D-cultured control or LKB1-depleted ATII cells and 3D co-cultures of MRC5 with control or LKB1-depleted ATII cells**
Red indicates upregulation and blue downregulation. n=3 samples in each group.

5.5.4 2D/3D co-cultures of LKB1 depleted ATII cells with MRC5 lung fibroblasts suggest a paracrine signalling between LKB1-depleted ATII cells and fibroblasts augments myofibroblast activation.

To further explore the effect of paracrine signalling on fibroblast to myofibroblast transition and analysed *ACTA2* expression, the myofibroblasts markers - Smooth muscle aortic alpha-actin (α-SMA, *ACTA2*) has been evaluated and it is also significantly up-regulated (Figure. 5.14a). These results suggest that the increased expression of α-SMA may indicate the differentiation of myofibroblasts from residential human fibroblasts (MRC5). This behaviour appears to be triggered by the interaction between MRC5 and LKB1-depleted ATII cells. to confirm the paracrine influence of ATII cells on fibroblast differentiation, we treated MRC5 cells with conditioned media (CM) from ATII cells transfected with control or LKB1 siRNA

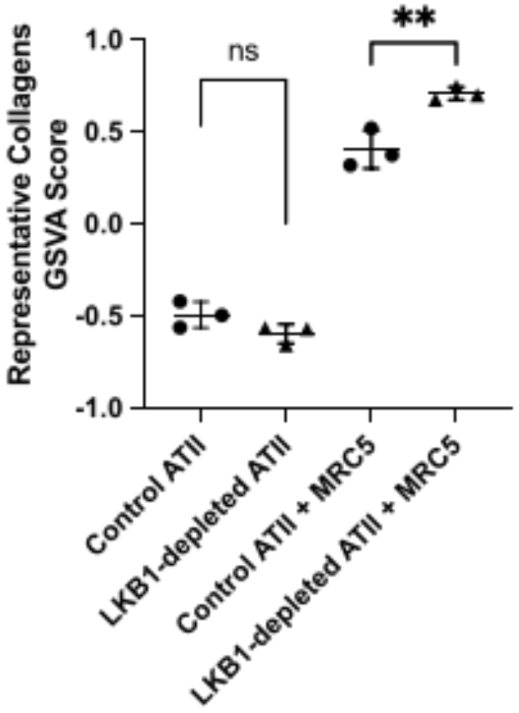

FIGURE 5.13: **Gene Set Variation Analysis (GSVA) scores using a collagen signature in 2D-cultured control or LKB1-depleted ATII cells, and 3D co-cultures of MRC5 with control or LKB1-depleted ATII cells**
Data are mean±s.d.;n=3 samples in each group. $**$ $P < 0.01$ and ns: not significant.

without or with the addition of transforming growth factor-β (TGF-β), and assessed levels of α-SMA. CM from ATII cells transfected with LKB1 siRNA without TGF-β had a similar effect on α-SMA expression compared to TGF-β treatment alone (Figure. 5.14b). Furthermore, CM from LKB1-depleted ATII cells together with TGF-β achieved a strong synergistic effect on α-SMA protein levels (Figure. 5.14b).

To better understand the influence of LKB1 depletion in ATII cells on fibroblasts, we utilised a machine learning method called CIBERSORTx can effectively analyze the dynamic alterations in the proportion and abundance of these two major cell types (ATII and fibroblasts) and their subtypes. Briefly, The CibersortX analysis was performed on the Kropski single-cell RNAseq dataset (GSE135893) (Arun C Habermann et al. 2020), through the CibersortX web portal to derive gene expression signatures associated with different cell types. These signatures were then mapped onto 2D or 3D LKB1 depletion RNAseq data to quantify the proportion of each cell type in individual samples to compare epithelial cells and fibroblast components.

the CibersortX analysis was conducted using the following parameters: batch correction was implemented since the 6 samples of LKB1 depletion ATII -MRC5 bulk RNAseq were provided as FPKM values, and the single-cell RNA-seq signature matrix was computed using raw counts for input. All other settings remained at their

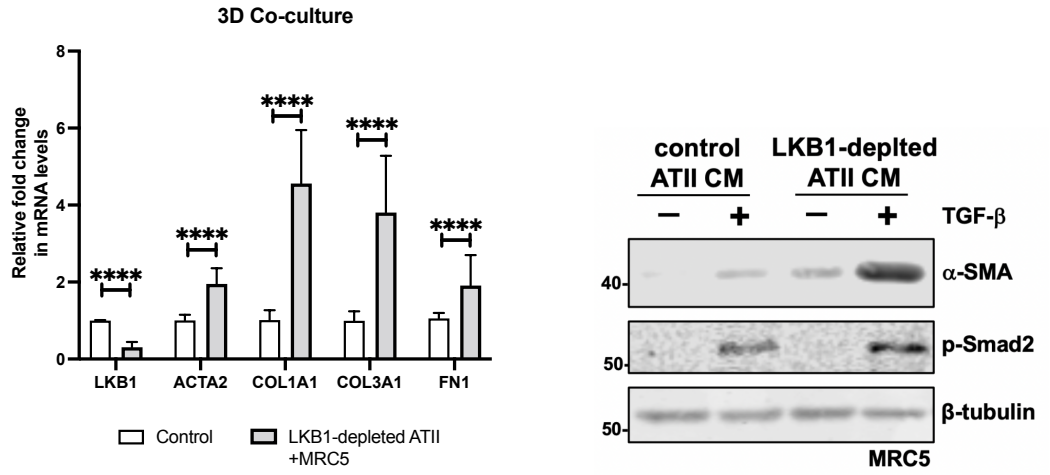

(A) (B)

FIGURE 5.14: **Relative mRNA expressions of *STK11* (LKB1), *ACTA2* (α-SMA), *COL1A1*, *COL3A1* and *FN1* in the spheroid samples from MRC5 co-cultured with control or LKB1-depleted ATII cells**

β-actin-normalised mRNA levels in ATII cells were used to set the baseline value at unity. Data are mean $\pm$ s.d. $n = 3$ samples per group. $*P < 0.05$; $**P < 0.01$; $***P < 0.001$ and ns: not significant

default values, and the cell type has been defined in that paper. The combined proportions obtained from the CibersortX analysis are displayed in figure. 5.15a, with cell types categorized as epithelial, and mesenchymal based on their classification. Notably, LKB1-depleted ATII co-culturing with MRC5 exhibit an increased presence of mesenchymal cell types along with a decreased proportion of epithelial cells, which is consistent with their established functional role in Epithelial-mesenchymal transition. Apart from that, the different mesenchymal cells including fibroblasts and other subtypes also have been mapped on the 3D dataset (Figure. 5.15b). Compared to other types of fibroblast, myofibroblasts show broadly enriched in LKB1 depleted ATII cells co-culturing with MRC5, suggesting that the LKB1 depletion can augment myofibroblasts activation in epithelial-mesenchymal microenvironment.

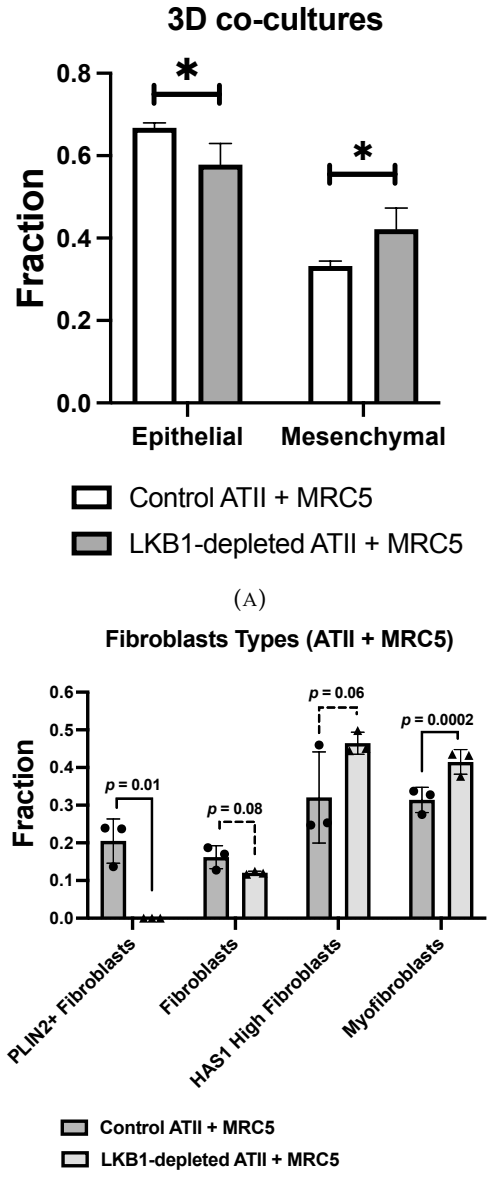

FIGURE 5.15: **Comparison of cell type abundance and expression from 3D co-culturing RNA-seq dataset**

Estimated epithelial and mesenchymal composition in 3D co-cultures obtained from CIBERSORTx (Chloé B Steen et al. 2020). Differences in fractions between LKB1-depleted ATII co-culturing with MRC5 and control group in RNA-seq dataset. B. Estimated fibroblast subtypes (PLIN2+fibroblast, fibroblasts, HAS1 high fibroblasts, myofibroblasts) composition obtained from CIBERSORTx. Differences in fractions between LKB1-depleted ATII co-culturing with MRC5 and control spheroid in RNA-seq dataset. Both analyses based on the signature Matrix were created by the scRNA-seq dataset acquired from GSE135893.

5.6 Discussion

The crucial interplay between epithelial and fibroblast cells has long been the subject of intensive research, particularly in the context of fibrotic diseases. Our prior studies indicated a pivotal role of reduced autophagy activity in mediating fibrosis through a disrupted epithelial-fibroblast dialogue (Charlotte Hill, Juanjuan Li, et al. 2019). The current experiment extends this discourse, focusing on the effects of LKB1 depletion in ATII cells.

Cell co-culture models are pivotal tools in cell biology, facilitating the observation of interactions between different cell types or between cells and their surrounding microenvironment (Noel et al. 2017). Depending on the desired investigation, cells can either be placed in direct contact or kept separate to study the influence of specific chemical factors on cell behaviour (K. MacDonald et al. 2005). These configurations are respectively termed "direct contact co-culture" and "indirect contact co-culture" models (Paschos et al. 2015). In the direct contact co-culture approach, cells can either be intimately mixed or layered upon a monolayer, such as a trophoblast. This setup involves co-cultivating two or more cell types in a defined ratio on a shared surface under controlled conditions. In the context of this chapter, the co-culture of ATII cells with MRC5 fibroblasts using the Nanoshuttle-PL method is highlighted. A primary advantage of this system is its ability to elucidate the interactions between alveolar epithelial type II cells (ATII) and human fibroblasts (MRC5), providing insights into discrepancies in the extracellular matrix components and fibroblast diversity. Notably, co-culturing LKB1-depleted ATII cells with fibroblasts revealed that LKB1 depletion not only instigated an epithelial-to-mesenchymal transition (EMT) in epithelial cells but also modulated secretory factors or paracrine signalling, promoting myofibroblast differentiation. Furthermore, the growth of co-cultured fibroblasts was observed to be enhanced by down-regulating LKB1 in ATII cells.

In employing the 3D co-culture model coupled with RNA-seq, we obtained a more physiologically relevant representation of cell-cell interactions. The CIBERSORTx method, a machine learning technique, further refined our analysis, enabling us to discern changes in cell populations with LKB1 depletion in ATII cells. Our results indicate a pronounced shift from the epithelial to the mesenchymal phenotype, which aligns with the well-documented EMT process observed in many fibrotic conditions. Particularly noteworthy is the marked increase in the myofibroblast population, a cell type integrally associated with fibrosis progression.

Cellular interactions or regulations aren't solely achieved through direct cell-to-cell contact. More often, they are facilitated by chemical signals disseminated within microenvironments. Given this, a co-culture system that precludes direct cellular interactions is sometimes requisite. Enter the indirect contact co-culture method: this involves cultivating diverse cell types in a manner that facilitates interaction via

chemical mediators present in the culture medium, without any direct physical contact. One prevalent approach is the use of conditioned media. Here, cell culture supernatants, rich in various growth factors or stimuli secreted by cells, are harvested. These supernatants are then employed to discern the effects of these factors on cellular growth or differentiation. For instance, The Western blot results are presented in figure. 5.14b show that when human fibroblasts (MRC5) are treated with TGFβ or left untreated, and then exposed to conditioned media harvested from ATII cells (either transfected with *STK11* siRNA or not), there are differential expression levels of α-SMA observed. This indirect co-culture approach is invaluable for probing cellular paracrine actions under distinct conditions and is amenable to quantitative analyses. Furthermore, additional regulators such as immune cytokines and secreted enhancers can also be added to the co-culture system to study intercellular interactions. For example, for the global transcriptomic investigation in LKB1-depleted ATII cells. The collagen gene expression data challenge the prevalent belief about EMT's direct role in collagen production. While LKB1-depleted ATII cells undergoing EMT did not manifest a significant uptick in collagen gene expression, a stark contrast was observed in the 3D co-culture model. This differential expression, further quantified by GSVA, underscores the importance of cellular context and interactions in gene expression dynamics. Additionally, the up-regulated expression of *ACTA2*, *COL1A1*, *COL3A1*, and *FN1* post-LKB1 depletion in ATII cells, as revealed by the RNA-seq and subsequently validated by real-time qPCR, supports the hypothesis that LKB1 plays a significant role in regulating ECM genes.

Co-culture systems have been engineered to closely mimic the intricate cellular interactions seen in vivo. However, these models aren't without their challenges. While they closely mimic in vivo conditions, they often lack essential components such as vasculature or immune cells. Combining multiple organoids into a larger structure can lead to central necrosis due to these missing components. Additionally, achieving standardization in these co-culture models remains a hurdle. The convergence of various techniques, including advanced culturing, biosensors, and microfluidics, holds promise for crafting more complex and reproducible in vitro tissue models. These multi-organ co-culture systems have already shown their worth in studies related to neurodevelopment, neuromodulatory mechanisms, and neurological diseases, heralding new research avenues. Despite these advancements, organoid-based co-culture systems are still nascent in the realm of human tissue research. Compared to traditional models, they are in their infancy, and challenges such as stability, reproducibility, scalability, and accurate control of microenvironmental conditions persist. Many of these systems, while promising, are still in their proof-of-concept stages rather than being fully realized alternatives to existing models. Each comes with its unique advantages and limitations (R. Liu et al. 2022).

Drawing upon these findings and our prior research (Charlotte Hill, Juanjuan Li, et al. 2019; L. Yao, Franco Conforti, et al. 2019), we posit that collagen production in IPF lungs may not be a direct consequence of EMT. Instead, epithelial cells might exert an indirect influence on myofibroblast differentiation through paracrine signalling. Such a perspective demands a more intricate understanding of the role of epithelial cells in fibrosis, emphasizing the necessity to discern between their direct and indirect contributions. As we continue unravelling the complexities of IPF, which is going to be discussed in the next chapter, it becomes increasingly evident that a singular lens may not suffice. The nuanced interplay of cellular interactions and signalling pathways warrants a multifaceted approach to decode the intricacies of this debilitating condition.

Chapter 6

Investigating the role of LKB1 using human patient samples and mouse model

Results shown throughout this chapter are part of the following publication: [1]

6.1 Abstract

Activation of LKB1 occurs via allosteric binding of LKB1 to STE20-related adaptor (STRAD) and mouse protein 25 (MO25, encoded by *CAB39* and *CAB39L*) (Zeqiraj et al. 2009). Given our in vitro findings, we compared the expressions of LKB1 (*STK11*), *STRADA*, *STRADB*, *CAB39* and *CAB39L* in IPF and control lungs in a transcriptomic dataset that we have recently established (GSE169500) (Brereton, L. Yao, Davies, Yilu Zhou, Vukmirovic, J. A. Bell, S. Wang, Ridley, Dean, Andriotis, et al. 2022a). Briefly, laser capture microdissection was performed upon Formalin-Fixed Paraffin-Embedded (FFPE) control non-fibrotic lung tissue (alveolar septae, n=10) and usual interstitial pneumonia/idiopathic pulmonary fibrosis FFPE lung tissue (fibroblast foci and adjacent non-affected alveolar septae, n=10 each), followed by RNA-seq. Among those subunits within the LKB1 complex, only the expression of *CAB39L*, the allosteric activator of LKB1, was down-regulated in IPF alveolar septae. By contrast, expressions of other subunits, including LKB1 (*STK11*), *STRADA*, *STRADB* and *CAB39*, did not significantly change in IPF lungs. Down-regulation of *CAB39L* in human IPF lungs was then verified using real-time qPCR and RNA in situ hybridisation, showing a reduced mRNA level of *CAB39L* in IPF lungs. Using the same dataset (GSE169500), we assessed the expression of *CAB39L*

[1] ***Xu Z***, *Davies E R, Yao L, et al. LKB1 depletion-mediated epithelial–mesenchymal transition induces fibroblast activation in lung fibrosis. Genes & Diseases, 2023, ISSN 2352-3042, https://doi.org/10.1016/j.gendis.2023.06.034.*

and *SNAI2* (Snail2) in alveolar septae from control and IPF lungs. We found that the levels of *CAB39L* were significantly inversely correlated with emphSNAI2 (Snail2). These observations agree with the finding that in IPF down-regulation of *CAB39L* leads to LKB1 inactivation and promotes EMT via the p62-NF κB pathway.

To determine whether the inactivation of Lkb1 in mouse alveolar epithelium induces the fibrotic process in murine tissue, mice deletion of Lkb1 is initiated by the introduction of Cre-expressing adenovirus. We first confirmed the expression of Lkb1 in murine lung interstitial and alveolar spaces. The result showed high efficiency in knocking out Lkb1 in mouse alveolar interstitial at a young age (3 months post-intubation) compared to the wild type. In this section of this part, we also quantified the proportion of alveolar spaces in the lung tissue by determining the ratio of the total area of alveolar spaces to the total area of the lung tissue section. The findings implied that the removal of Lkb1 in mice might lead to a degradation in lung function.

6.2 Introduction and Rationale

The exact progenitors of fibroblasts and myofibroblasts in IPF remain a subject of debate. Various studies have proposed different candidate progenitor cells, encompassing alveolar epithelial cells (AECs) through epithelial-mesenchymal transition (EMT), interstitial fibroblasts, lipofibroblasts, circulating fibrocytes, and pericytes. In particular, circulating fibrocytes are suggested to contribute to the myofibroblast population in IPF, driven by factors released from apoptotic and necroptotic AECs emitting CXCL13 and CCL2. Nonetheless, the specific lineage of these fibrocytes remains ambiguous, with some theories positing that they might be a subset of monocyte-derived macrophages. While certain studies using murine models have indicated that specific pericyte populations can differentiate into lung fibroblasts, this phenomenon has not yet been evidenced in IPF. Moreover, other lineage tracing experiments in mice have refuted a pericyte origin for lung fibroblasts. Recent research has pinpointed a group of lipofibroblasts as a possible precursor for activated myofibroblasts. As research progresses, the theory of an epithelial origin is becoming less favoured, with single-cell RNA sequencing (scRNA-seq) data bolstering the idea of a paracrine signalling role for AECs via EMT (Moss, Ryter, and Rosas 2022). Given the evidence presented, it is crucial to ascertain the role of LKB1 in IPF and to determine whether the loss of LKB1 in alveolar epithelial cells impacts mouse lung function.

6.3 Objectives

1. Determine the role of LKB1 as either a protein kinase or an activator within specific complexes, and its association with downregulation in human IPF lungs. This will involve analyzing existing IPF databases and patient samples using bioinformatics strategies and conducting In Situ Hybridization (ISH) to accurately target relevant components.

2. Investigate the impact of Lkb1 deletion in mouse lung epithelial cells on lung function and the potential development of irreversible lung fibrosis. This will be achieved by generating Lkb1-deficient mice through the administration of an adenovirus expressing Cre recombinase. The virus will be delivered to the lungs of anaesthetized mice via intratracheal instillation, allowing for targeted infection of the pulmonary alveoli.

6.4 Methodology

All primary human lung sections and transcriptomic profiling database was from Brooke Lab, Clinical and Experimental Sciences, University of Southampton. (University Southampton Hospital, UK), especially by Dr Mark Jones and Franco Conforti, as described in their previous work (Franco Conforti et al. 2017). Details were described in section 2.14. The RNAscope ISH (In Situ Hybridization) Assay refer to section 2.13.3. Briefly, the RNAscope in situ hybridization assay is performed to detect the mRNA probe in IPF patients and healthy donors. The procedure consists of the following steps outlined below. tissue sections were baked for 1 h at 60 $^{\circ}C$, deparaffinized, and treated with pre-treat 1 for 10 min at room temperature (RT). Target retrieval was performed for 15 min at 100 $^{\circ}C$, followed by protease treatment for 15 min at 40 $^{\circ}C$. Probes were then hybridized for 2 h at 40 $^{\circ}C$ followed by RNAscope amplification followed by DAB chromogenic detection.

Mouse lung tissue isolated from inducible Lkb1 -/- mice where deletion of Lkb1 is initiated by the introduction of adenovirus expresses Cre recombinase and the viral delivery method when initiating an experiment. delivered Cre to the lungs of anaesthetized mice using intratracheal instillation (IT) to infect the whole pulmonary alveoli. Details were performed in section 2.10.

6.5 Results

6.5.1 Down-regulation of *CAB39L* in human IPF lungs.

In terms of the discussion in the last chapter, we evaluated that LKB1 plays an important role in inducible EMT in epithelial cells. Studies in animal models have shown that loss of LKB1 in lung epithelial cells can lead to the development of lung fibrosis, suggesting that LKB1 may play a protective role in preventing the development of IPF. We hypothesised that LKB1 appears to have significant up-regulation in established IPF. Laser Capture micro-dissection database (GSE169500) (Brereton, L. Yao, Davies, Yilu Zhou, Vukmirovic, J. A. Bell, S. Wang, Ridley, Dean, Andriotis, et al. 2022b) utilized to investigate the expression of LKB1 and its relative components in IPF tissue and healthy people.

In brief, a transcriptomic dataset of normal and IPF lungs was produced by laser capture micro-dissection microscopy, which can precisely excise samples from Formalin-fixed, paraffin-embedded alveolar septae in control lungs and IPF biopsies, as well as fibroblast foci from IPF lungs. After Dr. Mark Jones performed tissue procurement and laser capture micro-dissection at the University of Southampton, the sequencing and read assignment were performed at the University of Yale, and FPKM values were calculated from raw count data to normalize for sequencing depth and gene length. 10 control and 10 IPF tissue samples, with alveolar septae and fibroblast foci (FF) being dissected from the same IPF tissue samples, resulting in a total of 30 samples. An Ion Torrent Proton sequencer produced around 20 million single-end reads per sample, with each read being roughly 100bp in length. Post-processing and reads mapping to the University of California Santa Cruz hg19 human genome to calculate FPKM values. To assess RNA quality before sequencing, RNA integrity (RIN) numbers were measured.

LKB1 serves as both a protein kinase and a tumour suppressor, with mutations leading to its inactivation observed in a variety of sporadic cancers and tissue fibrosis instances. The inactivation mechanism in many diseases, however, may not always directly involve LKB1 (W. Li et al. 2018). CAB39 and its paralog CAB39L, are scaffolding proteins that interact with LKB1 and the STE20-Related Kinase Adaptor (STRAD), facilitating LKB1's activation (Jérôme Boudeau, Annette F Baas, et al. 2003a). This activation is critical as LKB1 is a recognized tumour suppressor and the primary kinase for phosphorylating AMPK. Located on chromosome 13q14.2, CAB39L, the β isoform of CAB39, forms part of the LKB1 complex. It can interact with the LKB1-STRAD complex, leading to the activation of LKB1, which consequently results in the phosphorylation and activation of AMPKα/β. To reveal these components, After comparing the expression of LKB1 (*STK11*), *STRADA*, *STRADB*, *CAB39* and *CAB39L* in IPF and control lung, only the expression of *CAB39L*, the

allosteric activator of LKB1, was down-regulated in IPF alveolar septae (Figure. 6.1,figure. 6.3a). Dr. Elizabeth R Davies thereby confirmed the expression of *CAB39L* in IPF tissues (Figure. 6.3b). the results suggested as same as in alveolar septae, which *CAB39L* had lower expression in IPF tissue compared to Healthy donors. These results gave us the hint that reduced *CAB39L* expression causes LKB1 to decrease via allosteric binding LKB1 complex in IPF, which can improve EMT via paracrine signalling. Based on this hypothesis, we created a Pearson correlation plot showing a correlation between *CAB39L* with *SNAI2*. The dataset (GSE169500) was subjected to Principal Component Analysis (PCA) to identify the primary sources of variation within the data. Notably, Plotting the two principal components of this analysis showed a strong segregation between *CAB39L* with *SNAI2*, both in IPF alveolar septae and control alveolar septae. in other words, it means that as the expression of *SNAI2* increases, the expression of *CAB39L* may decrease. this significant variation in the difference between the expression of *CAB39L* and *SNAI2*, indicating that there is a negative correlation between *CAB39L* and *SNAI2* in IPF dataset.

We then performed In situ detection of *CAB39L* mRNA on formalin-fixed paraffin-embedded (FFPE) tissue sections of human lungs from IPF patients or healthy donors (control) using RNAscope and this part was conducted by Dr.Elizabeth R Davies. The use of RNAscope in this study is particularly valuable for visualizing the expression of low-abundance *CAB39L* specifically expressed at a cellular level within lung tissue. The counterstaining with Gill's Hematoxylin and mounting of the tissue sections before imaging would help to enhance the visualization of the signals. Based on the results of the RNAscope analysis, it appears that the expression of *CAB39L* is significantly lower in the alveolar septae of IPF patients compared to healthy donors. This finding supports the previous observation that the expression of *CAB39L* is low in IPF tissue samples (Figure. 6.4). Overall, the results of this study suggest that the decreased expression of *CAB39L* may play a role in the pathogenesis of IPF, which is a valuable insight for further research into potential therapeutic targets for this disease.

6.5.2 The impact of Lkb1 deletion in mouse lung epithelia

To investigate whether the inactivation of Lkb1 in mouse alveolar epithelium induces the fibrotic process in murine tissue, we utilized an adenovirus expressing Cre to delete Lkb1 in mice. At both 3 months and 17 months post-intubation, mice were euthanized and their inflated right lungs were embedded in paraffin for subsequent H&E and trichrome staining, as well as immunohistochemistry (IHC). Additionally, the right lung tissue was prepared for RNA/protein extraction. We initially confirmed the expression of Lkb1 in murine lung interstitial and alveolar spaces. However, due to the overlapping cytoplasmic and nuclear stains of the LKB1 antibody, we utilized a deconvolution DAB method to obtain independent Lkb1 signals (Ruifrok,

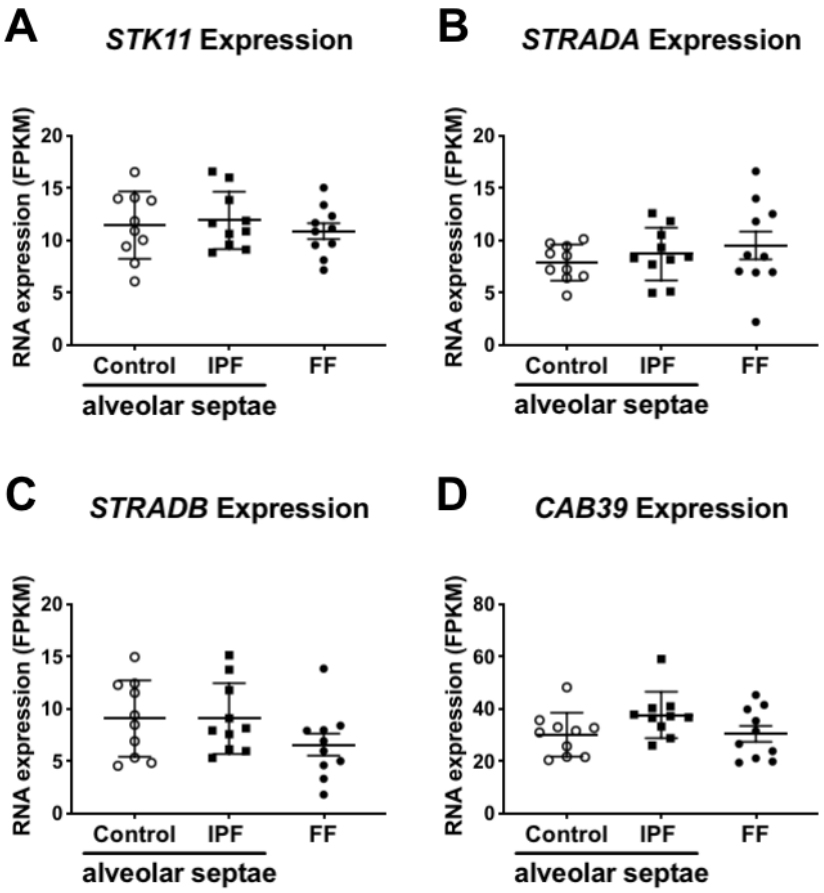

FIGURE 6.1: **Down-regulation of *CAB39L* in human IPF lungs**
Expression of *STK11* (LKB1) (A), *STRADA* (B), *STRADB* (C) and *CAB39* (D) in healthy (control) alveolar septae, IPF alveolar septae and IPF fibroblast foci(FF) ($n = 10$ individual healthy and IPF donors; GSE169500). Relative expression levels are calculated as Fragments Per Kilobase of transcript per Million mapped reads (FPKM). Data are mean $\pm$ s.d.; $n = 10$ samples in each group.

D. A. Johnston, et al. 2001). Our results demonstrate a high efficiency of Lkb1 knockout in mouse alveolar interstitial cells at a young age (3 months post-intubation) compared to the wild type (Figure. 6.5).

Dr.Elizabeth R Davies and I conducted experiments to investigate whether Lkb1 defective mice exhibit pathological features of pulmonary fibrosis, such as interstitial thickening and collagen deposition at an older age (17 months post-intubation). H&E staining was performed on interstitial tissue from both $Lkb1^{-/-}$ mice and WT mice at the same age, and the results were presented in Figure. 6.6 a. Our findings demonstrate that the interstitial tissue from $Lkb1^{-/-}$ mice exhibited a significantly greater degree of thickening compared to the WT mice. Additionally, We quantified the percentage of alveolar spaces in the whole lung tissue and found that the volume of alveolar space in $Lkb1^{-/-}$ mice was significantly reduced compared to the WT mice (Figure. 6.6 b). Briefly, we performed image analysis on the H&E-stained lung

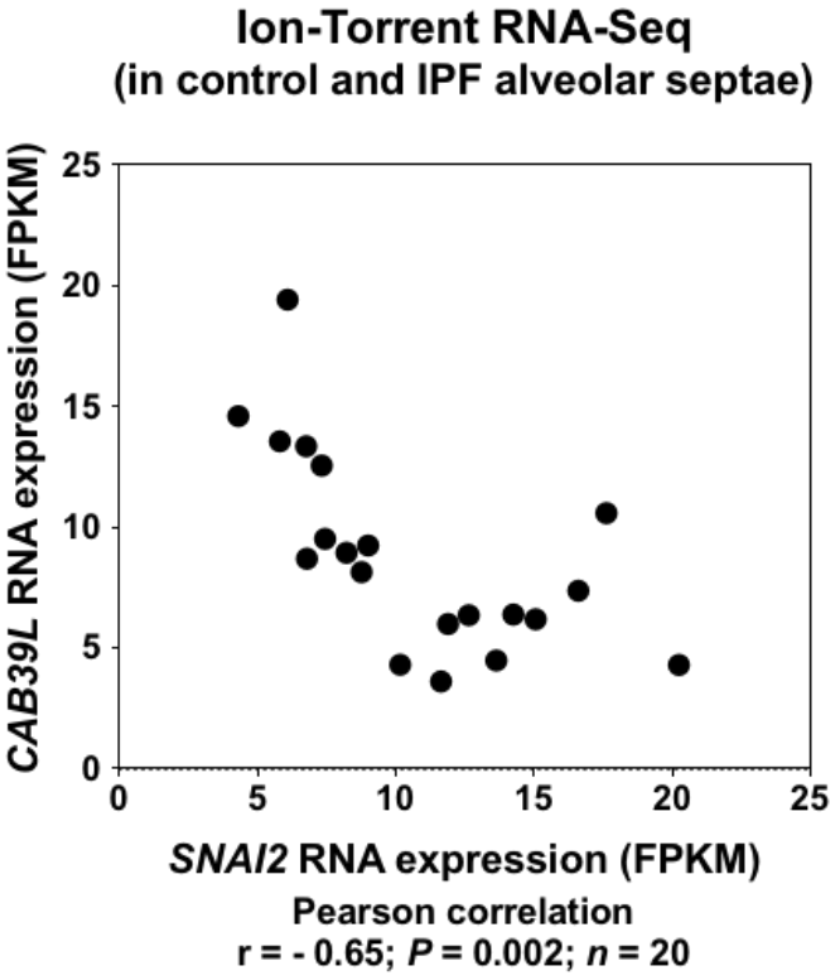

FIGURE 6.2: **Negative correlation of *CAB39L* with *SNAI2* in IPF**
Scatter plot to compare the expression of *CAB39L* and *SNAI2* (Snail2) in alveolar septae from healthy donors and IPF patients. (Pearson coefficient $r = -0.65$; $P = 0.002$; $n = 20$).

tissue sections and selected representative images of lung tissue sections from both Lkb1$^{-/-}$ mice and WT mice by sections scanner. Then, using image analysis software(Fiji), we outlined the alveolar spaces in each image and calculated the area of the alveolar spaces as well as the area of the entire lung tissue section. Finally, we calculated the percentage of alveolar spaces by dividing the total area of alveolar spaces by the total area of the lung tissue section. This allowed us to quantify the percentage of alveolar spaces in the whole lung tissue and compare the results between Lkb1$^{-/-}$ mice and WT mice. These results suggest that the deletion of Lkb1 in mice results in a loss of lung function. Taken together, our findings indicate that Lkb1 plays a crucial role in maintaining normal lung function and its deficiency leads to pathological features of pulmonary fibrosis in mice.

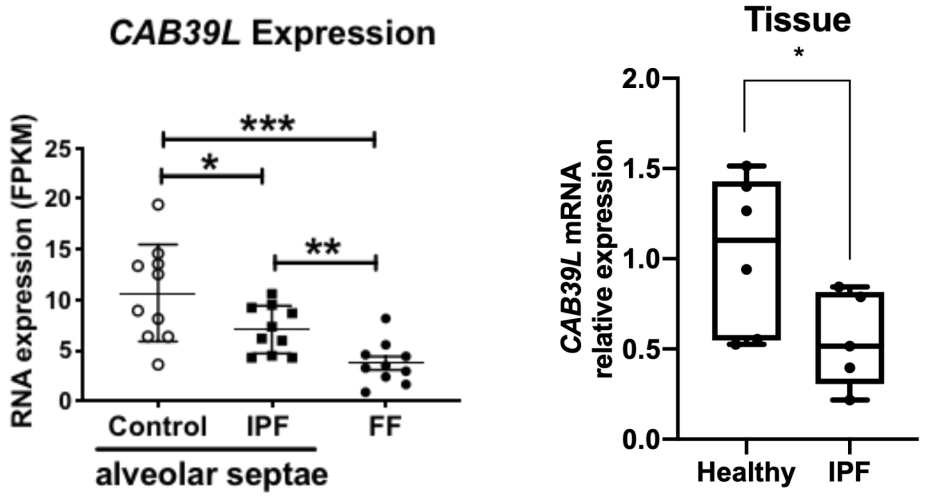

(A) A (B) B

FIGURE 6.3: **Down-regulation of *CAB39L* in human IPF lungs**
(A). Expression of *CAB39L* in healthy (control) alveolar septae, IPF alveolar septae and IPF fibroblast foci $n = 10$ individual healthy and IPF donors; GSE169500). Relative expression levels are calculated as Fragments Per Kilobase of transcript per Million mapped reads (FPKM). $*\ P < 0.05$; $**P < 0.01$, $***P < 0.001$. (B). Relative fold changes in the mRNA level of *CAB39L* in human healthy donor vs. IPF lungs. Data are mean $\pm$s.d.; $n = 6$ samples per group. $*P < 0.05$.

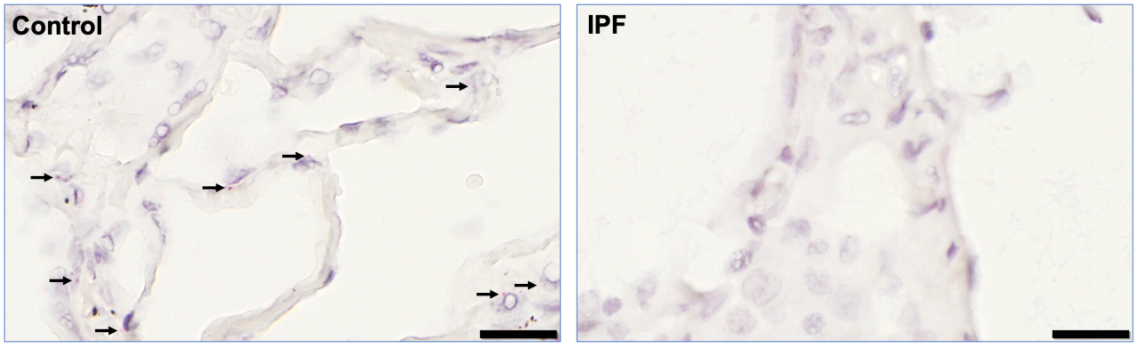

FIGURE 6.4: **Down-regulation of *CAB39L* in human IPF lungs**
Representative images of mRNA expression of *CAB39L* (red) in the lungs from healthy donors (control) or IPF patients (IPF) using RNAscope® RNA in-situ hybridisation. Scale bar: 20 μm.

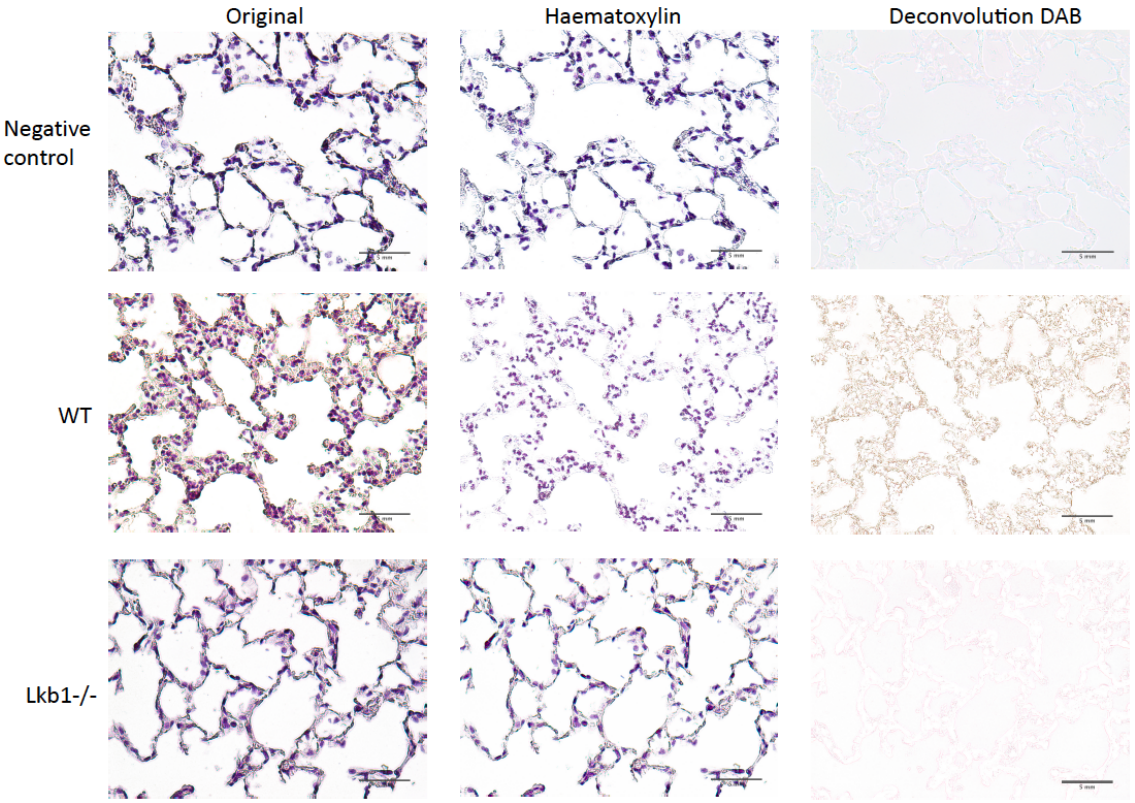

FIGURE 6.5: **Lkb1 is deleted in mouse lung alveolar interstitium compared to WT**
Each row showing immunohistochemistry of LKB1 antibody/TBS stained images is separated into haematoxylin and DAB channels. Lkb1 for WT and $lkb1^{-/-}$ mouse embedded tissue and TBS for negative control. Images with deconvolution DAB performed LKB1 cytoplasmic staining. 40× magnification, scale bar means 5 mm.

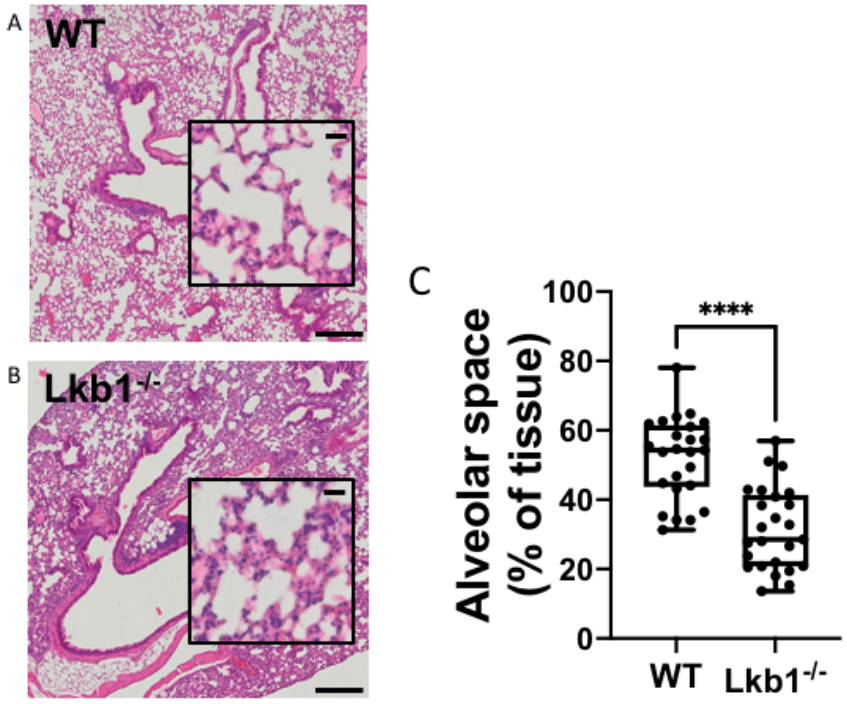

(A) A (B) B

FIGURE 6.6: **Lkb1 deletion in mice shows interstitial thickening** (A, B) Histologic images showing H&E staining for alveolar interstitial in WT and Lkb1$^{-/-}$ mice. Original magnification 20×, scale bar 200/20 μm. (C) Quantified percentage of WT and Lkb1$^{-/-}$ mice lung alveolar space in whole tissue. $****P < 0.0001$

6.5.3 Discussion

The centrality of LKB1's role, a well-recognized kinase, in various cellular processes, underscores the imperative of understanding its regulation. The allosteric activation of LKB1, mediated through its binding to STRAD and MO25, offers a multifaceted regulatory mechanism. The current findings, drawing from our in vitro observations and the transcriptomic IPF database, highlight the intriguing dynamics of the LKB1 complex within the context of IPF.

The differential expression of the LKB1 complex subunits in IPF offers the first point of discussion. Among these, CAB39L, an allosteric activator, emerged as the sole subunit manifesting down-regulation in IPF alveolar septae. The unaltered expression of other subunits, including LKB1 itself, accentuates the potential significance of CAB39L's regulation. This observation is further substantiated by the subsequent validation experiments, confirming the reduced mRNA levels of *CAB39L* in IPF lungs. The inverse correlation between *CAB39L* and *SNAI2* in alveolar septae further underlines the nuanced interplay between these molecules, suggesting an inverse relationship between LKB1 activation and EMT progression in IPF. Other researchers have been reporting the role of CAB39L in the LKB1 complex in gastric cancer (GC). CAB39L interacts with the LKB1-STRAD complex, leading to AMPK activation, and its suppression effects can be reversed by LKB1 knockdown. Further, CAB39L influences cellular energy metabolism by promoting oxidative phosphorylation and mitochondrial biogenesis, countering the Warburg effect—a characteristic metabolic shift in cancer cells. This metabolic influence is linked to improved patient outcomes; hence, CAB39L promoter methylation could serve as a prognostic biomarker for GC (W. Li et al. 2018).

The in vivo experiments, involving the targeted deletion of Lkb1 in mouse alveolar epithelium, provide additional insights. The choice of inducing Lkb1 deletion using Cre-expressing adenovirus offers a precise and controlled manipulation. The meticulous temporal analysis, examining effects at both 3 months and 17 months post-intubation, offers a longitudinal perspective. Confirming Lkb1 expression in murine lung interstitial and alveolar spaces lays the groundwork for evaluating the impact of its deletion. The innovative application of deconvolution DAB to discern Lkb1 signals, given the overlap challenges, underscores the necessity of methodological rigour in such experiments. The observed high-efficiency knockout in younger mice, juxtaposed against the wild type, hints at the potential age-related dynamics in LKB1 regulation and function.

The broader implications of these findings remain manifold. LKB1's regulation, particularly via CAB39L, could emerge as a potential therapeutic target in IPF. Moreover, the inverse dynamics between CAB39L and EMT progression might offer novel biomarkers or prognostic indicators for IPF. However, as we delve deeper into

the role of LKB1 in fibrotic processes, it's imperative to reconcile these observations with broader cellular and molecular contexts, ensuring that we appreciate the complexity and multi-factorial nature of IPF pathogenesis.

Chapter 7

Conclusion and Future Work

7.1 Final conclusion

Work discussed throughout this chapter is part of the following publications:[1]

In summary, In this study, LKB1 depletion in alveolar type II (ATII) cells led to significant transcriptomic changes, notably the activation of EMT and TNFα signalling pathways via NF κB, as evidenced by RNA-seq and GSEA analyses. This alteration was associated with an increase in mesenchymal markers, a decrease in epithelial markers, and inhibition of autophagy, as shown by changes in p62 and LC3-II levels. The findings suggest that LKB1 inactivation in ATII cells promotes EMT and fibrosis through a p62-NF κB dependent mechanism, aligning with previous observations of reduced fibrotic activity in myofibroblasts with activated AMPK, LKB1's downstream effector. this study not only provides novel insights into the role of epithelial LKB1 in pulmonary fibrosis but also highlights the potential therapeutic intervention by targeting this pathway in IPF. It explores the complex interplay between epithelial and fibroblast cells, particularly under conditions of fibrosis, focusing on the consequences of LKB1 depletion in alveolar type II (ATII) cells. Through cell co-culture models, the study demonstrates how LKB1 depletion leads to epithelial-to-mesenchymal transition (EMT), affecting paracrine signalling and promoting myofibroblast differentiation, impacting fibrosis progression. Utilizing both direct and indirect co-culture approaches, the research provides insights into cellular interactions and their role in fibrotic diseases like idiopathic pulmonary fibrosis (IPF). The findings suggest that collagen production in IPF may not directly result from EMT but may involve complex interactions and paracrine signalling between epithelial cells and myofibroblasts. This highlights the importance of advanced co-culture models in simulating in vivo conditions and understanding disease mechanisms. Apart from

[1] ***Xu Z***, *Davies E R, Yao L, et al. LKB1 depletion-mediated epithelial–mesenchymal transition induces fibroblast activation in lung fibrosis[J]. Genes & Diseases, 2023.*

that, the research highlights the pivotal role of the LKB1 complex, particularly emphasizing the allosteric activation by CAB39L in IPF. It was discovered that, within the complex, only CAB39L is down-regulated in IPF, suggesting its significant role in disease dynamics. In vivo experiments further elucidate LKB1's function in lung tissue, underlining the age-related differences in its expression and activity. These insights propose CAB39L's regulation and the LKB1 pathway as potential therapeutic targets and biomarkers in IPF, urging a more comprehensive understanding of their roles in the disease's pathogenesis (Figure. 7.1).

IPF is a progressive interstitial lung disease with limited treatment options available (Richeldi, H. Collard, and M. Jones 2017). Although the underlying cause of IPF is not fully understood, repetitive micro-injuries to aged alveolar epithelium are proposed to trigger aberrant wound healing processes, initiating an accumulation of ECM deposited by myofibroblasts (Moss, Ryter, and Rosas 2022), which are critical in the pathogenesis of IPF, with increased fibroblast foci associated with worse prognosis (T. King Jr et al. 2001). The origin of myofibroblasts in IPF is controversial and it was proposed that ATII cells undergone EMT may be a source of myofibroblasts in fibrotic diseases. However, findings from our group suggest that ATII cells undergoing EMT induced by RAS activation (L. Yao, Franco Conforti, et al. 2019) or autophagy inhibition (Charlotte Hill, Juanjuan Li, et al. 2019) produce extremely low levels of ECM genes. This is also the case when ATII cells undergo EMT induced by LKB1 depletion in this study (See chapter. 5). However, using conditioned media experiments or a 3D co-culture model in this study, we were able to demonstrate that although epithelial cells do not directly contribute to myofibroblast populations via EMT, they can promote myofibroblast differentiation through paracrine signalling.

LKB1 is an evolutionarily conserved serine/threonine protein kinase, which acts as an important regulator of cell polarity, proliferation, and cell metabolism in epithelial cells (Kullmann and M. Krahn 2018). Activation of LKB1 activation occurs via allosteric binding of LKB1 to STE20-related adaptor (*STRAD*) and mouse protein 25 (MO25, encoded by *CAB39* and *CAB39L*) (Momcilovic and D. Shackelford 2015a). Many of the best-known functions of LKB1 are attributable to its ability to activate AMPK, which is an important conserved regulator of cell growth and metabolism (M. Mihaylova and Shaw 2011). It was reported recently that activation of AMPK in myofibroblasts from IPF lungs displays lower fibrotic activity. In a bleomycin mouse model of lung fibrosis, metformin accelerates the resolution of well-established fibrosis in an AMPK-dependent manner (Rangarajan et al. 2018). This study supports the role of metformin in reversing established fibrosis by facilitating deactivation and apoptosis of myofibroblasts (ibid.). In line with this, Han and colleagues reported that kidney-specific deletion of Lkb1 induces severe renal fibrosis (S. Han et al. 2016). Similar to our findings, they found LKB1 (*STK11*) mRNA levels are not statistically significantly altered in fibrotic kidney samples. Instead, the expression of the allosteric

activator of LKB1, *CAB39L*, is significantly decreased in kidney fibrosis (ibid.), raising its potential role in the development of fibrotic disease. Coincidently, thymoquinone alleviates thioacetamide-induced hepatic fibrosis by activating the LKB1-AMPK signalling pathway in mice (Bai et al. 2014). Apart from AMPK, LKB1 also activates a family of 12 "AMPK-related kinases", including BRSK1, BRSK2, NUAK1, NUAK2, QIK, QSK, SIK, MARK1, MARK2, MARK3, MARK4 and MELK (J. Lizcano et al. 2004). It was shown earlier that LKB1 suppresses EMT-transcriptional factor Snail1 (Goodwin et al. 2014) and ZEB1 (Roy et al. 2010) expression via MARK1/4 and miR-200a/c, respectively. In this study, we demonstrated that LKB1 depletion induces Snail2 expression via autophagy inhibition-p62-NFκB pathway in ATII cells, in consistence with our previous reports (Charlotte Hill, Juanjuan Li, et al. 2019; Wang et al. 2019).

As a highly conserved process (Hill and Wang 2020), autophagy has been associated with several human diseases, including pulmonary fibrosis (Hill and Wang 2021). It has been reported that LKB1 modulates autophagy activity via an AMPK-mTORC1 (Gurumurthy et al. 2010; Araya and S. Nishimura 2010) or AMPK-ULK1 (ATG1) axis (Sanchez-Garrido and Shenoy 2021). In ATII cells, upon LKB1 inhibition, autophagy activity is reduced, leading to EMT via the p62-NFκB pathway (See chapter 4). This drives local myofibroblast differentiation via paracrine signalling.

Although the role of metformin for IPF treatment remains controversial (Spagnolo et al. 2018; Teague et al. 2022), our results suggest that IPF patients with lower *CAB39L* expression might benefit from metformin treatment. Prospective validation of these findings is warranted which could inform stratified approaches for the treatment of pulmonary fibrosis.

7.2 Future Work

As described in the previous sections, there are numerous opportunities for further investigation based on our current findings. These future endeavours will contribute to a deeper understanding of the pathogenesis of IPF and aid in the development of innovative therapeutic approaches.

7.2.1 A potential role of Wnt5a upregulation in lung fibroblasts

We have previously shown that in alveolar epithelial cells, autophagy inhibition fosters epithelial-mesenchymal transition (EMT). This process plays a critical role in embryonic development, wound healing, cancer metastasis, and fibrosis. Furthermore, the depletion of *STK11* (serine/threonine kinase 11, encoding LKB1) in

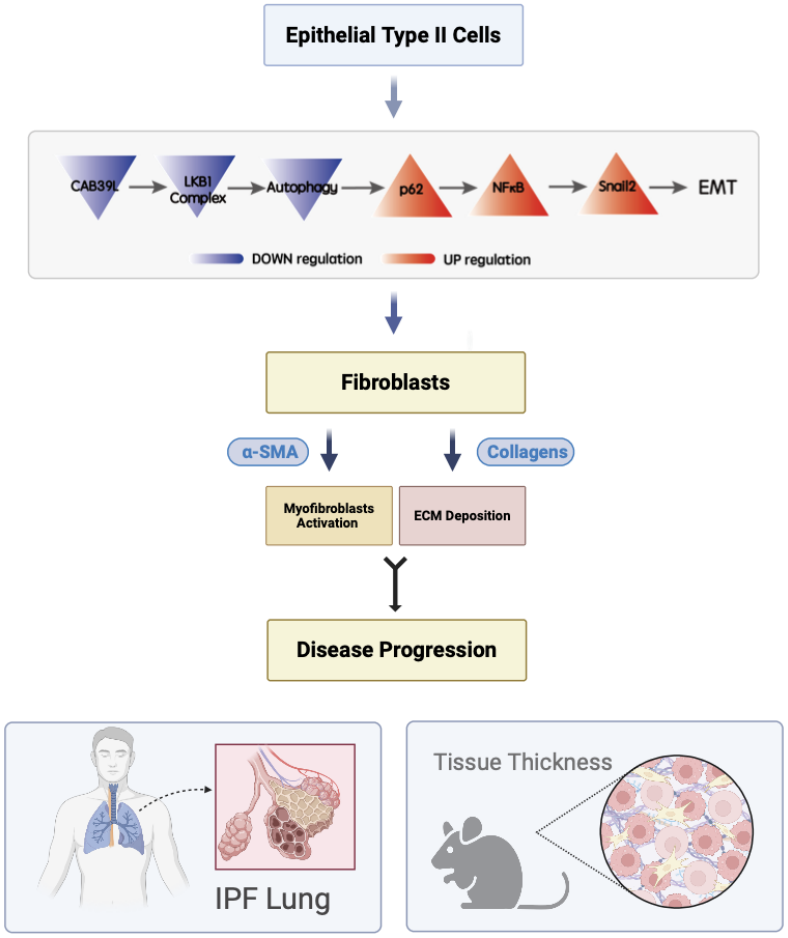

FIGURE 7.1: **LKB1 Depletion in Epithelial Cells: Inducing Crosstalk with Fibroblasts, Myofibroblast Activation, and Collagen Deposition to Drive Disease Progression**
Diagram depicting the pathway where CAB39L downregulation inactivates the LKB1 complex, leading to the inhibition of autophagy and induction of epithelial-mesenchymal transition (EMT) through the p62-NF κB-Snail2 pathway in alveolar type II (ATII) cells. This process mediates crosstalk between epithelial cells and fibroblasts, contributing to the progression of IPF.

alveolar epithelial type II (ATII) cells leads to autophagy inhibition, culminating in EMT via the NFκB – Snail2 signalling pathway. Given this backdrop, a crucial question this project seeks to address is how fibroblasts respond to these epithelial signals. Our global transcriptomic analysis revealed numerous differentially expressed genes (DEGs), some of which are pivotal in regulating fibroblast proliferation and reorganization (as detailed in Chapter 5). To understand the primary mediators facilitating paracrine signalling between LKB1-depleted ATII cells and fibroblasts, we compared DEGs from 2D culture datasets (Chapter 3). Notably, the expression of *wnt5a* emerged as having significant potential to interact with the myofibroblast.

To dissect these signalling pathways further, we utilized Metascape (Yingyao Zhou

et al. 2019). Our analysis of up-regulated and down-regulated pathways, analogous to the approach in Figure 5.9, revealed an overlapping signalling subgroup that encapsulates the interaction between LKB1-edited ATII cells and MRC5 fibroblasts. This interaction was identified by comparing up-regulated signalling in the 3D group with non-up-regulated signalling in the 2D group. Unlike merely overlapping the DEGs, this signalling interaction provides a more comprehensive visualization of the relative enrichment of signalling pathways in comparison to the entire genome. It also highlights key bio-markers within these enriched pathways. Our integrated analysis of the pathways and gene symbols pinpointed *wnt5a* as a potential influencer of fibroblast cell growth in the LKB1-depleted ATII co-culture with the MRC5 model. Preliminary results support this hypothesis (see Figure B.4). Specifically, the expression of *wnt5a* in LKB1-depleted ATII cells versus the control in the 3D co-culturing model suggests that the increased expression of *wnt5a* is influenced more by the co-culturing environment than solely by LKB1 depletion in ATII cells. Furthermore, an RNAscope in-situ hybridization assay on histological sections of 3D co-culturing spheroids mirrored these findings, showing an elevated expression of *wnt5a* in the co-culturing model compared to control spheroids. Protein expression assays of wnt5a/b in MRC5, conditioned with media from LKB1-depleted ATII cells, further underscored that the LKB1-depleted ATII-MRC5 microenvironment enhances the protein levels of wnt5a/b. Preliminary cell growth studies, where ATP levels were gauged using the CellTiter-Glo 2.0 Luminescent Cell Viability Assay, corroborated these findings. Our data potentially suggest that LKB1 inactivation not only can induce EMT of alveolar epithelial cells but also contributes to fibroblast proliferation via regulating wnt5a expression within aberrant epithelial–fibroblast crosstalk. Moving forward, a deeper exploration of the role of *wnt5a* within the epithelial-fibroblast microenvironment is imperative. To fortify our findings, the protein and mRNA levels of *wnt5a* expression should be re-evaluated in multiple replicates, ensuring the robustness and reproducibility of our data. Additionally, to unravel the intricate relationship between fibroblast growth and LKB1 inactivation, further investigations are warranted. By consolidating such evidence, we can achieve a more comprehensive understanding of these cellular dynamics and their implications.

7.2.2 Identify inactivation of LKB1 release secret proteins mediating epithelial-mesenchymal crosstalk

Paracrine factors, secreted molecules, operate over short distances, influencing neighbouring cells in a brief timeframe. Crucially, in paracrine signalling, the gradient of the received factor determines the cellular response. Given this, our focus has intensified on the types of transcript factors and secreted proteins within the paracrine signalling microenvironment. The transcriptomic profiling described in Chapter 6(6)

(GSE169500) encompasses 10 samples from the alveolar epithelium of IPF patients and 10 healthy controls. The DEGs concerning CAB39L, spotlighting genes such as *SNAI2*, *MMPs*, and *TIMP1*, are negatively correlated with CAB39L. Notably, the significant inverse expression of Snail2 (SNAI2) with CAB39L aligns with the LKB1-depleted ATII cell RNA-Seq data in Chapter 3. This underscores that Snail2's regulation is influenced not just by LKB1 depletion but also by CAB39L. Apart from that, Comparing the RNA-Seq dataset linked to LKB1(*STK11*) with the CAB39L-related transcriptomic database, the Venn diagram in Fig. B.5 highlights an intersection of 63 genes, suggesting their association with the LKB1 complex in both tissue and ATII cells. Importantly, when these 63 genes were overlaid with predicted proteins (Figure. B.6), a key focus emerged: identifying mediators influencing epithelial and fibroblast crosstalk. Among the six identified secreted proteins, Peroxidasin homolog (PXDN) stands out. It's reported that myofibroblasts release PXDN, which then forms a fibril-like network in the extracellular space, co-localizing with fibronectin and aiding extracellular matrix formation. Additionally, the down-regulation of metallopeptidase inhibitor 1 (TIMP1), akin to a-SMA and TGFβ, signifies reduced fibrosis, echoing previous studies. Intriguingly, both PXDN and TIMP1, with differential expression in IPF versus control, are also documented in the LungDisease Analysis database. Their expression levels in both patient databases and RNA-Seq data are detailed in Fig. B.7.

The upregulated secreted proteins, induced by LKB1(*STK11*) silencing in ATII cells, notably TIMP1 and PXDN, demand further investigation. It's pivotal to ascertain if their secretion from epithelial cells, consequent to LKB1 loss, orchestrates the dialogue between epithelial cells and fibroblasts.

7.2.3 Identify the factor(s) responsible for Snail2-regulated paracrine signalling.

In Chapter 3 and from previous findings in our group, we discovered that the dramatically up-regulated expression of Snail2 is not only determined by LKB1 depletion in alveolar epithelial cells but is also influenced by Zeb1-related KRAS-induced EMT. This necessitates our attention to the series of downstream cascades caused by the upregulation of Snail2. Snail2, also known as Slug, is a transcriptional repressor pivotal in various biological processes, particularly in embryonic development and tumour progression. A key function of Snail2 is its regulatory role in the Epithelial-Mesenchymal Transition (EMT) process where it promotes EMT by suppressing the expression of E-cadherin, a protein essential for maintaining epithelial cell adhesion. Beyond EMT, Snail2 is implicated in cell migration and invasion, critical components of tumour progression and metastasis. It can also inhibit the activity of P53, thereby increasing cell resistance to damage and suppressing apoptosis. Moreover, Snail2 is believed to influence the cell cycle,

particularly concerning cell proliferation and differentiation. In specific contexts, Snail2 can also enhance the stem cell-like characteristics of cells, pivotal in both tumour formation and regenerative medicine. Additionally, evidence suggests that Snail2 can assist tumour cells in evading immune responses, thus providing favourable conditions for tumour growth and metastasis. Finally, Snail2's influence extends to the extracellular matrix, where it can alter its composition and structure, further affecting cell migration and invasion. The intricacies of Snail2's roles and its subsequent pathways might differ based on cell type, tissue environment, and other biological contexts.

7.2.4 Restoring LKB1 activity might have therapeutic potential in fibrotic conditions.

It has some results show that LKB1 inactivation can regulate the expression of epithelial targets and relative transcription factors, but it remains understood that the role of LKB1 in fibrotic conditions, characterized by the excessive deposition of extracellular matrix components and the progressive scarring of tissues, poses significant challenges to current therapeutic strategies. One promising avenue that has emerged from recent studies is the potential role of Liver Kinase B1 (LKB1) in modulating fibrotic responses. However, its function extends beyond oncology, with mounting evidence suggesting its critical role in cellular energy metabolism, cell polarity, and tissue homeostasis.LKB1 in Cellular Homeostasis: LKB1 plays a pivotal role in maintaining cellular energy homeostasis. By activating AMP-activated protein kinase (AMPK) and other related kinases, LKB1 helps to ensure that cells can respond adequately to energy stress. Given that disrupted cellular metabolism and energy dysregulation are often observed in fibrotic conditions, restoring LKB1 activity could potentially rectify these imbalances, thereby mitigating the fibrotic response. Unfortunately, Based on my lab test that the metformin activated AMPK in epithelial cells to check whether the responses to EMT affected by the LKB1-AMPK pathway, the autophagy-related NFκB signallings mediating EMT might not enhanced by LKB1-AMPK activity in my experimental models. consequently, it remains to be confirmed whether the LKB1 and other related downstream kinase should be the checkpoint involved in Cellular Homeostasis by LKB1 inactivation.

The role of LKB1 in cell polarity and tissue architecture further underscores its potential relevance in fibrosis. Disrupted cell polarity and tissue architecture are hallmarks of fibrotic conditions. In this project, we firstly confirmed that the LKB1 inactivation in epithelial cells can induce the process of lung fibrosis by paracrine signallings, but it still needs to verify if enhancing LKB1 activity might be possible to restore normal tissue architecture, thereby preventing or even reversing fibrotic changes. On the other hand, Given that LKB1 can modulate inflammatory responses,

particularly through its interactions with mTOR signalling, strategies aimed at restoring LKB1 activity could attenuate the chronic inflammatory signals that drive fibrosis. the Potential Therapeutic Strategies: Several approaches could be considered to restore LKB1 activity. These might include small molecule activators, gene therapy to reintroduce functional LKB1 or targeted protein therapies. The feasibility and efficacy of each approach would need rigorous testing in preclinical models before transitioning to clinical trials. While the therapeutic potential of LKB1 is promising, several challenges remain. Firstly, the precise molecular mechanisms linking LKB1 to fibrosis need further elucidation. Additionally, while LKB1 restoration might benefit fibrotic conditions, its broader effects on cellular function and potential oncogenic pathways must be carefully considered to ensure patient safety.

Appendix A

Buffers and Reagents

A.1 siRNA Oligos Sequences

A.2 Protein lysis buffer

Items	Sources	Concentration
Urea	Sigma-Aldrich	8M
Tiourea	Sigma-Aldrich	1M
dithiothreitol	Sigma-Aldrich	50mM
spermine	Sigma-Aldrich	24mM
CHAPS	Sigma-Aldrich	0.5%

TABLE A.1: **Protein lysis buffer**

A.3 SDS-PAGE Gel preparation

A.3.1 Resolving gel

Solution Components	Sources	Volume
dH2O	-	3ml
30% Acrylamide	Severn Biotech Ltd	2.5ml
1.5 M Tris. HCl (pH 8.8)	Severn Biotech Ltd	1.9ml
10% SDS	Severn Biotech Ltd, Kidderminster, UK	75ul
10% Ammonia Persulphate	Sigma-Aldrich	75ul
TEMED	ThermoFisher Scientific	3ul
Total	-	7.5ml

TABLE A.2: **Resolving gel**

A.3.2 Stacking gel

Solution Components	Sources	Volume
dH2O	-	2.1ml
30% Acrylamide	Severn Biotech Ltd	0.5ml
1.0 M Tris. HCl (pH 6.8)	Severn Biotech Ltd	0.38ml
10% SDS	Severn Biotech Ltd, Kidderminster, UK	30ul
10% Ammonia Persulphate	Sigma-Aldrich	30ul
TEMED	ThermoFisher Scientific	3ul
Total	-	5ml

TABLE A.3: **Stacking gel**

A.4 Running Buffer for SDS-PAGE

Solution Components	Sources	Concentration
Tris	Severn Biotech Ltd	25 mM
Glycine	Fisher Scientific	192 mM
SDS	Sigma-Aldrich	0.1%
Adjusted pH to 8.3		

TABLE A.4: **Running Buffer for SDS-PAGE**

A.5 Transfer buffer

Solution Components	Sources	Concentration
Tris	Severn Biotech Ltd	25 mM
Glycine	Fisher Scientific	192 mM
Methanol	Fisher Scientific	20%

TABLE A.5: **Transfer buffer**

A.6 0.1% Tween -Tris Buffered Saline (TBS) (TBST)

Solution Components	Sources	Concentration
Sodium Chloride	Fisher Scientific	150 mM mM
1M Tris.cl (ph7.5-8)	Severn Biotech Ltd	100 mM
tween20	Sigma-Aldrich	0.1%

TABLE A.6: **TBST**

A.6.0.1 A.5.3 Blocking buffer

5% skimmed milk in TBST

Appendix B

Supplementary information

B.1 Tables

B.1.1 Top DEGs in LKB1-depleted alveolar type II (ATII) cells.

B.1.1.1 Top 100 Up-regulated DEGs in Alveolar type II cells transfected with siRNA against LKB1

Gene_name	baseMean	log2FoldChange	P-value	Padj	Change
BTNL8	14.3680896	7.87277238	3.93E-09	2.03E-08	up
IGFN1	136.767309	7.06754128	6.69E-31	1.11E-29	up
TMEM156	8.29460912	6.83059204	4.66E-07	2.03E-06	up
GSDMA	5.62304678	6.00273202	1.20E-05	4.52E-05	up
SERPINB4	43.8758941	5.90833159	1.04E-15	8.45E-15	up
CHI3L2	33.1109775	5.84869025	3.59E-12	2.33E-11	up
KCNQ3	4.90126681	5.66167118	4.09E-05	0.00014398	up
LINC01537	28.7216837	5.65143443	2.74E-11	1.67E-10	up
PLCZ1	4.68097614	5.64912367	3.90E-05	0.00013742	up
SCN7A	4.60202612	5.6488888	3.85E-05	0.00013599	up
KRT8P14	4.48105684	5.54141197	4.94E-05	0.00017194	up
LINC02454	33.5841369	5.48784614	1.96E-13	1.38E-12	up
SPRY4-AS1	11.3789508	5.44039871	2.10E-06	8.58E-06	up
TEX29	32.3113926	5.42346696	4.96E-13	3.41E-12	up
RN7SKP11	3.98771347	5.29495725	0.00010091	0.00033855	up
ART2P	8.7106851	5.00919181	1.33E-05	4.98E-05	up
LINC02621	3.68614347	4.94699545	0.0002804	0.00088411	up
LINC02273	3.44653422	4.93647421	0.00025866	0.00082071	up
LINC00520	58.536492	4.80992155	4.78E-25	6.14E-24	up

XIRP2	3.23803911	4.78180703	0.0004145	0.00127477	up
AC093567.1	3.44913107	4.74577277	0.00047862	0.00145879	up
AC107016.1	7.20043128	4.64806767	4.30E-05	0.00015086	up
HECW2	40.0140403	4.62446035	2.15E-18	2.02E-17	up
AC091173.1	22.015536	4.53286143	1.01E-10	5.90E-10	up
AC034223.1	6.68939883	4.48682666	7.97E-05	0.00027064	up
AC008555.2	6.62429521	4.48283981	7.42E-05	0.00025298	up
HMGB3P32	2.90857473	4.47074618	0.00072811	0.00215549	up
SERPINB2	66.9049352	4.42586699	1.67E-30	2.74E-29	up
MYH16	91.6021548	4.41955602	2.25E-40	5.06E-39	up
TSGA10IP	5.75233485	4.19412663	0.00018648	0.00060254	up
SLCO2B1	8.8344241	4.18913213	3.49E-05	0.00012397	up
AC090673.1	20.87817	4.18802076	1.67E-10	9.66E-10	up
TNFSF8	2.68720057	4.16082278	0.00149798	0.00421316	up
CCL7	13.7724666	4.02376755	2.25E-07	1.01E-06	up
LINC02137	5.16571995	3.97356714	0.00037014	0.00114641	up
SPOCD1	133.676924	3.96521194	1.89E-57	6.60E-56	up
CCR4	2.48130233	3.92412091	0.00182415	0.00505209	up
AC003092.1	7.80882666	3.90768751	0.00014564	0.00047701	up
HTR3A	22.5615652	3.90254751	2.01E-11	1.24E-10	up
AC090377.1	5.05200974	3.87138689	0.00043298	0.00132713	up
HMGA2	1639.70182	3.82220198	0	0	up
KCNQ5-IT1	7.12595738	3.79507888	0.00016128	0.00052491	up
GAPLINC	11.7696817	3.78901249	1.52E-06	6.31E-06	up
DMBT1	142.344585	3.7250927	9.02E-62	3.46E-60	up
IVL	4.56382577	3.68898399	0.00075662	0.00223529	up
PAPPA	62.7657925	3.64239832	7.71E-28	1.12E-26	up
GAP43	4.44072021	3.63111931	0.00084604	0.00248523	up
IL24	1800.66201	3.61191108	0	0	up
GPR3	239.902968	3.51605718	1.22E-97	9.02E-96	up
RPL35P2	10.3351581	3.51584339	8.53E-06	3.27E-05	up
AC010327.4	12.0617287	3.49902111	1.32E-06	5.50E-06	up
TTC9B	8.13097159	3.49371259	5.66E-05	0.00019543	up
LNCOG	33.5425767	3.47099433	8.23E-15	6.31E-14	up
ETV4	1742.93096	3.46480312	0	0	up
DIRC3	7.90637767	3.45608394	6.80E-05	0.00023274	up
FOLR3	32.8740655	3.45146724	8.32E-15	6.37E-14	up
AREG	24.9625803	3.45127513	1.58E-11	9.78E-11	up
AL133330.1	6.0259098	3.43018782	0.00053646	0.00162058	up
CCL26	7.75215797	3.42408659	9.14E-05	0.00030856	up
KCP	7.62346904	3.37724192	0.00012302	0.00040676	up

FGF5	184.586874	3.344119	3.65E-72	1.73E-70	up
MPZ	16.0176242	3.30049038	4.33E-08	2.06E-07	up
MYEOV	166.765915	3.28035325	1.82E-66	7.76E-65	up
ABCC9	3.91358894	3.27798795	0.00184853	0.00511538	up
SEMA7A	956.413118	3.2652162	4.08E-297	2.48E-294	up
TMEM200A	426.256653	3.25405715	7.67E-160	1.38E-157	up
INSC	98.113315	3.12066114	5.40E-37	1.10E-35	up
SBSN	636.299968	3.09628909	2.69E-202	7.32E-200	up
SH2D2A	33.3605908	3.08473	1.62E-13	1.14E-12	up
NT5E	7036.92489	3.0737899	0	0	up
AC090192.2	13.9377995	3.05196763	4.42E-07	1.93E-06	up
AC078850.1	9.53060199	3.04605147	3.64E-05	0.00012887	up
PDE2A	138.028975	3.0276408	1.99E-50	5.94E-49	up
FOSL1	11061.0395	2.99823309	8.51E-275	4.28E-272	up
APCDD1L	331.199469	2.99533979	4.09E-107	3.47E-105	up
AL354740.1	58.5236057	2.97333775	3.73E-23	4.42E-22	up
DNAH3	4.75309466	2.95186276	0.0021106	0.005777	up
RGS17	110.753187	2.92997367	1.64E-39	3.60E-38	up
ARL2-SNX15	3.34773507	2.91557444	0.00356857	0.00939179	up
ANXA10	89.3539117	2.90800312	7.07E-31	1.17E-29	up
MPP4	27.1245515	2.89835659	3.99E-11	2.40E-10	up
AP005233.2	15.2108506	2.888201	4.01E-07	1.76E-06	up
SERPINB7	366.349389	2.88107453	2.04E-122	2.30E-120	up
LINC01204	55.9380614	2.87675462	6.25E-21	6.61E-20	up
DCAF4L1	3.30955849	2.85649772	0.00383586	0.01004136	up
PLCXD3	258.599608	2.8509827	1.46E-83	8.70E-82	up
AC024909.1	4.58215323	2.84693884	0.00260507	0.00702807	up
ANGPTL4	82.892873	2.83071155	5.17E-30	8.28E-29	up
SPAG11A	4.70618953	2.81585833	0.0027254	0.00732614	up
SLC28A3	79.6569847	2.81572339	1.99E-26	2.73E-25	up
AC010343.3	33.6849387	2.80664452	1.67E-13	1.17E-12	up
TAGLN3	53.7670748	2.80565479	1.66E-19	1.65E-18	up
AC093001.1	8.55253987	2.78423361	0.00013398	0.00044101	up
CCR5AS	24.4012757	2.78064915	4.15E-10	2.32E-09	up
SIGLEC9	8.22884821	2.7756446	0.00012502	0.00041291	up
SPRY4	354.88083	2.74431715	7.73E-112	7.00E-110	up
SERPINB3	9.55059062	2.72967733	7.14E-05	0.00024389	up
CHI3L1	350.902616	2.70201842	1.13E-106	9.55E-105	up
EML1	55.6973409	2.69881703	6.52E-20	6.62E-19	up
PDCD1LG2	807.390361	2.69263408	7.15E-235	2.87E-232	up

B.1.1.2 Top 100 down-regulated DEGs in Alveolar type II cells transfected with siRNA against LKB1

Gene_name	baseMean	log2FoldChange	P-value	Padj	Change
CD244	33.34390234	-5.772502946	5.73E-12	3.67E-11	down
ITLN2	18.39833349	-5.372947823	7.60E-08	3.55E-07	down
UPB1	41.21309433	-5.172871539	7.41E-17	6.45E-16	down
LGR5	3.942444094	-5.172532564	0.000148928	0.000487149	down
SYT8	9.307593626	-5.029493891	1.18E-05	4.44E-05	down
LSP1	27.07143358	-4.534927116	1.91E-12	1.26E-11	down
ZNF725P	3.054581907	-4.443950191	0.000869229	0.00254924	down
SLCO4C1	10.49793772	-4.428033653	1.20E-05	4.51E-05	down
AL354714.1	2.840652295	-4.261649293	0.001086231	0.003138955	down
ALPP	35.42870654	-4.19282629	1.94E-16	1.65E-15	down
AL354861.3	2.76527635	-4.142132297	0.001417699	0.00400811	down
AC015909.4	2.706773968	-4.048659321	0.00161779	0.004528596	down
PDE11A	11.35068629	-3.617580871	3.24E-06	1.30E-05	down
HSD3B1	40.0549662	-3.57650412	2.24E-17	2.00E-16	down
AC104248.1	18.50149078	-3.533954594	1.40E-08	6.93E-08	down
KEL	24.50439597	-3.446552072	1.95E-10	1.12E-09	down
LINC00639	45.42612702	-3.402065189	2.46E-19	2.43E-18	down
IGBP1P4	7.91511094	-3.380446946	0.000117613	0.000390301	down
AC021066.1	13.56640938	-3.319167632	5.80E-07	2.50E-06	down
IGFBP5	326.9455636	-3.286012791	1.14E-113	1.07E-111	down
LINC02302	35.65911351	-3.230698691	9.03E-15	6.89E-14	down
ODAM	75.97864243	-3.185866378	4.05E-30	6.51E-29	down
BMP5	96.35989676	-3.167691657	1.12E-36	2.25E-35	down
NTM	25.91272646	-3.161199165	2.36E-11	1.45E-10	down
LINC01505	13.8164298	-3.129728112	7.09E-07	3.04E-06	down
NOTUM	8.69622599	-3.112819261	5.98E-05	0.000205801	down
CHST9	5.442695391	-3.029201601	0.001359745	0.003856191	down
SMIM1	577.504321	-3.017279347	1.26E-177	2.66E-175	down
COL9A2	273.9409227	-3.002595063	2.95E-88	1.90E-86	down
COL2A1	13.1236539	-2.973458012	2.95E-06	1.19E-05	down
SYNPO2L	89.35673709	-2.966133122	2.45E-32	4.28E-31	down
PDE1A	31.98446283	-2.963700948	5.57E-13	3.81E-12	down
MAP2K6	101.7655368	-2.953112124	7.02E-36	1.38E-34	down
OLFML1	9.426432305	-2.945086087	3.92E-05	0.000138086	down
AC025154.2	96.23460936	-2.934723857	9.92E-34	1.82E-32	down
LGI3	3.526395242	-2.912819203	0.003670287	0.009641816	down
NPPB	12.03192715	-2.901839968	6.06E-06	2.36E-05	down

CCN5	23.63523327	-2.895059397	1.09E-09	5.92E-09	down
POM121L9P	3.537169694	-2.881777726	0.003928118	0.010252531	down
GRAMD4P7	20.15575618	-2.880972711	7.52E-09	3.82E-08	down
LINC00987	6.831377338	-2.866892704	0.000642371	0.001916059	down
RIPOR2	4.789132926	-2.8598301	0.002359485	0.006411103	down
AC005515.1	6.528662958	-2.856942889	0.000731877	0.002166008	down
ABAT	11.33541468	-2.833104216	1.24E-05	4.66E-05	down
ITLN1	1204.558562	-2.802901726	0	0	down
AC106785.2	4.736967062	-2.778397687	0.002998911	0.008003722	down
AC022034.1	18.45732688	-2.76524081	2.04E-07	9.18E-07	down
SUSD2	26.05775001	-2.745157642	5.54E-10	3.08E-09	down
IL22RA2	5.858079122	-2.73631505	0.001272125	0.003625601	down
EPHA3	6.083974971	-2.726972596	0.001034144	0.002998647	down
AC005586.2	77.91014251	-2.712420661	8.85E-26	1.18E-24	down
CDH5	53.89018869	-2.690880683	1.66E-17	1.50E-16	down
CHAC1	269.5212203	-2.675885028	2.79E-27	3.98E-26	down
PRELP	206.6292784	-2.661859938	1.83E-62	7.15E-61	down
LINC02593	128.8050623	-2.656894615	4.01E-40	8.94E-39	down
TYRP1	119.6044336	-2.648903387	3.37E-37	6.90E-36	down
ID2	874.5453899	-2.635177034	7.79E-225	2.61E-222	down
LINC01203	36.3837638	-2.631595607	7.77E-13	5.26E-12	down
DLX2	19.7447127	-2.628797138	1.71E-07	7.75E-07	down
LINC02385	15.79079917	-2.627662915	1.12E-06	4.69E-06	down
PLA2G1B	4.427330771	-2.623924495	0.00393722	0.010273251	down
LINC01929	48.14598734	-2.622646581	2.82E-16	2.38E-15	down
SLC12A5-AS1	3.407542116	-2.563691333	0.004755579	0.012204266	down
ELAVL2	91.26244242	-2.548965787	7.72E-28	1.12E-26	down
TSPAN8	772.9502534	-2.542291535	3.09E-150	4.97E-148	down
SOWAHD	73.40842002	-2.529021243	1.48E-21	1.62E-20	down
HMCN2	5.313304733	-2.517759219	0.002181635	0.005960074	down
SSC4D	65.10899972	-2.50312557	1.49E-18	1.41E-17	down
MYOD1	6.564798572	-2.501998672	0.000850247	0.002496848	down
SAMD11	282.2297524	-2.490164763	3.44E-72	1.64E-70	down
GLYAT	23.20538723	-2.479721473	3.96E-08	1.90E-07	down
TSPAN32	5.781957001	-2.478219703	0.001809056	0.005015122	down
TMEM26	21.96749872	-2.475794958	4.65E-08	2.21E-07	down
GAL3ST1	19.59432409	-2.458894841	3.13E-07	1.39E-06	down
PDE6A	25.69377507	-2.403699182	8.91E-09	4.49E-08	down
PLP1	56.84024376	-2.377483609	2.31E-17	2.06E-16	down
ZDHHC22	6.261794417	-2.372277577	0.001350533	0.003831146	down
MYOZ1	29.66355047	-2.371111078	5.73E-10	3.19E-09	down

PRSS35	51.34641674	-2.369340284	3.14E-15	2.47E-14	down
LINC01836	13.15254199	-2.369245969	1.67E-05	6.18E-05	down
IL21-AS1	5.059291478	-2.365485277	0.003405414	0.009006004	down
HOXC12	22.72689602	-2.352271467	3.71E-08	1.78E-07	down
AL358334.2	14.39503141	-2.344871849	6.85E-06	2.65E-05	down
SLC15A2	58.06202082	-2.343243953	1.24E-16	1.07E-15	down
MYL7	6.731902263	-2.333199197	0.001268746	0.003616996	down
EWSAT1	49.62132876	-2.316226767	1.45E-13	1.02E-12	down
ATOH8	1250.490837	-2.312863531	1.14E-248	4.86E-246	down
APOBR	19.60487317	-2.289129877	3.90E-07	1.71E-06	down
A2M	1279.074482	-2.279676166	1.52E-264	7.26E-262	down
SMO	27.95126853	-2.276249176	1.10E-08	5.53E-08	down
ACSS1	82.81730078	-2.275442481	5.53E-23	6.50E-22	down
PLEKHA6	484.3522587	-2.270519092	9.13E-98	6.77E-96	down
LMO1	15.45564401	-2.260428044	6.13E-06	2.38E-05	down
CXCL16	509.2996991	-2.259321635	6.45E-118	6.68E-116	down
LYPD6B	6.868941656	-2.251662877	0.001074559	0.003106563	down
OLR1	131.5533416	-2.249891321	1.29E-32	2.27E-31	down
STEAP4	94.58836034	-2.238287058	8.63E-23	1.00E-21	down
CA14	17.28396374	-2.233600146	2.13E-06	8.66E-06	down
CST2	20.07417705	-2.227425378	8.28E-07	3.52E-06	down
SLC7A11	437.9863223	-2.223607606	7.85E-75	3.91E-73	down

Hallmarks	Gene Count	ES	NES	P-value	FDR
HALLMARK_TNFA_SIGNALING_VIA_NFKB	186	0.56153923	2.3563566	0.00000045	0
HALLMARK_KRAS_SIGNALING_UP	147	0.50381	2.0710256	0.0000032	0
HALLMARK_EPITHELIAL_MESENCHYMAL_TRANSITION	180	0.46019462	1.9392318	0.000072	3.46E-04
HALLMARK_IL2_STAT5_SIGNALING	163	0.45989358	1.9131495	0.000032	2.59E-04
HALLMARK_MYC_TARGETS_V2	58	0.5008566	1.7863066	0.00012	0.001843339
HALLMARK_INFLAMMATORY_RESPONSE	150	0.4173048	1.7290806	0.0001	0.00371051
HALLMARK_COMPLEMENT	156	0.4100694	1.6807551	0.001760563	0.005819444
HALLMARK_COAGULATION	92	0.41114324	1.5844904	0.008576329	0.017239956
HALLMARK_HYPOXIA	181	0.35982743	1.5158093	0.006920415	0.028101308
HALLMARK_UV_RESPONSE_DN	141	0.34294215	1.4167479	0.020477816	0.068416566
HALLMARK_P53_PATHWAY	188	0.3141299	1.3431394	0.01584507	0.114279985
HALLMARK_MYC_TARGETS_V1	197	0.30677688	1.3225087	0.027729636	0.124488324
HALLMARK_HEDGEHOG_SIGNALING	30	0.43116638	1.3162637	0.12569316	0.12035076
HALLMARK_APICAL_JUNCTION	170	0.30825827	1.3066916	0.036842104	0.121433504
HALLMARK_ESTROGEN_RESPONSE_EARLY	179	0.30269855	1.2702984	0.07504363	0.15099576
HALLMARK_IL6_JAK_STAT3_SIGNALING	67	0.34253323	1.2493705	0.12820514	0.1657848
HALLMARK_GLYCOLYSIS	179	0.26625893	1.1204782	0.20758122	0.37915763
HALLMARK_APICAL_SURFACE	38	0.343115	1.1072423	0.29657796	0.387341
HALLMARK_APOPTOSIS	144	0.26778972	1.1070529	0.23498233	0.36736524
HALLMARK_UV_RESPONSE_UP	141	0.26954317	1.1033033	0.24333926	0.3579447
HALLMARK_ALLOGRAFT_REJECTION	127	0.25073856	1.0169203	0.41323793	0.554614
HALLMARK_REACTIVE_OXYGEN_SPECIES_PATHWAY	45	0.28926784	0.9736572	0.49725777	0.6494038
HALLMARK_TGF_BETA_SIGNALING	52	0.26209804	0.9099873	0.6056604	0.8060223
HALLMARK_CHOLESTEROL_HOMEOSTASIS	73	0.24228792	0.8915974	0.6820604	0.8243782
HALLMARK_ADIPOGENESIS	185	0.20802891	0.88619417	0.77717394	0.8054468
HALLMARK_WNT_BETA_CATENIN_SIGNALING	36	0.2102777	0.68229824	0.92897195	1
HALLMARK_G2M_CHECKPOINT	199	0.13531494	0.5754945	1	1
HALLMARK_OXIDATIVE_PHOSPHORYLATION	197	0.091877036	0.3893004	1	0.9999655

TABLE B.3: **GSEA in ATII cells transfected with siRNA against LKB1**

List of 28 enriched Hallmark pathways from the molecular signature database (MSigDB) in LKB1 depletion samples, in which 9 significant up-regulation has been highlighted (FDR <0.05)"Gene Count" is the number of genes in the gene set after filtering out those genes not in the expression dataset. "ES" is the enrichment score for the gene set, that is, the degree to which this gene set is overrepresented at the top or bottom of the ranked list of genes in the expression dataset."NES" is the normalized enrichment score, that is, the enrichment score for the gene set after it has been normalized across analysed gene sets."P-value" is the Nominal Pvalue, that is, the statistical significance of the enrichment score. The nominal Pvalue has not adjusted for gene set size or multiple hypothesis testing. "FDR" is the false discovery rate, that is, the estimated probability that the normalized enrichment score represents a false positive finding. The data list is organized here from maximal to minimal NES.

B.1.2 GSEA in ATII cells transfected with siRNA against LKB1.

B.1.3 Top 10 GO terms enrichment analysis in LKB1-depleted ATII cells.

Category	ID	terms	q-value FDR	Hit Count
MF	GO:0005201	extracellular matrix structural constituent	1.67E-04	20
MF	GO:0005102	signaling receptor binding	1.67E-04	89
MF	GO:0048018	receptor ligand activity	7.94E-04	34
MF	GO:0030546	signaling receptor activator activity	7.94E-04	34
MF	GO:0030545	signaling receptor regulator activity	4.35E-03	34
MF	GO:0033549	MAP kinase phosphatase activity	7.63E-03	5
MF	GO:0005125	cytokine activity	7.68E-03	19
MF	GO:0005539	glycosaminoglycan binding	1.28E-02	19
MF	GO:0005126	cytokine receptor binding	1.28E-02	21
MF	GO:0008330	protein tyrosine/threonine phosphatase activity	1.94E-02	4
BP	GO:0007155	cell adhesion	2.05E-08	90
BP	GO:0022610	biological adhesion	2.05E-08	90
BP	GO:0030334	regulation of cell migration	6.08E-08	69
BP	GO:2000145	regulation of cell motility	2.01E-07	70
BP	GO:0040012	regulation of locomotion	2.01E-07	72
BP	GO:0006935	chemotaxis	2.01E-07	51
BP	GO:0042330	taxis	2.20E-07	51
BP	GO:0051270	regulation of cellular component movement	5.60E-07	72
BP	GO:0016477	cell migration	5.60E-07	93
BP	GO:0000165	MAPK cascade	6.57E-06	60
CC	GO:0031226	intrinsic component of plasma membrane	2.54E-05	89
CC	GO:0009986	cell surface	3.50E-05	59
CC	GO:0005887	integral component of plasma membrane	3.50E-05	84
CC	GO:0031012	extracellular matrix	1.14E-04	40

CC	GO:0030312	external encapsulating structure	1.14E-04	40
CC	GO:0009897	external side of plasma membrane	3.71E-04	32
CC	GO:0062023	collagen-containing extracellular matrix	6.78E-04	32
CC	GO:0097478	leaflet of membrane bilayer	3.85E-03	38
CC	GO:0098552	side of membrane	3.85E-03	38
CC	GO:0070161	anchoring junction	5.46E-03	44
CC	GO:0045121	membrane raft	9.83E-03	25

TABLE B.4: **Top 10 GO terms enrichment analysis in LKB1-depleted ATII cells**

B.1.4 Top DEGs in 3D co-cultured LKB1-depleted ATII cells and MRC5

B.1.4.1 Top 100 up-regulated DEGs in 3D co-cultured LKB1-depleted ATII cells and MRC5

Gene_name	baseMean	log2FoldChange	pvalue	padj	Change
CDH6	409.7453737	2.747980507	1.43E-44	7.79E-42	up
FENDRR	1390.604667	2.124740099	7.46E-41	2.91E-38	up
SELE	94.68260529	5.316665401	2.70E-30	4.24E-28	up
COL1A1	10389.9406	1.593733429	2.12E-27	2.63E-25	up
FGF7	3613.327066	1.625589592	4.13E-27	4.93E-25	up
PRKG2	208.2296686	2.463567341	4.84E-25	5.07E-23	up
MAP1A	2452.213394	2.281145841	9.22E-25	9.40E-23	up
TBX2	2698.297634	1.756072436	1.31E-24	1.31E-22	up
BHMT2	202.3098855	2.378831056	1.79E-24	1.75E-22	up
COLEC12	779.5879577	2.578775733	3.27E-24	3.06E-22	up
SMOC1	1526.145071	2.14564131	9.41E-24	8.61E-22	up
ENC1	577.6583625	2.113757912	9.84E-24	8.94E-22	up
TSPYL5	339.9679348	1.809811519	5.87E-23	5.04E-21	up
WNT5A	6289.851217	1.425691333	1.52E-22	1.28E-20	up
REX1BD	554.7257628	1.690168115	2.45E-21	1.91E-19	up
CCDC68	1352.231994	1.829082095	3.73E-21	2.82E-19	up
VWA5A	479.8353632	1.858628398	9.59E-21	7.05E-19	up
MLLT11	786.4177914	2.436838132	1.00E-20	7.34E-19	up
UCHL1	4255.157537	2.413641839	6.03E-20	4.18E-18	up
EHD3	357.7661619	1.810476682	4.10E-19	2.65E-17	up
CCDC9B	861.9867979	1.422407118	4.34E-19	2.79E-17	up
GPX8	872.6436708	1.545946319	6.89E-19	4.33E-17	up
ANTXR1	3257.82589	1.186706586	8.42E-19	5.26E-17	up
ZNF70	357.9862111	1.426464838	6.69E-18	3.83E-16	up
SLC2A10	1629.015629	1.289341859	8.84E-18	5.02E-16	up
PSMG3-AS1	114.7169894	2.481103249	1.19E-17	6.72E-16	up
TMEM98	508.1914393	1.730728996	1.45E-17	8.12E-16	up
TMEM119	358.4601795	1.71437161	2.34E-17	1.28E-15	up
TMEM168	352.1392796	1.464917814	2.34E-17	1.28E-15	up
RAMP1	584.443489	1.64405841	2.43E-17	1.32E-15	up
PTGIR	293.813821	2.053337961	4.08E-17	2.19E-15	up
ZNF362	268.6496228	1.499766527	6.23E-17	3.30E-15	up
C14orf132	1379.936416	1.28123441	8.75E-17	4.54E-15	up
COL7A1	47910.29178	1.362520635	1.17E-16	5.96E-15	up
RIPOR2	429.6427661	1.480327485	2.40E-16	1.19E-14	up

ZNF618	366.4252708	1.767706654	2.42E-16	1.20E-14	up
FOXF1	3213.177638	1.452657817	4.22E-16	2.06E-14	up
CXCL5	9864.988634	1.958200544	4.28E-16	2.09E-14	up
FER1L6	458.7495816	1.692429653	5.56E-16	2.69E-14	up
IL11	65211.28155	2.006487554	6.93E-16	3.33E-14	up
SYT11	900.3170268	1.122600653	7.30E-16	3.49E-14	up
MIR34AHG	530.3435122	1.348214432	7.45E-16	3.56E-14	up
ADGRL4	252.1753369	1.600372409	7.77E-16	3.70E-14	up
CLGN	1212.862919	1.465643872	1.29E-15	5.98E-14	up
PHLDA3	749.9607558	1.240089351	3.21E-15	1.43E-13	up
SMO	401.6541318	1.621032135	3.24E-15	1.45E-13	up
ZDHHC1	356.2099864	1.309078859	3.35E-15	1.49E-13	up
F2RL2	395.0189007	1.638417353	3.85E-15	1.71E-13	up
TRNP1	428.7760487	1.433725572	3.96E-15	1.75E-13	up
JAM3	432.3950599	1.310711714	4.54E-15	2.00E-13	up
PDGFRA	3477.1459	1.934782908	6.07E-15	2.64E-13	up
AEBP1	3964.380232	1.244844207	9.93E-15	4.17E-13	up
EID1	2293.937695	1.193858555	1.02E-14	4.25E-13	up
TECPR1	517.5019553	1.28100707	1.27E-14	5.29E-13	up
SEPTIN11	2789.714416	1.225529817	1.61E-14	6.66E-13	up
KLHL5	4706.097085	1.06012294	1.68E-14	6.92E-13	up
SLC6A15	2345.536269	1.422821528	2.04E-14	8.35E-13	up
KRCC1	290.6709892	1.312604418	2.44E-14	9.87E-13	up
EMILIN1	7450.941273	1.475779066	2.49E-14	1.01E-12	up
PKD2	1260.286068	1.461676061	2.75E-14	1.10E-12	up
PDLIM3	259.3663995	1.50766833	3.32E-14	1.31E-12	up
ADAM33	565.0105349	1.293551396	3.29E-14	1.31E-12	up
FKBP14	1259.090192	1.178989435	5.35E-14	2.08E-12	up
BPGM	367.1264313	1.526770927	5.56E-14	2.16E-12	up
CBSL	92.27293863	2.396142886	6.53E-14	2.51E-12	up
LDAH	141.2348921	1.684888517	7.09E-14	2.70E-12	up
DGKI	323.0573588	1.837742712	7.87E-14	2.99E-12	up
UCN2	1067.662102	1.437941874	8.06E-14	3.06E-12	up
CRLF1	315.2377412	1.680917854	8.77E-14	3.32E-12	up
SLC35B4	693.540881	1.340558016	9.30E-14	3.49E-12	up
SERPINB7	1385.575617	1.34781893	1.42E-13	5.22E-12	up
TMEM204	370.6304222	1.250367495	1.52E-13	5.56E-12	up
ADAM23	183.3229438	1.568445313	1.87E-13	6.78E-12	up
DPY19L3	656.5169531	1.079669895	1.92E-13	6.93E-12	up
TNIP3	101.3753587	1.797925612	2.42E-13	8.69E-12	up
CD248	1049.603193	1.884494828	2.56E-13	9.14E-12	up

RAB36	150.8693968	1.68342741	2.89E-13	1.02E-11	up
TBX2-AS1	155.1953682	1.655011283	3.25E-13	1.14E-11	up
TCF21	385.0935224	1.958206409	3.48E-13	1.22E-11	up
IGFBP5	136483.7555	1.645425979	4.03E-13	1.40E-11	up
TMEM132B	229.8206913	2.331060019	4.18E-13	1.44E-11	up
RRM2B	1223.274808	1.070652007	4.59E-13	1.57E-11	up
TBXAS1	404.4737035	1.43002178	4.73E-13	1.62E-11	up
GSPT2	171.0521422	1.521163514	5.29E-13	1.81E-11	up
IDH1	321.0593592	1.289261005	5.80E-13	1.97E-11	up
VPS9D1	651.2208691	1.112256708	6.24E-13	2.12E-11	up
SEL1L3	1270.741651	1.482303228	7.68E-13	2.57E-11	up
IDE	610.1265202	1.375150305	8.33E-13	2.79E-11	up
LINC00205	465.7125691	1.21051423	9.04E-13	3.00E-11	up
TRIM2	286.1647338	1.439494134	1.09E-12	3.58E-11	up
ABCC4	1393.771294	1.057968458	1.12E-12	3.65E-11	up
SLC25A15	389.8023253	1.640747794	1.22E-12	3.95E-11	up
GNG11	2186.89214	1.1925748	1.27E-12	4.13E-11	up
PTGS1	9183.925389	1.252154344	1.36E-12	4.39E-11	up
PDGFRB	2248.167926	1.082238871	1.41E-12	4.56E-11	up
TRPV4	120.050221	1.659648868	1.73E-12	5.54E-11	up
ITGA2	12453.01785	1.145736674	1.92E-12	6.10E-11	up
COLEC10	305.2943106	2.024851245	2.30E-12	7.22E-11	up
IFFO1	589.5338684	1.148729487	2.31E-12	7.22E-11	up
DESI1	953.8175143	1.345853703	2.56E-12	7.93E-11	up

B.1.4.2 Top 100 down-regulated DEGs in 3D co-cultured LKB1-depleted ATII cells and MRC5

Gene_name	baseMean	log2FoldChange	pvalue	padj	Change
SERPINA1	2242.082957	-3.692463121	8.83E-110	1.72E-105	down
KRT19	1292.800162	-3.335782433	1.05E-108	1.02E-104	down
ZBED6CL	1131.138773	-3.635387171	6.93E-91	4.50E-87	down
L1CAM	736.9731496	-3.264851229	2.90E-77	1.41E-73	down
C1QL1	1527.274384	-2.754238322	1.02E-73	3.97E-70	down
MATN2	672.030288	-3.142334941	5.63E-71	1.83E-67	down
TERT	1899.799858	-2.841204935	2.17E-70	6.04E-67	down
NNMT	782.9941012	-3.364993724	1.14E-69	2.78E-66	down
UBE2C	748.4617212	-3.475645218	1.77E-67	3.82E-64	down
NAV2	1153.27016	-2.649792122	2.58E-67	5.02E-64	down
ITGA6	524.1272356	-3.046646941	4.32E-60	7.64E-57	down

DLGAP5	412.6249101	-3.133844272	6.22E-57	1.01E-53	down
C4B	452.854585	-4.49251396	3.26E-56	4.89E-53	down
TOP2A	1738.785417	-2.877331679	7.62E-54	1.06E-50	down
BIRC5	406.0854769	-2.758232673	1.33E-53	1.72E-50	down
MELTF	1513.835845	-2.797738896	1.48E-52	1.80E-49	down
AURKB	523.0845907	-3.062576301	6.66E-52	7.64E-49	down
KIFC1	534.7551867	-2.693027899	1.72E-51	1.86E-48	down
DEPP1	681.8055447	-3.525953307	3.85E-51	3.94E-48	down
ITGB4	295.4735911	-3.421057431	4.49E-51	4.38E-48	down
CIT	489.2366303	-2.880226707	7.95E-51	7.37E-48	down
C4A	409.0181502	-3.395296808	1.22E-49	1.08E-46	down
SERPINE1	8375.693791	-2.127962861	3.38E-49	2.86E-46	down
FUCA1	380.1102112	-3.399434458	6.28E-49	5.10E-46	down
CFB	1077.337883	-2.606987628	8.07E-49	6.29E-46	down
NUP210	422.093697	-2.786470762	1.97E-48	1.48E-45	down
TK1	954.1608608	-2.655232657	4.83E-47	3.48E-44	down
TNFSF10	359.2052713	-3.550779328	2.07E-46	1.44E-43	down
GPRC5A	892.3962128	-2.884813992	7.45E-46	5.01E-43	down
TMEM178B	281.136978	-2.822801496	1.64E-45	1.06E-42	down
SEMA6B	256.6228678	-3.105468247	1.77E-45	1.11E-42	down
SEMA3B	2135.631804	-2.695264977	4.75E-45	2.89E-42	down
PCOLCE2	304.3404505	-3.576134991	1.11E-44	6.55E-42	down
KIF20A	342.3313086	-3.064315845	1.31E-44	7.50E-42	down
KIF18B	507.3657787	-2.762455949	1.44E-44	7.79E-42	down
MAP3K9	506.8609454	-2.629161973	8.75E-44	4.61E-41	down
ANLN	578.129545	-2.794935431	1.35E-43	6.94E-41	down
PIMREG	279.7856572	-2.819597088	2.06E-43	1.03E-40	down
AQP3	303.1852522	-3.192515439	3.34E-43	1.63E-40	down
PLEKHS1	133.0434273	-4.247680633	4.07E-43	1.93E-40	down
HMGB2	990.4648901	-2.305695314	5.42E-43	2.51E-40	down
ARFGEF3	377.8198978	-2.872439924	7.82E-43	3.54E-40	down
ARHGEF4	608.1836407	-2.726775159	1.25E-42	5.54E-40	down
GPRC5C	250.2334072	-2.76252638	1.72E-42	7.46E-40	down
MKI67	957.2913421	-2.782650795	2.15E-42	9.12E-40	down
DMBT1	1238.890737	-4.148248498	3.21E-42	1.33E-39	down
PODXL	1408.965517	-2.690700738	1.08E-41	4.38E-39	down
CELSR1	505.8455016	-2.2384679	1.83E-41	7.29E-39	down
KIF2C	384.1213802	-2.754775528	8.69E-41	3.32E-38	down
CPE	3380.601829	-2.671692811	1.01E-40	3.77E-38	down
TPD52	304.3221687	-2.521875664	1.79E-40	6.59E-38	down
PTTG1	615.452802	-2.353959034	2.07E-40	7.46E-38	down

AURKA	536.9201933	-2.873401981	2.34E-40	8.30E-38	down
TROAP	267.7178781	-2.739433811	2.93E-40	1.02E-37	down
ASPM	277.934154	-2.90713249	6.60E-40	2.26E-37	down
ITPR3	3341.924007	-1.966226639	9.44E-40	3.17E-37	down
TPX2	786.433699	-2.925337528	1.80E-39	5.94E-37	down
MET	987.0538404	-2.23578841	6.13E-39	1.99E-36	down
CPVL	158.2278453	-3.577349562	7.40E-39	2.36E-36	down
FAM160A1	362.9975198	-2.823219458	1.47E-38	4.63E-36	down
F11R	400.2379438	-2.328238035	1.76E-38	5.44E-36	down
KRT8	2400.833018	-1.943554866	2.38E-38	7.26E-36	down
KIF4A	299.4252998	-2.698627602	3.68E-38	1.10E-35	down
AC007786.2	180.0947943	-2.921997004	1.04E-37	3.06E-35	down
ITGA3	6905.660781	-2.143691508	1.37E-37	3.99E-35	down
TGFA	138.2263301	-4.143785711	1.59E-37	4.55E-35	down
HHIPL2	165.7614304	-3.219909309	1.81E-37	5.11E-35	down
CD74	1847.125449	-3.419741635	3.70E-37	1.03E-34	down
EFNA1	257.3352671	-2.919083318	4.09E-37	1.12E-34	down
WT1	133.6409553	-3.695705653	4.16E-37	1.13E-34	down
APOL1	560.5133335	-2.181921801	4.91E-37	1.31E-34	down
PTX3	2995.505783	-3.072252426	5.27E-37	1.39E-34	down
PROS1	1026.742544	-2.094175692	6.23E-37	1.62E-34	down
KIAA1217	1408.069873	-2.234616425	2.27E-36	5.79E-34	down
GRIN2A	264.521928	-2.872833424	2.29E-36	5.79E-34	down
SYNE2	1391.270574	-2.491677756	2.75E-36	6.88E-34	down
NCAPG2	1797.022703	-2.171173867	9.21E-36	2.27E-33	down
AC015712.2	209.982463	-3.613118726	1.02E-35	2.49E-33	down
MGP	120.8598345	-4.141746955	1.92E-35	4.61E-33	down
CEP55	265.3658663	-2.799932976	2.56E-35	6.07E-33	down
CTSV	120.0287111	-4.560747848	3.42E-35	8.02E-33	down
CDT1	858.4906646	-1.990831862	7.69E-35	1.78E-32	down
NFIB	426.6811512	-2.914951327	1.18E-34	2.71E-32	down
CDK1	572.8548181	-2.711965885	1.40E-34	3.17E-32	down
ACTR3C	194.4068323	-2.793196615	1.51E-34	3.38E-32	down
KIF11	313.2359319	-2.3907684	3.02E-34	6.68E-32	down
RRAD	3423.913208	-2.10110595	3.48E-34	7.61E-32	down
PAEP	167.5721305	-2.912943533	6.00E-34	1.30E-31	down
GGH	955.274433	-1.935498963	6.64E-34	1.41E-31	down
EZR	2018.276408	-2.055037634	6.67E-34	1.41E-31	down
E2F1	1241.448541	-2.148235285	6.93E-34	1.45E-31	down
CENPF	403.4299857	-2.790284763	7.02E-34	1.46E-31	down
HES4	480.7174644	-2.107153912	8.50E-34	1.74E-31	down

RACGAP1	417.7940205	-2.076840834	1.16E-33	2.36E-31	down
IQGAP3	302.9040411	-2.340124055	1.34E-33	2.70E-31	down
LAMA3	614.628731	-2.46361122	3.55E-33	7.06E-31	down
CHRDL1	177.6238374	-2.652111351	4.42E-33	8.70E-31	down
EZH2	1594.722783	-2.15702744	6.04E-33	1.18E-30	down
ASF1B	754.0148022	-2.154347548	6.58E-33	1.27E-30	down
MSLN	178.0422495	-2.934387789	9.89E-33	1.89E-30	down

B.1.5 List of collagen genes used for GSVA calculation

gene symbols	control_ATII	control_ATII	control_ATII	siLKB1_ATII	siLKB1_ATII	siLKB1_ATII	Change	control_ATII+MR(	control_ATII+MR(	control_ATII+MR(	siLKB1_ATII+MR(	siLKB1_ATII+MR(	siLKB1_ATII+MR(	Change
COL10A1	7.367536978	8.558956	2.60375001	1.709089628	0.873863395	2.998697412	NS	6.349856196	4.319124553	6.744750086	8.748603705	6.22362954	10.34317213	up
COL12A1	6648.67587	6609.416022	6762.806693	5122.141614	5624.184809	4541.52723	down	17134.02864	18123.04663	14259.52581	31268.60322	31323.52748	38734.23935	up
COL14A1	41.04770602	63.71667244	53.81083354	34.18179255	36.70226258	34.48502023	none	99.4810804	112.2972384	157.377502	179.346376	160.0361882	79.92451194	up
COL15A1	23.15511622	29.48084844	32.11291679	106.8181017	108.359061	91.46027105	up	129.1137427	169.3096825	139.3915018	206.6857625	183.1525265	554.7701417	up
COL16A1	106.3030335	116.9723987	110.2254171	151.254432	150.3045039	134.9413835	up	6126.55292	6267.913552	5781.374949	11745.00047	10398.79587	8837.770444	up
COL18A1	2335.509222	2495.411171	2478.770009	2419.216368	2440.700462	2659.844604	NS	8088.658484	8947.498425	7312.433218	11503.3203	10736.65005	6235.992508	up
COL1A1	695.7059918	693.275436	669.1637526	293.1088711	279.6362864	260.8866748	down	4925.371789	5675.329663	4728.06981	16078.84004	16698.88715	14233.14514	up
COL1A2	6991.792592	6820.536937	6860.881276	3574.560956	3820.530762	3725.881534	down	11365.18428	14348.99559	17027.12159	37575.25291	39789.44183	18099.61095	up
COL22A1	0	0	0	0	0	0	NS	32.80759035	7.774424196	29.22725037	129.0419047	109.3580619	47.95470716	up
COL23A1	0	0	0	0	0	0	NS	6.349856196	3.455299643	6.744750086	3.28072639	0.889089934	12.22374888	up
COL24A1	1.052505283	5.705970666	4.33958335	2.563634441	0.873863395	2.998697412	NS	365.1167313	446.5974788	393.443755	1176.687198	1362.085779	475.7859181	up
COL27A1	539.93521	534.4592524	529.4291687	612.7086315	632.6770979	580.2479491	up	3640.584219	3577.098955	2597.852908	4255.102127	4437.447862	2834.029165	up
COL3A1	14.73507396	19.97089733	19.96208341	16.23635146	9.612497344	14.99348706	NS	8432.609028	10635.4123	11182.79564	30539.18838	31114.59134	13526.04829	up
COL4A1	2400.76455	2416.478577	2336.431676	2144.052938	2177.66758	2111.082978	down	6928.751419	7142.104362	5854.443075	10283.98366	9906.240048	11509.12972	up
COL4A2	6475.012498	6584.690149	6615.260859	5758.7775	6026.161971	5784.487307	down	16509.62611	17172.83922	13618.77455	21741.37378	21093.65869	18462.56226	up
COL4A5	2635.473228	2616.187551	2731.33376	1391.198957	1511.783673	1527.836331	down	2741.021258	3165.054473	4954.018938	4628.01136	4853.541952	3620.110247	up
COL6A3	249.443752	229.1898218	279.4691677	204.2362105	262.1590185	209.9088188	NS	17751.023	18998.10126	15945.71333	30877.1032	29449.3259	30753.07162	up
COL6A6	4.21002113	3.803980444	0.86791667	5.127268883	9.612497344	4.498046117	NS	2.116618732	0.863824911	5.620625072	2.187150926	1.778179869	5.641730255	up
COL7A1	358.9043014	320.4853524	359.3175014	320.4543052	316.3385489	265.3847209	NS	23859.58466	23650.66223	31682.3394	74051.46249	70572.40263	63645.29929	up
COL8A1	1157.755811	1159.26304	1163.008338	1145.09005	1113.301965	1126.010878	NS	2534.650932	2814.341559	4181.745053	5385.859156	6057.369723	3259.03951	up
COL8A2	66.3078328	64.66766755	59.01833356	23.92725479	38.44998937	34.48502023	down	41.27406527	41.46359571	40.46850052	74.3631315	53.34539606	101.5511446	up
GSVA score	**-0.4981905**	**-0.4219135**	**-0.5649982**	**-0.6591056**	**-0.5702732**	**-0.566273**	**NS**	**0.3728837**	**0.3168435**	**0.5176085**	**0.7456441**	**0.6997919**	**0.6745149**	**up**

TABLE B.7: **List of collagen genes used for GSVA calculation in Figure. 5.12**

"Gene symbols" are representative up-regulated collagen relative gene symbols described in Figure. 5.12. The "GEO dataset" is the uploaded RNAseq dataset used for the analysis. "GSVA score" is the gene set variation score calculated by normalised raw count, performed by GSVA package in R. "Change" is the direction of the up or down regulations of DEGs.

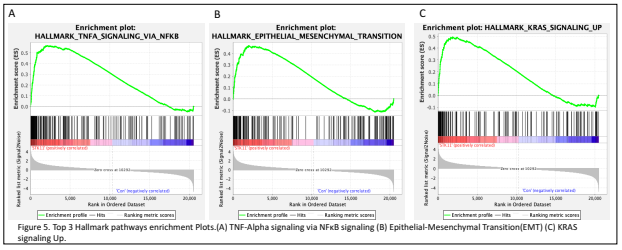

FIGURE B.1: **Gene set enrichment analysis (GSEA) plot showing enrichment of Hallmark TNF α Signaling Via NF κB in LKB1-depleted ATII cells**

Normalised enrichment score (NES) and false discovery rate (FDR) are indicated.

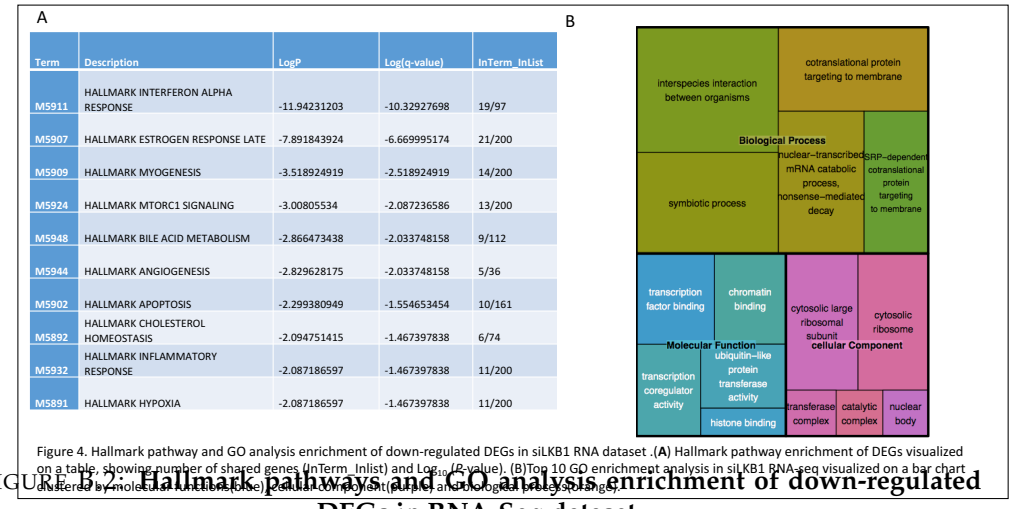

FIGURE B.2: **Hallmark pathways and GO analysis enrichment of down-regulated DEGs in RNA-Seq dataset.**

(A) REVIGO TreeMap showing Gene Ontology (GO) analysis of down-regulated differentially expressed genes (DEGs) in RNA-Seq from ATII cells transfected with LKB1 siRNA or control siRNA. Common colours represent groupings based on parent GO terms, and each rectangle is proportional to the relative enrichment of the GO term compared to the whole genome. Genes with false discovery rate (FDR) <0.05 were considered as DEGs (differentially expressed genes). (B) Hallmark pathway enrichment of DEGs visualized on a table, showing the number of shared genes (InTerm_Inlist) and Log10 (P-value).

B.2 Figures

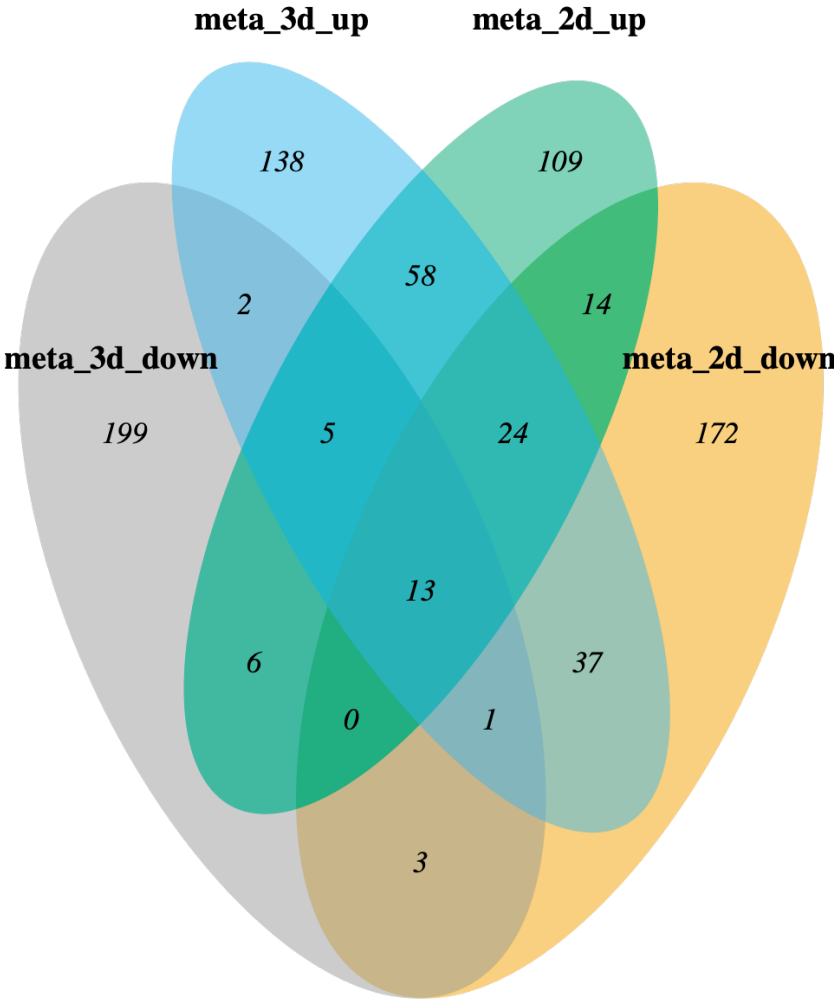

FIGURE B.3: **Distribution of up or down-regulated relative KEGG pathways and GO items in 3D co-culturing model or 2d LKB1 depleted ATII cells**
Venn Diagram showing the comparison between up-regulated and down-regulated KEGG and GO items analysed via Metacapes in LKB1 depletion in ATII cell (2D) with 3D co-culturing RNA-seq datasets. Numbers showing the KEGG and GO items significantly enriched at indicated DEGs(meta_3d_down/meta_3d_up: up-regulated DEGs in 3D co-culturing model; meta_2d_down/meta_2d_up: up-regulated DEGs in 2D culturing LKB1 depleted ATII cells.) cutoff was 0.05.

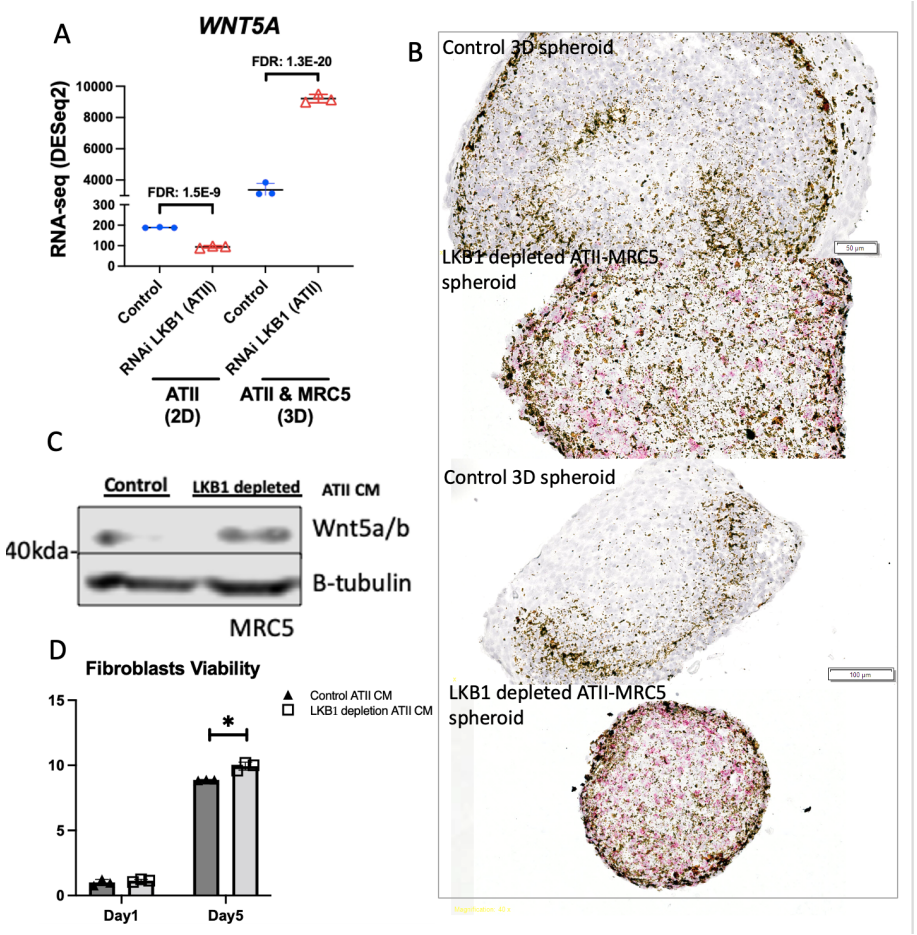

FIGURE B.4: **LKB1 depletion in ATII cells potentially drives the Fibroblast proliferation via Wnt5a upregulation**

Figure A representative figures for expression of *wnt5a* in LKB1 depletion vs control in ATII cells and 3D co-culturing model. Figure B shows that an RNAscope in-situ hybridization assay was performed on histological sections of 3D co-culturing spheroids. Red spots indicate *wnt5a* signals. Protein expression of wn5a/b in MRC5 incubated with conditional media collected in LKB1 depleted ATII cells shown in Figure C. ATP levels were determined by luminescence using the CellTiter-Glo 2.0 Luminescent Cell Viability Assay related luminescence units were normalised to control.

No.	Symbol	No.	Symbol	No.	Symbol
1	CDCP1	22	KIAA0930	43	HOXB7
2	SERINC2	23	MANF	44	ZCRB1
3	PPIF	24	SGTB	45	RAD23B
4	PPP1R14B	25	RELT	46	NDUFAB1
5	SNAI2	26	HYOU1	47	GTF2E2
6	CD276	27	NEIL2	48	LTB4R
7	VOPP1	28	FXYD5	49	NGRN
8	ELOVL1	29	RCC1	50	PXDN
9	TMEM158	30	NAA20	51	TFB2M
10	MMP14	31	HSP90B1	52	C5orf15
11	BASP1	32	GPI	53	CCDC88A
12	OCIAD2	33	SCFD2	54	ATP2C1
13	ITGAX	34	VASP	55	MRPL12
14	LIMK1	35	MAST4	56	ATP6AP1
15	FAM3C	36	SH3BGRL3	57	TIMP1
16	LOX	37	MPC2	58	PSMC1
17	UBE2D1	38	SPR	59	ZNRF1
18	PTGFRN	39	GBP3	60	CCDC47
19	SPRED1	40	NAGA	61	ABHD12
20	PLEKHM2	41	PLGRKT	62	IARS2
21	PBX3	42	CEP55	63	RPN1

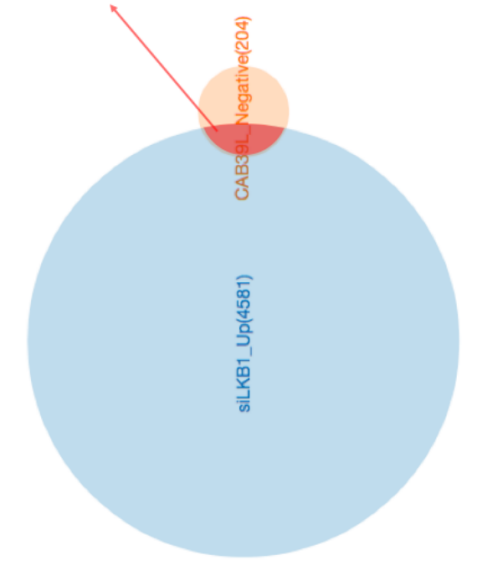

FIGURE B.5: **63 up-regulated genes in RNA-Seq overlapped with CAB39L negative-related DEGs in IPF**

Venn diagram of intersection between up-regulated gene expression in RNA-Seq dataset and CAB39L Negative-related gene to the expression of CAB39L in IPF transcriptomic profiling. the table shows the total 63 genes/proteins for the intersection. Venn diagram created by Meta-chart online.

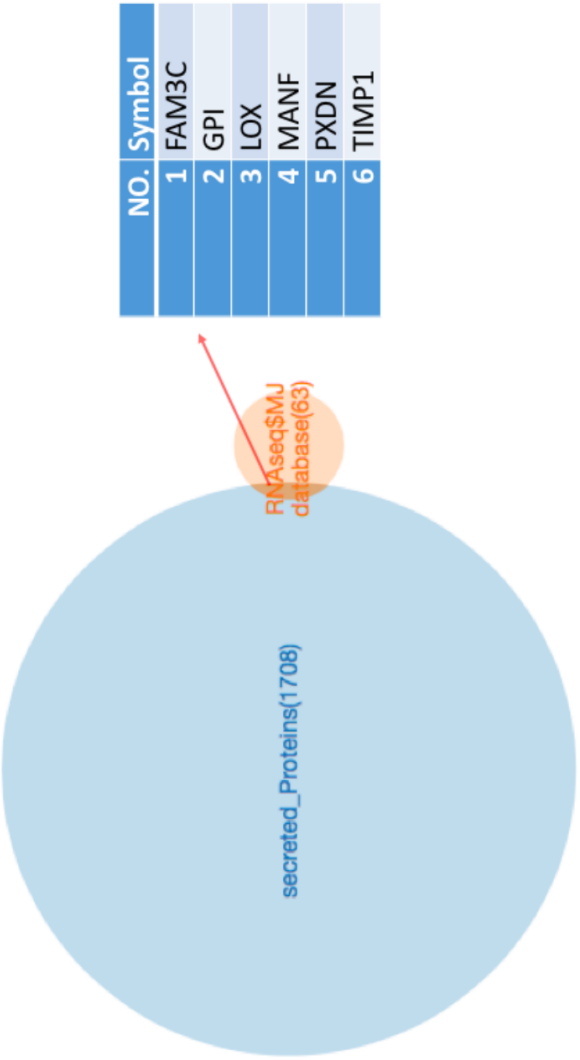

FIGURE B.6: **6 secreted proteins encoded by genes from 63 overlapped datasets**
Venn diagram of the intersection between predicted secreted proteins and the 63 genes/proteins selected by the above indication. The table shows the total 6 proteins in the intersection areas. Venn diagram created by Meta-chart online.

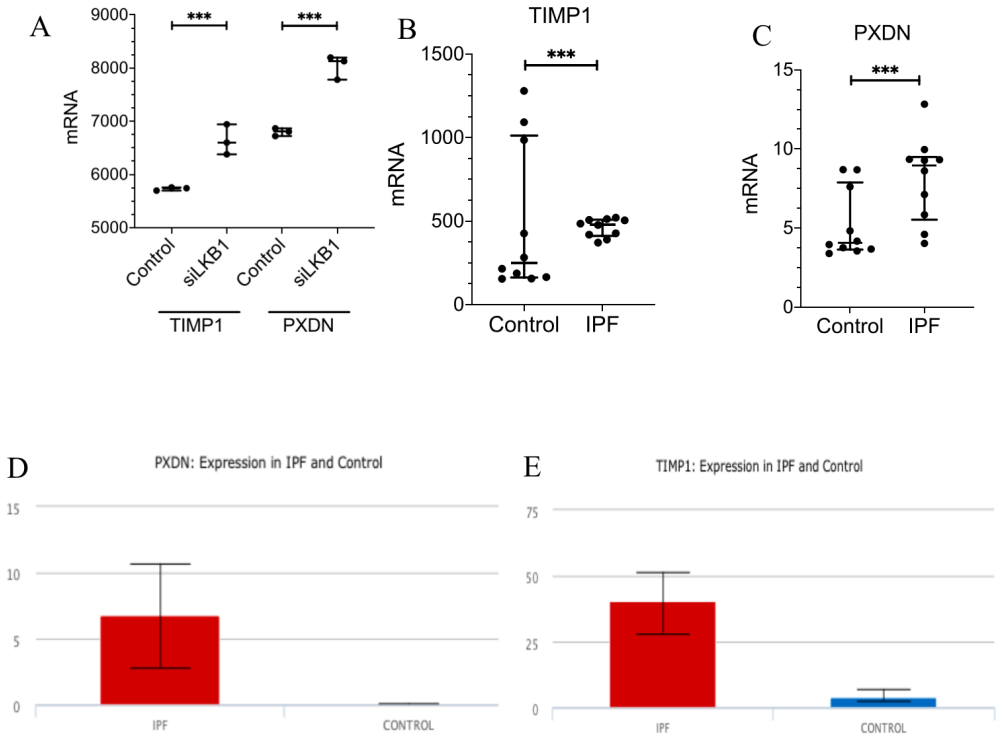

FIGURE B.7: **Secreted proteins of PXDN and TIMP1 are up-regulated by LKB1 depletion in ATII cells and down-regulated in IPF**

Representative figures for the expression of PXDN and TIMP1 in LKB1 depletion vs. control RNA-Seq data and IPF patient's transcriptomic database. $***P < 0.001$. (A). mRNA level of TIMP1 and PXDN in RNA-seq. (B, C). The expression of TIMP1 and PXDN in the IPF patient's transcriptomic database. PXDN and TIMP1 are differentially expressed in IPF vs. Control as identified in LGEA (Lung Disease Analysis). (D). P-value $= 0.0015$ and fold change $= 353.336$ (up-regulated). (E). P-value $= 0.0048$ and fold change $= 10.089$ (up-regulated).

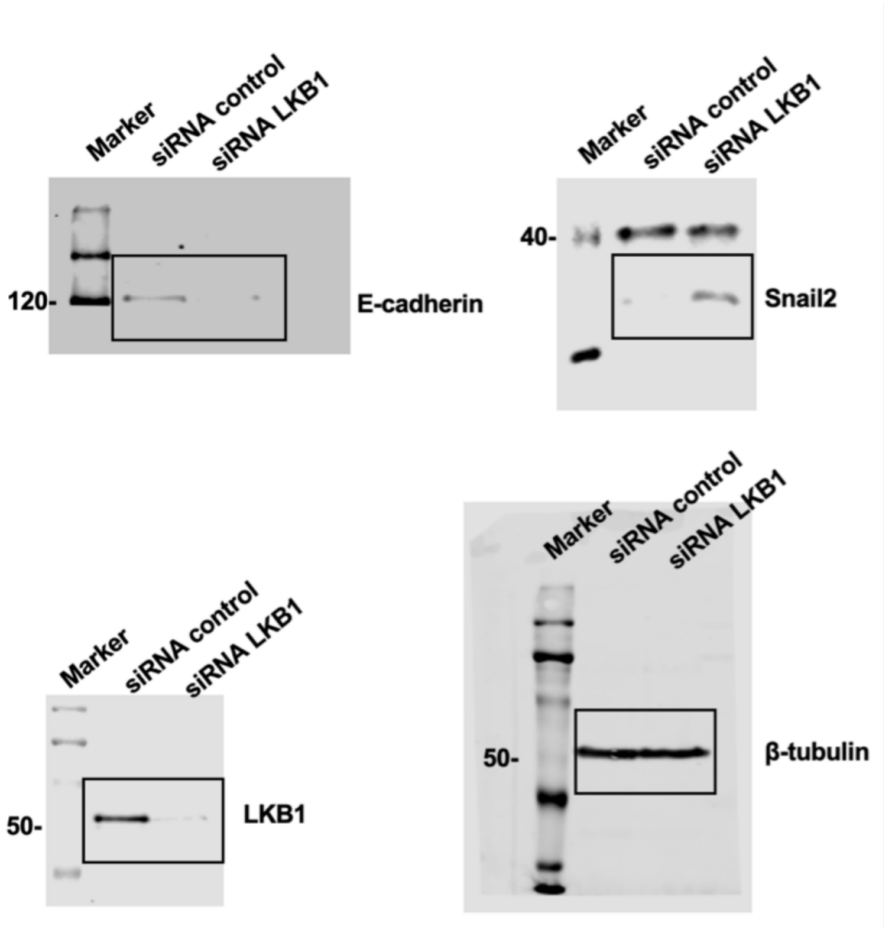

FIGURE B.8

B.3 Raw data for western blots

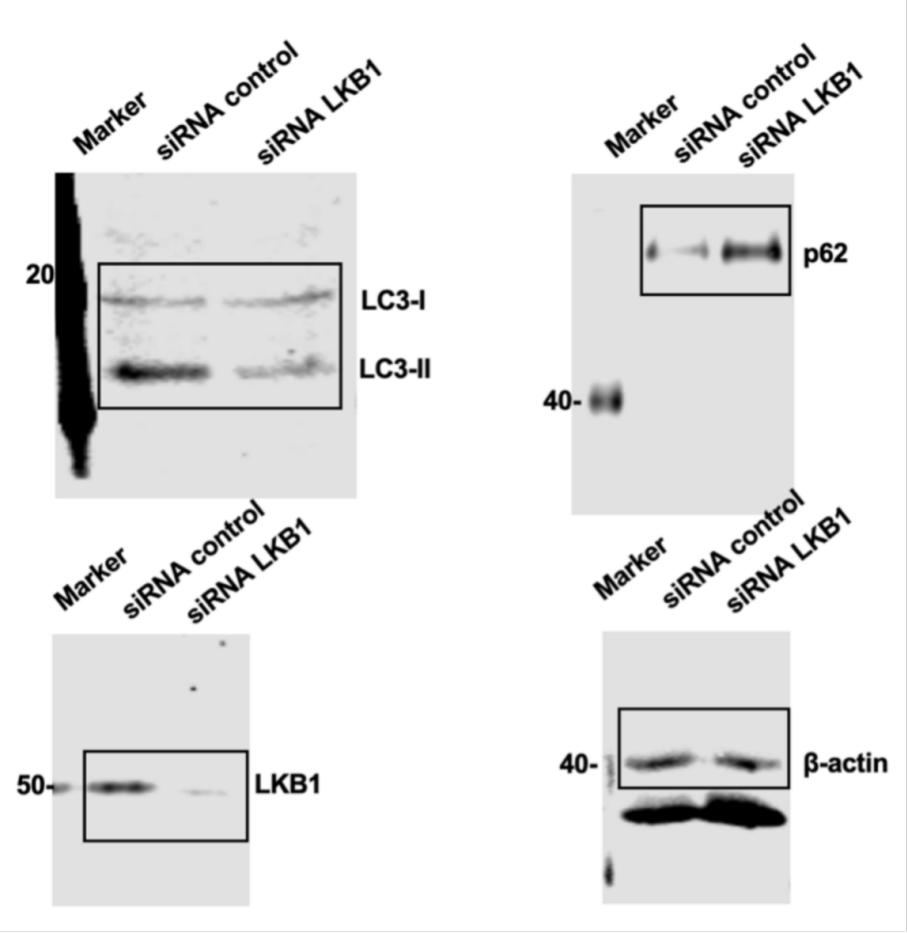
Marker
siRNA control
siRNA LKB1
20
LC3-I
LC3-II
Marker
siRNA control
siRNA LKB1
p62
40-
Marker
siRNA control
siRNA LKB1
50-
LKB1
Marker
siRNA control
siRNA LKB1
40-
β-actin

FIGURE B.9

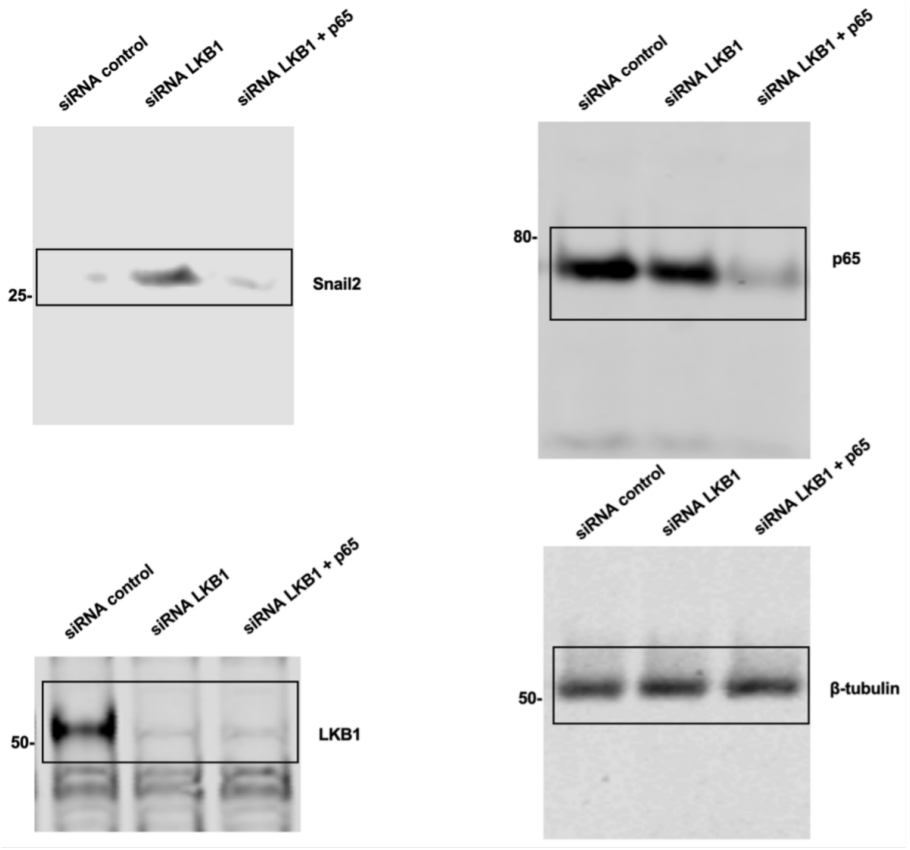
siRNA control
siRNA LKB1
siRNA LKB1 + p65
25-
Snail2
siRNA control
siRNA LKB1
siRNA LKB1 + p65
80-
p65
siRNA control
siRNA LKB1
siRNA LKB1 + p65
50-
LKB1
siRNA control
siRNA LKB1
siRNA LKB1 + p65
50-
β-tubulin

FIGURE B.10

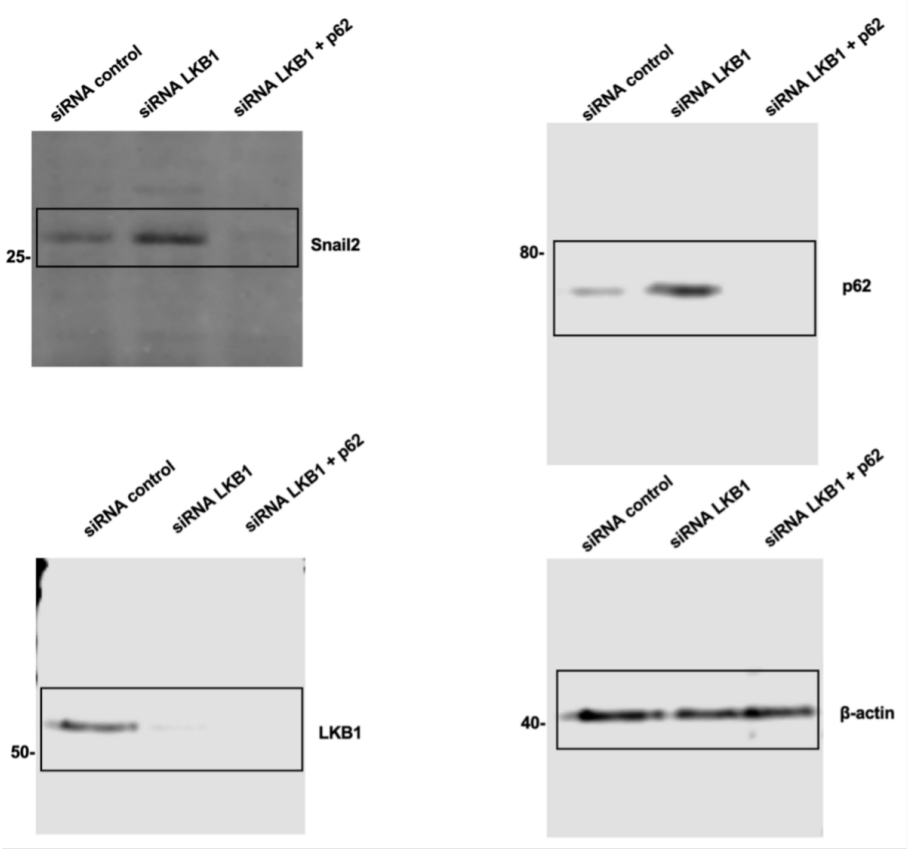
siRNA control
siRNA LKB1
siRNA LKB1 + p62
25-
Snail2
siRNA control
siRNA LKB1
siRNA LKB1 + p62
80-
p62
siRNA control
siRNA LKB1
siRNA LKB1 + p62
50-
LKB1
siRNA control
siRNA LKB1
siRNA LKB1 + p62
40-
β-actin

FIGURE B.11

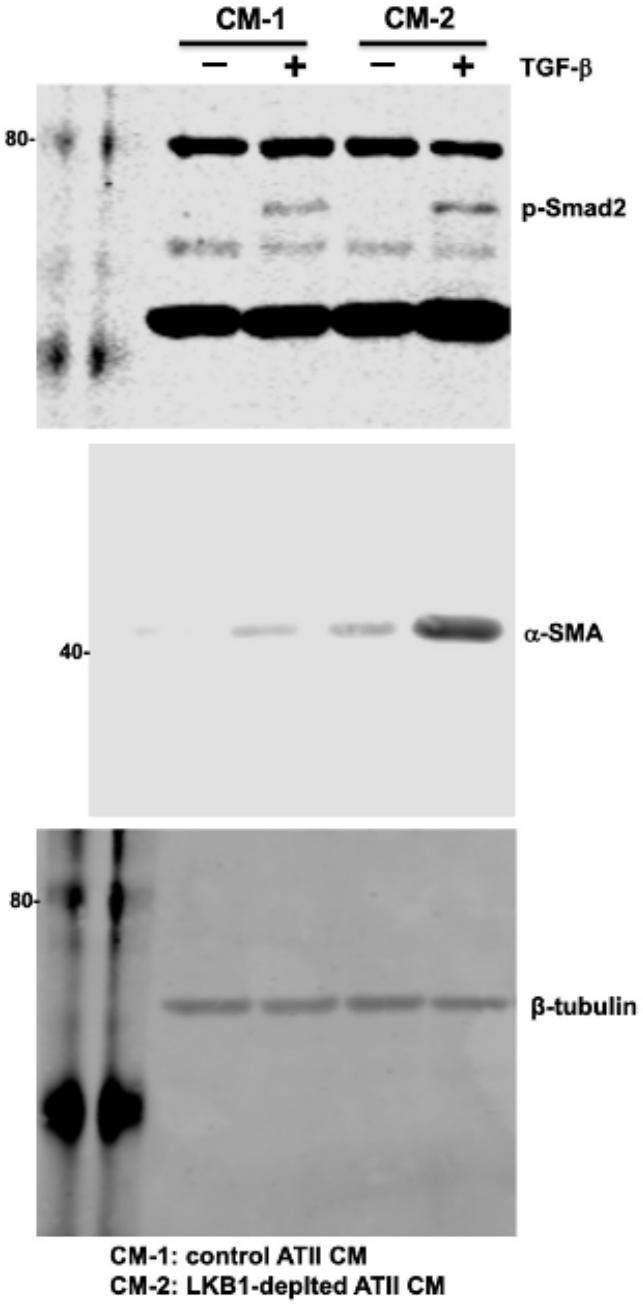
CM-1
CM-2
−
+
−
+
TGF-β
80-
p-Smad2
40-
α-SMA
80-
β-tubulin
CM-1: control ATII CM
CM-2: LKB1-deplted ATII CM

FIGURE B.12

B.4 R script

Raw data were imported into `RStudio (version 4.2.0)`.
`RStudio Version 1.4.1717 for IOS` and R scripts were run.
% Set the working directory before running
`setwd("C:/Users/zx2n18/RNA-seq")`

B.4.1 R code for Figure. 3.5

```
library(ggplot2)
data <- read.csv("Hallmark_gsea_Up.csv")
p <- ggplot(data, aes(NES, NAME))
p + geom_point(aes(colour=FDR.q.val, size=SIZE)) +
scale_color_gradientn(colours=rainbow(4), limits=c(0, 1)) +
geom_vline(xintercept=0, size=0.5, colour="gray50") +
theme(axis.text = element_text(size = 8, face = "bold"),
panel.background=element_rect(fill="gray95", colour="gray95"),
panel.grid.major=element_line(size=0.45,linetype='solid',
colour="gray90"),
panel.grid.minor=element_line(size=0.45,linetype='solid',
colour="gray90"),
axis.title.y=element_blank()) +
expand_limits(x=c(0,3)) +
scale_x_continuous(breaks=c(0,0.5,1,1.5,2,2.5,3)) +
scale_y_discrete(limits=rev(data$NAME))
```

B.4.2 R codes for Figure. 5.12

```
library(gplots)
a1<-read.csv("colleagen_up.csv")
a1<-as.matrix(a1)
a1<-as.numeric(a1)
distCor <- function(a1) as.dist(1-cor(t(a1)))
hclustAvg <- function(a1) hclust(a1, method="average")
pdf("collagen_heatmap.pdf",width=20, height=20)
colorbar<-colorRampPalette(c('darkblue','grey','red'))(n=1000)
###set the color for heatmap
heatmap.2(a1, trace="none",
density='none',margin=c(5,10),scale="row",cexRow = 1.3,
    labRow = labels, cexCol = 0.8, zlim=c(-10,10),Colv = T,Rowv =
T,srtCol=45,adjCol=c(1,0),
    hclustfun = hclustAvg,distfun=distCor,symbreak=FALSE,key = T,keysize
= 1.5,
    labRow =c(as.character(DEP_ras_expression_fc_pvalue$P.Value..)),
    ColSideColors = condition_colors, RowSideColors=row_annotation))
dev.off()
```

B.4.3 R codes for Figure. 5.13

```
BiocManager::install("GSVA")
library("GSVA")
data <-read.csv("2d_3d_exprMatrix.rpm2.csv")
rownames(data)<-data[,1]
data<-data[,-1]
data<-as.matrix(data)
geneset<-read.csv("col_up_3d.csv")
GSVA <- gsva(data, geneSets, mx.diff=1)
```

B.4.4 R codes for Figure. 3.4

```
library(treemap)
revigo.names <-
c("term_ID","description","frequency","value","uniqueness","dispensability","represent
revigo.data <- read.csv("GO_data.csv")
stuff <- data.frame(revigo.data);
names(stuff) <- revigo.names;
stuff$value <- as.numeric( as.character(stuff$value) );
stuff$frequency <- as.numeric( as.character(stuff$frequency) );
stuff$uniqueness <- as.numeric( as.character(stuff$uniqueness) );
stuff$dispensability <- as.numeric( as.character(stuff$dispensability)
);
# by default, outputs to a PDF file
pdf( file="revigo_treemap.pdf", width=16, height=9 )
# check the tmPlot command documentation for all possible parameters -
there are a lot more
treemap(
    stuff,
    index = c("representative","description"),
    vSize = "value",
    type = "categorical",
    vColor = "representative",
    title = "Revigo TreeMap",
    inflate.labels = FALSE,
    lowerbound.cex.labels = 0,
    bg.labels = "#CCCCCCAA",
    position.legend = "none"
)
dev.off()
```

B.4.5 R codes for Figure. 3.5

```
mytheme <- theme(axis.title=element_text(face="bold", size=10,colour =
'gray25'),
Go_Up<-read.xlsx('/Toppgene_2dup_result.xlsx',sheet = 1)
Go_Up$Count<-sapply(Go_Up$InTerm_InList,function(x)
strsplit(x,"/")[[1]][1]) %>%as.numeric()
Go_Up$Member<-sapply(Go_Up$InTerm_InList,function(x)
strsplit(x,"/")[[1]][2])%>%as.numeric()
Go_Up$GeneRatio<-as.numeric(Go_Up[,10])/as.numeric(Go_Up[,11])
Go_Up<-Go_Up[grepl('Member',Go_Up$GroupID),]
Go_Up$`P.adjust`<-10^(Go_Up$`Log(q-value)`)
Go_Up<-Go_Up[order(Go_Up$GeneRatio),]
Go_Up$Description<-factor(Go_Up$Description,levels = (Go_Up$Description))
#Plot
p<-ggplot(Go_Up,aes(GeneRatio,Description)) +
geom_point(aes(size=Count,color=`P.adjust`))+scale_colour_gradient(high='blue',low='red',n.br
    theme_bw()+
    theme(axis.title=element_text(face="bold", size=10,colour =
'black'),
ggsave('Up_Go_result.pdf',width = 9,height = 8)
```

References

Abdul-Hafez, A., R. Shu, and B. D. Uhal (2003). "JunD and HIF-1 mediate transcriptional activation of angiotensinogen by TGF-1 in human lung fibroblasts". In: *American Journal of Physiology-Lung Cellular and Molecular Physiology* 284, pp. L501–L507.

Adamali, Huzaifa I et al. (2012). "Non-pharmacological treatment of idiopathic pulmonary fibrosis". In: *Current Respiratory Care Reports* 1, pp. 208–215.

Aimo, Alberto et al. (2020). "Pirfenidone is a cardioprotective drug: mechanisms of action and preclinical evidence". In: *Pharmacological research* 155, p. 104694.

Alder, Jonathan K, Christina E Barkauskas, et al. (2015). "Telomere dysfunction causes alveolar stem cell failure". In: *Proceedings of the National Academy of Sciences* 112.16, pp. 5099–5104.

Alder, Jonathan K, Susan E Stanley, et al. (2015a). "Exome sequencing identifies mutant TINF2 in a family with pulmonary fibrosis". In: *Chest* 147.5, pp. 1361–1368.

– (2015b). "Exome sequencing identifies mutant TINF2 in a family with pulmonary fibrosis". In: *Chest* 147.5, pp. 1361–1368.

Alexander, Angela et al. (2010). "ATM signals to TSC2 in the cytoplasm to regulate mTORC1 in response to ROS". In: *Proceedings of the National Academy of Sciences* 107.9, pp. 4153–4158.

Altarejos, Judith Y et al. (2005). "Myocardial ischemia differentially regulates LKB1 and an alternate 5≠AMP-activated protein kinase kinase". In: *Journal of Biological Chemistry* 280.1, pp. 183–190.

Aluwihare, Poshala and John S Munger (2008). "What the lung has taught us about latent TGF-β activation". In: *American journal of respiratory cell and molecular biology* 39.5, pp. 499–502.

Alvarado-Kristensson, Maria et al. (2009). "SADB phosphorylation of γ-tubulin regulates centrosome duplication". In: *Nature cell biology* 11.9, pp. 1081–1092.

Alvira, Cristina M (2014). "Nuclear factor-kappa-B signaling in lung development and disease: one pathway, numerous functions". In: *Birth Defects Research Part A: Clinical and Molecular Teratology* 100.3, pp. 202–216.

Anagnostopoulou, Vasileia et al. (2013). "Differential effects of dehydroepiandrosterone and testosterone in prostate and colon cancer cell apoptosis: the role of nerve growth factor (NGF) receptors". In: *Endocrinology* 154.7, pp. 2446–2456.

Andersson-Sjöland, Annika et al. (2008). "Fibrocytes are a potential source of lung fibroblasts in idiopathic pulmonary fibrosis". In: *The international journal of biochemistry & cell biology* 40.10, pp. 2129–2140.

Annes, Justin P, John S Munger, and Daniel B Rifkin (2003). "Making sense of latent TGFβ activation". In: *Journal of cell science* 116.2, pp. 217–224.

Antoniades, H. and et al. (1990). "Platelet-derived growth factor in idiopathic pulmonary fibrosis". In: *The Journal of clinical investigation* 86, pp. 1055–1064.

Antoniades, HN et al. (1990). "Platelet-derived growth factor in idiopathic pulmonary fibrosis." In: *The Journal of clinical investigation* 86.4, pp. 1055–1064.

Aparicio, IM et al. (2016). "Autophagy-related proteins are functionally active in human spermatozoa and may be involved in the regulation of cell survival and motility". In: *Scientific reports* 6.1, p. 33647.

Araya, J and SL Nishimura (2010). "Fibrogenic reactions in lung disease". In: *Annual Review of Pathology: Mechanisms of Disease* 5, pp. 77–98.

Araya, Jun, Stephanie Cambier, et al. (2007). "Squamous metaplasia amplifies pathologic epithelial-mesenchymal interactions in COPD patients". In: *The Journal of clinical investigation* 117.11, pp. 3551–3562.

Araya, Jun, Jun Kojima, et al. (2013). "Insufficient autophagy in idiopathic pulmonary fibrosis". In: *American Journal of Physiology-Lung Cellular and Molecular Physiology* 304.1, pp. L56–L69.

Armanios, Mary Y et al. (2007). "Telomerase mutations in families with idiopathic pulmonary fibrosis". In: *New England Journal of Medicine* 356.13, pp. 1317–1326.

Ashley, Shanna L et al. (2017). "Periostin regulates fibrocyte function to promote myofibroblast differentiation and lung fibrosis". In: *Mucosal immunology* 10.2, pp. 341–351.

Baas, AF et al. (2003). "Activation of the tumour suppressor kinase LKB1 by the STE20-like pseudokinase STRAD". In: *The EMBO journal* 22.12, pp. 3062–3072.

Baas, Annette F. et al. (2003). "Activation of the Tumor Suppressor Kinase LKB1 by the STE20-like Pseudokinase STRAD". In: *EMBO Journal* 22, pp. 3062–3072. DOI: 10.1093/emboj/cdg292.

Baddini-Martinez, José and Carlos Alberto Pereira (2015). "How many patients with idiopathic pulmonary fibrosis are there in Brazil?" In: *Jornal Brasileiro de Pneumologia* 41, pp. 560–561.

Badr-Eldin, Shaimaa M et al. (2022). "Three-Dimensional In Vitro Cell Culture Models for Efficient Drug Discovery: Progress So Far and Future Prospects". In: *Pharmaceuticals* 15.8, p. 926.

Bai, T et al. (2014). "Thymoquinone alleviates thioacetamide-induced hepatic fibrosis by activating the LKB1-AMPK signaling pathway in mice". In: *International immunopharmacology* 19.2, pp. 351–357.

Bai, Ting et al. (2014). "Thymoquinone alleviates thioacetamide-induced hepatic fibrosis and inflammation by activating LKB1–AMPK signaling pathway in mice". In: *International immunopharmacology* 19.2, pp. 351–357.

Balch, William E et al. (2014). "Malfolded protein structure and proteostasis in lung diseases". In: *American journal of respiratory and critical care medicine* 189.1, pp. 96–103.

El-Bassouny, Dalia Refaat et al. (2021). "Role of nuclear factor-kappa B in bleomycin induced pulmonary fibrosis and the probable alleviating role of ginsenoside: histological, immunohistochemical, and biochemical study". In: *Anatomy & Cell Biology* 54.4, pp. 448–464.

Bates, Richard C et al. (2005). "Transcriptional activation of integrin β6 during the epithelial-mesenchymal transition defines a novel prognostic indicator of aggressive colon carcinoma". In: *The Journal of clinical investigation* 115.2, pp. 339–347.

Baumgartner, Kathy B et al. (2000). "Occupational and environmental risk factors for idiopathic pulmonary fibrosis: a multicenter case-control study". In: *American journal of epidemiology* 152.4, pp. 307–315.

Berkhof, Farida F et al. (2013). "Azithromycin and cough-specific health status in patients with chronic obstructive pulmonary disease and chronic cough: a randomised controlled trial". In: *Respiratory research* 14, pp. 1–8.

Bernard, Monique et al. (2014). "Autophagy fosters myofibroblast differentiation through MTORC2 activation and downstream upregulation of CTGF". In: *Autophagy* 10.12, pp. 2193–2207.

Bhaskaran, Madhu et al. (2003). "Angiotensin II induces apoptosis in renal proximal tubular cells". In: *American Journal of Physiology-Renal Physiology* 284.5, F955–F965.

Bhaskaran, Madhusudhanan and et al. (2003). "Angiotensin II induces apoptosis in renal proximal tubular cells". In: *American Journal of Physiology-Renal Physiology* 284, F955–F965.

Białas, Adam Jerzy et al. (2016). "The role of mitochondria and oxidative/antioxidative imbalance in pathobiology of chronic obstructive pulmonary disease". In: *Oxidative medicine and cellular longevity* 2016.

Birring, Surinder S et al. (2017). "A novel formulation of inhaled sodium cromoglicate (PA101) in idiopathic pulmonary fibrosis and chronic cough: a randomised, double-blind, proof-of-concept, phase 2 trial". In: *The Lancet Respiratory Medicine* 5.10, pp. 806–815.

Bjoraker, Julie A et al. (1998). "Prognostic significance of histopathologic subsets in idiopathic pulmonary fibrosis". In: *American journal of respiratory and critical care medicine* 157.1, pp. 199–203.

Bjørkøy, Geir et al. (2005). "p62/SQSTM1 forms protein aggregates degraded by autophagy and has a protective effect on huntingtin-induced cell death". In: *The Journal of cell biology* 171.4, pp. 603–614.

Blackwell, Timothy S et al. (2021). "A phase I randomized, controlled, clinical trial of valganciclovir in idiopathic pulmonary fibrosis". In: *Annals of the American Thoracic Society* 18.8, pp. 1291–1297.

Bois, Roland M du et al. (2011). "Ascertainment of individual risk of mortality for patients with idiopathic pulmonary fibrosis". In: *American journal of respiratory and critical care medicine* 184.4, pp. 459–466.

Bolaños, Alfredo Lozano et al. (2012). "Role of Sonic Hedgehog in idiopathic pulmonary fibrosis". In: *American Journal of Physiology-Lung Cellular and Molecular Physiology* 303.11, pp. L978–L990.

Bolaños, Ana L. and et al. (2012). "Role of Sonic Hedgehog in idiopathic pulmonary fibrosis". In: *American Journal of Physiology-Lung Cellular and Molecular Physiology* 303, pp. L978–L990.

Bonniaud, Philippe et al. (2005). "Progressive transforming growth factor β1–induced lung fibrosis is blocked by an orally active ALK5 kinase inhibitor". In: *American journal of respiratory and critical care medicine* 171.8, pp. 889–898.

Booth, Adam J et al. (2012). "Acellular normal and fibrotic human lung matrices as a culture system for in vitro investigation". In: *American journal of respiratory and critical care medicine* 186.9, pp. 866–876.

Border, Wayne A and Nancy A Noble (1994). "Transforming growth factor β in tissue fibrosis". In: *New England journal of medicine* 331.19, pp. 1286–1292.

Boudeau, Jérôme, Annette F Baas, et al. (2003a). "MO25α/β interact with STRADα/β enhancing their ability to bind, activate and localize LKB1 in the cytoplasm". In: *The EMBO journal* 22.19, pp. 5102–5114.

Boudeau, Jérôme, Annette F. Baas, et al. (2003b). "MO25$\alpha\beta$ interact with STRAD$\alpha\beta$ enhancing their ability to bind, activate and localize LKB1 in the cytoplasm". In: *EMBO Journal* 22, pp. 5102–5114. DOI: 10.1093/emboj/cdg490.

Boudeau, Jérôme, Maria Deak, et al. (2003). "Heat-shock protein 90 and Cdc37 interact with LKB1 and regulate its stability". In: *Biochemical Journal* 370.3, pp. 849–857.

Boyette, Lisa B and Rocky S Tuan (2014). "Adult stem cells and diseases of aging". In: *Journal of clinical medicine* 3.1, pp. 88–134.

Brereton, Christopher J, Liudi Yao, Elizabeth R Davies, Yilu Zhou, Milica Vukmirovic, Joseph A Bell, Siyuan Wang, Robert A Ridley, Lareb SN Dean, Orestis G Andriotis, et al. (2022a). "Pseudohypoxic HIF pathway activation dysregulates collagen structure-function in human lung fibrosis". In: *Elife* 11, e69348.

Brereton, Christopher J, Liudi Yao, Elizabeth R Davies, Yilu Zhou, Milica Vukmirovic, Joseph A Bell, Siyuan Wang, Robert A Ridley, Lareb SN Dean, Orestis G Andriotis, et al. (Feb. 2022b). "Pseudohypoxic HIF pathway activation dysregulates collagen structure-function in human lung fibrosis". In: *eLife* 11. Ed. by

Gordana Vunjak-Novakovic, Paul W Noble, and Gianni Carraro, e69348. ISSN: 2050-084X. DOI: 10.7554/eLife.69348. URL: https://doi.org/10.7554/eLife.69348.

Brezniceanu, M.-L. and et al. (2010). "Reactive oxygen species promote caspase-12 expression and tubular apoptosis in diabetic nephropathy". In: *Journal of the American Society of Nephrology* 21, pp. 943–954.

Brune, Kieran et al. (2015). "Pulmonary epithelial barrier function: some new players and mechanisms". In: *American Journal of Physiology-Lung Cellular and Molecular Physiology* 308.8, pp. L731–L745.

Bueno, Marta et al. (2015). "PINK1 deficiency impairs mitochondrial homeostasis and promotes lung fibrosis". In: *The Journal of clinical investigation* 125.2, pp. 521–538.

Burgstaller, Gerald et al. (2017). "The instructive extracellular matrix of the lung: basic composition and alterations in chronic lung disease". In: *European Respiratory Journal* 50.1.

Bustos, Martha L et al. (2014). "Aging mesenchymal stem cells fail to protect because of impaired migration and antiinflammatory response". In: *American journal of respiratory and critical care medicine* 189.7, pp. 787–798.

Byun, Hae-Ok et al. (2015). "From cell senescence to age-related diseases: differential mechanisms of action of senescence-associated secretory phenotypes". In: *BMB reports* 48.10, p. 549.

Cabrera, Sandra et al. (2015). "Essential role for the ATG4B protease and autophagy in bleomycin-induced pulmonary fibrosis". In: *Autophagy* 11.4, pp. 670–684.

Calle, Elizabeth A et al. (2015). "Fate of distal lung epithelium cultured in a decellularized lung extracellular matrix". In: *Tissue Engineering Part A* 21.11-12, pp. 1916–1928.

Campo, Ilaria et al. (2014). "A large kindred of pulmonary fibrosis associated with a novel ABCA3 gene variant". In: *Respiratory research* 15.1, pp. 1–15.

Carroll, Bernadette et al. (2018). "Oxidation of SQSTM1/p62 mediates the link between redox state and protein homeostasis". In: *Nature communications* 9.1, p. 256.

Castelino, Flavia V and John Varga (2010). "Interstitial lung disease in connective tissue diseases: evolving concepts of pathogenesis and management". In: *Arthritis research & therapy* 12.4, pp. 1–11.

Chambers, Daniel C et al. (2017). "The registry of the International Society for Heart and Lung Transplantation: thirty-fourth adult lung and heart-lung transplantation report—2017; focus theme: allograft ischemic time". In: *The Journal of Heart and Lung Transplantation* 36.10, pp. 1047–1059.

Chanda, Diptiman et al. (2019). "Developmental pathways in the pathogenesis of lung fibrosis". In: *Molecular aspects of medicine* 65, pp. 56–69.

Chang, Wenteh et al. (2014). "A critical role for the mTORC2 pathway in lung fibrosis". In: *PloS one* 9.8, e106155.

El-Chemaly, Souheil et al. (2010). "Familial pulmonary fibrosis: natural history of preclinical disease". In: *B40. INTERSTITIAL LUNG DISEASE: EPIDEMIOLOGY AND OUTCOMES*. American Thoracic Society, A2980–A2980.

Chen, Kui-Jun et al. (2016). "Bleomycin (BLM) induces epithelial-to-mesenchymal transition in cultured A549 cells via the TGF-β/Smad signaling pathway". In: *Journal of Cancer* 7.11, p. 1557.

Chen, Ying et al. (2020). "p62/SQSTM1, a central but unexploited target: advances in its physiological/pathogenic functions and small molecular modulators". In: *Journal of Medicinal Chemistry* 63.18, pp. 10135–10157.

Cheng, Hailing et al. (2009). "SIK1 couples LKB1 to p53-dependent anoikis and suppresses metastasis". In: *Science signaling* 2.80, ra35–ra35.

Cheng, Yusi et al. (2019). "CircRNA-012091/PPP1R13B–mediated lung fibrotic response in silicosis via endoplasmic reticulum stress and autophagy". In: *American journal of respiratory cell and molecular biology* 61.3, pp. 380–391.

Chiang, Hui-Ling et al. (1989). "A role for a 70-kilodalton heat shock protein in lysosomal degradation of intracellular proteins". In: *Science* 246.4928, pp. 382–385.

Cho, Monique E and Jeffrey B Kopp (2010). "Pirfenidone: an anti-fibrotic therapy for progressive kidney disease". In: *Expert opinion on investigational drugs* 19.2, pp. 275–283.

Cigna, Nathalie and et al. (2012). "The hedgehog system machinery controls transforming growth factor-β–dependent myofibroblastic differentiation in humans: involvement in idiopathic pulmonary fibrosis". In: *The American journal of pathology* 181, pp. 2126–2137.

Collard, Harold R, Luca Richeldi, et al. (2017). "Acute exacerbations in the INPULSIS trials of nintedanib in idiopathic pulmonary fibrosis". In: *European Respiratory Journal* 49.5.

Collard, Harold R, Christopher J Ryerson, et al. (2016). "Acute exacerbation of idiopathic pulmonary fibrosis. An international working group report". In: *American journal of respiratory and critical care medicine* 194.3, pp. 265–275.

Comeglio, P et al. (2019). "Therapeutic effects of obeticholic acid (OCA) treatment in a bleomycin-induced pulmonary fibrosis rat model". In: *Journal of Endocrinological Investigation* 42, pp. 283–294.

Conforti, F. and et al. (2020). "Paracrine SPARC signaling dysregulates alveolar epithelial barrier integrity and function in lung fibrosis". In: *Cell death discovery* 6, pp. 1–11.

Conforti, Franco et al. (2017). "The histone deacetylase inhibitor, romidepsin, as a potential treatment for pulmonary fibrosis". In: *Oncotarget* 8.30, p. 48737.

Cook, Donald N, David M Brass, and David A Schwartz (2002). "A matrix for new ideas in pulmonary fibrosis". In: *American journal of respiratory cell and molecular biology* 27.2, pp. 122–124.

Coward, William R, Gauri Saini, and Gisli Jenkins (2010). "The pathogenesis of idiopathic pulmonary fibrosis". In: *Therapeutic advances in respiratory disease* 4.6, pp. 367–388.

Cox, Nehemiah, Darrell Pilling, and Richard H Gomer (2014). "Serum amyloid P: a systemic regulator of the innate immune response". In: *Journal of leukocyte biology* 96.5, pp. 739–743.

Cronkhite, Jennifer T et al. (2008). "Telomere shortening in familial and sporadic pulmonary fibrosis". In: *American journal of respiratory and critical care medicine* 178.7, pp. 729–737.

Darby, I, O Skalli, and G Gabbiani (1990). "Alpha-smooth muscle actin is transiently expressed by myofibroblasts during experimental wound healing." In: *Laboratory investigation; a journal of technical methods and pathology* 63.1, pp. 21–29.

De Wever, Olivier et al. (2008). "Stromal myofibroblasts are drivers of invasive cancer growth". In: *International journal of cancer* 123.10, pp. 2229–2238.

Decaris, Martin L et al. (2021). "Dual inhibition of $\alpha v\beta 6$ and $\alpha v\beta 1$ reduces fibrogenesis in lung tissue explants from patients with IPF". In: *Respiratory research* 22.1, pp. 1–14.

Degryse, Amber L et al. (2011). "TGFβ signaling in lung epithelium regulates bleomycin-induced alveolar injury and fibroblast recruitment". In: *American Journal of Physiology-Lung Cellular and Molecular Physiology* 300.6, pp. L887–L897.

Demedts, Maurits et al. (2005). "High-dose acetylcysteine in idiopathic pulmonary fibrosis". In: *New England Journal of Medicine* 353.21, pp. 2229–2242.

Desai, Tushar J, Douglas G Brownfield, and Mark A Krasnow (2014). "Alveolar progenitor and stem cells in lung development, renewal and cancer". In: *Nature* 507.7491, pp. 190–194.

Distler, Jörg HW et al. (2019). "Shared and distinct mechanisms of fibrosis". In: *Nature Reviews Rheumatology* 15.12, pp. 705–730.

Doncheva, Nadezhda T et al. (2018). "Cytoscape StringApp: network analysis and visualization of proteomics data". In: *Journal of proteome research* 18.2, pp. 623–632.

Douglas, William W, Jay H Ryu, and Darrell R Schroeder (2000). "Idiopathic pulmonary fibrosis: impact of oxygen and colchicine, prednisone, or no therapy on survival". In: *American journal of respiratory and critical care medicine* 161.4, pp. 1172–1178.

Dowman, L, CJ Hill, and AE Holland (2014). "Pulmonary rehabilitationforinterstitiallungdisease". In: *Cochrane Database Syst Rev. https://doi.org/10.1002/14651858. CD006322. pub3*.

Drakopanagiotakis, F et al. (2018). "Biomarkers in idiopathic pulmonary fibrosis". In: *Matrix Biology* 68, pp. 404–421.

Dunsmore, SARAH E and D Eugene Rannels (1996). "Extracellular matrix biology in the lung". In: *American Journal of Physiology-Lung Cellular and Molecular Physiology* 270.1, pp. L3–L27.

Egan, Jim J et al. (1995). "Epstein-Barr virus replication within pulmonary epithelial cells in cryptogenic fibrosing alveolitis." In: *Thorax* 50.12, pp. 1234–1239.

Egan, JJ (2011). "Follow-up and nonpharmacological management of the idiopathic pulmonary fibrosis patient". In: *European Respiratory Review* 20.120, pp. 114–117.

Eggers, Carrie M et al. (2012). "STE20-related kinase adaptor protein α (STRADα) regulates cell polarity and invasion through PAK1 signaling in LKB1-null cells". In: *Journal of Biological Chemistry* 287.22, pp. 18758–18768.

Enomoto, Tatsuji et al. (2003). "Diabetes mellitus may increase risk for idiopathic pulmonary fibrosis". In: *Chest* 123.6, pp. 2007–2011.

Estany, Susanna et al. (2014). "Lung fibrotic tenascin-C upregulation is associated with other extracellular matrix proteins and induced by TGFβ1". In: *BMC pulmonary medicine* 14.1, pp. 1–9.

Fanny, Manoussa et al. (2018). "The IL-33 receptor ST2 regulates pulmonary inflammation and fibrosis to bleomycin". In: *Frontiers in immunology* 9, p. 1476.

Faverio, Paola et al. (2018). "Management of acute respiratory failure in interstitial lung diseases: overview and clinical insights". In: *BMC pulmonary medicine* 18.1, pp. 1–13.

Féréol, Sophie et al. (2008). "Cell mechanics of alveolar epithelial cells (AECs) and macrophages (AMs)". In: *Respiratory physiology & neurobiology* 163.1-3, pp. 3–16.

Fernández Fabrellas, Estrella et al. (2018). "Prognosis and follow-up of idiopathic pulmonary fibrosis". In: *Medical Sciences* 6.2, p. 51.

Fingerlin, Tasha E et al. (2013). "Genome-wide association study identifies multiple susceptibility loci for pulmonary fibrosis". In: *Nature genetics* 45.6, pp. 613–620.

Force, Seth D et al. (2011). "Bilateral lung transplantation offers better long-term survival, compared with single-lung transplantation, for younger patients with idiopathic pulmonary fibrosis". In: *The Annals of thoracic surgery* 91.1, pp. 244–249.

Frangogiannis, Nikolaos G (2020). "Transforming growth factor–β in tissue fibrosis". In: *Journal of Experimental Medicine* 217.3.

Frantz, Christian, Kathleen M Stewart, and Valerie M Weaver (2010). "The extracellular matrix at a glance". In: *Journal of cell science* 123.24, pp. 4195–4200.

Froese, Aaron R et al. (2016). "Stretch-induced activation of transforming growth factor-β1 in pulmonary fibrosis". In: *American journal of respiratory and critical care medicine* 194.1, pp. 84–96.

Fukuchi, Yoshinosuke (2009). "The aging lung and chronic obstructive pulmonary disease: similarity and difference". In: *Proceedings of the American Thoracic Society* 6.7, pp. 570–572.

Fukuda, Yuh et al. (1998). "Localization of matrix metalloproteinases-1,-2, and-9 and tissue inhibitor of metalloproteinase-2 in interstitial lung diseases." In: *Laboratory investigation; a journal of technical methods and pathology* 78.6, pp. 687–698.

Gabbiani, G (1981). "The myofibroblast: a key cell for wound healing and fibrocontractive diseases". In: *Prog Clin Biol Res* 54, pp. 183–194.

Gabbiani, GRGB, GB Ryan, and G Majno (1971). "Presence of modified fibroblasts in granulation tissue and their possible role in wound contraction". In: *Experientia* 27.5, pp. 549–550.

Gagnon, Lyne et al. (2018). "A newly discovered antifibrotic pathway regulated by two fatty acid receptors: GPR40 and GPR84". In: *The American Journal of Pathology* 188.5, pp. 1132–1148.

Galiè, Nazzareno et al. (2005). "Sildenafil citrate therapy for pulmonary arterial hypertension". In: *New England Journal of Medicine* 353.20, pp. 2148–2157.

Gargus, Matthew et al. (2015). "Human esophageal myofibroblasts secrete proinflammatory cytokines in response to acid and Toll-like receptor 4 ligands". In: *American Journal of Physiology-Gastrointestinal and Liver Physiology* 308.11, G904–G923.

Geiser, Thomas et al. (2004). "H2O2 inhibits alveolar epithelial wound repair in vitro by induction of apoptosis". In: *American Journal of Physiology-Lung Cellular and Molecular Physiology* 287, pp. L448–L453.

Giacomini, Marilyn M et al. (2012). "Epithelial cells utilize cortical actin/myosin to activate latent TGF-β through integrin $\alpha v\beta 6$-dependent physical force". In: *Experimental cell research* 318.6, pp. 716–722.

Gilani, Syed R et al. (2010). "CD28 down-regulation on circulating CD4 T-cells is associated with poor prognoses of patients with idiopathic pulmonary fibrosis". In: *PloS one* 5.1, e8959.

Glaspole, Ian N et al. (2017). "Determinants and outcomes of prolonged anxiety and depression in idiopathic pulmonary fibrosis". In: *European Respiratory Journal* 50.2.

Goldmann, Torsten et al. (2018). "Human alveolar epithelial cells type II are capable of TGFβ-dependent epithelial-mesenchymal-transition and collagen-synthesis". In: *Respiratory research* 19.1, pp. 1–13.

Gómez-Batiste, Xavier et al. (2010). "Models of care, organization and quality improvement for the care of advanced and terminal patients and their families: the contribution of palliative care". In: *Medicina Clınica* 135.2, pp. 83–89.

Goodwin, JM et al. (2014). "An AMPK-independent signaling pathway downstream of the LKB1 tumor suppressor controls Snail1 and metastatic potential". In: *Molecular cell* 55.3, pp. 436–450.

Grahovac, Jelena and Alan Wells (2014). "Matrikine and matricellular regulators of EGF receptor signaling on cancer cell migration and invasion". In: *Laboratory Investigation* 94, pp. 31–40.

Grande, M Teresa et al. (2015). "Snail1-induced partial epithelial-to-mesenchymal transition drives renal fibrosis in mice and can be targeted to reverse established disease". In: *Nature medicine* 21.9, pp. 989–997.

Gribbin, Jonathan et al. (2006). "Incidence and mortality of idiopathic pulmonary fibrosis and sarcoidosis in the UK". In: *Thorax* 61.11, pp. 980–985.

GROUP*, NOCTURNAL OXYGEN THERAPY TRIAL (1980). "Continuous or nocturnal oxygen therapy in hypoxemic chronic obstructive lung disease: a clinical trial". In: *Annals of internal medicine* 93.3, pp. 391–398.

Gui, Xianhua et al. (2018). "Leptin promotes pulmonary fibrosis development by inhibiting autophagy via PI3K/Akt/mTOR pathway". In: *Biochemical and Biophysical Research Communications* 498.3, pp. 660–666.

Gui, Yao-Song et al. (2015). "mTOR overactivation and compromised autophagy in the pathogenesis of pulmonary fibrosis". In: *PloS one* 10.9, e0138625.

Gulack, Brian C et al. (2015). "What is the optimal transplant for older patients with idiopathic pulmona ry fibrosis?" In: *The Annals of thoracic surgery* 100.5, pp. 1826–1833.

Guo, Tao et al. (2021). "Respiratory outcomes in patients following COVID-19-related hospitalization: a meta-analysis". In: *Frontiers in Molecular Biosciences* 8, p. 750558.

Gurumurthy, S et al. (2010). "The Lkb1 metabolic sensor maintains haematopoietic stem cell survival". In: *Nature* 468.7324, pp. 659–663.

Habermann, AC et al. (2020). "Single-cell RNA sequencing reveals profibrotic roles of distinct epithelial and mesenchymal lineages in pulmonary fibrosis". In: *Science Advances* 6.28, eaba1972.

Habermann, Arun C et al. (2020). "Single-cell RNA sequencing reveals profibrotic roles of distinct epithelial and mesenchymal lineages in pulmonary fibrosis". In: *Science advances* 6.28, eaba1972.

Habiel, David M and Cory M Hogaboam (2017). "Heterogeneity of fibroblasts and myofibroblasts in pulmonary fibrosis". In: *Current pathobiology reports* 5, pp. 101–110.

Hagimoto, Naoki and et al. (2002). "TGF-*beta*1 as an enhancer of Fas-mediated apoptosis of lung epithelial cells". In: *The Journal of Immunology* 168, pp. 6470–6478.

Hallstrand, TS et al. (2005). "The timed walk test as a measure of severity and survival in idiopathic pulmonary fibrosis". In: *European Respiratory Journal* 25.1, pp. 96–103.

Han, Dong et al. (2013). "LKB1/AMPK/mTOR signaling pathway in non-small-cell lung cancer". In: *Asian pacific journal of cancer prevention* 14.7, pp. 4033–4039.

Han, Seung Hyeok et al. (2016). "Deletion of Lkb1 in renal tubular epithelial cells leads to CKD by altering metabolism". In: *Journal of the American Society of Nephrology* 27.2, pp. 439–453.

Han, SH et al. (2016). "Deletion of Lkb1 in renal tubular epithelial cells leads to CKD by altering metabolism". In: *Journal of the American Society of Nephrology* 27.2, pp. 439–453.

Hanmandlu, Ankit et al. (2022). "Transcriptomic and epigenetic profiling of fibroblasts in idiopathic pulmonary fibrosis". In: *American Journal of Respiratory Cell and Molecular Biology* 66.1, pp. 53–63.

Hänzelmann, S, R Castelo, and J Guinney (2013). "GSVA: gene set variation analysis for microarray and RNA-Seq data". In: *BMC Bioinformatics* 14.1, p. 7.

Harada, Taishi et al. (2010). "Epithelial–mesenchymal transition in human lungs with usual interstitial pneumonia: quantitative immunohistochemistry". In: *Pathology international* 60.1, pp. 14–21.

Hardie, D Grahame (2005). "New roles for the LKB1→ AMPK pathway". In: *Current opinion in cell biology* 17.2, pp. 167–173.

Hardie, D Grahame and Dario R Alessi (2013). "LKB1 and AMPK and the cancer-metabolism link-ten years after". In: *BMC biology* 11.1, pp. 1–11.

Hardinge, Maxine et al. (2015). "British Thoracic Society guidelines for home oxygen use in adults: accredited by NICE". In: *Thorax* 70.Suppl 1, pp. i1–i43.

Hawley, SA et al. (2003). "Complexes between the LKB1 tumor suppressor". In: *STRADα/β and MO24α/β are upstream kinases in the AMP-activated protein kinase cascade http://jbiol. com/content/2/4/28 [Europe PMC free article]*.

Hayashi, Hiromitsu and Takao Sakai (2012). "Biological significance of local TGF-β activation in liver diseases". In: *Frontiers in physiology* 3, p. 12.

Hebert, Morgan et al. (2016). "The story of an exceptional serine protease, tissue-type plasminogen activator (tPA)". In: *Revue neurologique* 172, pp. 186–197.

Hecker, Louise et al. (2014). "Reversal of persistent fibrosis in aging by targeting Nox4-Nrf2 redox imbalance". In: *Science translational medicine* 6.231, 231ra47–231ra47.

Hemminki, Akseli et al. (1998a). "A serine/threonine kinase gene defective in Peutz–Jeghers syndrome". In: *Nature* 391.6663, pp. 184–187.

– (1998b). "A serine/threonine kinase gene defective in Peutz–Jeghers syndrome". In: *Nature* 391.6663, pp. 184–187.

Henderson, Neil C, Florian Rieder, and Thomas A Wynn (2020). "Fibrosis: from mechanisms to medicines". In: *Nature* 587.7835, pp. 555–566.

Herrera, Iliana et al. (2013). "Matrix metalloproteinase (MMP)-1 induces lung alveolar epithelial cell migration and proliferation, protects from apoptosis, and represses mitochondrial oxygen consumption". In: *Journal of Biological Chemistry* 288.36, pp. 25964–25975.

Hill, C and Y Wang (2020). "The importance of epithelial-mesenchymal transition and autophagy in cancer drug resistance". In: *Cancer drug resistance (Alhambra, Calif)* 3.1, p. 38.

– (2021). "Autophagy in Pulmonary Fibrosis: Friend or Foe?" In: *Genes & Diseases*.

Hill, Charlotte, Mark G Jones, et al. (2019). "Epithelial-mesenchymal transition contributes to pulmonary fibrosis via aberrant epithelial/fibroblastic cross-talk". In: *Journal of lung health and diseases* 3.2, p. 31.

Hill, Charlotte, Juanjuan Li, et al. (2019). "Autophagy inhibition-mediated epithelial–mesenchymal transition augments local myofibroblast differentiation in pulmonary fibrosis". In: *Cell death & disease* 10.8, p. 591.

Hill, Charlotte and Yihua Wang (2020). "The importance of epithelial-mesenchymal transition and autophagy in cancer drug resistance". In: *Cancer Drug Resistance* 3.1, p. 38.

– (2022). "Autophagy in pulmonary fibrosis: friend or foe?" In: *Genes & Diseases* 9.6, pp. 1594–1607.

Hinz, Boris (2006). "Masters and servants of the force: the role of matrix adhesions in myofibroblast force perception and transmission". In: *European journal of cell biology* 85.3-4, pp. 175–181.

Hinz, Boris, Giuseppe Celetta, et al. (2001). "Alpha-smooth muscle actin expression upregulates fibroblast contractile activity". In: *Molecular biology of the cell* 12.9, pp. 2730–2741.

Hinz, Boris, Sem H Phan, et al. (2007). "The myofibroblast: one function, multiple origins". In: *The American journal of pathology* 170.6, pp. 1807–1816.

Hirahara, Kiyoshi et al. (2019). "The immunopathology of lung fibrosis: amphiregulin-producing pathogenic memory T helper-2 cells control the airway fibrotic responses by inducing eosinophils to secrete osteopontin". In: *Seminars in Immunopathology*. Vol. 41. Springer, pp. 339–348.

Hirani, Nikhil et al. (2021). "Target inhibition of galectin-3 by inhaled TD139 in patients with idiopathic pulmonary fibrosis". In: *European Respiratory Journal* 57.5.

Hook, Jaime L et al. (2012). "Titrated oxygen requirement and prognostication in idiopathic pulmonary fibrosis". In: *European Respiratory Journal* 39.2, pp. 359–365.

Horan, Gerald S et al. (2008). "Partial inhibition of integrin $\alpha v\beta 6$ prevents pulmonary fibrosis without exacerbating inflammation". In: *American journal of respiratory and critical care medicine* 177.1, pp. 56–65.

Hostettler, Katrin E et al. (2014). "Anti-fibrotic effects of nintedanib in lung fibroblasts derived from patients with idiopathic pulmonary fibrosis". In: *Respiratory research* 15.1, pp. 1–9.

Hou, Jiwei et al. (2018). "TNF-α-induced NF-κB activation promotes myofibroblast differentiation of LR-MSCs and exacerbates bleomycin-induced pulmonary fibrosis". In: *Journal of cellular physiology* 233.3, pp. 2409–2419.

Hu, Kaihong et al. (2007). "Tissue-type plasminogen activator promotes murine myofibroblast activation through LDL receptor–related protein 1–mediated integrin signaling". In: *The Journal of clinical investigation* 117, pp. 3821–3832.

Huang, N-Y et al. (2013). "Pharmacokinetics, safety and tolerability of pirfenidone and its major metabolite after single and multiple oral doses in healthy Chinese subjects under fed conditions". In: *Drug research*, pp. 388–395.

Huang, Steven et al. (2007). "Prostaglandin E2 inhibits collagen expression and proliferation in patient-derived normal lung fibroblasts via E prostanoid 2 receptor and cAMP signaling". In: *American Journal of Physiology-Lung Cellular and Molecular Physiology* 292.2, pp. L405–L413.

Huang, Xiangwei et al. (2012). "Matrix stiffness–induced myofibroblast differentiation is mediated by intrinsic mechanotransduction". In: *American journal of respiratory cell and molecular biology* 47.3, pp. 340–348.

Hubbard, R (2001). "Occupational dust exposure and the aetiology of cryptogenic fibrosing alveolitis". In: *European Respiratory Journal* 18.32 suppl, 119S–121S.

Humphreys, Benjamin D et al. (2010). "Fate tracing reveals the pericyte and not epithelial origin of myofibroblasts in kidney fibrosis". In: *The American journal of pathology* 176.1, pp. 85–97.

Hung, Chi et al. (2013). "Role of lung pericytes and resident fibroblasts in the pathogenesis of pulmonary fibrosis". In: *American journal of respiratory and critical care medicine* 188.7, pp. 820–830.

Huppmann, Patrick et al. (2013). "Effects of inpatient pulmonary rehabilitation in patients with interstitial lung disease". In: *European Respiratory Journal* 42.2, pp. 444–453.

Hutchinson, John et al. (2015). "Global incidence and mortality of idiopathic pulmonary fibrosis: a systematic review". In: *European Respiratory Journal* 46.3, pp. 795–806.

Hwang, Jin-Taek et al. (2006). "Selenium regulates cyclooxygenase-2 and extracellular signal-regulated kinase signaling pathways by activating AMP-activated protein kinase in colon cancer cells". In: *Cancer research* 66.20, pp. 10057–10063.

Ichimura, Yoshinobu and Masaaki Komatsu (2018). "Activation of p62/SQSTM1–Keap1–nuclear factor erythroid 2-related factor 2 pathway in cancer". In: *Frontiers in oncology* 8, p. 210.

Imokawa, Shiro et al. (1997). "Tissue factor expression and fibrin deposition in the lungs of patients with idiopathic pulmonary fibrosis and systemic sclerosis". In: *American journal of respiratory and critical care medicine* 156.2, pp. 631–636.

Inami, Yoshihiro et al. (2011). "Persistent activation of Nrf2 through p62 in hepatocellular carcinoma cells". In: *Journal of Cell Biology* 193.2, pp. 275–284.

Iyer, SN, G Gurujeyalakshmi, and SN Giri (1999). "Effects of pirfenidone on transforming growth factor-β gene expression at the transcriptional level in bleomycin hamster model of lung fibrosis". In: *Journal of Pharmacology and Experimental Therapeutics* 291.1, pp. 367–373.

Jackson, Robert M et al. (2014). "Exercise limitation in IPF patients: a randomized trial of pulmonary rehabilitation". In: *Lung* 192, pp. 367–376.

Jayachandran, Aparna et al. (2009). "SNAI transcription factors mediate epithelial–mesenchymal transition in lung fibrosis". In: *Thorax* 64.12, pp. 1053–1061.

Jeon, Sang-Min, Navdeep S Chandel, and Nissim Hay (2012). "AMPK regulates NADPH homeostasis to promote tumour cell survival during energy stress". In: *Nature* 485.7400, pp. 661–665.

Jiang, Peidu and Noboru Mizushima (2015). "LC3- and p62-based biochemical methods for the analysis of autophagy progression in mammalian cells". In: *Methods*

75. Autophagy, pp. 13–18. ISSN: 1046-2023. DOI: https://doi.org/10.1016/j.ymeth.2014.11.021. URL: https://www.sciencedirect.com/science/article/pii/S1046202314003843.

Johansen, Terje and Trond Lamark (2011). "Selective autophagy mediated by autophagic adapter proteins". In: *Autophagy* 7.3, pp. 279–296.

Jones, Russell G et al. (2005). "AMP-activated protein kinase induces a p53-dependent metabolic checkpoint". In: *Molecular cell* 18.3, pp. 283–293.

Justice, Jamie N et al. (2019). "Senolytics in idiopathic pulmonary fibrosis: results from a first-in-human, open-label, pilot study". In: *EBioMedicine* 40, pp. 554–563.

Kalluri, Meena et al. (2018). "Beyond idiopathic pulmonary fibrosis diagnosis: multidisciplinary care with an early integrated palliative approach is associated with a decrease in acute care utilization and hospital deaths". In: *Journal of Pain and Symptom Management* 55.2, pp. 420–426.

Kalluri, Raghu, Robert A Weinberg, et al. (2009). "The basics of epithelial-mesenchymal transition". In: *The Journal of clinical investigation* 119.6, pp. 1420–1428.

Kärkkäinen, Miia et al. (2018). "Underlying and immediate causes of death in patients with idiopathic pulmonary fibrosis". In: *BMC Pulmonary Medicine* 18, pp. 1–10.

Karuman, Philip et al. (2001). "The Peutz-Jegher gene product LKB1 is a mediator of p53-dependent cell death". In: *Molecular cell* 7.6, pp. 1307–1319.

Kasai, Hidenori et al. (2005). "TGF-β1 induces human alveolar epithelial to mesenchymal cell transition (EMT)". In: *Respiratory research* 6.1, pp. 1–15.

Katzenstein, Anna-Luise A and Jeffrey L Myers (1998). "Idiopathic pulmonary fibrosis: clinical relevance of pathologic classification". In: *American journal of respiratory and critical care medicine* 157.4, pp. 1301–1315.

Kendall, Ryan T and Carol A Feghali-Bostwick (2014). "Fibroblasts in fibrosis: novel roles and mediators". In: *Frontiers in pharmacology* 5, p. 123.

Kenyon, NJ et al. (2003). "TGF-β1 causes airway fibrosis and increased collagen I and III mRNA in mice". In: *Thorax* 58.9, pp. 772–777.

Khalil, N. et al. (1996). "TGF-beta 1, but not TGF-beta 2 or TGF-beta 3, is differentially present in epithelial cells of advanced pulmonary fibrosis: an immunohistochemical study". In: *American journal of respiratory cell and molecular biology* 14, pp. 131–138.

Khalil, Nasreen et al. (1996). "TGF-beta 1, but not TGF-beta 2 or TGF-beta 3, is differentially present in epithelial cells of advanced pulmonary fibrosis: an immunohistochemical study." In: *American journal of respiratory cell and molecular biology* 14.2, pp. 131–138.

Khan, Abdul Q et al. (2019). "RAS-mediated oncogenic signaling pathways in human malignancies". In: *Seminars in cancer biology*. Vol. 54. Elsevier, pp. 1–13.

Khor, Yet H et al. (2022). "Antacid medication and antireflux surgery in patients with idiopathic pulmonary fibrosis: a systematic review and meta-analysis". In: *Annals of the American Thoracic Society* 19.5, pp. 833–844.

Kim, Jungwook et al. (2009). "Reactive oxygen species/oxidative stress contributes to progression of kidney fibrosis following transient ischemic injury in mice". In: *American Journal of Physiology-Renal Physiology* 297, F461–F470.

Kim, Kevin K, Matthias C Kugler, et al. (2006). "Alveolar epithelial cell mesenchymal transition develops in vivo during pulmonary fibrosis and is regulated by the extracellular matrix". In: *Proceedings of the National Academy of Sciences* 103.35, pp. 13180–13185.

Kim, Kevin K, Dean Sheppard, and Harold A Chapman (2018). "TGF-β1 signaling and tissue fibrosis". In: *Cold Spring Harbor perspectives in biology* 10.4, a022293.

Kimura, Shunsuke, Naonobu Fujita, et al. (2009). "Monitoring autophagy in mammalian cultured cells through the dynamics of LC3". In: *Methods in enzymology* 452, pp. 1–12.

Kimura, Shunsuke, Takeshi Noda, and Tamotsu Yoshimori (2007). "Dissection of the autophagosome maturation process by a novel reporter protein, tandem fluorescent-tagged LC3". In: *Autophagy* 3.5, pp. 452–460.

King, Connor T et al. (2022). "Liver Kinase B1 Regulates Remodeling of the Tumor Microenvironment in Triple-Negative Breast Cancer". In: *Frontiers in molecular biosciences* 9, p. 847505.

King, Talmadge E, Annie Pardo, and Moisés Selman (2011). "Idiopathic pulmonary fibrosis". In: *The Lancet* 378.9807, pp. 1949–1961.

King Jr, Talmadge E, Williamson Z Bradford, et al. (2014). "A phase 3 trial of pirfenidone in patients with idiopathic pulmonary fibrosis". In: *New England Journal of Medicine* 370.22, pp. 2083–2092.

King Jr, Talmadge E, Annie Pardo, and Moisés Selman (2011). "Idiopathic pulmonary fibrosis". In: *The Lancet* 378.9807, pp. 1949–1961.

KING JR, TALMADGE E et al. (2001). "Idiopathic pulmonary fibrosis: relationship between histopathologic features and mortality". In: *American journal of respiratory and critical care medicine* 164.6, pp. 1025–1032.

King Jr, TE et al. (2001). "Idiopathic pulmonary fibrosis: relationship between histopathologic features and mortality". In: *American journal of respiratory and critical care medicine* 164.6, pp. 1025–1032.

Kistler, Kristin D et al. (2014). "Lung transplantation in idiopathic pulmonary fibrosis: a systematic review of the literature". In: *BMC pulmonary medicine* 14.1, pp. 1–12.

Klingberg, Franco, Boris Hinz, and Eric S White (2013). "The myofibroblast matrix: implications for tissue repair and fibrosis". In: *The Journal of pathology* 229.2, pp. 298–309.

Knippenberg, Sarah et al. (2015). "Streptococcus pneumoniae triggers progression of pulmonary fibrosis through pneumolysin". In: *Thorax* 70.7, pp. 636–646.

Kolb, Martin and et al. (2001). "Transient expression of IL-1β induces acute lung injury and chronic repair leading to pulmonary fibrosis". In: *The Journal of clinical investigation* 107, pp. 1529–1536.

Komatsu, Masaaki and Yoshinobu Ichimura (2010). "Physiological significance of selective degradation of p62 by autophagy". In: *FEBS letters* 584.7, pp. 1374–1378.

Komatsu, Masaaki, Satoshi Waguri, et al. (2007). "Homeostatic levels of p62 control cytoplasmic inclusion body formation in autophagy-deficient mice". In: *Cell* 131.6, pp. 1149–1163.

Kondoh, Yasuhiro, Vincent Cottin, and Kevin K Brown (2017). "Recent lessons learned in the management of acute exacerbation of idiopathic pulmonary fibrosis". In: *European Respiratory Review* 26.145.

Königshoff, Melanie and et al. (2009). "WNT1-inducible signaling protein–1 mediates pulmonary fibrosis in mice and is upregulated in humans with idiopathic pulmonary fibrosis". In: *The Journal of clinical investigation* 119, pp. 772–787.

Königshoff, Melanie, Monika Kramer, et al. (2009). "WNT1-inducible signaling protein–1 mediates pulmonary fibrosis in mice and is upregulated in humans with idiopathic pulmonary fibrosis". In: *The Journal of clinical investigation* 119.4, pp. 772–787.

Korfei, Martina, Poornima Mahavadi, and Andreas Guenther (2022). "Targeting histone deacetylases in idiopathic pulmonary fibrosis: a future therapeutic option". In: *Cells* 11.10, p. 1626.

Kornum, Jette B et al. (2008). "The incidence of interstitial lung disease 1995–2005: a Danish nationwide population-based study". In: *BMC Pulmonary Medicine* 8, pp. 1–7.

Koslowski, R. et al. (2003). "Cathepsins in bleomycin-induced lung injury in rat". In: *European Respiratory Journal* 22, pp. 427–435.

Kotani, Izumi et al. (1995). "Increased procoagulant and antifibrinolytic activities in the lungs with idiopathic pulmonary fibrosis". In: *Thrombosis research* 77.6, pp. 493–504.

Kou, Bo et al. (2022). "LKB1 inhibits proliferation, metastasis and angiogenesis of thyroid cancer by upregulating SIK1". In: *Journal of Cancer* 13.9, p. 2872.

Kreuter, Michael, Elisabeth Bendstrup, et al. (2017). "Palliative care in interstitial lung disease: living well". In: *The Lancet Respiratory Medicine* 5.12, pp. 968–980.

Kreuter, Michael, Ulrich Costabel, et al. (2018). "Statin therapy and outcomes in trials of nintedanib in idiopathic pulmonary fibrosis". In: *Respiration* 95.5, pp. 317–326.

Kreuter, Michael, Svenja Ehlers-Tenenbaum, et al. (2016). "Impact of comorbidities on mortality in patients with idiopathic pulmonary fibrosis". In: *PloS one* 11.3, e0151425.

Kropski, Jonathan A, Daphne B Mitchell, et al. (2014). "A novel dyskerin (DKC1) mutation is associated with familial interstitial pneumonia". In: *Chest* 146.1, e1–e7.

Kropski, Jonathan A, Jason M Pritchett, et al. (2015). "Extensive phenotyping of individuals at risk for familial interstitial pneumonia reveals clues to the pathogenesis of interstitial lung disease". In: *American journal of respiratory and critical care medicine* 191.4, pp. 417–426.

Kugler, Matthias C et al. (2015). "Sonic hedgehog signaling in the lung. From development to disease". In: *American journal of respiratory cell and molecular biology* 52.1, pp. 1–13.

Kuhn, Charles and JA1886011 McDonald (1991). "The roles of the myofibroblast in idiopathic pulmonary fibrosis. Ultrastructural and immunohistochemical features of sites of active extracellular matrix synthesis." In: *The American journal of pathology* 138.5, p. 1257.

Kulasekaran, Prabha and et al. (2009). "Endothelin-1 and transforming growth factor-β1 independently induce fibroblast resistance to apoptosis via AKT activation". In: *American journal of respiratory cell and molecular biology* 41, pp. 484–493.

Kulasekaran, Priya et al. (2009). "Endothelin-1 and transforming growth factor-β1 independently induce fibroblast resistance to apoptosis via AKT activation". In: *American journal of respiratory cell and molecular biology* 41.4, pp. 484–493.

Kulkarni, Ashok B et al. (1993). "Transforming growth factor beta 1 null mutation in mice causes excessive inflammatory response and early death." In: *Proceedings of the National Academy of Sciences* 90.2, pp. 770–774.

Kulkarni, Tejaswini et al. (2016). "Matrix remodeling in pulmonary fibrosis and emphysema". In: *American journal of respiratory cell and molecular biology* 54.6, pp. 751–760.

Kullmann, L and MP Krahn (2018). "Controlling the master—upstream regulation of the tumor suppressor LKB1". In: *Oncogene* 37.23, pp. 3045–3057.

Kullmann, Lars and Michael P Krahn (2018). "Controlling the master—upstream regulation of the tumor suppressor LKB1". In: *Oncogene* 37.23, pp. 3045–3057.

Kunz, Joachim B, Heinz Schwarz, and Andreas Mayer (2004). "Determination of four sequential stages during microautophagy in vitro". In: *Journal of Biological Chemistry* 279.11, pp. 9987–9996.

Kuwano, Kazuyoshi et al. (2001). "Attenuation of bleomycin-induced pneumopathy in mice by a caspase inhibitor". In: *American Journal of Physiology-Lung Cellular and Molecular Physiology* 280.2, pp. L316–L325.

Lai, Chih-Cheng et al. (2012). "Idiopathic pulmonary fibrosis in Taiwan–a population-based study". In: *Respiratory medicine* 106.11, pp. 1566–1574.

Lancaster, Lisa H et al. (2009). "Obstructive sleep apnea is common in idiopathic pulmonary fibrosis". In: *Chest* 136.3, pp. 772–778.

Larsen, Kenneth Bowitz et al. (2010). "A reporter cell system to monitor autophagy based on p62/SQSTM1". In: *Autophagy* 6.6, pp. 784–793.

Larsson, Ola et al. (2008). "Fibrotic myofibroblasts manifest genome-wide derangements of translational control". In: *PloS one* 3.9, e3220.

Lasithiotaki, Ismini et al. (2011). "Detection of herpes simplex virus type-1 in patients with fibrotic lung diseases". In: *PloS one* 6.12, e27800.

Laurent, GJ et al. (2007). "Regulation of matrix turnover: fibroblasts, forces, factors and fibrosis". In: *Biochemical Society Transactions* 35.4, pp. 647–651.

LeBleu, Valerie S et al. (2013). "Origin and function of myofibroblasts in kidney fibrosis". In: *Nature medicine* 19.8, pp. 1047–1053.

Lederer, David J and Fernando J Martinez (2018). "Idiopathic pulmonary fibrosis". In: *New England Journal of Medicine* 378.19, pp. 1811–1823.

Lee, Chun Geun et al. (2004). "Early growth response gene 1–mediated apoptosis is essential for transforming growth factor β1–induced pulmonary fibrosis". In: *The Journal of experimental medicine* 200.3, pp. 377–389.

Lee, HE et al. (2016). "Incidence and prevalence of idiopathic interstitial pneumonia and idiopathic pulmonary fibrosis in Korea". In: *The International Journal of Tuberculosis and Lung Disease* 20.7, pp. 978–984.

Lee, JH et al. (2006). "JNK pathway mediates apoptotic cell death induced by tumor suppressor LKB1 in Drosophila". In: *Cell Death & Differentiation* 13.7, pp. 1110–1122.

Lee, Sang Hoon et al. (2015). "Association between occupational dust exposure and prognosis of idiopathic pulmonary fibrosis". In: *Chest* 147.2, pp. 465–474.

Lenz, AG, U Costabel, and KL Maier (1996). "Oxidized BAL fluid proteins in patients with interstitial lung diseases". In: *European Respiratory Journal* 9.2, pp. 307–312.

Lettieri, Christopher J et al. (2006). "The distance-saturation product predicts mortality in idiopathic pulmonary fibrosis". In: *Respiratory medicine* 100.10, pp. 1734–1741.

Ley, Brett, Williamson Z Bradford, et al. (2015). "Unified baseline and longitudinal mortality prediction in idiopathic pulmonary fibrosis". In: *European Respiratory Journal* 45.5, pp. 1374–1381.

Ley, Brett, Harold R Collard, and Talmadge E King Jr (2011a). "Clinical course and prediction of survival in idiopathic pulmonary fibrosis". In: *American journal of respiratory and critical care medicine* 183.4, pp. 431–440.

– (2011b). "Clinical course and prediction of survival in idiopathic pulmonary fibrosis". In: *American journal of respiratory and critical care medicine* 183.4, pp. 431–440.

Ley, Brett, Christopher J Ryerson, et al. (2012). "A multidimensional index and staging system for idiopathic pulmonary fibrosis". In: *Annals of internal medicine* 156.10, pp. 684–691.

Li, Kai et al. (2020). "Circular RNA circGSK3B promotes cell proliferation, migration, and invasion by sponging miR-1265 and regulating CAB39 expression in hepatocellular carcinoma". In: *Frontiers in oncology* 10, p. 598256.

Li, Li et al. (2015). "Metformin attenuates gefitinib-induced exacerbation of pulmonary fibrosis by inhibition of TGF-β signaling pathway". In: *Oncotarget* 6.41, p. 43605.

Li, Mo and et al. (2011). "Epithelium-specific deletion of TGF-β receptor type II protects mice from bleomycin-induced pulmonary fibrosis". In: *The Journal of clinical investigation* 121, pp. 277–287.

Li, Nian-Shuang et al. (2016). "LKB1/AMPK inhibits TGF-β1 production and the TGF-β signaling pathway in breast cancer cells". In: *Tumor Biology* 37, pp. 8249–8258.

Li, Weilin et al. (2018). "CAB39L elicited an anti-Warburg effect via a LKB1-AMPK-PGC1α axis to inhibit gastric tumorigenesis". In: *Oncogene* 37.50, pp. 6383–6398.

Li, Xiangde and et al. (2003). "Bleomycin-induced apoptosis of alveolar epithelial cells requires angiotensin synthesis de novo". In: *American Journal of Physiology-Lung Cellular and Molecular Physiology* 284, pp. L501–L507.

– (2007). "Attenuation of bleomycin-induced pulmonary fibrosis by intratracheal administration of antisense oligonucleotides against angiotensinogen mRNA". In: *Current pharmaceutical design* 13, pp. 1257–1268.

Li, Xiaoming and et al. (2006). "Extravascular sources of lung angiotensin peptide synthesis in idiopathic pulmonary fibrosis". In: *American Journal of Physiology-Lung Cellular and Molecular Physiology* 291, pp. L887–L895.

Li, Xiaopeng et al. (2006). "Extravascular sources of lung angiotensin peptide synthesis in idiopathic pulmonary fibrosis". In: *American Journal of Physiology-Lung Cellular and Molecular Physiology* 291.5, pp. L887–L895.

Liang, Jiurong et al. (2016). "Hyaluronan and TLR4 promote surfactant-protein-C-positive alveolar progenitor cell renewal and prevent severe pulmonary fibrosis in mice". In: *Nature medicine* 22.11, pp. 1285–1293.

Liebow, AACC (1969). "The interstitial pneumonias". In: *Frontiers of pulmonary radiology*, pp. 102–141.

Lieubeau, Blandine et al. (1994). "The role of transforming growth factor β1 in the fibroblastic reaction associated with rat colorectal tumor development". In: *Cancer research* 54.24, pp. 6526–6532.

Liu, Fei et al. (2010). "Feedback amplification of fibrosis through matrix stiffening and COX-2 suppression". In: *Journal of Cell Biology* 190.4, pp. 693–706.

Liu, Gang et al. (2019). "Fibulin-1c regulates transforming growth factor–β activation in pulmonary tissue fibrosis". In: *JCI insight* 4.16.

Liu, Hong et al. (2013). "Interleukin 17A inhibits autophagy through activation of PIK3CA to interrupt the GSK3B-mediated degradation of BCL2 in lung epithelial cells". In: *Autophagy* 9.5, pp. 730–742.

Liu, Junfeng et al. (2016). "Mesenchymal stem cell-conditioned media suppresses inflammation-associated overproliferation of pulmonary artery smooth muscle cells in a rat model of pulmonary hypertension". In: *Experimental and Therapeutic Medicine* 11.2, pp. 467–475.

Liu, Lidan et al. (2012). "Deregulated MYC expression induces dependence upon AMPK-related kinase 5". In: *Nature* 483.7391, pp. 608–612.

Liu, Rongrong et al. (2022). "From 2D to 3D co-culture systems: a review of co-culture models to study the neural cells interaction". In: *International Journal of Molecular Sciences* 23.21, p. 13116.

Liu, Yongqing et al. (2008). “Zeb1 links epithelial-mesenchymal transition and cellular senescence”. In: *The Company of Biologists*.

Liu, Yujing et al. (2008). “Zeb1 links epithelial-mesenchymal transition and cellular senescence”. In: *Development* 135, pp. 579–588.

Lizcano, JM et al. (2004). “LKB1 is a master kinase that activates 13 kinases of the AMPK subfamily, including MARK/PAR-1”. In: *The EMBO Journal* 23.4, pp. 833–843.

Lizcano, Jose M et al. (2004a). “LKB1 is a master kinase that activates 13 kinases of the AMPK subfamily, including MARK/PAR-1”. In: *The EMBO journal* 23.4, pp. 833–843.

– (2004b). “LKB1 is a master kinase that activates 13 kinases of the AMPK subfamily, including MARK/PAR-1”. In: *The EMBO journal* 23.4, pp. 833–843.

Lomas, Nicola J et al. (2012). “Idiopathic pulmonary fibrosis: immunohistochemical analysis provides fresh insights into lung tissue remodelling with implications for novel prognostic markers”. In: *International journal of clinical and experimental pathology* 5.1, p. 58.

López-Lluch, Guillermo et al. (2015). “Mitochondrial responsibility in ageing process: innocent, suspect or guilty”. In: *Biogerontology* 16, pp. 599–620.

López-Otın, Carlos et al. (2013). “The hallmarks of aging”. In: *Cell* 153.6, pp. 1194–1217.

Love, Michael I, Wolfgang Huber, and Simon Anders (2014a). “Moderated estimation of fold change and dispersion for RNA-seq data with DESeq2”. In: *Genome biology* 15.12, pp. 1–21.

– (2014b). “Moderated estimation of fold change and dispersion for RNA-seq data with DESeq2”. In: *Genome biology* 15.12, pp. 1–21.

Lowery, Erin M et al. (2013). “The aging lung”. In: *Clinical interventions in aging*, pp. 1489–1496.

MacDonald, Bryan T, Keiko Tamai, and Xi He (2009). “Wnt/β-catenin signaling: components, mechanisms, and diseases”. In: *Developmental cell* 17.1, pp. 9–26.

MacDonald, Kelli et al. (2005). “Cytokine expanded myeloid precursors function as regulatory antigen-presenting cells and promote tolerance through IL-10-producing regulatory T cells”. In: *The Journal of Immunology* 174.4, pp. 1841–1850.

Maher, Toby M, Ellen M van der Aar, et al. (2018). “Safety, tolerability, pharmacokinetics, and pharmacodynamics of GLPG1690, a novel autotaxin inhibitor, to treat idiopathic pulmonary fibrosis (FLORA): a phase 2a randomised placebo-controlled trial”. In: *The Lancet Respiratory Medicine* 6.8, pp. 627–635.

Maher, Toby M, Iona C Evans, et al. (2010). “Diminished prostaglandin E2 contributes to the apoptosis paradox in idiopathic pulmonary fibrosis”. In: *American journal of respiratory and critical care medicine* 182.1, pp. 73–82.

Maher, Toby M. and et al. (2010). “Diminished prostaglandin E2 contributes to the apoptosis paradox in idiopathic pulmonary fibrosis”. In: *American journal of respiratory and critical care medicine* 182, pp. 73–82.

Majno, G et al. (1971). "Contraction of granulation tissue in vitro: similarity to smooth muscle". In: *Science* 173.3996, pp. 548–550.

Marignani, Paola A, Fumihiko Kanai, and Christopher L Carpenter (2001). "LKB1 associates with Brg1 and is necessary for Brg1-induced growth arrest". In: *Journal of Biological Chemistry* 276.35, pp. 32415–32418.

Marinković, Aleksandar et al. (2012). "Improved throughput traction microscopy reveals pivotal role for matrix stiffness in fibroblast contractility and TGF-β responsiveness". In: *American Journal of Physiology-Lung Cellular and Molecular Physiology* 303.3, pp. L169–L180.

Martinet, Wim et al. (2006). "In situ detection of starvation-induced autophagy". In: *Journal of Histochemistry & Cytochemistry* 54.1, pp. 85–96.

Martinez, Fernando J et al. (2017a). "Idiopathic pulmonary fibrosis". In: *Nature reviews Disease primers* 3.1, pp. 1–19.

– (2017b). "Idiopathic pulmonary fibrosis". In: *Nature reviews Disease primers* 3.1, pp. 1–19.

Matsumura, Takuma et al. (2018). "The effects of pirfenidone in patients with an acute exacerbation of interstitial pneumonia". In: *The Clinical Respiratory Journal* 12.4, pp. 1550–1558.

Meley, Daniel et al. (2006). "AMP-activated protein kinase and the regulation of autophagic proteolysis". In: *Journal of biological chemistry* 281.46, pp. 34870–34879.

Mendoza-Milla, Criselda et al. (2013). "Dehydroepiandrosterone has strong antifibrotic effects and is decreased in idiopathic pulmonary fibrosis". In: *European Respiratory Journal* 42.5, pp. 1309–1321.

Mi, Su et al. (2011). "Blocking IL-17A promotes the resolution of pulmonary inflammation and fibrosis via TGF-β1–dependent and–independent mechanisms". In: *The Journal of Immunology* 187.6, pp. 3003–3014.

Mih, Justin D et al. (2012). "Matrix stiffness reverses the effect of actomyosin tension on cell proliferation". In: *Journal of cell science* 125.24, pp. 5974–5983.

Mihaylova, Maria M and Reuben J Shaw (2011a). "The AMPK signalling pathway coordinates cell growth, autophagy and metabolism". In: *Nature cell biology* 13.9, pp. 1016–1023.

– (2011b). "The AMPK signalling pathway coordinates cell growth, autophagy and metabolism". In: *Nature cell biology* 13.9, pp. 1016–1023.

– (2011c). "The AMPK signalling pathway coordinates cell growth, autophagy and metabolism". In: *Nature cell biology* 13.9, pp. 1016–1023.

Mihaylova, MM and RJ Shaw (2011). "The AMPK signalling pathway coordinates cell growth, autophagy and metabolism". In: *Nature Cell Biology* 13.9, pp. 1016–1023.

Milara, Javier et al. (2018). "JAK2 mediates lung fibrosis, pulmonary vascular remodelling and hypertension in idiopathic pulmonary fibrosis: an experimental study". In: *Thorax* 73.6, pp. 519–529.

Millan-Billi, Paloma et al. (2018). "Comorbidities, Complications and Non-Pharmacologic Treatment in Idiopathic Pulmonary Fibrosis". In: *Medical Sciences* 6.3. ISSN: 2076-3271. DOI: 10.3390/medsci6030059. URL: https://www.mdpi.com/2076-3271/6/3/59.

Minagawa, Shunsuke et al. (2011). "Accelerated epithelial cell senescence in IPF and the inhibitory role of SIRT6 in TGF-β-induced senescence of human bronchial epithelial cells". In: *American Journal of Physiology-Lung Cellular and Molecular Physiology* 300.3, pp. L391–L401.

Miyake, Yoshihiro et al. (2005). "Occupational and environmental factors and idiopathic pulmonary fibrosis in Japan". In: *Annals of occupational hygiene* 49.3, pp. 259–265.

Mizushima, Noboru (2007). "Autophagy: process and function". In: *Genes & development* 21.22, pp. 2861–2873.

Mizushima, Noboru and Masaaki Komatsu (2011). "Autophagy: renovation of cells and tissues". In: *Cell* 147.4, pp. 728–741.

Molyneaux, Phillip L et al. (2014). "The role of bacteria in the pathogenesis and progression of idiopathic pulmonary fibrosis". In: *American journal of respiratory and critical care medicine* 190.8, pp. 906–913.

Momcilovic, M and DB Shackelford (2015a). "Targeting LKB1 in cancer – exposing and exploiting vulnerabilities". In: *Br J Cancer* 113.4, pp. 574–584.

– (2015b). "Targeting LKB1 in cancer–exposing and exploiting vulnerabilities". In: *British journal of cancer* 113.4, pp. 574–584.

Morishima, Yoh and et al. (2001). "Triggering the induction of myofibroblast and fibrogenesis by airway epithelial shedding". In: *American journal of respiratory cell and molecular biology* 24, pp. 1–11.

Morishima, Yuko et al. (2001). "Triggering the induction of myofibroblast and fibrogenesis by airway epithelial shedding". In: *American journal of respiratory cell and molecular biology* 24.1, pp. 1–11.

Moscat, Jorge and Maria T Diaz-Meco (2012). "p62: a versatile multitasker takes on cancer". In: *Trends in biochemical sciences* 37.6, pp. 230–236.

Moss, Benjamin J, Stefan W Ryter, and Ivan O Rosas (2022). "Pathogenic mechanisms underlying idiopathic pulmonary fibrosis". In: *Annual Review of Pathology: Mechanisms of Disease* 17, pp. 515–546.

Moustakas, Aristidis and Carl-Henrik Heldin (2009). "The regulation of TGFβ signal transduction". In: *Development* 136.22, pp. 3699–3714.

Mulero, Maria Carmen et al. (2019). "Genome reading by the NF-κB transcription factors". In: *Nucleic acids research* 47.19, pp. 9967–9989.

Munger, John S et al. (1999). "The integrin alpha v beta 6 binds and activates latent TGF beta 1: a mechanism for regulating pulmonary inflammation and fibrosis." In: *Cell* 96.3, pp. 319–328.

Muñoz-Espın, Daniel and Manuel Serrano (2014). "Cellular senescence: from physiology to pathology". In: *Nature reviews Molecular cell biology* 15.7, pp. 482–496.

Muro, Andrés F et al. (2008). "An essential role for fibronectin extra type III domain A in pulmonary fibrosis". In: *American journal of respiratory and critical care medicine* 177.6, pp. 638–645.

Mutlu, Gökhan M et al. (2012). "Proteasomal inhibition after injury prevents fibrosis by modulating TGF-β1 signalling". In: *Thorax* 67.2, pp. 139–146.

Naik, Payal K et al. (2012). "Periostin promotes fibrosis and predicts progression in patients with idiopathic pulmonary fibrosis". In: *American Journal of Physiology-Lung Cellular and Molecular Physiology* 303.12, pp. L1046–L1056.

Naikawadi, Ram P et al. (2016). "Telomere dysfunction in alveolar epithelial cells causes lung remodeling and fibrosis". In: *JCI insight* 1.14.

Nakaya, Michio et al. (2017). "Cardiac myofibroblast engulfment of dead cells facilitates recovery after myocardial infarction". In: *The Journal of clinical investigation* 127.1, pp. 383–401.

Nathan, Steven D et al. (2011). "Long-term course and prognosis of idiopathic pulmonary fibrosis in the new millennium". In: *Chest* 140.1, pp. 221–229.

Natsuizaka, Motoki et al. (2014). "Epidemiologic survey of Japanese patients with idiopathic pulmonary fibrosis and investigation of ethnic differences". In: *American journal of respiratory and critical care medicine* 190.7, pp. 773–779.

Navaratnam, V et al. (2011). "The rising incidence of idiopathic pulmonary fibrosis in the UK". In: *Thorax* 66.6, pp. 462–467.

Negreros, Miguel et al. (2019). "Transforming growth factor beta 1 induces methylation changes in lung fibroblasts". In: *PloS one* 14.10, e0223512.

Newman, AM et al. (2019). "Determining cell type abundance and expression from bulk tissues with digital cytometry". In: *Nature Biotechnology* 37.7, pp. 773–782.

Newton, Chad A et al. (2019). "Telomere length and use of immunosuppressive medications in idiopathic pulmonary fibrosis". In: *American journal of respiratory and critical care medicine* 200.3, pp. 336–347.

Nho, Richard Seonghun and Polla Hergert (2014). "IPF fibroblasts are desensitized to type I collagen matrix-induced cell death by suppressing low autophagy via aberrant Akt/mTOR kinases". In: *PloS one* 9.4, e94616.

Nishimura, Stephen L (2009). "Integrin-mediated transforming growth factor-β activation, a potential therapeutic target in fibrogenic disorders". In: *The American journal of pathology* 175.4, pp. 1362–1370.

Noble, Paul W et al. (2011). "Pirfenidone in patients with idiopathic pulmonary fibrosis (CAPACITY): two randomised trials". In: *The Lancet* 377.9779, pp. 1760–1769.

Noel, Gaelle et al. (2017). "A primary human macrophage-enteroid co-culture model to investigate mucosal gut physiology and host-pathogen interactions". In: *Scientific reports* 7.1, p. 45270.

Nony, Pascale et al. (2003). "Stability of the Peutz–Jeghers syndrome kinase LKB1 requires its binding to the molecular chaperones Hsp90/Cdc37". In: *Oncogene* 22.57, pp. 9165–9175.

Noth, Imre et al. (2013a). "Genetic variants associated with idiopathic pulmonary fibrosis susceptibility and mortality: a genome-wide association study". In: *The Lancet respiratory medicine* 1.4, pp. 309–317.

– (2013b). "Genetic variants associated with idiopathic pulmonary fibrosis susceptibility and mortality: a genome-wide association study". In: *The Lancet respiratory medicine* 1.4, pp. 309–317.

O'Dwyer, David N et al. (2013). "The Toll-like receptor 3 L412F polymorphism and disease progression in idiopathic pulmonary fibrosis". In: *American journal of respiratory and critical care medicine* 188.12, pp. 1442–1450.

Oakhill, Jonathan S et al. (2011). "AMPK is a direct adenylate charge-regulated protein kinase". In: *Science* 332.6036, pp. 1433–1435.

Okamoto, Atsuko et al. (2017). "Atrial natriuretic peptide protects against bleomycin-induced pulmonary fibrosis via vascular endothelial cells in mice". In: *Respiratory Research* 18.1, pp. 1–10.

Oldham, Justin M et al. (2015). "Thyroid disease is prevalent and predicts survival in patients with idiopathic pulmonary fibrosis". In: *Chest* 148.3, pp. 692–700.

Organ, Louise A et al. (2019). "Biomarkers of collagen synthesis predict progression in the PROFILE idiopathic pulmonary fibrosis cohort". In: *Respiratory research* 20, pp. 1–10.

Ossipova, Olga et al. (2003). "LKB1 (XEEK1) regulates Wnt signalling in vertebrate development". In: *Nature cell biology* 5.10, pp. 889–894.

Pakshir, Pardis and Boris Hinz (2018). "The big five in fibrosis: Macrophages, myofibroblasts, matrix, mechanics, and miscommunication". In: *Matrix Biology* 68, pp. 81–93.

Pakshir, Pardis, Nina Noskovicova, et al. (2020). "The myofibroblast at a glance". In: *Journal of Cell Science* 133.13, jcs227900.

Palmer, Scott M et al. (2018). "Randomized, double-blind, placebo-controlled, phase 2 trial of BMS-986020, a lysophosphatidic acid receptor antagonist for the treatment of idiopathic pulmonary fibrosis". In: *Chest* 154.5, pp. 1061–1069.

Pan, L. and et al. (2001). "Type II alveolar epithelial cells and interstitial fibroblasts express connective tissue growth factor in IPF". In: *European Respiratory Journal* 17, pp. 1220–1227.

Pan, LH et al. (2001). "Type II alveolar epithelial cells and interstitial fibroblasts express connective tissue growth factor in IPF". In: *European Respiratory Journal* 17.6, pp. 1220–1227.

Paolocci, Giulia et al. (2018). "Occupational risk factors for idiopathic pulmonary fibrosis in Southern Europe: a case-control study". In: *BMC pulmonary medicine* 18.1, pp. 1–6.

Papiris, Spyros A et al. (2015). "Survival in idiopathic pulmonary fibrosis acute exacerbations: the non-steroid approach". In: *BMC pulmonary medicine* 15.1, pp. 1–9.

Pardo, Annie and et al. (2005). "Up-regulation and profibrotic role of osteopontin in human idiopathic pulmonary fibrosis". In: *PLoS Med* 2, e251.

Pardo, Annie, Kevin Gibson, et al. (2005). "Up-regulation and profibrotic role of osteopontin in human idiopathic pulmonary fibrosis". In: *PLoS medicine* 2.9, e251.

Pardo, Annie and Moisés Selman (2002). "Molecular mechanisms of pulmonary fibrosis". In: *Frontiers in Bioscience-Landmark* 7.4, pp. 1743–1761.

– (2006). "Matrix metalloproteases in aberrant fibrotic tissue remodeling". In: *Proceedings of the American Thoracic Society* 3, pp. 383–388.

Park, Jong Sun et al. (2014). "Clinical significance of mTOR, ZEB1, ROCK1 expression in lung tissues of pulmonary fibrosis patients". In: *BMC pulmonary medicine* 14, pp. 1–9.

Parker, Matthew W et al. (2014). "Fibrotic extracellular matrix activates a profibrotic positive feedback loop". In: *The Journal of clinical investigation* 124.4.

Paschos, Nikolaos K et al. (2015). "Advances in tissue engineering through stem cell-based co-culture". In: *Journal of tissue engineering and regenerative medicine* 9.5, pp. 488–503.

Patel, AS et al. (2012). "Autophagy in idiopathic pulmonary fibrosis". In: *PloS one* 7.7, e41394.

Patel, Avignat S, Ling Lin, et al. (2012). "Autophagy in idiopathic pulmonary fibrosis". In: *PloS one* 7.7, e41394.

Patel, Avignat S, Danielle Morse, and Augustine MK Choi (2013). "Regulation and functional significance of autophagy in respiratory cell biology and disease". In: *American journal of respiratory cell and molecular biology* 48.1, pp. 1–9.

Pierce, Eric M. and et al. (2007). "Idiopathic pulmonary fibrosis fibroblasts migrate and proliferate to CC chemokine ligand 21". In: *European Respiratory Journal* 29, pp. 1082–1093.

Piguet, PF et al. (1993). "Expression and localization of tumor necrosis factor-alpha and its mRNA in idiopathic pulmonary fibrosis." In: *The American journal of pathology* 143.3, p. 651.

Piguet, Pierre et al. (1993). "Expression and localization of tumor necrosis factor-alpha and its mRNA in idiopathic pulmonary fibrosis". In: *The American journal of pathology* 143, p. 651.

Plataki, Maria et al. (2005). "Expression of apoptotic and antiapoptotic markers in epithelial cells in idiopathic pulmonary fibrosis". In: *Chest* 127.1, pp. 266–274.

Powis, Garth and Lynn Kirkpatrick (2004). "Hypoxia inducible factor-1α as a cancer drug target". In: *Molecular cancer therapeutics* 3.5, pp. 647–654.

Pozharskaya, Veronika et al. (2009). "Twist: a regulator of epithelial-mesenchymal transition in lung fibrosis". In: *PloS one* 4.10, e7559.

Proetzel, Gabriele et al. (1995). "Transforming growth factor–β3 is required for secondary palate fusion". In: *Nature genetics* 11.4, pp. 409–414.

Prunotto, Marco and et al. (2012). "Epithelial–mesenchymal crosstalk alteration in kidney fibrosis". In: *The Journal of pathology* 228, pp. 131–147.

Prunotto, Marco, David C Budd, et al. (2012). "Epithelial–mesenchymal crosstalk alteration in kidney fibrosis". In: *The Journal of pathology* 228.2, pp. 131–147.

Psathakis, K et al. (2006). "Exhaled markers of oxidative stress in idiopathic pulmonary fibrosis". In: *European journal of clinical investigation* 36.5, pp. 362–367.

Psathakis, K. and et al. (2006). "Exhaled markers of oxidative stress in idiopathic pulmonary fibrosis". In: *European journal of clinical investigation* 36, pp. 362–367.

Puddicombe, Sarah M. and et al. (2000). "Involvement of the epidermal growth factor receptor in epithelial repair in asthma". In: *The FASEB Journal* 14, pp. 1362–1374.

Putman, RK et al. (2016). "Evaluation of COPD Longitudinally to Identify Predictive Surrogate Endpoints (ECLIPSE) Investigators; COPDGene Investigators. Association between interstitial lung abnormalities and all-cause mortality". In: *JAMA* 315.7, pp. 672–81.

Qin, Xing et al. (2018). "Cancer-associated fibroblast-derived IL-6 promotes head and neck cancer progression via the osteopontin-NF-kappa B signaling pathway". In: *Theranostics* 8.4, p. 921.

Qunn, Lei et al. (2002). "Hyperplastic epithelial foci in honeycomb lesions in idiopathic pulmonary fibrosis". In: *Virchows Archiv* 441, pp. 271–278.

Rabinowitz, Joshua D and Eileen White (2010). "Autophagy and metabolism". In: *Science* 330.6009, pp. 1344–1348.

Raghu, Ganesh, Valeria C Amatto, et al. (2015). "Comorbidities in idiopathic pulmonary fibrosis patients: a systematic literature review". In: *European Respiratory Journal* 46.4, pp. 1113–1130.

Raghu, Ganesh, Shih-Yin Chen, et al. (2014). "Idiopathic pulmonary fibrosis in US Medicare beneficiaries aged 65 years and older: incidence, prevalence, and survival, 2001–11". In: *The lancet Respiratory medicine* 2.7, pp. 566–572.

Raghu, Ganesh, Harold R Collard, et al. (2011a). "An official ATS/ERS/JRS/ALAT statement: idiopathic pulmonary fibrosis: evidence-based guidelines for diagnosis and management". In: *American journal of respiratory and critical care medicine* 183.6, pp. 788–824.

– (2011b). "An official ATS/ERS/JRS/ALAT statement: idiopathic pulmonary fibrosis: evidence-based guidelines for diagnosis and management". In: *American journal of respiratory and critical care medicine* 183.6, pp. 788–824.

Raghu, Ganesh, Ellen Morrow, et al. (2016). "Laparoscopic anti-reflux surgery for idiopathic pulmonary fibrosis at a single centre". In: *European Respiratory Journal* 48.3, pp. 826–832.

Raghu, Ganesh, Derek Weycker, et al. (2006). "Incidence and prevalence of idiopathic pulmonary fibrosis". In: *American journal of respiratory and critical care medicine* 174.7, pp. 810–816.

Ramírez, Geny I. and et al. (2011). "Absence of Thy-1 results in TGF-β induced MMP-9 expression and confers a profibrotic phenotype to human lung fibroblasts". In: *Laboratory investigation* 91, pp. 1206–1218.

Ramos, C. and et al. (2001). "Fibroblasts from idiopathic pulmonary fibrosis and normal lungs differ in growth rate, apoptosis, and tissue inhibitor of metalloproteinases expression". In: *American journal of respiratory cell and molecular biology* 24, pp. 591–598.

Rangarajan, S et al. (2018). "Metformin reverses established lung fibrosis in a bleomycin model". In: *Nature medicine* 24.8, pp. 1121–1127.

Rangarajan, Sunad et al. (2018). "Metformin reverses established lung fibrosis in a bleomycin model". In: *Nature medicine* 24.8, pp. 1121–1127.

Richeldi, L, HR Collard, and MG Jones (2017). "Idiopathic pulmonary fibrosis". In: *The Lancet* 389.10082, pp. 1941–1952.

Richeldi, Luca, Harold R Collard, and Mark G Jones (2017). "Idiopathic pulmonary fibrosis". In: *The Lancet* 389.10082, pp. 1941–1952.

Richeldi, Luca, Roland M Du Bois, et al. (2014). "Efficacy and safety of nintedanib in idiopathic pulmonary fibrosis". In: *New England Journal of Medicine* 370.22, pp. 2071–2082.

Rochester, Carolyn L et al. (2015). "An official American Thoracic Society/European Respiratory Society policy statement: enhancing implementation, use, and delivery of pulmonary rehabilitation". In: *American journal of respiratory and critical care medicine* 192.11, pp. 1373–1386.

Rock, Jason R et al. (2011). "Multiple stromal populations contribute to pulmonary fibrosis without evidence for epithelial to mesenchymal transition". In: *Proceedings of the National Academy of Sciences* 108.52, E1475–E1483.

Rockey, Don C, P Darwin Bell, and Joseph A Hill (2015). "Fibrosis—a common pathway to organ injury and failure". In: *New England Journal of Medicine* 372.12, pp. 1138–1149.

Rohde, Volker et al. (2000). "Expression of the human telomerase reverse transcriptase is not related to telomerase activity in normal and malignant renal tissue". In: *Clinical cancer research* 6.12, pp. 4803–4809.

Roy, BC et al. (2010). "Involvement of LKB1 in epithelial–mesenchymal transition (EMT) of human lung cancer cells". In: *Lung Cancer* 70.2, pp. 136–145.

Rozencwajg, Sacha and Matthieu Schmidt (2016). "Extracorporeal membrane oxygenation for interstitial lung disease: what is on the other side of the bridge?" In: *Journal of Thoracic Disease* 8.8, p. 1918.

Rozin, GF et al. (2005). "Collagen and elastic system in the remodelling process of major types of idiopathic interstitial pneumonias (IIP)". In: *Histopathology* 46.4, pp. 413–421.

Ruifrok, Arnout C, Dennis A Johnston, et al. (2001). "Quantification of histochemical staining by color deconvolution". In: *Analytical and quantitative cytology and histology* 23.4, pp. 291–299.

Rusten, Tor Erik and Harald Stenmark (2010). "p62, an autophagy hero or culprit?" In: *Nature cell biology* 12.3, pp. 207–209.

Ruwanpura, Saleela M, Belinda J Thomas, and Philip G Bardin (2020). "Pirfenidone: molecular mechanisms and potential clinical applications in lung disease". In: *American journal of respiratory cell and molecular biology* 62.4, pp. 413–422.

Ryerson, Christopher and Brett Ley (2020). "Prognosis and monitoring of idiopathic pulmonary fibrosis". In: *UpToDate. Waltham*.

Sabry, Mostafa (2020). "TLR4/NF-KB signaling pathway is a key pathogenic event of lung injury in bleomycin-induced pulmonary fibrosis in a mouse model". In: *Al-Azhar Journal of Pharmaceutical Sciences* 61.1, pp. 92–103.

Sakai, Norihiko and Andrew M. Tager (2013). "Fibrosis of two: Epithelial cell-fibroblast interactions in pulmonary fibrosis". In: *Biochimica et Biophysica Acta (BBA)-Molecular Basis of Disease* 1832, pp. 911–921.

Sakamoto, Kei et al. (2006). "Deficiency of LKB1 in heart prevents ischemia-mediated activation of AMPKα2 but not AMPKα1". In: *American Journal of Physiology-Endocrinology and Metabolism* 290.5, E780–E788.

Saleh, Daniel and et al. (1997). "Elevated expression of endothelin-1 and endothelin-converting enzyme-1 in idiopathic pulmonary fibrosis: possible involvement of proinflammatory cytokines". In: *American journal of respiratory cell and molecular biology* 16, pp. 187–193.

Saleh, Dina et al. (1997). "Elevated expression of endothelin-1 and endothelin-converting enzyme-1 in idiopathic pulmonary fibrosis: possible involvement of proinflammatory cytokines." In: *American journal of respiratory cell and molecular biology* 16.2, pp. 187–193.

Sanchez-Cespedes, M (2007). "A role for LKB1 gene in human cancer beyond the Peutz–Jeghers syndrome". In: *Oncogene* 26.57, pp. 7825–7832.

Sanchez-Garrido, J and AR Shenoy (2021). "Regulation and repurposing of nutrient sensing and autophagy in innate immunity". In: *Autophagy* 17.7, pp. 1571–1591.

Sanford, L Philip et al. (1997). "TGFβ2 knockout mice have multiple developmental defects that are non-overlapping with other TGFβ knockout phenotypes". In: *Development* 124.13, pp. 2659–2670.

Santos, Alba and David Lagares (2018). "Matrix stiffness: the conductor of organ fibrosis". In: *Current Rheumatology Reports* 20, pp. 1–13.

Sapkota, G. P. et al. (2002). "Identification and Characterization of Four Novel Phosphorylation Sites (Ser31, Ser325, Thr336 and Thr366) on LKB1/STK11, the

Protein Kinase Mutated in Peutz-Jeghers Cancer Syndrome". In: *Biochemical Journal* 362, pp. 481–490. DOI: 10.1042/bj3620481.

Sato, Toshihiko et al. (2015). "Long-term results and predictors of survival after surgical resection of patients with lung cancer and interstitial lung diseases". In: *The Journal of thoracic and cardiovascular surgery* 149.1, pp. 64–70.

Sava, Parid et al. (2017). "Human pericytes adopt myofibroblast properties in the microenvironment of the IPF lung". In: *JCI insight* 2.24.

Schiller, Herbert B et al. (2015). "Time-and compartment-resolved proteome profiling of the extracellular niche in lung injury and repair". In: *Molecular systems biology* 11.7, p. 819.

Schuster, Ronen et al. (2021). "The inflammatory speech of fibroblasts". In: *Immunological reviews* 302.1, pp. 126–146.

Schwartz, David A (2016). "Idiopathic pulmonary fibrosis is a complex genetic disorder". In: *Transactions of the American Clinical and Climatological Association* 127, p. 34.

Scotton, Chris J et al. (2009). "Increased local expression of coagulation factor X contributes to the fibrotic response in human and murine lung injury". In: *The Journal of clinical investigation* 119.9, pp. 2550–2563.

Seibold, Max A et al. (2011). "A common MUC5B promoter polymorphism and pulmonary fibrosis". In: *New England Journal of Medicine* 364.16, pp. 1503–1512.

Selman, Moises et al. (2004). "Idiopathic pulmonary fibrosis: pathogenesis and therapeutic approaches". In: *Drugs* 64, pp. 405–430.

Selman, Moisés and et al. (2004). "Idiopathic pulmonary fibrosis". In: *Drugs* 64, pp. 405–430.

Selman, Moisés, Ivette Buendıa-Roldán, and Annie Pardo (2016). "Aging and pulmonary fibrosis". In: *Revista de Investigación Clınica* 68.2, pp. 75–83.

Selman, Moisés, Carlos López-Otın, and Annie Pardo (2016). "Age-driven developmental drift in the pathogenesis of idiopathic pulmonary fibrosis". In: *European Respiratory Journal* 48.2, pp. 538–552.

Selman, Moisés and Annie Pardo (2014). "Revealing the pathogenic and aging-related mechanisms of the enigmatic idiopathic pulmonary fibrosis. an integral model". In: *American journal of respiratory and critical care medicine* 189.10, pp. 1161–1172.

– (2020). "The leading role of epithelial cells in the pathogenesis of idiopathic pulmonary fibrosis". In: *Cellular signalling* 66, p. 109482.

Selman, Moisés, Annie Pardo, and Naftali Kaminski (2008). "Idiopathic pulmonary fibrosis: aberrant recapitulation of developmental programs?" In: *PLoS Med* 5, e62.

Semren, Nora et al. (2015). "Regulation of 26S proteasome activity in pulmonary fibrosis". In: *American journal of respiratory and critical care medicine* 192.9, pp. 1089–1101.

Serasanambati, Mamatha and Shanmuga Reddy Chilakapati (2016). "Function of nuclear factor kappa B (NF-kB) in human diseases-a review". In: *South Indian Journal of Biological Sciences* 2.4, pp. 368–87.

Seto, Yoshiki et al. (2013). "Photosafety assessments on pirfenidone: photochemical, photobiological, and pharmacokinetic characterization". In: *Journal of Photochemistry and Photobiology B: Biology* 120, pp. 44–51.

Sgalla, Giacomo et al. (2020). "Pamrevlumab for the treatment of idiopathic pulmonary fibrosis". In: *Expert Opinion on Investigational Drugs* 29.8, pp. 771–777.

Shackelford, David B, Evan Abt, et al. (2013). "LKB1 inactivation dictates therapeutic response of non-small cell lung cancer to the metabolism drug phenformin". In: *Cancer cell* 23.2, pp. 143–158.

Shackelford, David B and Reuben J Shaw (2009). "The LKB1–AMPK pathway: metabolism and growth control in tumour suppression". In: *Nature Reviews Cancer* 9.8, pp. 563–575.

Shamskhou, Elya A et al. (2019). "Hydrogel-based delivery of Il-10 improves treatment of bleomycin-induced lung fibrosis in mice". In: *Biomaterials* 203, pp. 52–62.

Shaw, Reuben J (2009). "LKB1 and AMP-activated protein kinase control of mTOR signalling and growth". In: *Acta physiologica* 196.1, pp. 65–80.

Shaw, Reuben J, Nabeel Bardeesy, et al. (2004). "The LKB1 tumor suppressor negatively regulates mTOR signaling". In: *Cancer cell* 6.1, pp. 91–99.

Shaw, Reuben J, Monica Kosmatka, et al. (2004). "The tumor suppressor LKB1 kinase directly activates AMP-activated kinase and regulates apoptosis in response to energy stress". In: *Proceedings of the National Academy of Sciences* 101.10, pp. 3329–3335.

Shaw, Tanya J and Paul Martin (2016). "Wound repair: a showcase for cell plasticity and migration". In: *Current opinion in cell biology* 42, pp. 29–37.

Shaw, Tanya J and Emanuel Rognoni (2020). "Dissecting fibroblast heterogeneity in health and fibrotic disease". In: *Current rheumatology reports* 22, pp. 1–10.

Shaykhiev, Renat et al. (2013). "EGF shifts human airway basal cell fate toward a smoking-associated airway epithelial phenotype". In: *Proceedings of the National Academy of Sciences* 110.29, pp. 12102–12107.

Sheppard, Dean (2006a). "Transforming growth factor β: a central modulator of pulmonary and airway inflammation and fibrosis". In: *Proceedings of the American Thoracic Society* 3.5, pp. 413–417.

– (2006b). "Transforming growth factor β: a central modulator of pulmonary and airway inflammation and fibrosis". In: *Proceedings of the American Thoracic Society* 3, pp. 413–417.

Shulgina, Ludmila et al. (2013). "Treating idiopathic pulmonary fibrosis with the addition of co-trimoxazole: a randomised controlled trial". In: *Thorax* 68.2, pp. 155–162.

Shull, Marcia M et al. (1992). "Targeted disruption of the mouse transforming growth factor-β1 gene results in multifocal inflammatory disease". In: *Nature* 359.6397, pp. 693–699.

Sime, Patricia J et al. (1997). "Adenovector-mediated gene transfer of active transforming growth factor-beta1 induces prolonged severe fibrosis in rat lung." In: *The Journal of clinical investigation* 100.4, pp. 768–776.

Skalli, Omar et al. (1986). "A monoclonal antibody against alpha-smooth muscle actin: a new probe for smooth muscle differentiation." In: *The Journal of cell biology* 103.6, pp. 2787–2796.

Society, American Thoracic et al. (2000). "Idiopathic pulmonary fibrosis: diagnosis and treatment: international consensus statement". In: *Am J Respir Crit Care Med* 161, pp. 646–664.

Solovyan, Vladislav T. and Juhani Keski-Oja (2006). "Proteolytic activation of latent TGF-β precedes caspase-3 activation and enhances apoptotic death of lung epithelial cells". In: *Journal of cellular physiology* 207, pp. 445–453.

Somogyi, Vivien et al. (2019). "The therapy of idiopathic pulmonary fibrosis: what is next?" In: *European Respiratory Review* 28.153.

Sosulski, Meredith L et al. (2015). "Deregulation of selective autophagy during aging and pulmonary fibrosis: the role of TGF β1". In: *Aging cell* 14.5, pp. 774–783.

Spagnolo, P et al. (2018). "Metformin Does Not Affect Clinically Relevant Outcomes in Patients with Idiopathic Pulmonary Fibrosis". In: *Respiration* 96.4, pp. 314–322.

Stankovic, Sanja, Mihailo Stjepanovic, and Milika Asanin (2021). "Biomarkers in Idiopathic Pulmonary Fibrosis". In: *Idiopathic Pulmonary Fibrosis*. IntechOpen.

Stanley, Susan E and Mary Armanios (2015). "The short and long telomere syndromes: paired paradigms for molecular medicine". In: *Current opinion in genetics & development* 33, pp. 1–9.

Steen, Chloé B et al. (2020). "Profiling cell type abundance and expression in bulk tissues with CIBERSORTx". In: *Stem Cell Transcriptional Networks: Methods and Protocols*, pp. 135–157.

Strieter, Robert M (2008). "What differentiates normal lung repair and fibrosis? Inflammation, resolution of repair, and fibrosis". In: *Proceedings of the American Thoracic Society* 5.3, pp. 305–310.

Strnad, P et al. (2008). "Mallory–Denk-bodies: Lessons from keratin-containing hepatic inclusion bodies". In: *Biochimica et Biophysica Acta (BBA)-Molecular Basis of Disease* 1782.12, pp. 764–774.

Strongman, Helen, Imran Kausar, and Toby M Maher (2018). "Incidence, prevalence, and survival of patients with idiopathic pulmonary fibrosis in the UK". In: *Advances in therapy* 35, pp. 724–736.

Stuart, Bridget D et al. (2015). "Exome sequencing links mutations in PARN and RTEL1 with familial pulmonary fibrosis and telomere shortening". In: *Nature genetics* 47.5, pp. 512–517.

Subramanian, Aravind et al. (2005). “Gene set enrichment analysis: a knowledge-based approach for interpreting genome-wide expression profiles”. In: *Proceedings of the National Academy of Sciences* 102.43, pp. 15545–15550.

Suganuma, Hiroyuki and et al. (1995). “Enhanced migration of fibroblasts derived from lungs with fibrotic lesions”. In: *Thorax* 50, pp. 984–989.

Sundaram, Kumaran et al. (2011). “Mutant p62P392L stimulation of osteoclast differentiation in Paget’s disease of bone”. In: *Endocrinology* 152.11, pp. 4180–4189.

Suter, Marianne et al. (2006). “Dissecting the role of 5≠AMP for allosteric stimulation, activation, and deactivation of AMP-activated protein kinase”. In: *Journal of Biological Chemistry* 281.43, pp. 32207–32216.

Suzuki, Atsushi and Yasuhiro Kondoh (2017). “The clinical impact of major comorbidities on idiopathic pulmonary fibrosis”. In: *Respiratory Investigation* 55.2, pp. 94–103.

Tai, Yifan et al. (2021). “Myofibroblasts: function, formation, and scope of molecular therapies for skin fibrosis”. In: *Biomolecules* 11.8, p. 1095.

Takeda, Shintaro et al. (2007). “LKB1 is crucial for TRAIL-mediated apoptosis induction in osteosarcoma”. In: *Anticancer research* 27.2, pp. 761–768.

Takezaki, Akio et al. (2019). “A homozygous SFTPA1 mutation drives necroptosis of type II alveolar epithelial cells in patients with idiopathic pulmonary fibrosis”. In: *Journal of Experimental Medicine* 216.12, pp. 2724–2735.

Taliaferro-Smith, L et al. (2009). “LKB1 is required for adiponectin-mediated modulation of AMPK–S6K axis and inhibition of migration and invasion of breast cancer cells”. In: *Oncogene* 28.29, pp. 2621–2633.

Tang, Haiying et al. (2016). “Salidroside protects against bleomycin-induced pulmonary fibrosis: activation of Nrf2-antioxidant signaling, and inhibition of NF-κB and TGF-β1/Smad-2/-3 pathways”. In: *Cell Stress and Chaperones* 21, pp. 239–249.

Tanida, Isei, Takashi Ueno, and Eiki Kominami (2008). “LC3 and Autophagy”. In: *Autophagosome and phagosome*, pp. 77–88.

Tanjore, Harikrishna, Dong-Sheng Cheng, et al. (2011). “Alveolar epithelial cells undergo epithelial-to-mesenchymal transition in response to endoplasmic reticulum stress”. In: *Journal of biological chemistry* 286.35, pp. 30972–30980.

Tanjore, Harikrishna, Xiaochuan C Xu, et al. (2009). “Contribution of epithelial-derived fibroblasts to bleomycin-induced lung fibrosis”. In: *American journal of respiratory and critical care medicine* 180.7, pp. 657–665.

Teague, TT et al. (2022). “Evaluation for clinical benefit of metformin in patients with idiopathic pulmonary fibrosis and type 2 diabetes mellitus: a national claims-based cohort analysis”. In: *Respiratory Research* 23.1, p. 91.

Thannickal, Victor J. and Barry L. Fanburg (2000). “Reactive oxygen species in cell signaling”. In: *American Journal of Physiology-Lung Cellular and Molecular Physiology* 279, pp. L1005–L1028.

Thannickal, Victor J. and Jeffrey C. Horowitz (2006). "Evolving concepts of apoptosis in idiopathic pulmonary fibrosis". In: *Proceedings of the American Thoracic Society* 3, pp. 350–356.

Thiery, Jean Paul et al. (2009). "Epithelial-mesenchymal transitions in development and disease". In: *cell* 139.5, pp. 871–890.

Thomas, Alan Q et al. (2002). "Heterozygosity for a surfactant protein C gene mutation associated with usual interstitial pneumonitis and cellular nonspecific interstitial pneumonitis in one kindred". In: *American journal of respiratory and critical care medicine* 165.9, pp. 1322–1328.

Thomas, George V et al. (2006). "Hypoxia-inducible factor determines sensitivity to inhibitors of mTOR in kidney cancer". In: *Nature medicine* 12.1, pp. 122–127.

Thong, Lorraine, Enda James McElduff, and Michael Thomas Henry (2023). "Trials and treatments: an update on pharmacotherapy for idiopathic pulmonary fibrosis". In: *Life* 13.2, p. 486.

Tiainen, Marianne, Kari Vaahtomeri, et al. (2002). "Growth arrest by the LKB1 tumor suppressor: induction of p21WAF1/CIP1". In: *Human molecular genetics* 11.13, pp. 1497–1504.

Tiainen, Marianne, Antti Ylikorkala, and Tomi P Mäkelä (1999). "Growth suppression by Lkb1 is mediated by a G1 cell cycle arrest". In: *Proceedings of the National Academy of Sciences* 96.16, pp. 9248–9251.

Tian, Sheng-Lan et al. (2018). "Emodin attenuates bleomycin-induced pulmonary fibrosis via anti-inflammatory and anti-oxidative activities in rats". In: *Medical Science Monitor: International Medical Journal of Experimental and Clinical Research* 24, p. 1.

Tilborghs, Sam et al. (2017). "The role of nuclear factor-kappa B signaling in human cervical cancer". In: *Critical reviews in oncology/hematology* 120, pp. 141–150.

Tomasek, James J et al. (2002). "Myofibroblasts and mechano-regulation of connective tissue remodelling". In: *Nature reviews Molecular cell biology* 3.5, pp. 349–363.

Travis, William D et al. (2002). "American Thoracic Society/European Respiratory Society international multidisciplinary consensus classification of the idiopathic interstitial pneumonias". In: *American journal of respiratory and critical care medicine* 165.2, pp. 277–304.

Trethewey, Samuel P and Gareth I Walters (2018). "The role of occupational and environmental exposures in the pathogenesis of idiopathic pulmonary fibrosis: a narrative literature review". In: *Medicina* 54.6, p. 108.

Trudzinski, Franziska C et al. (2016). "Outcome of patients with interstitial lung disease treated with extracorporeal membrane oxygenation for acute respiratory failure". In: *American journal of respiratory and critical care medicine* 193.5, pp. 527–533.

Turner-Warwick, M, B Burrows, and AJ Johnson (1980). "Cryptogenic fibrosing alveolitis: response to corticosteroid treatment and its effect on survival". In: *Thorax* 35.8, pp. 593–599.

Uchida, Masaru et al. (2012). “Periostin, a matricellular protein, plays a role in the induction of chemokines in pulmonary fibrosis”. In: *American journal of respiratory cell and molecular biology* 46.5, pp. 677–686.

Uh, Soo-Taek et al. (1998). “Morphometric analysis of insulin-like growth factor-I localization in lung tissues of patients with idiopathic pulmonary fibrosis”. In: *American Journal of Respiratory and Critical Care Medicine* 158.5, pp. 1626–1635.

Uhal, Bruce D. and et al. (1995). “Fibroblasts isolated after fibrotic lung injury induce apoptosis of alveolar epithelial cells in vitro”. In: *American Journal of Physiology-Lung Cellular and Molecular Physiology* 269, pp. L819–L828.

Umemura, Atsushi et al. (2016). “p62, upregulated during preneoplasia, induces hepatocellular carcinogenesis by maintaining survival of stressed HCC-initiating cells”. In: *Cancer cell* 29.6, pp. 935–948.

Vallance, Bruce A et al. (2005). “TGF-β1 gene transfer to the mouse colon leads to intestinal fibrosis”. In: *American Journal of Physiology-Gastrointestinal and Liver Physiology* 289.1, G116–G128.

Vancheri, C et al. (2010). “Idiopathic pulmonary fibrosis: a disease with similarities and links to cancer biology”. In: *European Respiratory Journal* 35.3, pp. 496–504.

Vancheri, Carlo et al. (2018). “Nintedanib with add-on pirfenidone in idiopathic pulmonary fibrosis. Results of the INJOURNEY trial”. In: *American journal of respiratory and critical care medicine* 197.3, pp. 356–363.

Velagacherla, Varalakshmi et al. (2022). “Molecular pathways and role of epigenetics in the idiopathic pulmonary fibrosis”. In: *Life Sciences*, p. 120283.

Veleva-Rotse, Biliana O et al. (2014). “STRAD pseudokinases regulate axogenesis and LKB1 stability”. In: *Neural Development* 9.1, pp. 1–13.

Vianello, Andrea (2014). “Noninvasive ventilation in patients with idiopathic pulmonary fibrosis is not a futile intervention!” In: *Journal of Critical Care* 29.6, p. 1129.

Vierhout, Megan et al. (2021). “Monocyte and macrophage derived myofibroblasts: Is it fate? A review of the current evidence”. In: *Wound Repair and Regeneration* 29.4, pp. 548–562.

Volmer, Martin W et al. (2005). “Differential proteome analysis of conditioned media to detect Smad4 regulated secreted biomarkers in colon cancer”. In: *Proteomics* 5.10, pp. 2587–2601.

Waghray, Meghna and et al. (2005). “Hydrogen peroxide is a diffusible paracrine signal for the induction of epithelial cell death by activated myofibroblasts”. In: *The FASEB journal* 19, pp. 1–16.

Wagner, Tracy M, James E Mullally, and FA Fitzpatrick (2006). “Reactive lipid species from cyclooxygenase-2 inactivate tumor suppressor LKB1/STK11: cyclopentenone prostaglandins and 4-hydroxy-2-nonenal covalently modify and inhibit the AMP-kinase kinase that modulates cellular energy homeostasis and protein translation”. In: *Journal of Biological Chemistry* 281.5, pp. 2598–2604.

Walters, Matthew S et al. (2014). "Smoking accelerates aging of the small airway epithelium". In: *Respiratory research* 15.1, pp. 1–13.

Wang, Angela et al. (1996). "Differential regulation of airway epithelial integrins by growth factors." In: *American journal of respiratory cell and molecular biology* 15.5, pp. 664–672.

Wang, Hong-Miao et al. (2020). "HPV16 E6/E7 promote the translocation and glucose uptake of GLUT1 by PI3K/AKT pathway via relieving miR-451 inhibitory effect on CAB39 in lung cancer cells". In: *Therapeutic Advances in Chronic Disease* 11, p. 2040622320957143.

Wang, Rui and et al. (1999). "Human lung myofibroblast-derived inducers of alveolar epithelial apoptosis identified as angiotensin peptides". In: *American Journal of Physiology-Lung Cellular and Molecular Physiology* 277, pp. L1158–L1164.

Wang, Ting et al. (2017). "Interleukin-17 induces human alveolar epithelial to mesenchymal cell transition via the TGF-β1 mediated Smad2/3 and ERK1/2 activation". In: *PLoS One* 12.9, e0183972.

Wang, Y et al. (2019). "Autophagy inhibition specifically promotes epithelial-mesenchymal transition and invasion in RAS-mutated cancer cells". In: *Autophagy* 15.5, pp. 886–899.

Wang, Yihua, Fangfang Bu, et al. (2014). "ASPP2 controls epithelial plasticity and inhibits metastasis through β-catenin-dependent regulation of ZEB1". In: *Nature cell biology* 16.11, pp. 1092–1104.

Wang, Yihua, Hua Xiong, et al. (2019). "Autophagy inhibition specifically promotes epithelial-mesenchymal transition and invasion in RAS-mutated cancer cells". In: *Autophagy* 15.5, pp. 886–899.

Wang, Yongliang et al. (2013). "Pirfenidone attenuates cardiac fibrosis in a mouse model of TAC-induced left ventricular remodeling by suppressing NLRP3 inflammasome formation". In: *Cardiology* 126.1, pp. 1–11.

Wang, Yongyu et al. (2009). "Genetic defects in surfactant protein A2 are associated with pulmonary fibrosis and lung cancer". In: *The American Journal of Human Genetics* 84.1, pp. 52–59.

Wang, Zhong et al. (2001). "Antagonistic controls of autophagy and glycogen accumulation by Snf1p, the yeast homolog of AMP-activated protein kinase, and the cyclin-dependent kinase Pho85p". In: *Molecular and cellular biology* 21.17, pp. 5742–5752.

Weill, David et al. (2015). "A consensus document for the selection of lung transplant candidates: 2014—an update from the Pulmonary Transplantation Council of the International Society for Heart and Lung Transplantation". In: *The Journal of Heart and Lung Transplantation* 34.1, pp. 1–15.

Wells, Athol U et al. (2003). "Idiopathic pulmonary fibrosis: a composite physiologic index derived from disease extent observed by computed tomography". In: *American journal of respiratory and critical care medicine* 167.7, pp. 962–969.

Willis, Brigham C and Zea Borok (2007). "TGF-β-induced EMT: mechanisms and implications for fibrotic lung disease". In: *American Journal of Physiology-Lung Cellular and Molecular Physiology* 293.3, pp. L525–L534.

Willis, Brigham C, Janice M Liebler, et al. (2005). "Induction of epithelial-mesenchymal transition in alveolar epithelial cells by transforming growth factor-β1: potential role in idiopathic pulmonary fibrosis". In: *The American journal of pathology* 166.5, pp. 1321–1332.

Wilson, Edward CF et al. (2014). "Treating idiopathic pulmonary fibrosis with the addition of co-trimoxazole: an economic evaluation alongside a randomised controlled trial". In: *Pharmacoeconomics* 32, pp. 87–99.

Wilson, William R and Michael P Hay (2011). "Targeting hypoxia in cancer therapy". In: *Nature Reviews Cancer* 11.6, pp. 393–410.

Wind, Sven et al. (2019). "Clinical pharmacokinetics and pharmacodynamics of nintedanib". In: *Clinical pharmacokinetics* 58, pp. 1131–1147.

Wollin, Lutz et al. (2015). "Mode of action of nintedanib in the treatment of idiopathic pulmonary fibrosis". In: *European Respiratory Journal* 45.5, pp. 1434–1445.

Woods, Angela et al. (2003). "LKB1 is the upstream kinase in the AMP-activated protein kinase cascade". In: *Current biology* 13.22, pp. 2004–2008.

Wooten, Marie W et al. (2005). "The p62 scaffold regulates nerve growth factor-induced NF-κB activation by influencing TRAF6 polyubiquitination". In: *Journal of Biological Chemistry* 280.42, pp. 35625–35629.

Wrobel, Louise K et al. (2002). "Contractility of single human dermal myofibroblasts and fibroblasts". In: *Cell motility and the cytoskeleton* 52.2, pp. 82–90.

Wu, Haijian et al. (2015). "Crosstalk between macroautophagy and chaperone-mediated autophagy: implications for the treatment of neurological diseases". In: *Molecular neurobiology* 52, pp. 1284–1296.

Wu, Jin'en et al. (2018). "MicroRNA roles in the nuclear factor kappa B signaling pathway in cancer". In: *Frontiers in Immunology* 9, p. 546.

Wu, Xiaojun et al. (2021). "3-month, 6-month, 9-month, and 12-month respiratory outcomes in patients following COVID-19-related hospitalisation: a prospective study". In: *The Lancet Respiratory Medicine* 9.7, pp. 747–754.

Wuyts, Wim A, Carlo Agostini, et al. (2013). "The pathogenesis of pulmonary fibrosis: a moving target". In: *European Respiratory Journal* 41.5, pp. 1207–1218.

Wuyts, Wim A, Katerina M Antoniou, et al. (2014). "Combination therapy: the future of management for idiopathic pulmonary fibrosis?" In: *The lancet Respiratory medicine* 2.11, pp. 933–942.

Wygrecka, Malgorzata et al. (2011). "Role of protease-activated receptor-2 in idiopathic pulmonary fibrosis". In: *American journal of respiratory and critical care medicine* 183.12, pp. 1703–1714.

Wynn, Thomas A (2011a). "Integrating mechanisms of pulmonary fibrosis". In: *Journal of Experimental Medicine* 208.7, pp. 1339–1350.

Wynn, Thomas A and Thirumalai R Ramalingam (2012). "Mechanisms of fibrosis: therapeutic translation for fibrotic disease". In: *Nature medicine* 18.7, pp. 1028–1040.

Wynn, Thomas A. (2011b). "Integrating mechanisms of pulmonary fibrosis". In: *Journal of Experimental Medicine* 208, pp. 1339–1350.

Xiang, Xiaoqin et al. (2004). "AMP-activated protein kinase activators can inhibit the growth of prostate cancer cells by multiple mechanisms". In: *Biochemical and biophysical research communications* 321.1, pp. 161–167.

Xu, Yan et al. (2016). "Single-cell RNA sequencing identifies diverse roles of epithelial cells in idiopathic pulmonary fibrosis". In: *JCI insight* 1.20.

Xue, Hua, Bingjian Lu, and Maode Lai (2008). "The cancer secretome: a reservoir of biomarkers". In: *Journal of translational medicine* 6, pp. 1–12.

Yanai, Hagai et al. (2015). "Cellular senescence-like features of lung fibroblasts derived from idiopathic pulmonary fibrosis patients". In: *Aging (Albany NY)* 7.9, p. 664.

Yang, Ivana V et al. (2014). "Relationship of DNA methylation and gene expression in idiopathic pulmonary fibrosis". In: *American journal of respiratory and critical care medicine* 190.11, pp. 1263–1272.

Yang, Jibing et al. (2013). "Activated alveolar epithelial cells initiate fibrosis through secretion of mesenchymal proteins". In: *The American journal of pathology* 183.5, pp. 1559–1570.

Yang, Zhifen and Daniel J Klionsky (2010). "Eaten alive: a history of macroautophagy". In: *Nature cell biology* 12.9, pp. 814–822.

Yao, Liudi, Franco Conforti, et al. (2019). "Paracrine signalling during ZEB1-mediated epithelial–mesenchymal transition augments local myofibroblast differentiation in lung fibrosis". In: *Cell Death & Differentiation* 26.5, pp. 943–957.

Yao, Liudi, Yilu Zhou, et al. (2021). "Bidirectional epithelial–mesenchymal crosstalk provides self-sustaining profibrotic signals in pulmonary fibrosis". In: *Journal of Biological Chemistry* 297.3.

Yogo, Yurika et al. (2009). "Macrophage derived chemokine (CCL22), thymus and activation-regulated chemokine (CCL17), and CCR4 in idiopathic pulmonary fibrosis". In: *Respiratory research* 10.1, pp. 1–11.

Yorimitsu, T and Daniel J Klionsky (2005). "Autophagy: molecular machinery for self-eating". In: *Cell Death & Differentiation* 12.2, pp. 1542–1552.

Zaafan, Mai A et al. (2016). "Pyrrolidinedithiocarbamate attenuates bleomycin-induced pulmonary fibrosis in rats: modulation of oxidative stress, fibrosis, and inflammatory parameters". In: *Experimental Lung Research* 42.8-10, pp. 408–416.

Zagórska, Anna et al. (2010). "New roles for the LKB1-NUAK pathway in controlling myosin phosphatase complexes and cell adhesion". In: *Science signaling* 3.115, ra25–ra25.

Zakikhani, Mahvash et al. (2006). "Metformin is an AMP kinase–dependent growth inhibitor for breast cancer cells". In: *Cancer research* 66.21, pp. 10269–10273.

Zeng, Ping-Yao and Shelley L Berger (2006). "LKB1 is recruited to the p21/WAF1 promoter by p53 to mediate transcriptional activation". In: *Cancer research* 66.22, pp. 10701–10708.

Zeqiraj, Elton et al. (2009). "Structure of the LKB1-STRAD-MO25 complex reveals an allosteric mechanism of kinase activation". In: *Science* 326.5960, pp. 1707–1711.

Zhang, Donna D and Mark Hannink (2003). "Distinct cysteine residues in Keap1 are required for Keap1-dependent ubiquitination of Nrf2 and for stabilization of Nrf2 by chemopreventive agents and oxidative stress". In: *Molecular and cellular biology*.

Zhang, Lijuan et al. (2016). "Combined pulmonary fibrosis and emphysema: a retrospective analysis of clinical characteristics, treatment and prognosis". In: *BMC Pulmonary Medicine* 16.1, pp. 1–8.

Zhao, Like et al. (2019). "Iguratimod ameliorates bleomycin-induced alveolar inflammation and pulmonary fibrosis in mice by suppressing expression of matrix metalloproteinase-9". In: *International journal of rheumatic diseases* 22.4, pp. 686–694.

Zhong, Li et al. (2008). "Identification of secreted proteins that mediate cell-cell interactions in an in vitro model of the lung cancer microenvironment". In: *Cancer research* 68.17, pp. 7237–7245.

Zhou, Yang et al. (2010). "Thy-1-integrin $\alpha v\beta 5$ interactions inhibit lung fibroblast contraction-induced latent transforming growth factor-$\beta 1$ activation and myofibroblast differentiation". In: *Journal of Biological Chemistry* 285, pp. 22382–22393.

Zhou, Yingyao et al. (2019). "Metascape provides a biologist-oriented resource for the analysis of systems-level datasets". In: *Nature communications* 10.1, p. 1523.

Zhou, Yong et al. (2013). "Inhibition of mechanosensitive signaling in myofibroblasts ameliorates experimental pulmonary fibrosis". In: *The Journal of clinical investigation* 123.3, pp. 1096–1108.

Zhu, Liangying et al. (2017). "M2 macrophages induce EMT through the TGF-β/Smad2 signaling pathway". In: *Cell biology international* 41.9, pp. 960–968.

Zhuang, Zhi-Gang et al. (2006). "Enhanced expression of LKB1 in breast cancer cells attenuates angiogenesis, invasion, and metastatic potential". In: *Molecular cancer research* 4.11, pp. 843–849.

Zissel, Gernot et al. (2000). "Human alveolar epithelial cells type II are capable of regulating T-cell activity." In: *Journal of investigative medicine: the official publication of the American Federation for Clinical Research* 48.1, pp. 66–75.